Distortional Static and Buckling Analysis of Wide Flange Steel Beams

Payam Pezeshky

Under the supervision of

Dr. Magdi E. Mohareb

Thesis submitted to the

Faculty of Graduate and Postdoctoral Studies

In partial fulfillment of the requirements

For the Ph.D. degree in Civil Engineering

Civil Engineering Department

Faculty of Engineering

University of Ottawa

To my beloved parents,

Soroush & Mahnaz Pezeshky

Acknowledgement

I would like to express my deepest gratitude to my supervisor, Dr. Magdi Mohareb, whose extensive knowledge, valuable advice, creative thought, technical and financial support, and commitment to the highest professional standards inspired me throughout this research.

I am also thankful to the members of my thesis proposal committee Dr. Khoo, Dr. Martín-Pérez, and Dr. Dragomirescu for their thoughtful advice and encouragement.

I would like to thank my dear friends Haleh and Farhood Nowzartash and their sweet daughters Leva and Ava for their moral support.

My highest appreciations go to my dear parents, Soroush and Mahnaz, my beloved sisters, Sanaz and Sarir, my kindhearted brother Parham, my adorable niece Ma'va and my lovely nephew Vala for their unconditional and continuous love, patience and support.

Special thanks go to the Baha'i Institute for Higher Education (B.I.H.E.) staff and colleagues in Iran for their sincere self-dedicated commitment towards the development of knowledge and growth of education. Indeed, without their sacrifice, I could not have made it up to this point.

Last but not least, I would like to thank the Baha'i community of Ottawa, my wonderful circle of friends and my officemates Amir and Leonardo for their company and support.

Abstract

Existing design provisions in design standards and conventional analysis methods for structural steel members are based on the simplifying kinematic Vlasov assumption that neglects cross-sectional distortional effects. While the non-distortional assumption can lead to reasonable predictions of beam static response and buckling strength in common situations, past work has shown the inadequacy of such assumption in a number of situations where it may lead to over-predicting the strength of the members. The present study thus develops a series of generalized theories/solutions for the static analysis and buckling analysis of steel members with wide flange cross-sections that capture distortional effects of the web. Rather than adopting the classical Vlasov assumption that postulates the cross-section to move and rotate in its own plane as a rigid disk, the present theories assume the web to be flexible in the plane of the cross-section and thus able to bend laterally, while both flanges to move as rigid plates within the plane of the cross-section to be treated as Euler-Bernouilli beams. The theories capture shear deformation effects in the web, as well as local and global warping effects. Based on the principle of minimum potential energy, a distortional theory is developed for the static analysis of wide flange steel beams with mono-symmetric cross-sections. The theory leads to two systems of differential equations of equilibrium. The first system consists of three coupled equilibrium differential equations that characterize the longitudinal-transverse response of the beam and the second system involves four coupled equilibrium differential equations of equilibrium and characterizes the lateral-torsional response of the beam. Closed form solutions are developed for both systems for general loading. Based on the kinematics of the new theory, two distortional finite elements are then developed. In the first element, linear and cubic Hermitian polynomials are employed to interpolate displacement fields while in the second element, the closed-form solutions developed are adopted to formulate special shape functions. For longitudinal-transverse response the elements consist of two nodes with four degree of freedom per node for longitudinal-transverse response and for lateral-torsional response, the elements consist of two nodes with eight degrees of freedom per node. The solution is able to predict the distortional deformation and stresses in a manner similar to shell solutions while keeping the modeling and computational effort to a minimum.

Applications of the new beam theory include (1) providing new insights on the response of steel beams under torsion whereby the top and bottom flanges may exhibit different angles of twist, (2) capturing the response of steel beams with a single restrained flange as may be the case when a concrete slab provides lateral and/or torsional restraint to the top flange of a steel beam, and (3) modelling the beneficial effect of transverse stiffeners in reducing distortional effects in the web.

The second part of the study develops a unified lateral torsional buckling finite element formulation for the analysis of beams with wide flange doubly symmetric cross-sections. The solution captures several non-conventional features. These include the softening effect due to web distortion, the stiffening effect induced by pre-buckling deformations, the pre-buckling nonlinear interaction between strong axis moments and axial forces, the contribution of pre-buckling shear deformation effects within the plane of the web, the destabilizing effects due to transverse loads being offset from the shear centre, and the presence of transverse stiffeners on web distortion. Within the framework of the present theory, it is possible to evoke or suppress any combination of the features and thus isolate the individual contribution of each effect or quantify the combined contributions of multiple effects on the member lateral torsional capacity. The new solution is then applied to investigate the influence of the ratios of beam span-to-depth, flange width-to-thickness, web height-to-thickness, and flange width-to-web height on the lateral torsional buckling strength of simply supported beams and cantilevers. Comparisons with conventional lateral torsional buckling solutions that omit distortional and pre-buckling effects quantify the influence of distortional and/or pre-buckling deformation effects. The theory is also used to investigate the influence of P-delta effects of beam-columns subjected to transverse and axial forces on their lateral torsional buckling resistance. The theory is used to investigate the load height effect relative to the shear centre. Comparisons are made with load height effects as predicted by non-distortional buckling theories. The solution is adopted to quantify the beneficial effect of transverse stiffeners in controlling/suppressing web distortion in beams and increasing their buckling resistance.

Table of Contents

Acknowledgement ..... **iii**

Abstract ..... **iv**

Table of Contents ..... **vi**

List of Figures ..... **xiii**

List of Tables ..... **xvi**

Glossary ..... **xvi**

1. Chapter 1 ..... **1**

Introduction **1**

1.1. General 1

1.2. Deformations in lateral torsional buckling 2

1.3. Motivation 4

1.3.1. Limitations of conventional beam theories in static analysis applications 4

1.3.1.1. Beams with restraints at one of the flanges 4

1.3.1.2. Effect of transverse stiffeners on web distortion 4

1.3.1.3. Wide flange beams under twisting moments 6

1.3.1.4. Beams with overhangs under twisting moments 7

1.3.2. Limitations of conventional beam theories in buckling applications 8

1.3.2.1. Effects of web distortion and PBD 9

1.3.2.2. Effect of load height 10

1.3.2.3. P-delta effect in pre-buckling analysis 10

1.3.2.4. Shear deformation in pre-buckling analysis 10

1.3.2.5. Effect of transverse stiffeners 11

1.3.2.6. Features of the Sought distortional buckling theory 11

1.4. Overview of the thesis 12

1.5. References 13

2. Chapter 2 ..... **16**

Literature review 16

2.1. General 16

2.2. Fundamentals of calculus of variation and Variational principles 16

2.3. Principle of stationary total potential energy 19

2.4. Kinematics of beam theories 21

2.4.1. Euler-Bernoulli beam theory 21

2.4.2. Timoshenko beam theory 22

2.4.3. Higher order beam theories 23

2.4.4. Vlasov thin-walled beam theory 23

2.4.5. Gjelsvik thin-walled beam theory 25

2.5. Geometrically nonlinear pre-buckling analysis 27

2.5.1. Background 27

2.5.2. Overview of eigen-value buckling solutions 28

2.5.2.1. Conventional approach based on linear pre-buckling analysis: 28

2.5.2.2. Accounting for non-linear effects in pre-bucking analysis: 29

2.5.2.3. Modifications to account for pre-bucking deformation effects: 29

2.6. References 30

3. Chapter 3 32

Distortional theory for the analysis of wide flange steel beams [(a)] 32

3.1. Abstract 32

3.2. Introduction and literature review 33

3.3. Statement of the problem 38

3.4. Assumptions and kinematics 41

3.4.1. Displacements in the plane of the cross-section 41

3.4.2. Longitudinal displacement 42

3.5. Expressions for strains and stresses 44

3.6. Energy formulation 45

3.7. Field equations and boundary conditions 48

3.8. Closed form solution 51

3.8.1. Homogenous solution for the longitudinal-transverse response 51

3.8.2. Homogenous lateral-torsional response 53

3.8.3. Particular solution 54

3.9. Numerical examples 55

3.9.1. Example 1: Longitudinal-transverse response 55

3.9.2. Example 2: Cantilever under torsion 57

3.9.3. Example 3: Cantilever under various types of twisting moments 59

3.9.4. Example 4: Cantilever beam with restrained top flange 61

3.9.5. Example 5: Cantilever under transverse uniform distributed load 62

3.10. Summary and conclusions 65

3.11. Appendix A 66

3.12. Appendix B 68

3.13. List of symbols 70

3.14. References 73

4. Chapter 4 76

Distortional Theory for the Analysis of Wide Flange Steel Beams –Finite Element Formulation[(a)] 76

4.1. Abstract 76

4.2. Introduction and Literature Review 77

4.3. Statement of the problem 78

4.4. Assumptions and Kinematics 79

4.5. Energy Formulation 80

4.6. Finite Element Formulation 1- Based on Polynomial Interpolation (FE1) 82

4.6.1. Longitudinal-transverse response 83

4.6.1.1. Displacement fields in terms of Nodal Displacement 83

4.6.1.2. Equilibrium Conditions 85

4.6.2. Lateral-torsional response 85

4.6.2.1. Displacement fields in terms of Nodal Displacement 85

4.6.2.2. Equilibrium Conditions 87

4.7. Finite Element Formulation 2- Based on Exact Shape Functions (FE2) 87

4.7.1. Longitudinal-transverse response 89

4.7.1.1. Displacement fields in terms of Nodal Displacement 89

4.7.1.2. Equilibrium Conditions 92

4.7.2. Lateral torsional response 92

4.7.2.1. Displacement fields in terms of Nodal Displacement 92

4.7.2.2. Equilibrium Conditions 95

4.8. Numerical Examples 95

4.8.1. Example 1: Cantilever under transverse loading 95

4.8.2. Example 2: Mesh Sensitivity Analysis 96

4.8.3. Example 3: Beam with Overhangs under Torsion 98

4.9. Summary and Conclusion 102

4.10. Appendix A- Closed form solution for lateral torsional response 102

4.11. Notations 104

4.12. Subscripts 107

4.13. References 107

5. Chapter 5 109

Geometric nonlinear analysis of shear-deformable beam-columns 109

5.1. Introduction and motivation 109

5.2. Statement of the problem 109

5.3. Geometry and coordinates 109

5.4. Assumptions and kinematics 110

5.5. Formulation 111

5.6. Finite element formulation 113

5.6.1. Total potential energy in terms of nodal displacement 114

5.6.2. Discretized equilibrium conditions 116

5.7. Coordinate transformations 117

5.8. Details of the iterative technique 117

5.9. Numerical examples 119

5.9.1. Example 1: Long-span simply supported member 119

5.9.2. Example 2: Short span cantilever 120

5.10. References 121

6. Chapter 6 122

Lateral torsional buckling of wide flange sections including distortional and pre-buckling effects 122

6.1. Abstract 122

6.2. Introduction and motivation 123

6.3. Literature review 124

6.3.1. Distortional buckling effect: 124

6.3.2. Pre-buckling deformation effect: 125

6.4. Statement of the problem 127

6.4.1. Assumptions 130

6.4.2. Kinematics 131

6.4.3. Pre-buckling Analysis 132

6.4.3.1. Finite element formulation ... 132
6.4.3.2. Expressions of pre-buckling stresses in terms of stress resultants ... 133
6.4.3.3. Expressions for pre-buckling displacements ... 133
6.4.4. Expressions for buckling displacements ... 135
6.4.4.1. Displacements for a generic point within the flanges ... 135
6.4.4.2. Displacements for a generic point within the web ... 137
6.5. Expressions for strains and stresses ... 138
6.5.1. Strains in the top flange ... 138
6.5.2. Strains in the web ... 139
6.5.3. Stress strain relations ... 140
6.6. Variational principle ... 140
6.6.1. Internal strain energy ... 141
6.6.1.1. Contribution of the web ... 141
6.6.1.2. Contributions of the Flanges ... 144
6.6.2. Load potential energy ... 151
6.7. Finite element formulation ... 151
6.7.1. Interpolation scheme ... 151
6.7.2. Second variation of Internal Strain energy ... 154
6.7.2.1. Second variation of load potential ... 154
6.8. Kinematic constraints to supress distortion at a beam end ... 154
6.9. Condition of neutral stability ... 156
6.10. Types of analysis: ... 157
6.10.1. Pre-buckling analysis ... 157
6.10.2. Buckling analysis ... 157
6.11. Convergence study and contribution of higher order terms ... 160
6.12. Verification ... 162
6.13. Numerical examples ... 163

6.13.1. Example 1-Parametric investigation: Simply supported beam under point load .. 163

6.13.2. Example 2-Parametric investigation: Cantilever under tip load 166

6.13.3. Example 3: Transverse load height effect 169

6.13.4. Example 4: Longitudinal load height effect 170

6.13.5. Example 5: P-delta effect in beam columns 171

6.13.6. Example 6: Effect of the stiffeners on distortional critical moments 173

6.14. Summary and conclusions 175

6.15. Appendix A – Matrices for the web 177

6.16. Appendix B – Matrices for flanges 178

6.17. Appendix C 181

6.18. List of symbols 182

6.19. References 187

7. Chapter 7 190

Summary-Conclusion-Recommendation-Future work 190

7.1. Summary of contributions 190

7.1.1. Contributions related to the distortional static theory 190

7.1.2. Contributions related to the distortional buckling theory: 191

7.1.3. Additional contributions 192

7.2. Conclusions 192

7.3. Recommendations for future work 194

List of Figures

Fig. 1-1 Vlasov's assumption a) Cross section remains undistorted after deformation b) shear deformation is negligible 1
Fig. 1-2 a) Distortion in slender wide flange cross section, b) distortional buckling modes in cold formed cross section 2
Fig. 1-3 Stages of buckling 3
Fig. 1-4 distortion in problems with partial restrains a) beam with concrete slab on the top flange b) deformed configuration 5
Fig. 1-5 Wide flange beam with transverse stiffeners 5
Fig. 1-6 Plate girder restrained by lateral braces at top flange 6
Fig. 1-7 Types of twisting moments (a) Type I- horizontal parallel forces, (b) Type II- transverse parallel forces on top flange, (c) Type III- transverse parallel forces on bottom flange (d) Twisting moments under the Vlasov theory 6
Fig. 1-8 Deformed configuration of beam under a) type I, b) Type II and c) Type III twisting moments 7
Fig. 1-9 a) Beam with overhangs seated on column b) deformed configuration in the absence of transverse stiffeners c)deformed configuration at the present of transverse stiffeners 8
Fig. 1-10 a) cross section kinematics in classical solutions b) cross section kinematics in reality c) beam onset of buckling in classical solutions d)beam onset of buckling in reality 11
Fig. 1-11 Load offset from the shear centre in a)classical solutions b)distortion solutions c) steel beam-beam connection 12
Fig. 1-12 Effect of transverse stiffeners on LTB of the plate girder 12
Fig. 2-1 Equilibrium position a)stable b)neutral c)unstable 20
Fig. 2-2 Right handed coordinate system 21
Fig. 2-3 a) Euler-Bernoulli beam b) Timoshenko beam c) Higher order beam (e.g., Bickford (1982), Reddy (1984b)) 23
Fig. 2-4 a) Kinematics of the Vlasov and Gjelsvic theories and b) Additional kinematic considerations in the Gjelsvic theory 26
Fig. 2-5 a) Wide flange beam under twist T, b) global warping response of the middle surface, and c) additional local warping response of the flange 27
Fig. 3-1. Cross section dimensions 39

Fig. 3-2. (a) Beam and axes (b) End tractions and stress resultants at z=0. (c) End tractions and stress resultants at z=L 40
Fig. 3-3. Coordinates and displacements 41
Fig. 3-4. Kinematics of top flange a) Deformed shape, b) Side view(Y-Z) and c) Plan view(X-Z) ... 42
Fig. 3-5. Tip deflection for transversely loaded beams 56
Fig. 3-6. Three scenarios for applying a twisting moment 19.2 kNm; a) Case a-Examples 2 and 3, b) Case b-Example 3, and c) Case c-Example 3 57
Fig. 3-7. Angles of twist along the cantilever span 58
Fig. 3-8. Cross section deformed configuration at the tip for cases (a), (b) and (c), (Displacement amplification factor=10) 60
Fig. 3-9. Deformed shape of the cross section at the tip with restrained top flange, (Displacement amplification factor=10) 61
Fig. 3-10 Deformed configuration for cantilever subject to line load 63
Fig. 3-11 Lateral displacements of top and bottom flanges and beam transvers displacement 64
Fig. 3-12 Angles of twist of top and bottom flanges 64
Fig. 4-1. Cross section dimensions, global and local coordinates 79
Fig. 4-2. Degrees of freedom of a) longitudinal-transverse element b) lateral torsional element 83
Fig. 4-3. Tip deflection under concentrated transverse force 96
Fig. 4-4. Cantilever subjected to parallel forces 96
Fig. 4-5. Multi-span beam, a) No Stiffeners provided b) Pair of stiffeners provided 99
Fig. 4-6. Point supports at beam-column junction, a) no stiffeners provided b) stiffeners provided. . 99
Fig. 4-7. Comparison of Lateral displacements along top and bottom flanges (mm) 100
Fig. 4-8. Angle of twist of top and bottom flanges under Hermitian FE and Abaqus (mm) 100
Fig. 4-9. Lateral displacement of top and bottom flanges of stiffened beam 101
Fig. 4-10. Angle of twist of top and bottom flanges of stiffened beam 101
Fig. 5-1. a) Cross section dimensions b) Loading scheme 110
Fig. 5-2 a) Displacements field of the beam b) shear deformations within the plane of the web 111
Fig. 5-3. Two-node finite element, a) degrees of freedom b) stress resultants 113
Fig. 5-4 Force-displacement diagram for a simply supported beam under transverse load acting at the mid-span and axial force acting the end 120

Fig. 5-5 Force-displacement diagram for a cantilever beam under transverse and axial loads acting at the tip 121

Fig. 6-1 a) Classical LTB kinematics b) distortion lateral torsional buckling c) beam configuration onset of buckling incorporating PBD effect 124

Fig. 6-2 a) Cross section dimensions b) Loading scheme pre-buckling analysis 129

Fig. 6-3 Stages of Deformation 130

Fig. 6-4 Two-node shear deformable element a) degrees of freedom b) nodal forces 133

Fig. 6-5 Distortional buckling finite element with 20 DOFs 153

Fig. 6-6 a) Distortional element without stiffeners, b) distortional element with stiffeners 156

Fig. 6-7 Convergence study for cantilever problem a) Non-distortional solutions b) Distortional solutions 162

Fig. 6-8 Examples a) cantilever under tip point load b) simply supported beam under mid-span point load 162

Fig. 6-9 a) Cross Section dimensions b) Loading scheme c-f) Ratio of various types of critical moments to the classical solution versus dimensionless parameters L/d, d/w, b/t and b/d 166

Fig. 6-10 a) Cross Section dimensions b) Loading scheme c-f) Ratio of various types of critical moments to the classical solution versus dimensionless parameters L/d, d/w, b/t and b/d 168

Fig. 6-11 a)Simply supported beam subjected to mid-span load offset from shear center b)geometric properties c) effect of load applied offset from the shear centre on critical moments d) effect of the load applied offset from the shear centre on the normalized critical moments 170

Fig. 6-12 Effect of the axial load offset from the shear centre on a) critical load b) normalized critical load 171

Fig. 6-13 a) Simply supported beam subjected to a mid-span transverse load and an axial end-node load b)geometric properties c) Buckling capacity resulting from interaction of transverse and axial forces d) force-displacement diagrams for $\alpha = 0.3$ and e) force-displacement diagrams for $\alpha = 1$. 173

Fig. 6-14 a) simply supported plate girder subjected to mid-span load b) geometric properties c) case (1) includes five stiffeners d) case (2) includes seven stiffeners e) effect of stiffeners on distortional normalized critical moment f) effect of middle stiffeners on normalized critical moments 175

List of Tables

Table 3-1. A comparison of distortional studies 37
Table 3-2 Vertical displacement at the tip of 4.00 m span cantilever 57
Table 3-3 Displacements and angles of twist at the tip of the cantilever 62
Table 4-1. Mesh sensitivity analysis 97
Table 6-1Types of analysis for beam analysis 159
Table 6-2 Comparison of critical moments (kNm) 163

Glossary

AISC	American Institute of Steel Construction
BC	Boundary Condition
BSI	British Standards Institution
CSA	Canadian Standards Association
DE	Differential Equation
DOF	Degree Of Freedom
FE	Finite Element
FEA	Finite Element Analysis
GBT	Generalised Beam Theory
LTB	Lateral Torsional Buckling
PBD	Pre-Buckling Deformation

Chapter 1

Introduction

1.1. General

Wide flange cross sections are commonly used in steel structures as beams, columns, and beam columns. Design provisions for such members are based on their yielding capacity, their buckling capacity, or a combination thereof. With the availability and use of higher strength steel, buckling considerations tend to govern the capacity of steel members as members become more prone to buckling than yielding. A common buckling mechanism in steel beams and beam-columns is Lateral Torsional Buckling (LTB) whereby a laterally unsupported member bent about its strong axis can attain a point of neutral stability at which it tends to undergo lateral movement and twist without increase in the applied load. LTB is recognized by various steel design standards (i.e., ANSI/AISC 360-16 (2016), EN-1993-1-1-05 (2005), CAN-CSA S16-14 (2014), Standards Association of Australia (1998)). Steel beam design provisions in standards for LTB are based on the idealized case of a simply supported member subjected to uniform bending moments about its strong axis. When such a member is bent about its strong axis, as moments increase, the member undergoes transverse displacements until the point of buckling onset is attained at which the member undergoes sudden lateral displacement and twist. The moment corresponding to this buckled state is referred to the buckling moment. The classical LTB treatment is based on the kinematics of the Vlasov thin-walled beam theory (Vlasov (1961)) which is based on two simplifying kinematic assumptions: a) cross section moves as a rigid disk in its own plane throughout deformation (i.e., cross section distortion is negligible) and b) shear strains along the section mid-surface is negligible, Fig. 1-1.

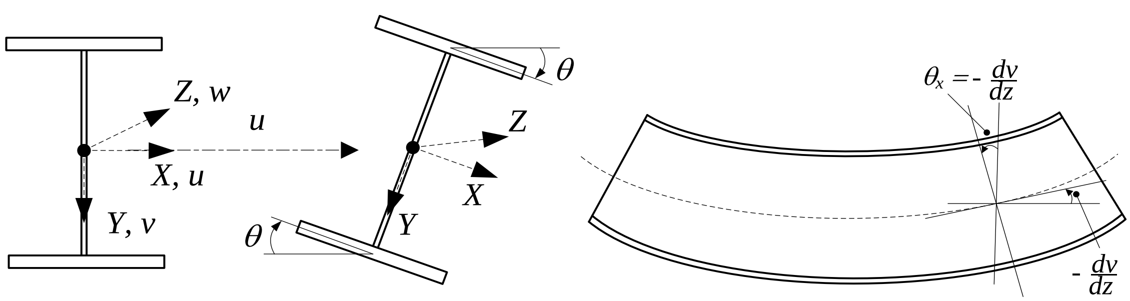

(a) **(b)**

Fig. 1-1 Vlasov's assumption a) Cross section remains undistorted after deformation b) shear deformation is negligible

While the first Vlasov assumption which omits distortional effects results in a simplified treatment, the significance of distortion has been recognized in various buckling problems (Section 2.5.2). Distortional effects were also reported to play an important role for members under twisting moments (Schardt (1994), Silvestre and Camotim (2002), Jönsson and Andreassen (2011), etc). Rolled members with stocky flanges and slender webs can buckle in a distortional mode where the flanges behave as rigid beams while the web bends in the plane of the cross-section (Fig. 1-2a). Distortional buckling have received attention in members with cold formed cross sections with typically thin segments (Fig. 1-2b) where each segment of the cross section distorts out of its own plane while the entire member buckles along its length. Less attention has been devoted to distortional effects in rolled sections, as it is generally assumed that, owing to their thicker segments, distortional effects tend to be less significant. One of the objectives of the present study is to examine the validity of the non-distortional assumption, and assess the conditions under which it is valid by developing a series of static and buckling theories that account for web distortion.

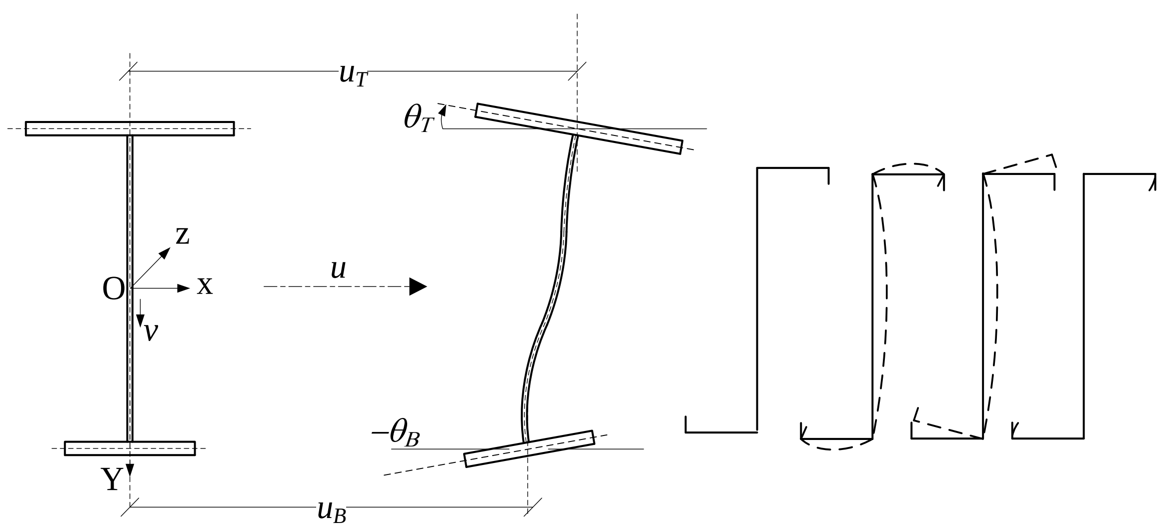

(a) **(b)**

Fig. 1-2 a) Distortion in slender wide flange cross section, b) distortional buckling modes in cold formed cross section

1.2. Deformations in lateral torsional buckling

A wide flange beam is shown in its un-deformed configuration (Fig. 1-3). During pre-buckling deformation (i.e., Stages 1-3) the beam undergoes transverse displacement $v(z)$ induced by transverse load q_y and moves from initial configuration 1 to equilibrium configuration 2. The applied reference load is assumed to gradually increase and, consequently, the associate pre-buckling transverse displacements are assumed to increase. At the onset of buckling (i.e. Stage 3 in Fig. 1-3), the applied transverse load is λq_y and the pre-buckling displacement is $v(\lambda, z)$ which is associated with the equilibrium at configuration 3. As the member buckles, the beam undergoes out of plane displacements and twist and moves to configuration 4. The displacements, strains, stresses and internal forces throughout stages 1-3 are pre-buckling variables and are obtained from a load-deformation pre-buckling analysis (i.e., Section1.3.1, Chapter 5) while the displacements, strains and stresses occurring in going from configuration 3 to configuration 4 are buckling variables. The load level λ at which the member has a tendency to undergo buckling displacement is obtained from an eigenvalue analysis (e.g., Section 1.3.2, Chapter 6)

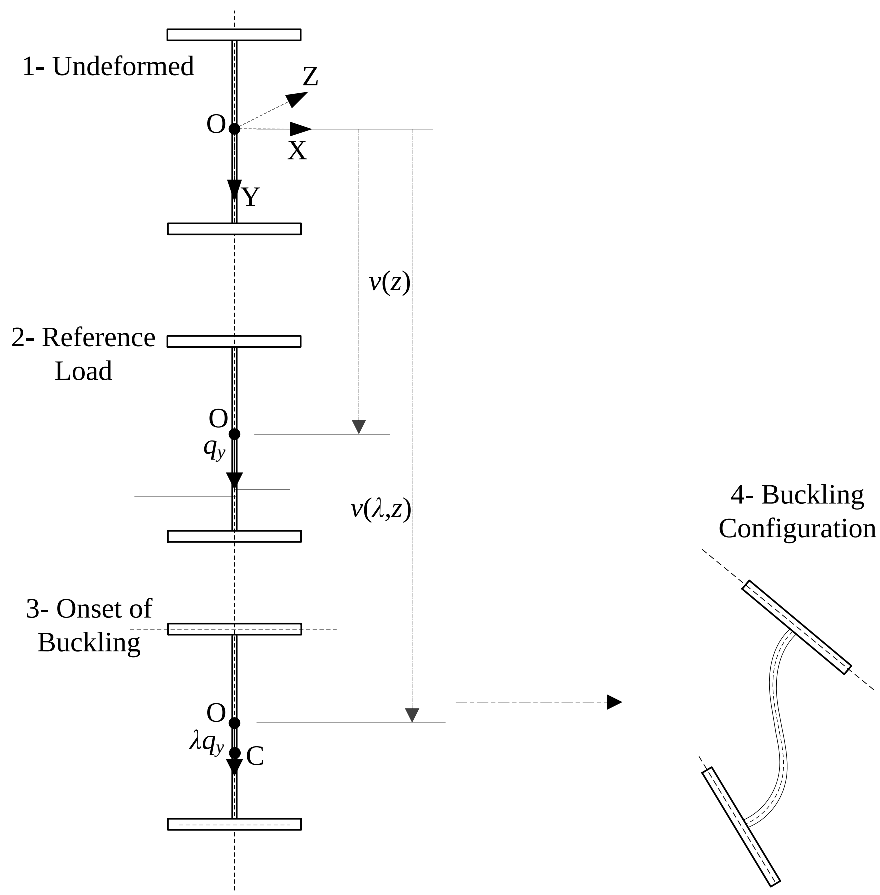

Fig. 1-3 Stages of buckling

1.3. Motivation

This section aims to present the limitations of conventional theories in the static and buckling analyses of wide flange beams. Limitations of conventional theories to static analysis applications are discussed in Section 1.3.1 while those for buckling applications are presented in Section 1.3.2.

1.3.1. Limitations of conventional beam theories in static analysis applications

In general, flanges of beams with deep and slender web subjected to twisting moments tend to exhibit different angles of twist. The presence of stiffeners and lateral braces reduce the tendency of the beam to distort. Classical beam theories are unable to capture distortion neither to accurately model the effect of lateral/twisting braces at the flanges. Illustrative applications are provided in Sections 1.3.1.1-1.3.1.4. The theories proposed in the present research capture distortional effects in a natural way and provide means to supress distortion when details such transverse stiffeners are provided.

1.3.1.1. Beams with restraints at one of the flanges

In composite steel-concrete beams, the top flange is typically restrained laterally and relative to twist by the concrete slab while the bottom flange may be free to translate laterally and twist. In such cases, the section is likely to distort under lateral forces (e.g. Fig. 1-4a). Classical theories (e.g. Vlasov (1961) and Gjelsvik (1981)) neglect the effect of web distortion by assuming a single angle of twist of the entire section. Under these theories, a twist restraint at the top flange would prevent the entire section from twisting. Such theories are unable to replicate the deformed configuration shown in Fig. 1-4b. The distortional beam theories to be develops in the present study aim at capturing such distortional effects.

Also, the wide flange beams with lateral braces either at the top flange (Detail A in Fig. 1-6) and/or bottom flange (Detail B in Fig. 1-6) are prone to distortion. The proposed distortional theories will capture such effects in a natural way.

1.3.1.2. Effect of transverse stiffeners on web distortion

The presence of a transverse stiffener at a given section (e.g., Fig. 1-5) tend to suppress distortion at the stiffener location by enforcing equal angles of twist for the top and bottom flanges while preventing the web from bending within the plane of the cross-section. A wide flange beam with multiple transvers stiffeners is shown in (Fig. 1-5). Distortion is fully suppressed at the location of the stiffeners but is present in between stiffeners. Such distortional effects are not captured by conventional beam theories but are captured in the theories developed in the present study. As the distance between stiffeners reduces, the distortional effects in between stiffeners is expected to reduce. Such a beneficial effect will also be quantified by the proposed theories.

Also, Details C and D in Fig. 1-6 supress distortion by forcing the angle of twist of top and bottom flanges to be equal. In the case of detail C, the presence of the column web below the bottom flange minimizes the angle of twist of the bottom flange and hence the angle of twist for the whole section is minimized. In contrast, the bottom flange of detail D is free to twist, and, while for section D distortion is supressed, the whole section is free to twist. The presence/absence of such stiffener effects will be modelled under the proposed theories.

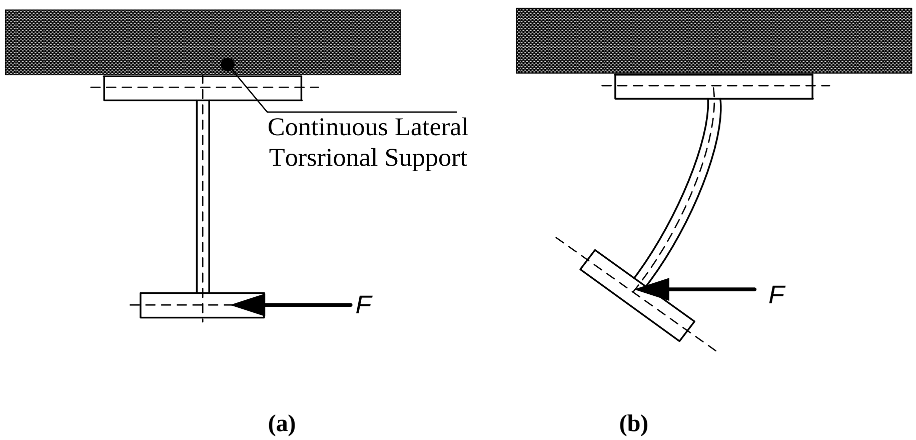

Fig. 1-4 distortion in problems with partial restrains a) beam with concrete slab on the top flange b) deformed configuration

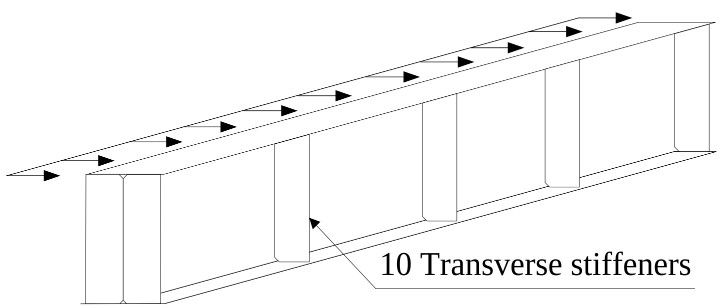

Fig. 1-5 Wide flange beam with transverse stiffeners

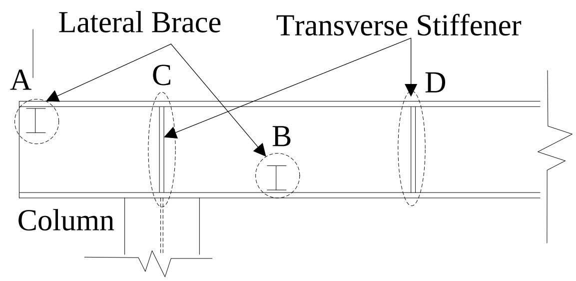

Fig. 1-6 Plate girder restrained by lateral braces at top flange

1.3.1.3. **Wide flange beams under twisting moments**

Wide flange steel members subjected to twisting moments are commonly analyzed using the Vlasov thin-walled beam theory (Vlasov (1961)) which incorporates both the Saint-Venant and Warping torsional effects. Under the Vlasov theory, twisting moments are assumed to induce a global angle of twist for a given cross-section. Specifically, the Vlasov theory does not distinguish between twisting moment $T = F_i d_i,\ i = 1..3$ types I, II and III, respectively shown in Fig. 1-7a-c. In such cases, shell finite element simulations (e.g., Abaqus/CAE model with with S4R elements) show that the deformational behaviour of such cases is associated with distortion and is fundamentally different depending to the type of twisting moment applied (Fig. 1-8a-c). This suggests the need to develop a more advanced beam theory capable of replicating the distortional behaviours observed in Fig. 1-8a-c and is the object of the proposed theories.

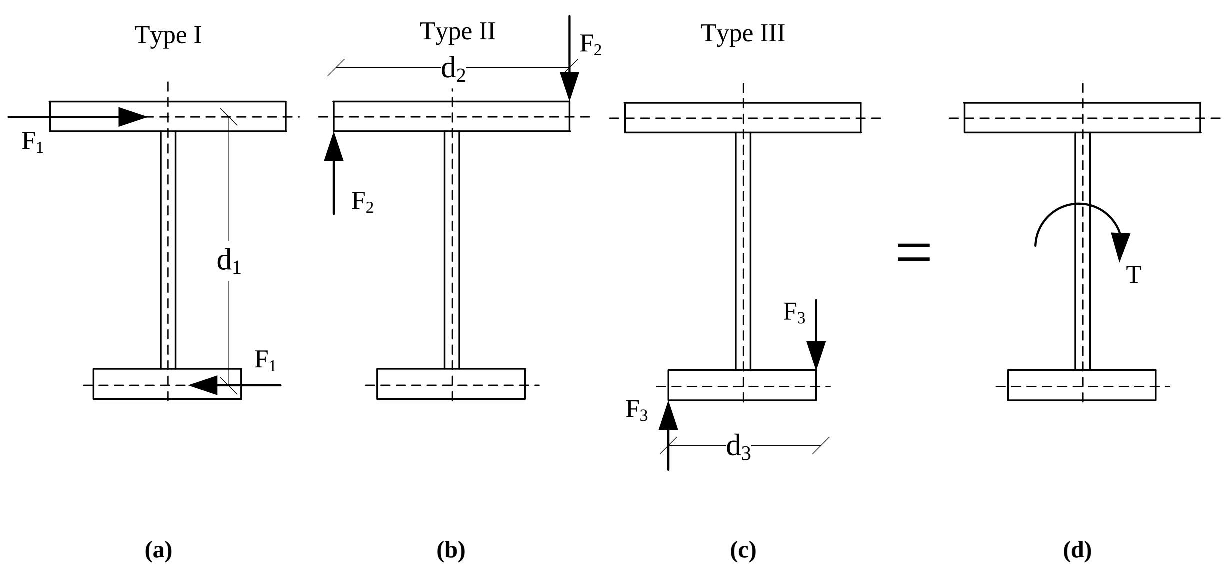

Fig. 1-7 Types of twisting moments (a) Type I- horizontal parallel forces, (b) Type II- transverse parallel forces on top flange, (c) Type III- transverse parallel forces on bottom flange (d) Twisting moments under the Vlasov theory

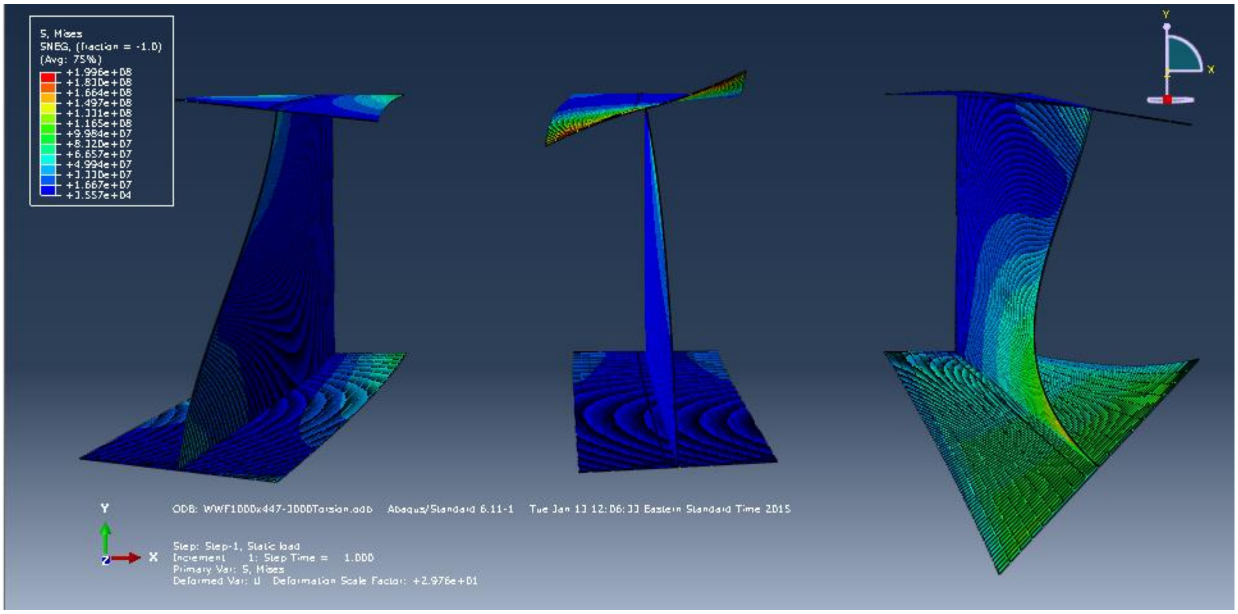

(a) **(b)** **(c)**

Fig. 1-8 Deformed configuration of beam under a) type I, b) Type II and c) Type III twisting moments

1.3.1.4. **Beams with overhangs under twisting moments**

Wide flange beams with overhangs with a bottom flange that is laterally restrained by the supporting columns (Fig. 1-9a) and subjected to eccentric lateral loads and/or twisting moments are likely to exhibit web distortion in the absence of transverse stiffeners. The presence of stiffeners at the column location will have a beneficial effect in controlling web distortion. (Fig. 1-9c). In the absence of transverse stiffeners, the beam twists and distorts in the presence of partial restrains provided at the point of columns (Fig. 1-9b). The proposed theory will enable the modelling of stiffener effects in such cases.

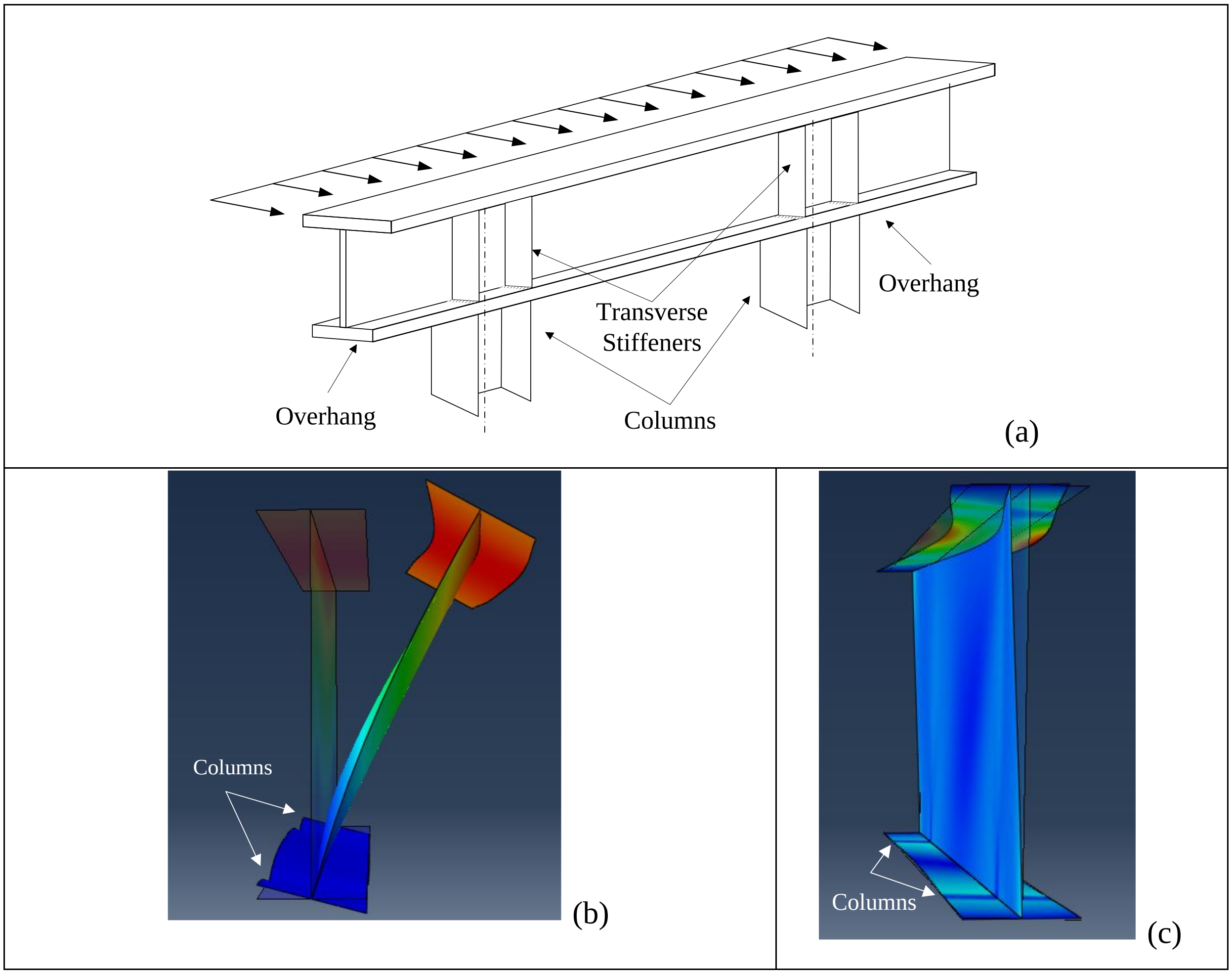

Fig. 1-9 a) Beam with overhangs seated on column b) deformed configuration in the absence of transverse stiffeners c)deformed configuration at the present of transverse stiffeners

1.3.2. **Limitations of conventional beam theories in buckling applications**

Conventional beam theories assume the cross section move as a rigid disk in its own plane throughout as the beam buckles (Fig. 1-10a). As a conservative assumption, they neglect the pre-buckling deformation effects (Fig. 1-10c) and thus assume that the beam at Configuration 3 in Fig. 1-3 is indistinguishable from un-deformed Configuration 1. The significance of distortional and Pre-Buckling Deformation (PBD) effects on the LTB of the beams are discussed under Section 1.3.2.1. In this respect, an innovative aspect of the theory developed in the present study is that it accounts for the interaction of both effects combined. Also, as will be discussed under Section 1.3.2.2, past distortional theories have not accounted for load height effects and a few PBD studies have investigated this effect. Other non-conventional effects captured in the present theories are non-linear second order moments (Section 1.3.2.3), shear deformation effects in the pre-buckling analysis (Section 1.3.2.4) and capturing the beneficial effect of transverse stiffeners (Section 1.3.2.5).

1.3.2.1. **Effects of web distortion and PBD**

The classical LTB solutions developed based on the Vlasov theory (i.e. Vlasov (1961)) neglect web distortion and pre-buckling deformation effects. Present LTB provisions in structural steel design standards (e.g., CAN-CSA S16-14 (2014), Standards Association of Australia (1998), ANSI/AISC 360-16 (2016), British Standards Institution (BSI) (2000)) are based on the Vlasov theory. As such, they suffer from the same limitations as those of the classical solution.

The neglect of distortional effects corresponds to the deformational behaviour depicted in Fig. 1-10a while Fig. 1-10b depicts an improved kinematic model that captures web distortion. The neglect of distortional effect is known to overestimate the critical moment capacity of the beam. Also, classical solutions assume that the pre-buckling deformation at the point of onset of buckling Fig. 1-10d. are negligible and thus the sagging configuration of the beam in Fig. 1-10d can be approximately represented by the straight configuration depicted in (Fig. 1-10c). The neglect of pre-buckling deformation is known to underestimate the critical moment capacity of the beam. Various studies have examined the destabilizing effects of web distortion on beam buckling capacity. Examples include the work of Bradford (1985), Vrcelj and Bradford (2006a), Chen and Ye (2010) and Wang et al. (1991) who showed distortional effects to be significant in wide flange beams with slender webs. Also, (Bradford (1992); Bradford (1992a)) documented the effect of web distortion on short-span cantilevers and beam with overhangs. Also, a few studies have documented that the pre-buckling deformation is beneficial. This includes the work of Trahair and Woolcock (1973), (Pi and Trahair (1992b); Pi and Trahair (1992c)). However, the study by Trahair and Woolcock (1973) suggests that pre-buckling deformation effects can be detrimental.

However, no theories have been developed to examine the interaction between both distortional and pre-buckling deformation effects. Thus, the present study develops a theory that captures both effects and thus enables examining their combined action on the predicted critical moments. Other aspects of the formulation include the incorporation of load height effect, the P-delta effects induced by strong axis moments and compressive forces in the pre-buckling analysis, and the presence of transverse stiffeners. Such effects are discussed in the following.

1.3.2.2. **Effect of load height**

The influence of load acting offset from the shear centre on the buckling resistance has been extensively investigated under classical solutions (Fig. 1-11a). The author was however unable to find any distortional theories that account for such effects in conjunction with web distortion (Fig. 1-11b). The interaction of load height effect with pre-buckling deformation effect has been investigated in the works of Roberts and Azizian (1983a), Pi and Trahair (1992b), Pi and Trahair (1992c), Mohri and Potier-Ferry (2006) and Erkmen and Attard (2011). In practical applications, loads are frequently offset from the shear centre (Fig. 1-11c). Such effects are thus captured under the present distortional buckling study.

1.3.2.3. **P-delta effect in pre-buckling analysis**

In beam-columns, the presence of compressive axial loads is expected to amplify the strong axis pre-buckling moments and accelerate the LTB of beam-columns. This effect is recognized in interaction equations of structural steel design provisions (e.g. CAN-CSA S16-14 (2014)) where a amplification factor (depending on the magnitude of the compressive axial force) is applied to the peak moments. While some distortional LTB theories account for the combined destabilizing effects of axial forces and strong axis moments (Hancock et al. (1980), Bradford and Trahair (1981), Bradford and Trahair (1982), Bradford (1990b) and Vrcelj and Bradford (2006a)), the author was unable to find any LTB theories that account for interaction of second order moments induced by axial compressive forces and bending moments during the pre-buckling stage. Thus the present study develops a step-wise non-linear pre-buckling procedure followed by eigen-value checks to identify the bifurcation point corresponding to LTB on the non-linear pre-buckling load deformation path.

1.3.2.4. **Shear deformation in pre-buckling analysis**

Since the primary objective of the present theory is to capture distortional effects and given that such effects are prominent in sections with deep and slender webs, it is natural to incorporate shear deformation effects when conducting the pre-buckling analysis. Thus, the present solution develops a shear deformable theory to capture the pre-buckling softening response induced by shear deformation in the web. The shear deformation effect is also observed to contribute in minor way to the stiffening effect due to pre-buckling deformation effects. The interaction of both effects is also captured in a natural way in the present study.

1.3.2.5. **Effect of transverse stiffeners**

Plate girders with slender web and deep section are prone to buckle in a distortional mode. The presence of transverse stiffeners (normally provided to increase the shear capacity of the web) are expected to also reduce distortional effects in the web thus increase the buckling resistance of the girder. The present theory develops a systematic means to model the beneficial effects of stiffener by enforcing appropriate kinematic constraints to suppress distortional effects at the location of stiffeners.

1.3.2.6. **Features of the Sought distortional buckling theory**

In summary, the sought distortional buckling theory will deviate from conventional solutions as it will include:

1- Web Distortional effects
2- Pre-buckling geometric non-linear effects
3- Pre-buckling deformation effects
4- Shear deformation effects
5- Load height effects
6- Modelling the presence of stiffeners

Such a theory will be presented in Chapter 6

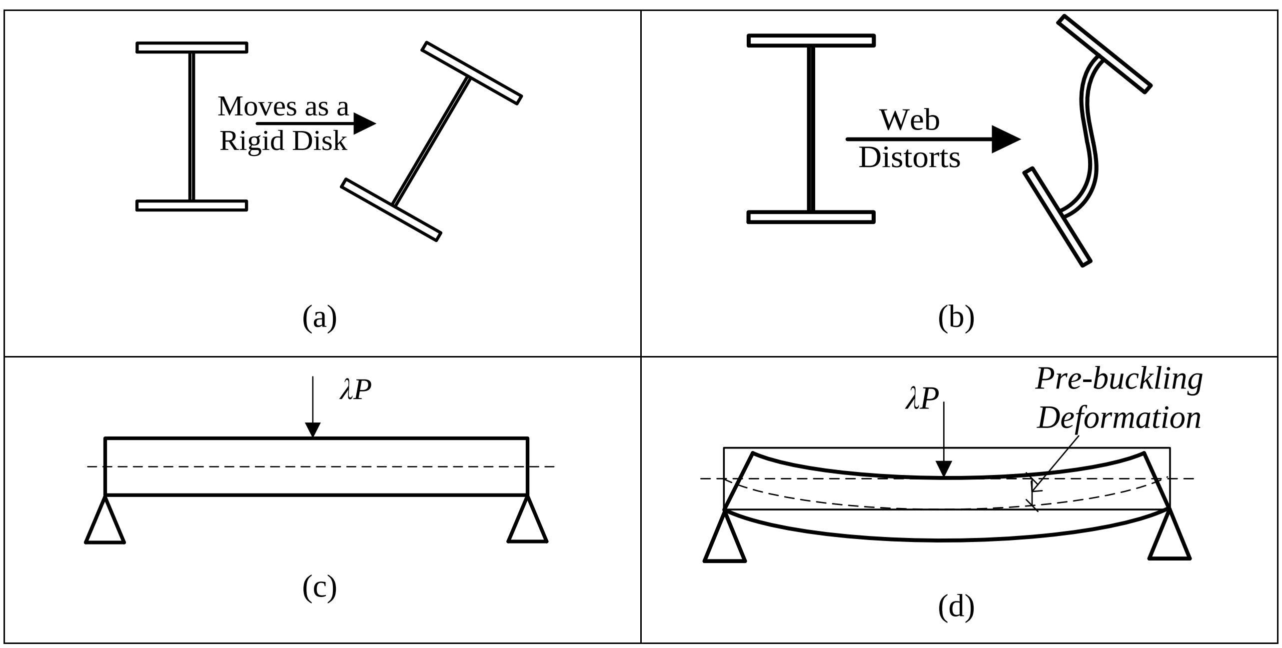

Fig. 1-10 a) cross section kinematics in classical solutions b) cross section kinematics in reality c) beam onset of buckling in classical solutions d)beam onset of buckling in reality

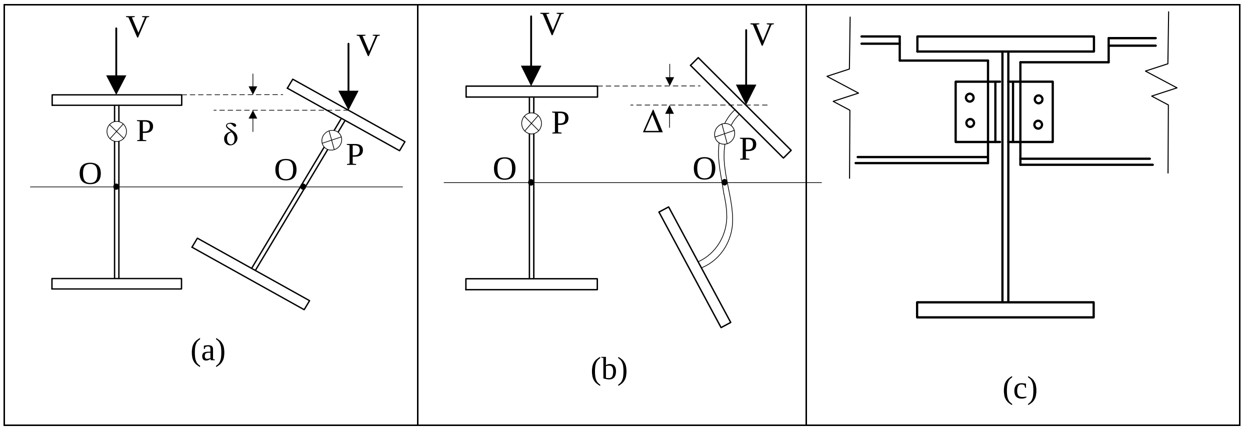

Fig. 1-11 Load offset from the shear centre in a)classical solutions b)distortion solutions c) steel beam-beam connection

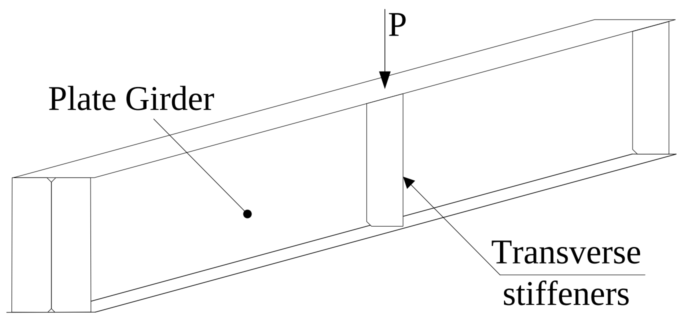

Fig. 1-12 Effect of transverse stiffeners on LTB of the plate girder

1.4. Overview of the thesis

Within the above context, the current thesis intends to avoid the limitations of previous theories by formulating new theories which capture distortional effects for static and buckling analyses. After the present introductory chapter, Chapter 2 provides a review of fundamental concepts key to the developments presented in Chapters 3 through 6. Chapters 3, 4, and 6 are written in a paper format with their own separate literature reviews, while Chapter 5 provides the specifics of the nonlinear analysis adopted in the developments of Chapter 6.

Chapter 3 develops new distortional theory for the static analysis of mono-symmetric wide flange beams under general loads. The governing equilibrium equations and associate boundary conditions (BCs) are derived and a closed form solution is developed for the resulting coupled system of differential equations. Examples are then solved to demonstrate the application of the theory and comparisons are provided against shell FEA solutions to assess the validity of the formulation. The formulation is able address the limitations raised under Sections 1.3.1.1-1.3.1.4. This contribution has been published in (Pezeshky and Mohareb (2014)).

Under certain boundary conditions (e.g., concentrated force at the mid-span, multi-span beams), the closed form solutions such as those developed under Chapter 3 become impractical. Thus, Chapter 4 extends the work of chapter 3 by developing four finite elements. The finite element formulations are able to address the limitations expressed under Section 1.3.1.4. The expressions for the stiffness matrices and energy equivalent nodal force vectors were developed and implemented under MATLAB (2011b). The convergence of the elements is investigated and the application of the formulation is illustrated through numerical examples. This contribution has been published in (Pezeshky and Mohareb (2015)).

Chapter 5 develops a geometrically nonlinear finite element formulation for shear deformable beam elements. An incremental iterative procedure is implemented to solve the nonlinear incremental force-displacement equilibrium equations under general transverse and longitudinal forces. The new formulation provides essential ingredients (e.g., pre-buckling internal forces and displacements P-delta effects, shear deformation effects) to conduct the buckling analysis in Chapter 6.

Chapter 6 develops a distortional finite element formulation for lateral torsional buckling of doubly-symmetric sections incorporating PBD effect that are neglected in classical solutions. The limitations discussed under Sections 1.3.2.1 to 1.3.2.5 are addressed by incorporating a series of features in the formulation (i.e., the load height effect, the geometric nonlinear effects in the pre-buckling stage, presence of transverse stiffeners, etc.) A parametric study is then performed and the influence of span-depth, flange width-flange thickness, depth-web thickness and flange width-depth ratios on distortion and PBD effects are quantified. The beneficial effects of transverse stiffeners on the distortional lateral torsional buckling resistance of plate girders are determined. Recommendations are provided regarding the most effective locations of transverse stiffeners. The formulations developed in Chapters 3-6 were coded in the Matlab environment.

Chapter 7 provides a summary of the theories developed and outlines their various features. A compilation of the conclusions is provided along with recommendations for future research and extensions of the present research.

1.5. References

ANSI/AISC 360-16 (2016). "ANSI/AISC 360-16." *Specification for structural steel buildings*, American Institute of Steel Construction (AISC), Chicago, IL.

Bradford, M. A. (1985). "Distortional buckling of monosymmetric I-beams." *Journal of Constructional Steel Research*, 5(2), 123-136.

Bradford, M. A. (1990b). "Stability of mono-symmetric beam-columns with thin webs." *Journal of Constructional Steel Research*, 15(4), 323-339.

Bradford, M. A. (1992). "Buckling of doubly-symmetric cantilevers with slender webs." *Engineering Structures*, 14(5), 327-334.

Bradford, M. A. (1992a). "Buckling of doubly-symmetric cantilevers with slender webs." *Engineering Structures*, 14(5), 327-334.

Bradford, M. A., and Trahair, N. S. (1981). "Distortional Buckling of I-Beams." *Journal of the Structural Division, ASCE*, 107(2), 355-370.

Bradford, M. A., and Trahair, N. S. (1982). "Distortional buckling of thin-web beam-columns." *Engineering Structures*, 4(1), 2-10.

British Standards Institution (BSI) (2000). "BS5950-1 Structural Use of Steelwork in Buildings – Part1." *Code of Practice for Design Rolled and Welded Sections*England.

CAN-CSA S16-14 (2014). "Handbook of Steel Construction." *CSA-S16-14 Specification*, Canadian Institute of Steel Construction, CA.

Chen, W. E. I., and Ye, J. (2010). "ELASTIC LATERAL AND RESTRAINED DISTORTIONAL BUCKLING OF DOUBLY SYMMETRIC I-BEAMS." *International Journal of Structural Stability and Dynamics*, 10(05), 983-1016.

EN-1993-1-1-05 (2005). "Eurocode 3: Design of Steel Structures-General Rules and Rules for Buildings." European Committee of Standardization (CEN), Brussels, Belgium.

Erkmen, R. E., and Attard, M. M. (2011). "Lateral–torsional buckling analysis of thin-walled beams including shear and pre-buckling deformation effects." *International Journal of Mechanical Sciences*, 53(10), 918-925.

Gjelsvik, A. (1981). *The theory of thin walled bars / Atle Gjelsvik*, Wiley, New York, NY, USA.

Hancock, G. J., Bradford, M. A., and Trahair, N. S. (1980). "Web distortion and flexural-torsional buckling." *Journal of the Structural Division, ASCE*, 106(7), 1557-1571.

Jönsson, J., and Andreassen, M. J. (2011). "Distortional eigenmodes and homogeneous solutions for semi-discretized thin-walled beams." *Thin-Walled Structures*, 49(6), 691-707.

MATLAB. 2011b. version 7.13.0.564The MathWorks.

Mohri, F., and Potier-Ferry, M. (2006). "EFFECTS OF LOAD HEIGHT APPLICATION AND PRE-BUCKLING DEFLECTIONS ON LATERAL BUCKLING OF THIN-WALLED BEAMS." *Journal of steel and composite structures*, 6(5), 401-415.

Pezeshky, P., and Mohareb, M. (2014). "Distortional theory for the analysis of wide flange steel beams." *Engineering Structures*, 75, 181-196.

Pezeshky, P., and Mohareb, M. (2015). "Finite-Element Formulations for the Distortional Analysis of Wide Flange Steel Beams." *Journal of Engineering Mechanics*, 04015071.

Pi, Y., and Trahair, N. (1992b). "Prebuckling Deflections and Lateral Buckling. I: Theory." *Journal of Structural Engineering*, 118(11), 2949-2966.

Pi, Y., and Trahair, N. (1992c). "Prebuckling Deflections and Lateral Buckling. II: Applications." *Journal of Structural Engineering*, 118(11), 2967-2985.

Roberts, T., and Azizian, Z. (1983a). "Instability of Thin Walled Bars." *Journal of Engineering Mechanics*, 109(3), 781-794.

Schardt, R. (1994). "Generalized beam theory—an adequate method for coupled stability problems." *Thin-Walled Structures*, 19(2–4), 161-180.

Silvestre, N., and Camotim, D. (2002). "First-order generalised beam theory for arbitrary orthotropic materials." *Thin-Walled Structures*, 40(9), 755-789.

Standards Association of Australia (1998). "AS 4100 steel structures."Sydney, Australia.

Trahair, N. S., and Woolcock, S. T. (1973). "Effect of Major Axis Curvature on I-Beam Stability." *Journal of Engineering Mechanics*, 99(1), 85-98.

Vlasov, V. Z. (1961). *Thin walled elastic beams*, Israel Program for Scientific Translations, Jerusalem, Israel. Available from Office of Technical Services, US Department of Commerce,Washington, D.C.

Vrcelj, Z., and Bradford, M. A. (2006a). "Elastic distortional buckling of continuously restrained I-section beam–columns." *Journal of Constructional Steel Research*, 62(3), 223-230.

Wang, C. M., Chin, C. K., and Kitipornchai, S. (1991). "Parametric study on distortional buckling of monosymmetric beam-columns." *Journal of Constructional Steel Research*, 18(2), 89-110.

Chapter 2

Literature review

2.1. General

This chapter reviews previous works related to the development of distortional theories in the current study. The principles of variational calculus are a cornerstone of the developments in the present work and are thus reviewed in Section 2.2. The developments are based on the principle of stationary total potential energy. The principle is covered in Section 2.3 and the related key concepts such as the stationarity condition, and the various types of stability conditions (stable, neutral and unstable) are presented. Section 2.3 provides the basis of the static distortional theory developed in Chapter 3, the finite element formulation in Chapter 4, the nonlinear pre-buckling analysis in Chapter 5 and the theory developed in Chapter 6.

The understanding of kinematics of existing beam theories and their limitations is important in developing the sought distortional theories are thus discussed under Section 2.4. This includes the Euler-Bernoulli theory, the shear deformable Timoshenko theory, the Vlasov theory and the Gjelsvik theory. A key aspect in developing the buckling theory in Chapter 6 is the incorporation of large deformation and moderate rotations. The influence of moderate rotation in the Vlasov theory is thus covered under Section 2.3.4. The development of the nonlinear pre-buckling formulation developed under chapter 5 entails an understanding of geometric non-linear analysis procedures and are thus covered under Section 2.5.

Another aspect relevant to the theories sought is the review of past distortional beam theories. In this regard, comprehensive reviews related to distortional theories will thus be provided in Section 3.2 with emphasis on studies with closed-form solutions, while Section 4.2 provides a survey of distortional theories with emphasis on approximate energy solutions and finite element formulations. A final aspect of the theory presented in Chapter 6 is the survey of past buckling theories that captured pre-buckling deformation effects. This aspect is covered under Section 6.3.

2.2. Fundamentals of calculus of variation and Variational principles

Variational principles are powerful tools in applied mechanics commonly used to derive the governing differential equations (DEs) characterizing the behaviour of a structure. A closed-form solution for the system of DEs is sought whenever possible. However, when such solutions are unattainable, the analyst may resort to numeric solutions such as finite element solution. Variational principles also provide a practical means to formulate such solutions.

In this case, finite element solution is used to approximate the solution of the complex system of governing DEs through a discrete system of algebraic equations. A functional π of a set of argument unknown functions $y_i = y_i(z)$, $(i=1,2,..k)$ is defined as

$$\pi = \int_a^b F\left(z, y_1, y_2, ..y_i, y_1', y_2', ..y_i', y_1^n, y_2^n, .., y_i^n\right)dz \qquad (i=1,2,..k) \tag{2.1}$$

where z is an independent functions and $y_i' = dy_i/dz$, $y_i'' = d^2 y_i/dz^2$, .., $y_i^n = d^n y_i/dz^n$ are the first, second and n[th] derivatives of unknown function y_i respectively. The variation $\Delta\pi$ of functional π due to a set of arbitrary functions δy_i is given by (e.g.,Lanczos (1893))

$$\begin{aligned}
&\Delta\pi\left(z, y_1, ..y_i, y_1', ..y_i', y_1^n, .., y_i^n\right) = \\
&\pi\left(y_1 + \delta y_1, ..y_i + \delta y_i, y_1' + \delta y_1', ..y_i' + \delta y_i', y_1^n + \delta y_1^n, .., y_i^n + \delta y_i^n\right) - \pi\left(z, y_1, ..y_i, y_1', ..y_i', y_1^n, .., y_i^n\right) \quad (2.2) \\
&= \delta\pi + \delta^2\pi + \delta\pi^3 + ..
\end{aligned}$$

where

$$\begin{aligned}
&\delta\pi = \sum_{p=0}^{n}\sum_{i=1}^{k}\left(\frac{\partial\pi}{\partial y_i^p}\right)\delta y_i^p \\
&\delta^2\pi = \frac{1}{2!}\sum_{p=0}^{n}\sum_{q=0}^{n}\sum_{i=1}^{k}\sum_{j=1}^{k}\left(\frac{\partial^2\pi}{\partial y_i^p \partial y_j^q}\right)\left(\delta y_i^p\right)\left(\delta y_j^q\right) \qquad (2.3)\text{a-c} \\
&\delta^3\pi = \frac{1}{3!}\sum_{p=0}^{n}\sum_{q=0}^{n}\sum_{r=0}^{n}\sum_{i=1}^{k}\sum_{j=1}^{k}\sum_{l=1}^{k}\left(\frac{\partial^3\pi}{\partial y_i^p \partial y_j^q \partial y_l^r}\right)\left(\delta y_i^p\right)\left(\delta y_j^q\right)\left(\delta y_l^r\right)
\end{aligned}$$

From Eq. (2.3)a, the first variation of the functional π (e.g., Wu (2010), Washizu (1982)) is given by

$$\delta\pi = \int_a^b\left(\frac{\partial F}{\partial y_i}\delta y_i + \frac{\partial F}{\partial y_i'}\delta y_i' + \frac{\partial F}{\partial y_i''}\delta y_i'' + .. + \frac{\partial F}{\partial y_i^n}\delta y_i^n\right)dz = 0 \qquad (i=1,2,..k) \tag{2.4}$$

Integrating Eq. (2.4) by parts and grouping like-terms, one obtains

$$\delta\pi = \int_a^b \left\{ \left[\frac{\partial F}{\partial y_1} - \frac{d}{dz}\left(\frac{\partial F}{\partial y_1'}\right) + \frac{d^2}{dz^2}\left(\frac{\partial F}{\partial y_1''}\right) - .. + \left(-1^n\right)\frac{d^n}{dz^n}\frac{\partial F}{\partial y_1^n} \right]\delta y_1 \right.$$
$$+ \left[\frac{\partial F}{\partial y_2} - \frac{d}{dz}\left(\frac{\partial F}{\partial y_2'}\right) + \frac{d^2}{dz^2}\left(\frac{\partial F}{\partial y_2''}\right) - .. + \left(-1^n\right)\frac{d^n}{dz^n}\frac{\partial F}{\partial y_2^n} \right]\delta y_2$$
$$+..$$
$$\left. + \left[\frac{\partial F}{\partial y_i} - \frac{d}{dz}\left(\frac{\partial F}{\partial y_i'}\right) + \frac{d^2}{dz^2}\left(\frac{\partial F}{\partial y_i''}\right) - .. + \left(-1^n\right)\frac{d^n}{dz^n}\frac{\partial F}{\partial y_i^n} \right]\delta y_i \right\} dz \qquad \left(i = 1, 2, ..k\right)$$
$$+ \left\langle \left\{ \left(\frac{\partial F}{\partial y_1'}\right)\delta y_1 + \left[\left(\frac{\partial F}{\partial y_1''}\right)\partial y_1' - \frac{d}{dz}\left(\frac{\partial F}{\partial y_1''}\right)\partial y_1 \right] + .. + \sum_{m=0}^{n-1}\left[\left(-1^m\right)\frac{d^m}{dz^m}\frac{\partial F}{\partial y_1^n}\delta y_1^{(n-m-1)} \right] \right\} \right.$$
$$+ \left\{ \left(\frac{\partial F}{\partial y_2'}\right)\delta y_2 + \left[\left(\frac{\partial F}{\partial y_2''}\right)\partial y_2' - \frac{d}{dz}\left(\frac{\partial F}{\partial y_2''}\right)\partial y_2 \right] + .. + \sum_{m=0}^{n-1}\left[\left(-1^m\right)\frac{d^m}{dz^m}\frac{\partial F}{\partial y_2^n}\delta y_2^{(n-m-1)} \right] \right\}$$
$$+..$$
$$\left. + \left\{ \left(\frac{\partial F}{\partial y_i'}\right)\delta y_i + \left[\left(\frac{\partial F}{\partial y_i''}\right)\partial y_i' - \frac{d}{dz}\left(\frac{\partial F}{\partial y_i''}\right)\partial y_i \right] + .. + \sum_{m=0}^{n-1}\left[\left(-1^m\right)\frac{d^m}{dz^m}\frac{\partial F}{\partial y_i^n}\delta y_i^{(n-m-1)} \right] \right\} \right\rangle \Bigg|_a^b = 0 \quad (2.5)$$

where the integral terms

$$\left.\begin{aligned}
&\left[\frac{\partial F}{\partial y_1} - \frac{d}{dz}\left(\frac{\partial F}{\partial y_1'}\right) + \frac{d^2}{dz^2}\left(\frac{\partial F}{\partial y_1''}\right) - .. + \left(-1^n\right)\frac{d^n}{dz^n}\frac{\partial F}{\partial y_1^n} \right] = 0 \\
&\left[\frac{\partial F}{\partial y_2} - \frac{d}{dz}\left(\frac{\partial F}{\partial y_2'}\right) + \frac{d^2}{dz^2}\left(\frac{\partial F}{\partial y_2''}\right) - .. + \left(-1^n\right)\frac{d^n}{dz^n}\frac{\partial F}{\partial y_2^n} \right] = 0 \\
&.. \\
&\left[\frac{\partial F}{\partial y_i} - \frac{d}{dz}\left(\frac{\partial F}{\partial y_i'}\right) + \frac{d^2}{dz^2}\left(\frac{\partial F}{\partial y_i''}\right) - .. + \left(-1^n\right)\frac{d^n}{dz^n}\frac{\partial F}{\partial y_i^n} \right] = 0
\end{aligned}\right\} \qquad \left(i = 1, 2, .., k\right) \qquad (2.6)$$

lead to the field equations and the boundary terms lead to the possible boundary conditions at the boundaries $z = a$ and $z = b$, i.e.

$$
\begin{aligned}
&At\ z=a:\ \left(i=1,2,..,\mathrm{k}\right)\\
&\qquad\left\{y_i=y_{ia-1}\ \text{or}\left[\frac{\partial F}{\partial y_1'}-\frac{d}{dz}\left(\frac{\partial F}{\partial y_1''}\right)+..\right]=\mathrm{f}_{ia-1}\right\},\left\{y_i'=y_{ia-2}\ \text{or}\left[\left(\frac{\partial F}{\partial y_1''}\right)+..\right]=\mathrm{f}_{ia-2}\right\},..\\
&\qquad,\left\{y_i^{n-1}\left(a\right)=y_{ia-n}\ \text{or}\ \frac{\partial F}{\partial y_i^n}=\mathrm{f}_{ia-n}\right\}\\
&At\ z=b:\ \left(i=1,2,..,\mathrm{k}\right)\\
&\qquad\left\{y_i=y_{ib-1}\ \text{or}\left[\frac{\partial F}{\partial y_1'}-\frac{d}{dz}\left(\frac{\partial F}{\partial y_1''}\right)+..\right]=\mathrm{f}_{ib-1}\right\},\left\{y_i'=y_{ib-2}\ \text{or}\left[\left(\frac{\partial F}{\partial y_1''}\right)+..\right]=\mathrm{f}_{ib-2}\right\},..\\
&\qquad,\left\{y_i^{n-1}\left(a\right)=y_{ib-n}\ \text{or}\ \frac{\partial F}{\partial y_i^n}=\mathrm{f}_{ib-n}\right\}
\end{aligned}
\tag{2.7)a-b}
$$

The second variation of the functional π as defined in Eq. (2.3)b can be expressed as

$$
\begin{aligned}
\delta^2\pi=\frac{1}{2}\int_a^b\Bigg\{&\sum_{i=1}^{k}\sum_{j=1}^{k}\left[\frac{\partial^2 F}{\partial y_i\partial y_j}\left(\partial y_i\partial y_j\right)+\frac{\partial^2 F}{\partial y_i\partial y_j'}\left(\partial y_i\partial y_j'\right)+\frac{\partial^2 F}{\partial y_i\partial y_j''}\left(\partial y_i\partial y_j''\right)+..+\frac{\partial^2 F}{\partial y_i\partial y_j^n}\left(\partial y_i\partial y_j^n\right)\right]\\
&+\sum_{i=1}^{k}\sum_{j=1}^{k}\left[\frac{\partial^2 F}{\partial y_i'\partial y_j}\left(\partial y_i'\partial y_j\right)+\frac{\partial^2 F}{\partial y_i'\partial y_j'}\left(\partial y_i'\partial y_j'\right)+\frac{\partial^2 F}{\partial y_i'\partial y_j''}\left(\partial y_i'\partial y_j''\right)+..+\frac{\partial^2 F}{\partial y_i'\partial y_j^n}\left(\partial y_i'\partial y_j^n\right)\right]\\
&+\sum_{i=1}^{k}\sum_{j=1}^{k}\left[\frac{\partial^2 F}{\partial y_i''\partial y_j}\left(\partial y_i''\partial y_j\right)+\frac{\partial^2 F}{\partial y_i''\partial y_j'}\left(\partial y_i''\partial y_j'\right)+\frac{\partial^2 F}{\partial y_i''\partial y_j''}\left(\partial y_i''\partial y_j''\right)+..+\frac{\partial^2 F}{\partial y_i''\partial y_j^n}\left(\partial y_i''\partial y_j^n\right)\right]\\
&+..\\
&+\sum_{i=1}^{k}\sum_{j=1}^{k}\left[\frac{\partial^2 F}{\partial y_i^n\partial y_j}\left(\partial y_i^n\partial y_j\right)+\frac{\partial^2 F}{\partial y_i^n\partial y_j'}\left(\partial y_i^n\partial y_j'\right)+\frac{\partial^2 F}{\partial y_i^n\partial y_j''}\left(\partial y_i^n\partial y_j''\right)+..+\frac{\partial^2 F}{\partial y_i^n\partial y_j^n}\left(\partial y_i^n\partial y_j^n\right)\right]\Bigg\}dz
\end{aligned}
\tag{2.8}
$$

2.3. Principle of stationary total potential energy

The total potential energy functional of a structure Π is the summation of the internal strain energy U stored in the beam and the load potential gain V by the external loads, i.e.

$$\Pi=U+V \tag{2.9}$$

For a structure with multiple degree of freedoms $q_i,\ i=1..n$, the stationarity condition of the total potential energy (e.g., Chajes (1974))

$$\delta\Pi\left(q_1,q_2,..,q_n\right)=\delta\left[U\left(q_1,q_2,..,q_n\right)+V\left(q_1,q_2,..,q_n\right)\right]=0 \tag{2.10}$$

provides the equilibrium condition of the structure. The equilibrium thus obtained can be either stable, neutral, or unstable (e.g., Trahair (1993)). A schematic description of the stability conditions for a single degree of freedom system is provided in Fig. 2-1a-c where position '1' in all cases is an equilibrium position corresponding to the condition $\delta\Pi(q)=0$. The three cases considered are fundamentally different in terms of stability. In Fig. 2-1a, if the ball is arbitrarily disturbed from its original position by a displacement δq , it tends to come back to its original equilibrium position. In such a case the system is considered stable as it satisfies the condition $\delta^2\Pi=\delta^2(U+V)=(1/2)\left(d^2\Pi/dq^2\right)\delta q^2>0$, $\forall\delta q$. Conversely, if for any δq, the ball in (Fig. 2-1c) tends to move away from the equilibrium position, such a system is deemed unstable and the condition $\delta^2\Pi=\delta^2(U+V)=(1/2)\left(d^2\Pi/dq^2\right)\delta q^2<0$ is satisfied. If the functional $\Pi(q)$ is a quadratic functional of q , $\delta\pi^3,\delta\pi^4,\ldots$ vanish. For the case of a ball on a flat surface illustrated in (Fig. 2-1b) lies at the border of stability and instability and meets the condition $\delta^2\Pi=\delta^2(U+V)=(1/2)\left(d^2\Pi/dq^2\right)\delta q^2=0$. Such an equilibrium is termed as neutrally stable. Buckling phenomena are typically associated with the positions of neutral equilibrium. For a multiple degree of freedom system, in addition to satisfying the equilibrium condition $\delta\Pi=0$, the variation with respect to the buckling displacements of second variation of total potential energy has to vanish to locate the position of neutral stability, i.e.,

$$\delta^2\Pi(q_1,q_2..,q_k)=\delta^2\left[U(q_1,q_2..,q_k)+V(q_1,q_2..,q_k)\right]=\frac{1}{2}\sum_{i=1}^{k}\sum_{j=1}^{k}\left(\frac{d^2\Pi}{dq_i dq_j}\right)\delta q_i\delta q_j=0 \qquad (2.11)$$

The stationarity condition in Eq. (2.10) denotes equilibrium and will be applied in chapter 3 to formulate the equilibrium equations of the system and associated boundary conditions. The condition will also be used in chapter 4 to enforce equilibrium in a weak sense by formulating finite element solutions. The equilibrium condition in Eq. (2.10) will also be adopted in Chapter 5 to characterize the pre-buckling equilibrium path while the neutral stability condition (2.11) will be adopted in Chapter 6 to locate the point on the equilibrium path where the equilibrium ceases to be stable and becomes unstable (i.e., the buckling point).

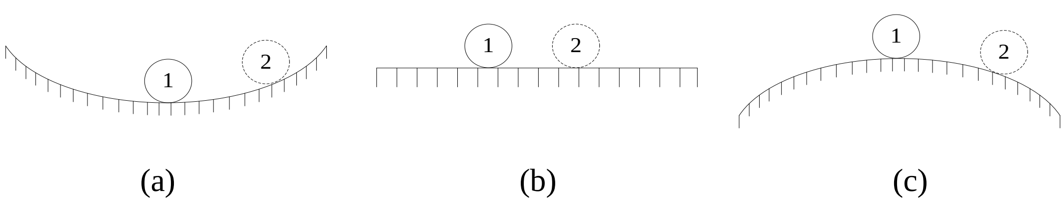

Fig. 2-1 Equilibrium position a)stable b)neutral c)unstable

2.4. **Kinematics of beam theories**

This section reviews a number of beam theories with emphasis on the kinematic assumptions and resulting displacement fields. A right-handed coordinate system (x,y,z) is defined (Fig. 2-2) and the corresponding lateral, transverse and longitudinal displacement fields are (u,v,w). Strictly speaking, each of the displacement fields depends on all three coordinates, i. e, $w=w(x,y,z)$, etc. which leads to complex models necessitating discretization in three dimensions. When one of the dimensions is significantly larger than the other two dimensions (as is the case for the longitudinal dimension z), kinematic assumptions can be postulated to transform the 3D problem into a 1D problem. Under such assumptions it is possible to reduce the dependence of the displacement fields on a single coordinate, i.e., $w=w(z)$, etc., leading to considerable simplifications in the solution. The following sections discuss the main kinematic assumptions and resulting displacement fields for the Euler-Bernoulli, Timoshenko, Higher order beams, Vlasov, and Gjelsvik beams given their relevance to the analysis of steel beams.

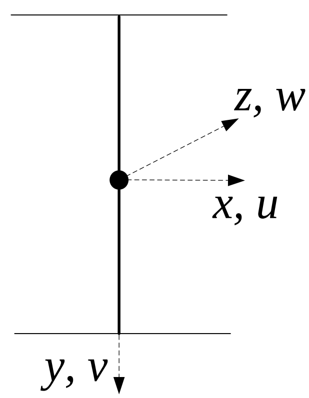

Fig. 2-2 Right handed coordinate system

2.4.1. **Euler-Bernoulli beam theory**

The Euler-Bernoulli beam theory is the simplest flexural beam theory for thin-walled members. The theory adopts the simplifying assumption that a cross-section originally normal to the beam centroidal axis remains planar and normal to the centroidal axis after deformation (Fig. 2-3a). This assumption signifies that the angle of rotation of the section is equal to the slope of the centroidal axis ($\theta_x(z)=-dv(z)/dz$) and the corresponding longitudinal displacement takes the form

$$\begin{aligned} w(y,z) &= w_0(z) - yv'(z) \\ v(y,z) &= v(z) \end{aligned} \tag{2.12}$$

where $w_0(z)$ is the longitudinal displacement of the beam at the centroid and $v(z)$ is the transverse displacement. The kinematic assumption of the Euler beam enables the expression of the equilibrium conditions for the beam in a simplified and approximate form in terms of displacement functions $w_0(z)$ and $v(z)$ in terms of simple ordinary differential equations rather than partial differential equations as is the case in the theory of elasticity. One of the limitations of the Euler-Bernoulli beam is that the normality condition between the section and the beam centroidal axis implies the neglect of shear deformation.

2.4.2. **Timoshenko beam theory**

Several approaches were developed to incorporate the effect of shear deformation and thus remedy the limitation of the Euler-Bernoulli beam. These include the Timoshenko (1921) (e.g., Timoshenko (1921), Friedman and Kosmatka (1993), Eisenberger (1994) which postulate that the cross section remains planar but non-normal to the beam axis. Hence, the angle of rotation of the cross-section θ_x differs from the slope i.e., $\theta_x \neq -dv/dz$. Under the Timoshenko beam assumption (Fig. 2-3b), the difference between both angles represents the shear strain which happens to be constant for a given section. Based on the kinematic assumption of the Timoshenko beam, the displacements fields are expressed as

$$\begin{aligned} w(y,z) &= w_0(z) + y\theta_x(z) \\ v(y,z) &= v(z) \end{aligned} \tag{2.13}$$

The above displacement fields lead to the three equilibrium conditions in terms of longitudinal and transverse displacements $w_0(z), v(z)$ and angle of rotation $\theta_x(z)$. Again the differential equations are ordinary. The fact that the shear deformation of the Timoshenko beam is independent of coordinate y implies that it does not vanish at the top and bottom surface of the beam and hence the corresponding shear stress is non-zero, which violates the traction boundary conditions at the top and bottom surfaces of the beam (which typically happen to vanish). Attempts to remedy the problem involve developing higher order beam theory as will be discussed under Section 2.4.3. Other lines of developments to account for the nonlinear distribution of shear stresses with coordinate y involve the development of shear factors (e.g., Cowper (1966), Reddy (1997)). Such treatment is non-universal and different theories predict different shear correction factors for the same cross-section.

2.4.3. **Higher order beam theories**

Higher order beam theories (e.g., Levinson (1980), Levinson (1981), Bickford (1982), Reddy (1984a), Reddy (1984b), and Heyliger and Reddy (1988)) relax the Euler-Bernoulli normality assumption of the section to the centroidal axis. In order to satisfy the traction boundary conditions at the top and bottom faces of the beam, a cubic distribution of the longitudinal displacement is postulated, i.e.,

$$w(y,z) = w_0(z) + y\theta_x(z) + y^3\psi(z)$$
$$v(y,z) = v(z)$$

where $\theta_x(z)$ and $\psi(z)$ define the non-linear nature of the deformed cross sectional line. One of the limitations of such developments is that they are limited to rectangular cross sections.

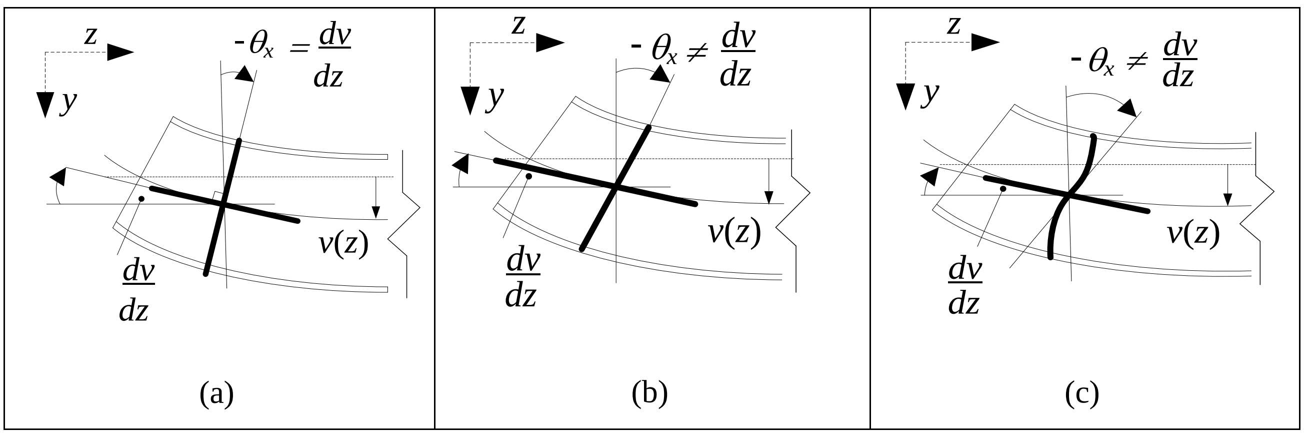

Fig. 2-3 a) Euler-Bernoulli beam b) Timoshenko beam c) Higher order beam (e.g., Bickford (1982), Reddy (1984b))

In the current work, shear deformation effects are captured in static the analyses (Chapters 3-4) and in non-linear geometric analysis (Chapter 5) in a manner similar to the Timoshenko beam solution. Unlike the conventional Timoshenko beam solution which is limited to linear analysis, a geometrically nonlinear analysis is developed in Chapter 5.

2.4.4. **Vlasov thin-walled beam theory**

When thin-walled members are twisted, they have a tendency to undergo longitudinal displacements whereby a plane section undergoes non-uniform longitudinal displacements (warping). When such longitudinal displacements are restrained, normal stresses σ_ω take place along with shear stresses τ_ω.

Vlasov (1961) developed a general theory for open thin-walled members subjected to combined effect of torsion and flexure. The theory is based on two kinematic assumptions

1- The cross section of the thin-walled member moves as a rigid disk in its own plane

2- The shear strain at the middle surface of the beam vanishes.

For a doubly symmetric wide flange section (Fig. 2-4a) where the centroid and shear centre of the cross section coincides at point O, the Vlasov assumptions allow the expression of the displacement fields $u(x,y,z), v(x,y,z), w(x,y,z)$ of any point (such as C on Fig. 2-4b) on the middle surface of the thin-walled beams in terms of the shear centre displacements $u_0(z)$, $v_0(z)$ and the angle of twist of the cross-section $\theta_z(z)$

Under the small rotation assumptions, the displacement fields are expressed as

$$\begin{aligned} u(x,y,z) &= u_0(z) - y\theta_z(z) \\ v(x,y,z) &= v_0(z) + x\theta_z(z) \\ w(x,y,z) &= w_0(z) - xu'(z) - yv'(z) - \bar{\omega}(x,y)\theta_z'(z) \end{aligned} \qquad (2.14)\text{a-c}$$

where $\bar{\omega}(x,y)$ is global warping function. For a doubly symmetric function the warping function takes the form

$$\bar{\omega}(x,y) = xy \qquad (2.15)$$

In the last of Eq. (2.14), the first three terms characterize the longitudinal displacement due to beam elongation, and biaxial bending while the last term characterizes the global warping deformation induced by twist. The warping deformation is depicted in (Fig. 2-5b) where the right top corner and bottom left corners move along the negative direction of the z-axis and the remaining two corners of the cross section move along the positive direction of the z-axis. The warping function gives rise to the warping constant of the section defined as $C_w = \int_A \bar{\omega}^2 dA$ where A is the cross-sectional area.

While the Vlasov theory captures the warping effects, it neglects any distortions that may take place in the section. Specifically, the Vlasov first assumption postulating the section to move as a rigid disc implies that any point (x,y) of given cross-section z undergoes the same angle of twist $\theta(z)$. For cross-sections with slender webs, such an assumption may yield inaccurate results as the web would likely bend in its own plane rather than move as a rigid body, the angle of twist of the top flange may differ from that of the bottom flange.

While the displacement fields in Eqs. (2.14) are valid under small deformations and rotations, they are inaccurate in stability problems, where the small rotation assumption no longer holds true. More accurate displacement fields expressions that account for moderate rotations have been developed in Pi and Trahair (1992b) take the following form

$$
\begin{aligned}
u(x,\mathrm{y},z) &= u - y\theta + \left\{-\frac{1}{2}x\left(u'^2+\theta^2+u'v'\theta\right)-\frac{1}{2}y\left(u'v'+u'^2\theta\right)-xyu'\left[\theta'+\frac{1}{2}\left(u''v'-u'v''\right)\right]\right\}\\
v(x,\mathrm{y},z) &= v + x\theta + \left\{-\frac{1}{2}x\left(u'v'+v'^2\theta\right)-\frac{1}{2}y\left(v'^2+\theta^2-u'v'\theta\right)-xyv'\left[\theta'+\frac{1}{2}\left(u''v'-u'v''\right)\right]\right\}\\
w(x,y,z) &= w - xu' - yv' - xy\theta' + \left\langle -x\left(v'\theta-\frac{1}{2}u'\theta^2\right)+y\left(u'\theta+\frac{1}{2}v'\theta^2\right)\right.\\
&\qquad \left. -\frac{1}{2}xy\left\{u'v''-u''v'-\left[\theta'+\frac{1}{2}\left(u''v'-u'v''\right)\right]\left(v'^2+u'^2\right)\right\}\right\rangle
\end{aligned}
\tag{2.16}
$$

The additional finite rotation terms also contribute to pre-buckling deformation effects. The distortional buckling theory developed in Chapter 6 modify Eq. (2.16) to account for web distortion.

2.4.5. **Gjelsvik thin-walled beam theory**

When the section is thin-walled, the Vlasov theory tends to characterize, reasonably well, the global warping deformations of the middle surface (Fig. 2-5b). However, as the thickness of the elements constituting the cross-section (flanges, webs, etc) become thicker, additional local warping take place where the extreme fibres of the element tend to warp relative to middle surface (Fig. 2-5c). The top right and bottom left corners of the top flange move out of the plane while the other corners of the flange move in the direction of z-axis. Similar local warping behaviour is observed for the other flange and the web.

Such local warping effects are captured within the Gjelsvik theory (Gjelsvik (1981). The theory adopts the two Vlasov assumptions. In addition, the Kirchhoff plate bending assumption is also postulated whereby a line normal to the middle-surface is assumed to remain normal to the middle-surface. The Kirchoff assumption captures the local warping effect in a natural way. A set of local coordinates (s,n) are defined to characterize the coordinates of a point offset from the middle surface by a distance n and s is a coordinate tangential to the middle surface (e.g., for a doubly symmetric wide flange section, $s=x$ for the flanges and $s=y$ for the web). The additional longitudinal displacement w_L of point B (Fig. 2-4b) relative to point C offset by a distance n from the middle surface is

$$w_L = -n\frac{\partial v}{\partial z} \tag{2.17}$$

From Eq. (2.14) by substituting into Eq. (2.17), one obtains the total longitudinal displacement of the flange, i.e.

$$w(x,y,z) = w_0(z) - xu'(z) - (y+n)v'(z) - \left[\bar{\omega}(x,y) + \bar{\bar{\omega}}(x,n)\right]\theta'(z) \tag{2.18}$$

where $\bar{\bar{\omega}}(x,n) = xn$ is local warping function for the flange. A similar equation can be derived for the longitudinal displacement of the web. In Eq. (2.18) the local and global warping functions can be summed to yield the total warping function, i.e.,

$$\omega = \bar{\omega} + \bar{\bar{\omega}} \tag{2.19}$$

The additional local warping effect contributes to the normal strains and stresses and increases the warping constant of the section defined as $C_w = \int_A \omega^2 dA$ under the Gjelsvik theory and gives rise to the transverse shear strains and stresses away from the middle surface. The transverse shear stresses give rise to the Saint-Venant torsional constant for thin-walled sections in a natural way. The local warping effect has been incorporated into the distortional static theories developed in Chapters 3-4 and the distortional buckling theory developed in Chapter 6.

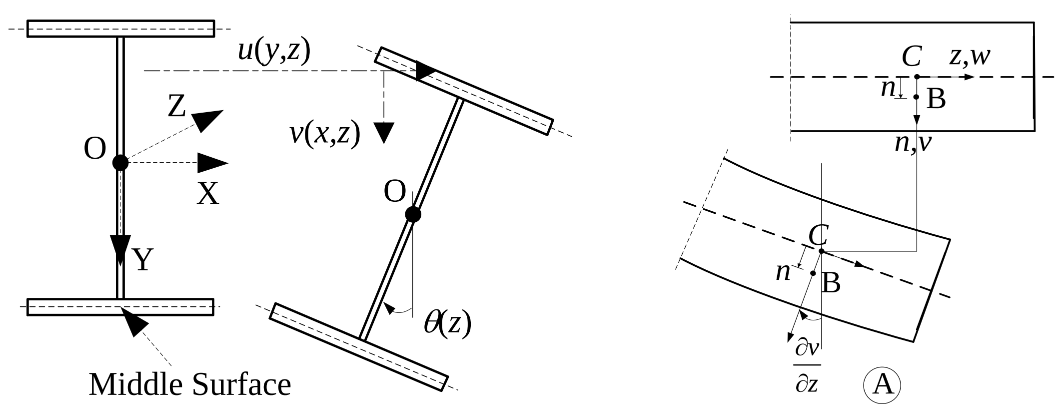

(a) **(b)**

Fig. 2-4 a) Kinematics of the Vlasov and Gjelsvic theories and b) Additional kinematic considerations in the Gjelsvic theory

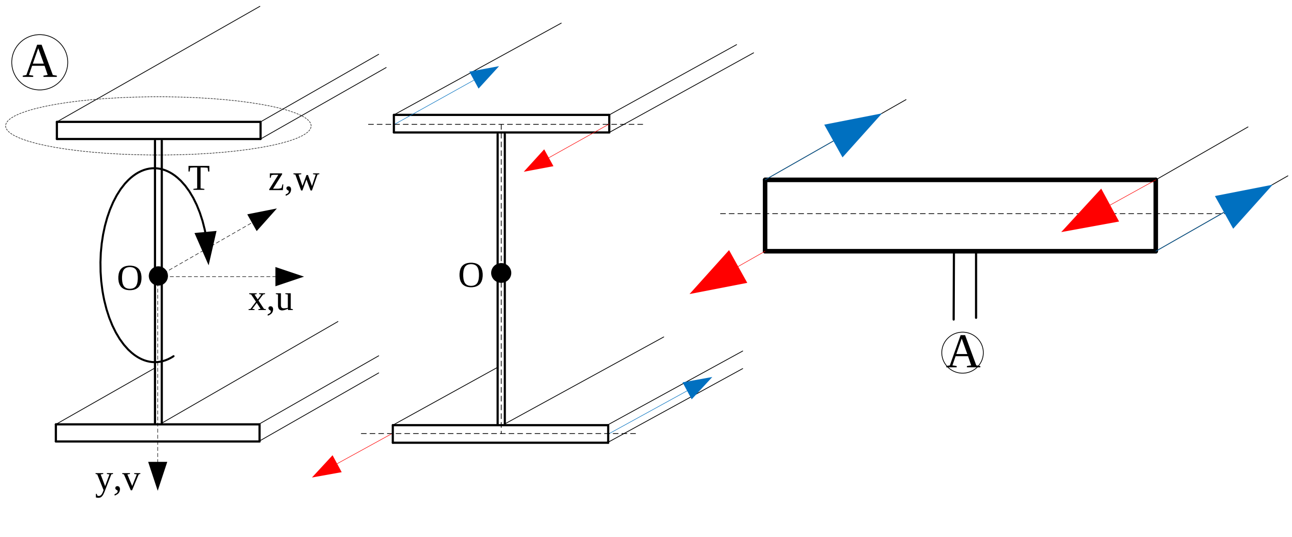

(a) **(b)** **(c)**

Fig. 2-5 a) Wide flange beam under twist T, b) global warping response of the middle surface, and c) additional local warping response of the flange

2.5. Geometrically nonlinear pre-buckling analysis

2.5.1. Background

Geometric nonlinear solution techniques have been investigated by many authors including Rajasekaran and Murray (1973) who investigated various solutions based on Taylor's series expansions (i.e., relaxation factors, pseudo load, initial value and alpha-constant techniques, etc) and adopted the incremental Newton-Raphson and modified Newton-Raphson iterative techniques. Bathe and Bolourchi (1979) developed two three dimensional nonlinear beam elements accounting for large rotations. In their study, the incremental updated Lagrangian and total Lagrangian formulation are employed where both techniques were shown to lead to identical stiffness matrices and nodal load vector. Chan and Kitipornchai (1987) investigated the nonlinear analysis of asymmetric thin-walled members. Their kinematics are based on the Vlasov theory while accounting for second order strains. The updated Lagrangian formulation was employed and arc-length technique was used to trace the nonlinear load-deflection path. Chajes and Churchill (1987) adopted variational principles to attain the stationary condition of total potential energy and developed a geometrically nonlinear beam element. In additional to the softening effect of stress resultants (e.g., axial forces and bending moments) within geometric stiffness matrices, the formulation is able to capture the effect of displacement changes, within the increments, in the displacement stiffness matrices. They adopted the incremental Newton-Raphson technique to obtain the equilibrium within increments using the direct methods or iterative procedures.

Zienkiewicz and Taylor (2000) developed a nonlinear beam element and proposed an incremental modified Newton-Raphson technique for the problems where tangent stiffness matrix is no longer positive definite. Siu-Lai and Chui (2000) provided a review of nonlinear solution techniques including Newton-Raphson, modified Newton-Raphson, direct Secant and pure incremental methods. They also elaborated on the iterative procedure of these techniques and derived the geometric stiffness matrix to conduct geometrically nonlinear analysis.

In the studies reviewed, shear deformation effect is neglected in the derivation of the geometric stiffness matrices. Thus in the current study, a geometrically nonlinear shear deformable element will be developed in Chapter 5 where variational principles are employed to attain the stationarity condition of total potential energy. The geometric and displacement stiffness matrices accounting for second order shear strains are derived and an incremental modified Newton-Raphson technique is adopted to trace the non-linear load-deflection path.

2.5.2. **Overview of eigen-value buckling solutions**

2.5.2.1. **Conventional approach based on linear pre-buckling analysis:**

The stages of deformation were discussed under Section 1.2. A static pre-buckling analysis is needed to capture the pre-buckling response of member, and associated internal forces (axial forces, shearing forces, and bending moments). Conventionally, it is assumed that pre-buckling analysis is linear (Trahair (1993)) and the corresponding discretized equilibrium conditions takes the form

$$\left[K_p\right]\left\{u_p\right\} = \left\{F\right\} \tag{20}$$

where $\left[K_p\right]$ is a deformation-independent (i.e., constant) pre-buckling elastic stiffness matrix, $\left\{u_p\right\}$ is the pre-buckling displacement vector, and $\left\{F\right\}$ is a nodal force vector. The system is solved for $\left\{u_p\right\}$. Given $\left\{u_p\right\}$, the pre-buckling internal forces are then determined.

In the second step, the internal forces obtained in Step 1 are scaled by a factor λ (based on the assumption that the displacement-force relationship is linear), and the buckling elastic matrix $\left[K_E\right]$ and geometric matrix $\lambda\left[K_G\right]$ are formed and a linearized buckling eigenvalue analysis of the type $\left(\left[K_E\right]-\lambda\left[K_G\right]\right)\left\{u_b\right\}=\left\{0\right\}$ is obtained where $\left\{u_b\right\}$ is the nodal buckling displacement vector.

2.5.2.2. **Accounting for non-linear effects in pre-bucking analysis:**

For a beam column, second order effects arise in the pre-buckling analysis due to the interaction between strong axis moments and axial forces leading to the so-called $P-\delta$ effect. In such a case, the pre-buckling response becomes non-linear and the corresponding equilibrium equations take the nonlinear form

$$\left[K_p\left(\left\{u_p\right\}\right)\right]_i\left\{u_p\right\}_i=\left\{F\right\}_i \tag{21}$$

Unlike the conventional solution in Eq. (20), it is noted here that at a force level $\left\{F\right\}_i$ the stiffness matrix $\left[K_p\right]_i$ is a function of the displacements $\left\{u_p\right\}_i$. An incremental solution based on the Newton-Raphson iterative scheme needs to be adopted to obtain the displacements and internal forces within each load increment. At a given load level $\left\{F\right\}_i$, the corresponding displacements $\left\{u_p\right\}_i$ are used to determine the internal forces. Neglecting pre-buckling deformation effects, one obtains the eigenvalue problem

$$\left(\left[K_E\right]_i-\lambda_i\left[K_G\left(\left\{u_p\right\}_i\right)\right]\right)\left\{u_b\right\}_i=\left\{0\right\} \tag{22}$$

which is to be solved for the eigen pairs (λ_i ,$\left\{u_b\right\}_i$). If the smallest value λ_i is found to meet the condition $\lambda_i>1$, the structure is deemed stable under the effect of the forces $\left\{F\right\}_i$. In this case, the magnitude of the loads is increased to $\left\{F\right\}_{i+1}$ and Eq. (21) is solved again for the corresponding pre-buckling nodal displacements $\left\{u_p\right\}_{i+1}$. The eigen pairs (λ_{i+1} ,$\left\{u_b\right\}_{i+1}$) are then determined by solving Eq. (22) and the process is repeated until the eigenvalue determined by Eq. (22) is equal to unity within a specified tolerance, in which case the system is deemed to be in a state of neutral stability (i.e., at the onset of bucking).

2.5.2.3. **Modifications to account for pre-bucking deformation effects:**

It is emphasized that the linearized eigenvalue problem defined by Eq. (22) stems from neglecting pre-buckling deformations. This is the case in the large majority of lateral torsional buckling solutions. Since the theory sought under the present work intends to incorporate the effect of pre-buckling deformations, the modifications would lead to a higher order eigenvalue problem of the form

$$\left(\left[K_E\right]_i-\lambda_i\left[K_{G1}\left(\left\{u_p\right\}_i\right)\right]-\lambda_i^2\left[K_{G2}\left(\left\{u_p\right\}_i\right)\right]\right)\left\{u_b\right\}=\left\{0\right\} \quad (23)$$

The procedure described under Section 2.5.2.2 remains valid with the exception that the eigenvalue check in Eq. (22)will be replaced by the form in Eq.(23).

2.6. References

Bathe, K.-J., and Bolourchi, S. (1979). "Large displacement analysis of three-dimensional beam structures." *International Journal for Numerical Methods in Engineering*, 14(7), 961-986.

Bickford, W. B. "Consistent higher order beam theory." *Proc., Developments in Theoretical and Applied Mechanics*, 137-150.

Chajes, A. (1974). *Principles of Structural Stability Theory*, Prentice-Hall, Inc, USA.

Chajes, A., and Churchill, J. (1987). "Nonlinear Frame Analysis by Finite Element Methods." *Journal of Structural Engineering*, 113(6), 1221-1235.

Chan, S. L., and Kitipornchai, S. (1987). "Geometric nonlinear analysis of asymmetric thin-walled beam-columns." *Engineering Structures*, 9(4), 243-254.

Cowper, G. R. (1966). "The Shear Coefficient in Timoshenko's Beam Theory." *Journal of Applied Mechanics*, 33(2), 335-340.

Eisenberger, M. (1994). "Derivation of shape functions for an exact 4-D.O.F. Timoshenko beam element." *Communications in Numerical Methods in Engineering*, 10(9), 673-681.

Friedman, Z., and Kosmatka, J. B. (1993). "An improved two-node timoshenko beam finite element." *Computers & Structures*, 47(3), 473-481.

Gjelsvik, A. (1981). *The theory of thin walled bars / Atle Gjelsvik*, Wiley, New York, NY, USA.

Heyliger, P. R., and Reddy, J. N. (1988). "A higher order beam finite element for bending and vibration problems." *Journal of Sound and Vibration*, 126(2), 309-326.

Lanczos, C. (1893). *The Variational Principles of Mechanics*, DOVER PUBLICATIONS, INC., Newyork.

Levinson, M. (1980). "An accurate, simple theory of the statics and dynamics of elastic plates." *Mechanics Research Communications*, 7(6), 343-350.

Levinson, M. (1981). "A new rectangular beam theory." *Journal of Sound and Vibration*, 74(1), 81-87.

Pi, Y., and Trahair, N. (1992b). "Prebuckling Deflections and Lateral Buckling. I: Theory." *Journal of Structural Engineering*, 118(11), 2949-2966.

Rajasekaran, S., and Murray, D. W. (1973). "Solution Techniques fo Geometrically Nonlinear Structures." Department of Civil Engineering, University of Alberta, Edmonton, Alberta.

Reddy, J. N. (1984a). *Energy and Variational Methods in Applied Mechanics*, John Wiley, New York.

Reddy, J. N. (1984b). "A Simple Higher-Order Theory for Laminated Composite Plates." *Journal of Applied Mechanics*, 51(4), 745-752.

Reddy, J. N. (1997). "On locking-free shear deformable beam finite elements." *Computer Methods in Applied Mechanics and Engineering*, 149(1–4), 113-132.

Siu-Lai, C., and Chui, P.-T. E. (2000). *Non-linear static and cyclic analysis of steel frames with semi-rigid connections*, Elsevier,.

Timoshenko, S. P. (1921). "On the correction for shear of the differential Equation for transverse vibration of prismatic beams." *Philosophical Magazine* 41, 744-746.

Trahair, N. S. (1993). *Flexural-torsional buckling of structures*, CRC Press, USA.

Vlasov, V. Z. (1961). *Thin walled elastic beams*, Israel Program for Scientific Translations, Jerusalem, Israel. Available from Office of Technical Services, US Department of Commerce,Washington, D.C.

Washizu, K. (1982). *Variational Methods in Elasticity & Plasticity*, Pergamon Press.

Wu, L. (2010). "Finite element formulations for lateral torsional buckling of shear deformable planar frames." Ph.D., University of Ottawa, Ottawa, CA.

Zienkiewicz, O. C., and Taylor, R. L. (2000). *The finite element method: Solid Mechanics*, Butterworth-Heinemann, Oxford.

Chapter 3

Distortional theory for the analysis of wide flange steel beams [(a)]

3.1. Abstract

A distortional theory is developed for the analysis of doubly symmetric and mono-symmetric wide flange beams under general loading. The governing differential equations of equilibrium and associated boundary conditions are derived based on the principle of potential energy. The theory captures shear deformation effects in the web and local and global warping effects. In contrast to classical beam theories, the present study captures web distortion by accounting for its flexibility within the plane of the cross-section while considering the flanges as Euler-Bernoulli beams. The formulation yields two systems of coupled differential equations of equilibrium in seven displacements fields. The first system governs the longitudinal transverse response and involves three displacement fields, and the second system governs the lateral torsional response and involves four displacement fields. Closed form solutions are then developed for both coupled systems under general loading. Numerical solutions for practical problems are then provided to illustrate the applicability of the formulation. Comparisons to results based on 3D shell finite element solutions show the validity of the results. The theory preserves the relative simplicity of one dimensional beam theories while effectively capturing the three-dimensional distortional phenomena normally captured within computationally expensive 3D FEA.

Keywords: Thin-Walled Beam, Distortion, Torsion, Warping, Coupling

[(a)] Pezeshky P., Mohareb M. Distortional theory for the analysis of wide flange steel beams. Engineering Structures. 2014;75:181-96.

3.2. **Introduction and literature review**

Conventionally, hot rolled and welded wide flange steel beams are analyzed using the Vlasov theory (Vlasov (1961)) which neglects distortional effects within the cross-section. Given that such cross-sections are relatively thick compared to cold-formed steel sections, it is often accepted that the Vlasov theory should reasonably predict their response. This is generally the case for a large number of applications. Nevertheless, some exceptions to this general rule are known to exist. This includes cross-sections with slender webs and thick flanges, short-span members, and/or when the applied loads are localized such that they deform a localized portion of the cross-section. In such cases, the web can undergo significant distortion and the application of the Vlasov theory or a variation thereof would lead to unreliable response predictions. The designer would typically need to resort to shell finite element analysis for an accurate response prediction. Another alternative is also available through various distortional beam theories which have been developed. A common theme among these theories has been to attempt to uncouple the distortion deformation from other conventional deformation modes, resulting in simple uncoupled equilibrium equations. The associated orthogonalization process is typically rather involved. Within this context, the present paper aims at developing a new distortional theory for wide flange sections. Rather than attempting to uncouple the resulting differential equations of equilibrium, the study develops a fully coupled system of governing equations and then provides a general closed form solution for the resulting system.

Classical theories such as the Euler-Bernoulli beam, the Timoshenko Beam (Timoshenko (1921), the thin walled beams Vlasov (1961) and Gjelsvik (1981) are based on the common assumption of neglecting cross-sectional distortional effects. More modern beam theories for the static analysis of beams which account for distortion include the work of Schardt (1989) who developed a Generalised Beam Theory (GBT), mostly for very thin walled members (e.g., cold form cross sections), in which he categorized the behaviour of the beam into: a) the four classical modes of deformation analogous of the Vlasov beam (Vlasov (1961)), i.e., axial, biaxial bending and twist), and b) distortion of the cross section in its own plane. His theory introduces distortional modes and associated warping functions that are orthogonal to the other four classical kinematic modes of deformation and thus consists of five uncoupled differential equations in four classical displacement fields in addition to a distortional field. Davies and Leach (1994) applied the GBT theory to cold formed sections. Using closed form solutions and the finite difference method, they solved the fourth order differential equation of distortion. Jönsson (1998) postulated that distortion has commonalities with torsion and thus leads to analogous internal forces. He extended the concept of sectorial coordinates, previously introduced by Vlasov, to characterize distortional deformation. He developed a one-dimensional finite element to determine the torsional and distortional warping functions and corresponding shear distribution within the cross-section. In two subsequent papers, Jönsson (1999b) and (1999a), combined the outcome of his previous study with the principle of stationary potential energy to formulate the distortional warping functions and corresponding shear stresses for open and closed sections. The resulting torsional and distortional equilibrium equations are observed to generally remain coupled. In another treatment, Rendek and Baláž (2004) adopted vector analysis to simplify the orthogonalization process between displacement modes normal to the cross-section and determine the associated modal loads and sectional properties. They approximated the transverse displacements by Hermitian cubic functions of the longitudinal coordinate and quantified the transverse bending moments and distortional sectional properties. Based on a modified version of Prokic theory, Saadé et al. (2006) developed a finite element which accounts for cross-sectional distortion. Later on, Gonçalves et al. (2010) devised a new approach to determine the deformation modes in which they subdivided the space of possible solutions into four sub-spaces based on four distinct kinematic hypotheses. Under each hypothesis, they identified the warping and in-plane modes. An orthogonalization process is then performed on the associated modes to determine the relevant cross-sectional constants. In their study, local deformations and shear deformations are also captured by introducing intermediate nodes. Jönsson and Andreassen (2011) developed a GBT solution in which they related the displacements within the plane of the cross section to the nodal displacements through Hermitian polynomials, thus capturing distortional effects. They orthogonalized the various modes by enforcing kinematic constraints, ultimately leading to two differential equations per segment which characterize distortion within the segment. Using polynomial interpolations of the longitudinal coordinate for conventional modes and exponential interpolations for distortional modes, they developed a finite element that captures distortion. In a more recent study, Andreassen and Jönsson (2012) generalized their previous work by incorporating the effect of distributed loads.

A common theme among the above studies is the various elaborate techniques devised by the authors to uncouple the resulting field equations governing distortion from the remaining classical modes of deformation, culminating in simpler field equations. The present theory deviates from the previous convention by avoiding the complications involved in the uncoupling process of the governing field equations, thus yielding a highly coupled system of equations, but then providing closed form solutions for the resulting systems of equations under general loads.

Distortional effects also have been received considerable attention in buckling investigations of thin-walled beams. This includes the work of Rajasekaran and Murray (1973) who developed a buckling finite element for wide flange beams based on overlaying the kinematics of the Vlasov thin walled beam theory on those of the Kirchhoff plate bending theory to capture the distortional behaviour of web and flanges. Johnson and Will (1974) developed a shell buckling finite element with 22 DOFs and applied it to capture the distortional buckling behaviour and predicting the buckling capacity of wide flange beams and columns. In a subsequent study, using the finite strip method, Hancock (1978) has shown that, in beams with slender webs and stocky flanges, the web is susceptible to distortion while the flanges remain undistorted. Hancock et al. (1980) developed an approximate distortional buckling solution for simply supported wide flange beams under uniform moments and axial forces. In their solution, they assumed that the web deforms as a cubic function along the height while both flanges undergo distinct angles of twist. Bradford and Trahair (1981) developed a finite element for I-shaped members under unequal end moments and compressive axial forces. Their element is based on Hermitian shape functions to interpolate the displacements along the span. Bradford and Trahair (1982) extended their work to other thin-walled sections such as lipped channels by retaining the flexible web assumption. Using a plate bending formulation, Roberts and Jhita (1983b) formulated the buckling characteristic equation of wide flange sections. In a series of papers, Bradford extended his previous work to develop distortional lateral buckling solutions for mono-symmetric cross-sections (1985), inelastic buckling of hot-rolled I-beams (Bradford 1986), mono-symmetric I-beams with flanges restrained by continuous lateral elastic restrains (1988a), beam columns (Bradford 1990b), cantilevers (Bradford 1992a), investigating the effects of end conditions, rotational and translational restraints for I-beams (Bradford 1992b), and beams laterally restrained at one flange (Bradford and Ronagh 1997). A common feature in all Bradford's work is the approximation of web lateral displacements through a cubic function. Based on the Rayleigh Ritz energy method, Wang et al. (1991) provided a comparison between distortional and non-distortional buckling for mono-symmetric simply supported beam-columns. Hughes and Ma (1996a) developed a distortional buckling solution for simply supported mono-symmetric I-beams under point loads and extended their work (Ma and Hughes 1996b) to beams under distributed transverse loads and unequal end moments. In their study, they assumed that the web distorts as a fifth order polynomial function. Dekker and Kemp (1998) developed a distortional buckling solution in which they idealized the flanges of an I-Beam as translational and rotational springs, while the flexible web remains as an elastic plate. In a study on simply supported I-beams, Pi and Trahair

(2000) developed a technique to quantify the torsional and warping rigidities which incorporates distortional effects. Their solution has incorporated pre-buckling and end-warping restrains effects. Ng and Ronagh (2004) developed a Fourier series solution to obtain the distortional buckling capacity of doubly-symmetric I-Beams, which models the effect of elastic restraints and loading offset from the shear centre. Based on shell FEA, Samanta and Kumar (2006b) investigated the distortional buckling of simply supported mono-symmetric I beams. Vrcelj and Bradford (2006a) investigated the effect of lateral and rotational restraints on the distortional buckling of I-beams with a tension flange seated on a support. Ádány and Schafer (2008) devised a mode decomposition technique within the constrained finite strip method to extract distortional buckling moments.Ádány and Schafer (2008) and Samanta and Kumar (2008) extended their previous work to cantilevers of mono-symmetric I cross-sections and investigated the effect of load position and bracing height on the distortional buckling capacity. Using the finite strip method, Zirakian (2008) studied the distortional buckling of doubly symmetric I-beams. He showed that AISC (2005) recommendations for lateral torsional buckling provisions of beams with slender webs, which neglects the Saint-Venant torsional stiffness, provide overly conservative means of incorporating the effect of distortion. By assuming a quadratic distribution of the web lateral displacement, Chen and Ye (2010) developed the potential energy expression for the distortional buckling of I-beams and applied the Ritz method to determine the buckling solution for simply supported beams with a single restrained flange. Using the effective section properties developed by Pi and Trahair (2000), Kalkan and Buyukkaragoz (2012) determined distortional critical moments and compared their results to those in AISC (2005), EC3 (2003), and AS 4100 (1998). Their study involved distortional buckling moments in the elastic and inelastic ranges.

A comparative summary for the above studies is provided in Table 1.

Table 3-1. A comparison of distortional studies

Reference	Displacement distribution in the longitudinal direction*	Analysis Type		Features		Solution Type								Details
		Static	Buckling	Local warping	Shear deformable in the plane of the web	Based on assumed web kinematics *	Generalized Beam Theory	Other mode orthogonalization techniques	Closed form	Finite element	Finite difference	Finite strip	Trigonometric series	
Rajasekaran and Murray (1973)	C	-	✓	-	✓	C	-	-	-	✓	-	-	-	
Johnson and Will (1974)	Qua	-	✓	-	✓	Qua	-	-	-	✓	-	-	-	4 node Shell element with 3 DOFs per node
(Hancock (1978); Hancock et al. (1980))	T	-	✓	-	✓	C	-	-	-	-	-	✓	✓	
Hancock et al. (1980)	T	-	✓	-	✓	C	-	-	-	-	-	-	✓	
(1985; 1986; 1992a; 1992b; Bradford and Trahair (1981); 1982)	C	-	✓	-	✓	C	-	-	-	✓	-	-	-	2 node beam element with 6,8.11 DOFs per node
(Bradford (1988a); Bradford 1990b; Roberts and Jhita (1983b)), Wang et al. (1991)	T	-	✓	-	✓	C	-	-	-	-	-	-	✓	
Davies and Leach (1994)	H-T	✓	-	-	-	-	✓	-	✓	✓	✓	-	-	Beam on elastic foundation (closed form solution)
(Hughes and Ma (1996a); 1996b)	T	-	✓	-	✓	Qui	-	-	-	-	-	-	✓	web nodal DOFs are displacement, slope and curvature
Bradford and Ronagh (1997)	C	-	✓	✓	✓	C	-	-	-	✓	-	-	-	2 node beam element with 8 DOFs per node
(Andreassen and Jönsson 2012; Jönsson (1998); Jönsson 1999a; Jönsson 1999b; Jönsson	H-T	✓	-	✓	✓	-	-	✓	✓	-	-	-	-	

Reference	Displacement distribution in the longitudinal direction*	Analysis Type		Features		Solution Type								Details
		Static	Buckling	Local warping	Shear deformable in the plane of the web	Based on assumed web kinematics *	Generalized Beam Theory	Other mode orthogonalization techniques	Closed form	Finite element	Finite difference	Finite strip	Trigonometric series	
and Andreassen 2011)														
(Ng and Ronagh (2004); Vrcelj and Bradford (2006a))	T	-	✓	-	✓	C	-	-	-	-	-	-	✓	
Rendek and Baláž (2004)	-	✓	-	-	-	C	✓	-	✓	-	-	-	-	beam on elastic foundation(closed form solution)
Saadé et al. (2006)	Qua-L	✓	-	✓	✓	-	-	✓	-	✓	-	-	-	
Ádány and Schafer (2008)	T	-	✓	-	✓	-	-	✓	-	-	-	✓	✓	
Chen and Ye (2010)	T	-	✓	-	✓	C	-	-	-	-	-	-	✓	
Gonçalves et al. (2010)	-	✓	-	-	✓	-	✓	-	-	-	-	-	-	systematic approach to determine deformation modes within GBT
Current Study	H-Qui	✓	-	✓	✓	C	-	-	✓	-	-	-	-	

* C: Cubic, H: Hyperbolic; L: Linear, Qua: Quadratic, Qui: Quintic, T: Trigonometric,

The majority of the above buckling studies assume that the lateral displacement of the web to have a cubic distribution along the height, while the flanges remain undistorted and having distinct angles of twist. In the present theory, we retain this kinematic assumption. Subsequent comparisons with shell FEA results will provide an assessment of the validity of this assumption.

3.3. Statement of the problem

Given is a beam of a wide flange mono-symmetric section with a slender web subjected to general member and end tractions. It is required to formulate the governing field equations and associated boundary conditions. A mono-symmetric I-shape section, shown in Fig. 3-1, has a bottom flange width b_B and thickness t_B and a top flange width b_T and thickness t_T. As a convention, all subscripts B denote parameters related to the bottom flange and subscripts T denotes those related to the top flange. Web height is denoted h and is defined as the distance between middle surfaces of both flanges and t_w denotes the web thickness.

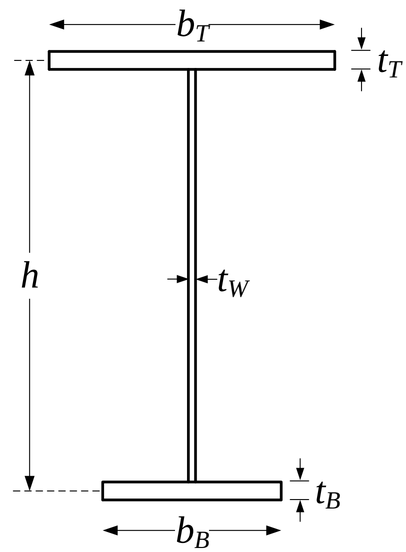

Fig. 3-1. Cross section dimensions

The beam member is subjected to the following general tractions (Fig. 3-2):

a) End tractions acting at both ends as:

$\bar{\sigma}_{zz}(x,y,0), \bar{\tau}_{zx}(x,y,0), \bar{\tau}_{zy}(x,y,0)$ and $\bar{\sigma}_{zz}(x,y,L), \bar{\tau}_{zx}(x,y,L), \bar{\tau}_{zy}(x,y,L)$.

Member tractions $p_z(s,n,z)$, $p_y(s,n,z)$ and $p_x(s,n,z)$ in longitudinal, transverse, and lateral directions, respectively, where the normal coordinate is $n = n_T, n_B, n_W$ for the top and bottom flanges and web, respectively. Also, the tangential coordinate s is along the middle surface and coincides with x_T, x_B and y_W within top and bottom flanges and the web, respectively, as shown in Fig. 3-1.

Furthermore, transverse distributed load can be applied vertically across the flange width on the top flange, while the longitudinal distributed load is applied across the entire cross section along the longitudinal direction.

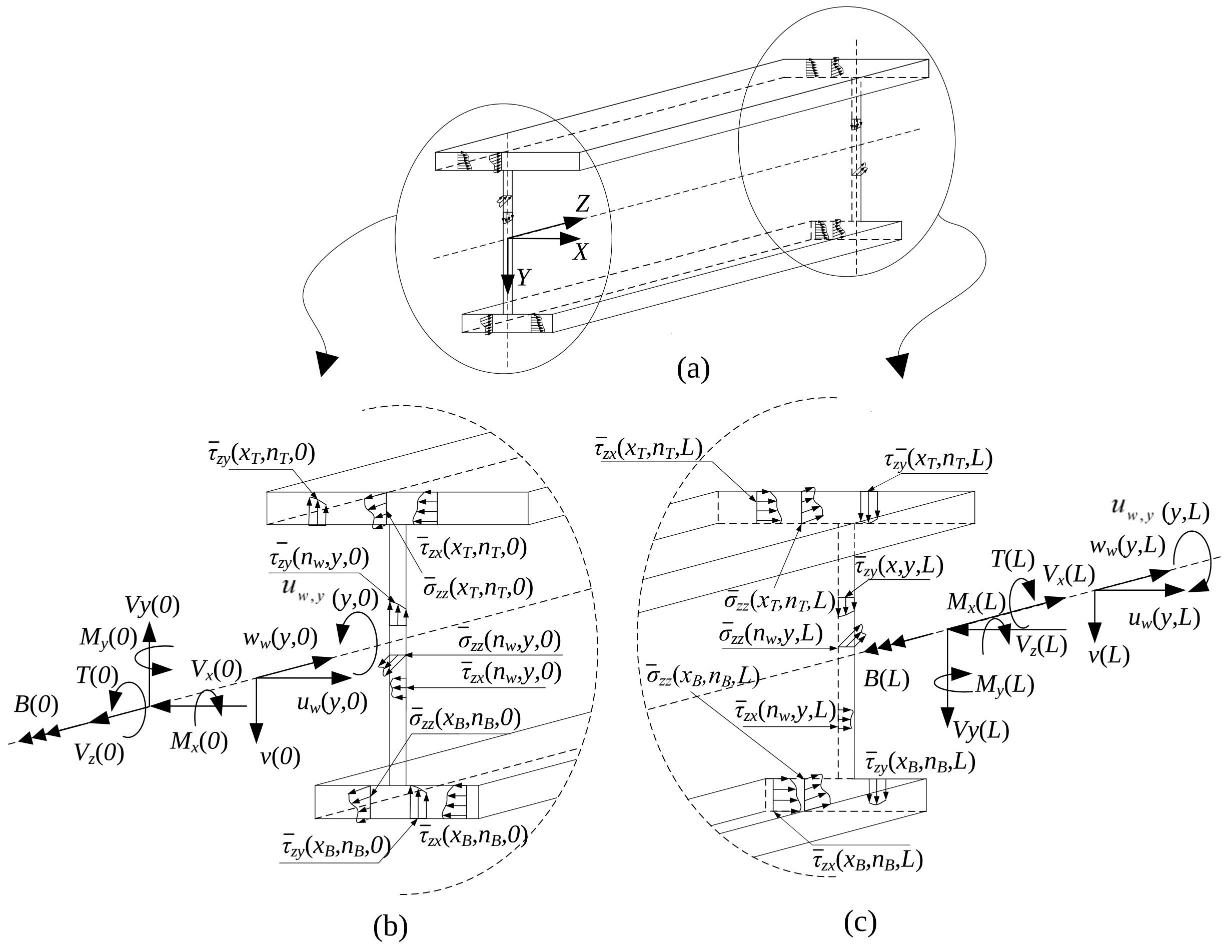

Fig. 3-2. (a) Beam and axes (b) End tractions and stress resultants at z=0. (c) End tractions and stress resultants at z=L

A global right handed $OXYZ$ coordinate system is introduced with an origin O located at web mid-height (Fig. 3-3). A local right handed coordinate system is also assigned to each of the flanges. For any point P offset from the middle surface, correspond local coordinates (x,n_T) and (x,n_B) at the top and bottom flanges, respectively. Displacements $\tilde{u}_T$ and $\tilde{u}_B$ denote the lateral displacements of points $P(x,n_T)$ and $R(x,n_B)$ relative to points $(0,n_T)$, $(0,n_B)$ lying on the middle surface of the section. Also, displacements $\tilde{v}_T$ and $\tilde{v}_B$ denote the transverse displacements relative to points $(0,n_T)$, $(0,n_B)$.

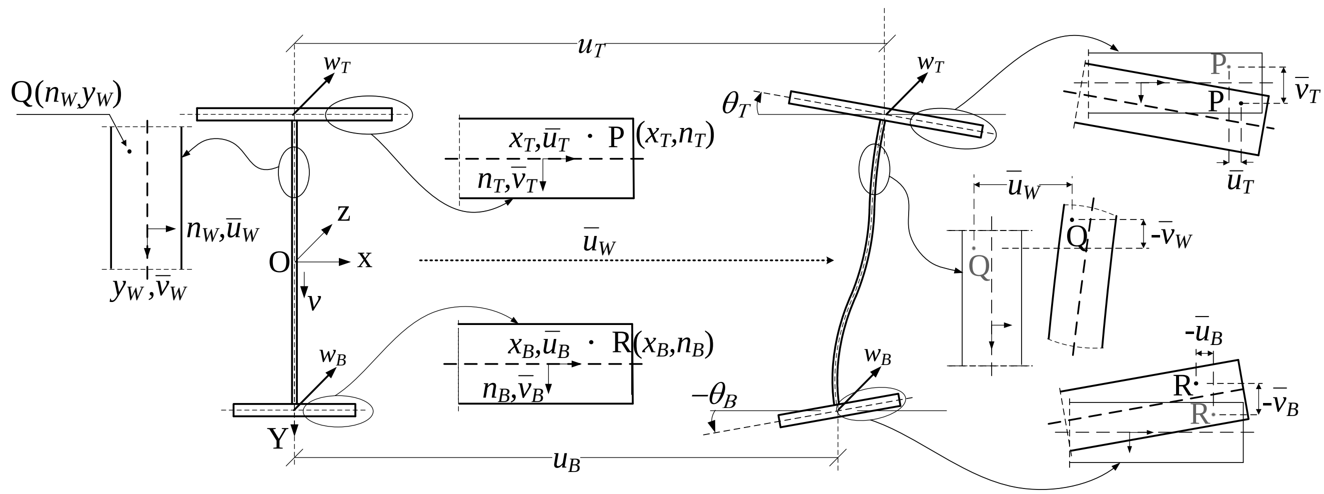

Fig. 3-3. Coordinates and displacements

3.4. Assumptions and kinematics

Strains and rotations are assumed small. The material is homogeneous, linearly elastic and isotropic and thus obeys Hooke's law. The formulation is restricted to prismatic beams with wide flange monosymmetric cross-sections. Additional kinematic assumptions are provided in the following subsections.

3.4.1. Displacements in the plane of the cross-section

Since the web is slender compared to the flanges, it is assumed to distort in the plane of the cross section through a cubic function (Fig. 3-3). The centroid of the top flange is assumed to translate laterally by a displacement $u_T(z)$ while that of the bottom flange is assumed to translate by displacement $u_B(z)$. The top flange is assumed to twist by an angle $\theta_T(z)$ and the bottom flange by a different angle $\theta_B(z)$. The transverse displacement at a generic point (y_W, n_W) on the web consists of two parts; a) a transverse displacement component $v(z)$ defined at the origin O, lying on the web middle surface, and b) a component $\bar{v}_{WP}$ due to the offset distance n_W undergoing a rotation within the plane of the cross-section (Fig. 3-3)

3.4.2. Longitudinal displacement

At a given section, the middle surface of the top flange is assumed to behave as a rigid line undergoing rotations $u'_T(z), v'(z)$ about the x and y axes and longitudinal displacement $w_T(z)$ (all primes denote differentiation with respect to Z, as a convention). Also, the bottom flange undergoes rotations $u'_B(z), v'(z)$ and longitudinal displacement $w_B(z)$.

Shear deformation within the plane of the flanges is assumed negligible in line with the conventional Euler-Bernoulli beam assumption. A line through (x, n_T) originally normal to the plane of the flange middle surface is assumed to remain normal to the middle surface of the flange, in line with the Kirchhoff plate bending theory.

Since the present theory is aimed at sections with deep and slender webs, it is appropriate to assume the web to act as a Timoshenko beam (rather than an Euler-Bernoulli beam), in which the web is assumed to rotate as a rigid line about the x-axis, i.e., the longitudinal displacement is assumed to take a linear distribution with respect to the y coordinate, but not necessarily remain perpendicular to the beam axis, i.e., $v'(z) \neq \left[w_T(z) - w_B(z)\right]/h$. A line through (y, n_W) originally normal to the web middle surface is assumed to remain normal to the web middle surface, in line with the Kirchoff plate bending theory.

In Fig. 3-3, the seven generalized displacements (e.g., $\bar{u}_T, \bar{w}_T, \bar{\theta}_T, \bar{v}, \bar{u}_B, \bar{w}_B, \bar{\theta}_B$) of the beam are shown. The displacements of the top flange are obtained by

$$\begin{aligned} \bar{u}_T(n_T, z) &= u_T(z) - n_T\theta_T(z) \\ \bar{v}_T(x_T, z) &= v(z) + x_T\theta_T(z) \end{aligned} \tag{3.1}$$

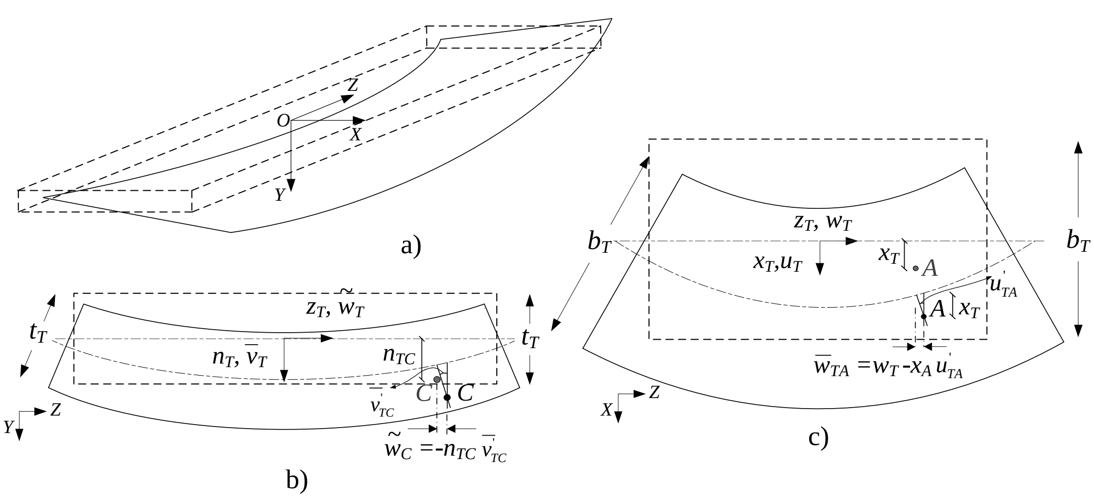

Fig. 3-4. Kinematics of top flange a) Deformed shape, b) Side view(Y-Z) and c) Plan view(X-Z)

The longitudinal displacement of a point A on the middle surface of the top flange (Fig. 3-4c) is

$$\bar{w}_{TA}\left(x_T, z\right) = w_T\left(z\right) - x_T u'_T\left(z\right) \tag{3.2}$$

The longitudinal displacement of Point C offset from the middle surface (Fig. 3-4b) is obtained by adding the relative displacement $-n_T\left[v'\left(z\right) + x_T\theta'_T\left(z\right)\right]$ to the longitudinal displacement $\bar{w}_{TA}$, i.e.,

$$\bar{w}_T\left(x_T, n_T, z\right) = w_T\left(z\right) - x_T u'_T\left(z\right) - n_T v'\left(z\right) - n_T x_T \theta'_T\left(z\right) \tag{3.3}$$

Also, the longitudinal displacement of the bottom flange is

$$\bar{w}_B\left(x_B, n_B, z\right) = w_B\left(z\right) - x_B u'_B\left(z\right) - n_B v'\left(z\right) - n_B x_B \theta'_B\left(z\right) \tag{3.4}$$

As stated in Section3.4, the web lateral displacement is assumed to be a cubic function of coordinate y. It is convenient to relate the web lateral displacement to the lateral displacements and angles of twist of both flanges $u_T\left(z\right), \theta_T\left(z\right), u_B\left(z\right), \theta_B\left(z\right)$, i.e.,

$$\bar{u}_W\left(y, z\right) = H_1\left(y\right)u_T\left(z\right) + H_2\left(y\right)\theta_T\left(z\right) + H_3\left(y\right)u_B\left(z\right) + H_4\left(y\right)\theta_B\left(z\right) \tag{3.5}$$

through the interpolation functions

$$\begin{aligned} H_1\left(y\right) &= \frac{1}{2} - \frac{3y}{2h} + \frac{2y^3}{h^3}, \qquad & H_2\left(y\right) &= \frac{h}{8} - \frac{y}{4} - \frac{y^2}{2h} + \frac{y^3}{h^2} \\ H_3\left(y\right) &= \frac{1}{2} + \frac{3y}{2h} - \frac{2y^3}{h^3}, \qquad & H_4\left(y\right) &= -\frac{h}{8} - \frac{y}{4} + \frac{y^2}{2h} + \frac{y^3}{h^2} \end{aligned} \tag{3.6}$$

Also, the longitudinal displacement of the web is linearly interpolated to the longitudinal displacements of both flanges through

$$w_W\left(y, z\right) = H_5\left(y\right)w_T\left(z\right) + H_6\left(y\right)w_B\left(z\right) \tag{3.7}$$

in which

$$H_5\left(y\right) = \left(\frac{1}{2} - \frac{y}{h}\right),\ H_6\left(y\right) = \left(\frac{1}{2} + \frac{y}{h}\right) \tag{3.8}$$

Based on the Kirchoff plate hypothesis, the longitudinal and transverse displacements of a point P $\left(n_w, y, z\right)$, on the web ($-\left(h - t_T\right)/2 \le y \le \left(h - t_B\right)/2$), relative to a point $(0, y, z)$ on the middle surface, one obtains

$$\bar{v}_{WP}(n_W, y, z) = -n_W \frac{\partial \bar{u}_W\left(y, z\right)}{\partial y} \quad , \bar{w}_{WP}(n_W, y, z) = -n_W \frac{\partial \bar{u}_W\left(y, z\right)}{\partial z} \tag{3.9}$$

The total displacements of the web are obtained by adding the plate contributions $\bar{v}_{wP}$, $\bar{w}_{wP}$ to the membrane components $v(z)$ and $w(z)$, i.e.,

$$\begin{aligned}
\bar{v}_W(n_W, y, z) &= -n_W \frac{\partial \bar{u}_W(y,z)}{\partial y} + v(z) \\
\bar{w}_W(n_W, y, z) &= -n_W \frac{\partial \bar{u}_W(y,z)}{\partial z} + \left(\frac{1}{2} - \frac{y}{h}\right) w_T(z) + \left(\frac{1}{2} + \frac{y}{h}\right) w_B(z)
\end{aligned} \tag{3.10}$$

3.5. **Expressions for strains and stresses**

The longitudinal strain ε_{zT} and shear strain γ_{xzT} within the top flange are given by

$$\begin{aligned}
\varepsilon_{zT} &= \frac{\partial \bar{w}_T}{\partial z} = w_T{}'(z) - x u_T''(z) - n_T v''(z) - x n_T \theta_T''(z) \\
\gamma_{xzT} &= \frac{\partial \bar{w}_T}{\partial x} + \frac{\partial \bar{u}_T}{\partial z} = -2 n_T \theta_T'(z)
\end{aligned} \tag{3.11}$$

Also, for the bottom flange, one has

$$\begin{aligned}
\varepsilon_{zB} &= w_B'(z) - x u_B''(z) - n_B v''(x,z) - x n_B \theta_B''(z) \\
\gamma_{xzB} &= -2 n_B \theta_B'(z)
\end{aligned} \tag{3.12}$$

It can be shown that $\gamma_{yzT} = \gamma_{yzB} = \gamma_{xyT} = \gamma_{xyB} = 0$. Web strains consist of a plate bending contribution and membrane contribution. The normal strain ε_{yP} , ε_{zP} and shear strain γ_{yzP} due to plate bending action of the web are given by

$$\begin{aligned}
\varepsilon_{yP} &= \frac{\partial \bar{v}_{WP}}{\partial y} = -n_W \frac{\partial^2 \bar{u}_W(y,z)}{\partial y^2} \\
\varepsilon_{zP} &= \frac{\partial \bar{w}_{WP}}{\partial z} = -n_W \frac{\partial^2 \bar{u}_W(y,z)}{\partial z^2} \\
\gamma_{yzP} &= \frac{\partial \bar{w}_{WP}}{\partial y} + \frac{\partial \bar{v}_{WP}}{\partial z} = -2 n_W \frac{\partial^2 \bar{u}_W}{\partial y \partial z}
\end{aligned} \tag{3.13}$$

The longitudinal strain ε_{zM} and shear strain γ_{yzM} of the web due to membrane action are

$$\begin{aligned}
\varepsilon_{zM} &= \frac{\partial \bar{w}_w}{\partial z} = \left(\frac{1}{2} + \frac{y}{h}\right) w_B'(z) + \left(\frac{1}{2} - \frac{y}{h}\right) w_T'(z) \\
\gamma_{yzM} &= \frac{\partial \bar{w}_w}{\partial y} + \frac{\partial v}{\partial z} = \left(\frac{w_B(z) - w_T(z)}{h}\right) + v'(z)
\end{aligned} \tag{3.14}$$

From Hooke's law, the stresses in the top and bottom flanges are obtained are

$$\sigma_{zT} = E\varepsilon_{zT} \ , \ \sigma_{zB} = E\varepsilon_{zB} \ , \ \tau_{xzT} = G\gamma_{xzT} \ , \ \tau_{xzB} = G\gamma_{xzB} \tag{3.15}$$

For the web, the plate bending stresses are given by

$$\sigma_{yP} = \frac{E}{1-\nu^2}\left(\varepsilon_{yP} + \nu\varepsilon_{zP}\right), \sigma_{zP} = \frac{E}{1-\nu^2}\left(\varepsilon_{zP} + \nu\varepsilon_{yP}\right), \tau_{yzP} = G\gamma_{yzP} \tag{3.16}$$

and the membrane stresses are

$$\sigma_{zM} = E\varepsilon_{zM}, \tau_{yzM} = G\gamma_{yzM} \tag{3.17}$$

3.6. **Energy formulation**

The total potential energy of the system, Π, is the sum of the internal strain energy U stored and the potential energy V gained by the loads. The internal strain energy U consists of the internal strain energy stored in the top flange U_T, that stored in the bottom flange U_B, and that stored in the web U_w. The potential energy V is the sum of the potential energy gain by the end tractions V_1 and member tractions V_2. Thus, the first variation of the total potential energy is

$$\delta\Pi = \left(\delta U_T + \delta U_B + \delta U_w\right) + \left(\delta V_1 + \delta V_2\right) \tag{3.18}$$

The first variation of internal strain energy in the top flange is due to normal and shear strains, i.e.,

$$\begin{aligned}\delta U_T &= \int_V \left(E\varepsilon_z \delta\varepsilon_z + G\gamma_{xz}\delta\gamma_{xz}\right) dV \\ &= \int_L \left(EA_T w_T' \delta w_T' + EI_{xxT} v''\delta v'' + EI_{yyT} u_T'' \delta u_T'' + EI_{\omega\omega T}\theta_T''\delta\theta_T'' + GJ_T \theta_T' \delta\theta_T'\right) dz\end{aligned} \tag{3.19}$$

in which, $\left(I_{xxT}, I_{yyT}, I_{\omega\omega T}, J_T\right) = \int_{A_T} \left(n_T^2, x_T^2, n_T^2 x_T^2, 4n_T^2\right) dA_T = \left(b_T t_T^3/12, b_T^3 t_T/12, b_T^3 t_T^3/144, b_T t_T^3/3\right)$ are cross-sectional properties of the top flange. In obtaining Eq. (3.19), the orthogonal cross-sectional properties, $\int_{A_T} \left(x, y, x^2 y, xy^2, xy\right) dA = \left(0,0,0,0,0\right)$, have been used. In a similar manner, one obtains the first variation of internal strain energy of the bottom flange as

$$\delta U_B = \int_L \left(EA_B w_B' \delta w_B' + EI_{xxB} v''\delta v'' + EI_{yyB} u_B'' \delta u_B'' + EI_{\omega\omega B}\theta_B''\delta\theta_B'' + GJ_B \theta_B' \delta\theta_B'\right) dz \tag{3.20}$$

in which $\left(I_{xxB}, I_{yyB}, I_{\omega\omega B}, J_B\right) = \int_{A_B} \left(n_B^2, x_B^2, n_B^2 x_B^2, 4n_B^2\right) dA_B = \left(b_B t_B^3/12, b_B^3 t_B/12, b_B^3 t_B^3/144, b_B t_B^3/3\right)$.

The first variation of the internal strain energy of the web consists of two contributions; the Membrane action δU_{wM} and the plate bending action δU_{wP}. These are given by

$$\delta U_{wM} = \int_V \left(E\varepsilon_{zM}\delta\varepsilon_{zM} + G\gamma_{yzM}\delta\gamma_{yzM} \right) dV$$
$$= \int_L E\left[\frac{A_w}{4}\left(w_T' + w_B' \right) + \frac{I_{xxw}}{h^2}\left(w_T' - w_B' \right) \right]\delta w_T' + E\left[\frac{A_w}{4}\left(w_B' + w_T' \right) + \frac{I_{xxw}}{h^2}\left(w_B' - w_T' \right) \right]\delta w_B' \quad (3.21)$$
$$+ \frac{GA_w}{h^2}\left[\left(w_T - w_B - hv' \right)\delta w_T + \left(w_B - w_T + hv' \right)\delta w_B + \left(hw_B - hw_T + h^2 v' \right)\delta v' \right] dz$$

and

$$\delta U_{wP} = \frac{E}{2(1-\nu^2)}\int_V \left(2\varepsilon_{zP}\delta\varepsilon_{zP} + 2\varepsilon_{yP}\delta\varepsilon_{yP} + 2\nu\left(\varepsilon_{zP}\delta\varepsilon_{yP} + \delta\varepsilon_{zP}\varepsilon_{yP} \right) + 2(1-\nu)\gamma_{yzP}\delta\gamma_{yzP} \right) dV$$
$$= D\iint_A \left\{ \left(\frac{\partial^2 \bar{u}_w}{\partial z^2} \right)\left(\delta\frac{\partial^2 \bar{u}_w}{\partial z^2} \right) + \left(\frac{\partial^2 \bar{u}_w}{\partial y^2} \right)\left(\delta\frac{\partial^2 \bar{u}_w}{\partial y^2} \right) + \nu\left[\left(\frac{\partial^2 \bar{u}_w}{\partial z^2} \right)\left(\delta\frac{\partial^2 \bar{u}_w}{\partial y^2} \right) + \left(\delta\frac{\partial^2 \bar{u}_w}{\partial z^2} \right)\left(\frac{\partial^2 \bar{u}_w}{\partial y^2} \right) \right] \right. \quad (3.22)$$
$$\left. + 2(1-\nu)\left[\left(\frac{\partial^2 \bar{u}_w}{\partial z \partial y} \right)\left(\delta\frac{\partial^2 \bar{u}_w}{\partial z \partial y} \right) \right] \right\} dA$$

in which D is the plate stiffness $D = Et_W{}^3 \big/ 12\left(1-\nu^2\right)$, and $\left(A_w, I_{xxw}\right) = \int_{A_w} \left(1, y^2\right) dA_w = \left\{ t_W\left[h - 0.5\left(t_T + t_B\right) \right],\ \ t_W\left[h - 0.5\left(t_T + t_B\right) \right]^3 \big/ 12 \right\}$ are web cross-sectional properties related to the axial and bending stiffness, respectively.

The variation of the potential energy gained by the specified tractions $\left(\bar{\tau}_{zx}, \bar{\tau}_{zy}, \bar{\sigma}_{zz} \right)_i$ acting at both ends of the member, $z = 0$ (denoted by subscript i=0) and $z = L$ (denoted by the subscript i=1) and undergoing displacements $\left(\bar{u}, \bar{v}, \bar{w} \right)_i$ is

$$\delta V_1 = -\int_A \sum_{i=0,1} \left(-1\right)^i \left(\left(\bar{\tau}_{zx}\delta\bar{u} + \bar{\tau}_{zy}\delta\bar{v} + \bar{\sigma}_{zz}\delta\bar{w} \right)_{i,T} + \left(\bar{\tau}_{zx}\delta\bar{u} + \bar{\tau}_{zy}\delta\bar{v} + \bar{\sigma}_{zz}\delta\bar{w} \right)_{i,B} + \left(\bar{\tau}_{zx}\delta\bar{u} + \bar{\tau}_{zy}\delta\bar{v} + \bar{\sigma}_{zz}\delta\bar{w} \right)_{i,W} \right) dA \quad (3.23)$$

From Eqs. (3.1)-(3.10), by substituting into Eq. (3.23) one obtains,

$$\delta V_1 = \sum_{i=0,1} \left(-1\right)^i \left[\bar{N}_T\delta w_T + \bar{N}_B\delta w_B + \bar{V}_{xT}\delta u_T + \bar{V}_{xB}\delta u_B + \bar{V}_y\delta v + \bar{M}_{yT}\delta u_T' + \bar{M}_{yB}\delta u_B' \right.$$
$$\left. + \bar{T}_T\delta\theta_T + \bar{T}_B\delta\theta_B + \left(\bar{M}_{xT} + \bar{M}_{xB} \right)\delta v' + \bar{B}_T\delta\theta_T' + \bar{B}_B\delta\theta_B' \right]_i \quad (3.24)$$

in which the following thirteen energy conjugate stress resultants arise naturally, i.e.,

$$\left(\bar{N}_T,\bar{N}_B,\bar{V}_y,\bar{M}_{xT},\bar{M}_{xB}\right)=\int_A\left\{\left[\bar{\sigma}_{zz}\left(1+H_5\right)\right],\left[\bar{\sigma}_{zz}\left(1+H_6\right)\right],\left(\bar{\tau}_{zy}\right),\left(-n_T\bar{\sigma}_{zz}\right),\left(-n_B\bar{\sigma}_{zz}\right)\right\}dA$$
$$\left(\bar{V}_{xT},\bar{V}_{xB}\right)=\int_A\left\{\left[\bar{\tau}_{zx}\left(1+H_1\right)-n_w\bar{\tau}_{zy}\left(dH_1/dy\right)\right],\left[\bar{\tau}_{zx}\left(1+H_3\right)-n_w\bar{\tau}_{zy}\left(dH_3/dy\right)\right]\right\}dA$$
$$\left(\bar{M}_{yT},\bar{M}_{yB}\right)=\int_A\left\{\left[-\bar{\sigma}_{zz}\left(x_T+n_wH_1\right)\right],\left[-\bar{\sigma}_{zz}\left(x_B+n_wH_3\right)\right]\right\}dA$$
$$\left(\bar{T}_T,\bar{T}_B\right)=\int_A\left\{\left[\bar{\tau}_{zx}\left(H_2-n_T\right)-\bar{\tau}_{zy}\left(n_w\,dH_2/dy-x_T\right)\right],\left[\bar{\tau}_{zx}\left(H_4-n_B\right)-\bar{\tau}_{zy}\left(n_w\,dH_4/dy-x_B\right)\right]\right\}dA$$
$$\left(\bar{B}_T,\bar{B}_B\right)=\int_A\bar{\sigma}_{zz}\left[\left(-x_Tn_T-n_wH_2\right),\left(-x_Bn_B-n_wH_4\right)\right]dA \tag{3.25}$$

In Eqs. (3.25) one recalls that H_1-H_6 are the interpolation functions defined in Eqs. (3.6) and (3.8). The first set of stress resultants denotes the longitudinal-transverse internal forces and the other energy conjugate terms denote lateral-torsional internal forces. The variation of the potential energy gained by the member tractions (p_x, p_y, p_z) undergoing displacements $\left(\bar{u},\bar{v},\bar{w}\right)_{T,B}$ and $\left(\bar{u},v,\bar{w}\right)_W$ is

$$\delta V_2=\int_A\left[\left(p_x\delta\bar{u}+p_y\delta\bar{v}+p_z\delta\bar{w}\right)_T+\left(p_x\delta\bar{u}+p_y\delta\bar{v}+p_z\delta\bar{w}\right)_B+\left(p_x\delta\bar{u}+p_y\delta v+p_z\delta\bar{w}\right)_W\right]dsdz \tag{3.26}$$

From Eq. (3.1), by substituting into Eq. (3.26), and performing the integral w. r. t. *ds*, one obtains,

$$\delta V_2=\int_L\left[q_{xT}\delta u_T\left(z\right)+q_{xB}\delta u_B\left(z\right)+q_y\delta v\left(z\right)+q_{zT}\delta w_T\left(z\right)+q_{zB}\delta w_B\left(z\right)+m_T\delta\theta_T\left(z\right)+m_B\delta\theta_B\left(z\right)\right]dz \tag{3.27}$$

where the following equivalent line loads arise.

$$q_{zT}\left(z\right)=\int_S\left(p_{zT}+p_{zw}H_5\right)ds,\quad q_{zB}\left(z\right)=\int_S\left(p_{zB}+p_{zw}H_6\right)ds$$
$$q_y\left(z\right)=\int_S\left\{\left[p_{yT}+n_T\left(\partial p_{zT}/\partial z\right)\right]+\left[p_{yB}+n_B\left(\partial p_{zB}/\partial z\right)\right]+\left(p_{yw}\right)\right\}ds$$
$$q_{xT}\left(z\right)=\int_S\left\{\left[p_{xT}+x_T\left(\partial p_{zT}/\partial z\right)\right]+\left[p_{xw}H_1-n_wp_{yw}\left(dH_1/dy\right)+n_w\left(\partial p_{zw}/\partial z\right)H_1\right]\right\}ds$$
$$q_{xB}\left(z\right)=\int_S\left\{\left[p_{xB}+x_B\left(\partial p_{zB}/\partial z\right)\right]+\left[p_{xw}H_3-n_wp_{yw}\left(dH_3/dy\right)+n_w\left(\partial p_{zw}/\partial z\right)H_3\right]\right\}ds$$
$$m_T\left(z\right)=\int_S\left\{\left[x_Tp_{yT}-n_Tp_{xT}+x_Tn_T\left(\partial p_{zT}/\partial z\right)\right]+\left[p_{xw}H_2-n_wp_{yw}\left(d^2H_2/dy^2\right)+n_w\left(\partial p_{zw}/\partial z\right)H_2\right]\right\}ds$$
$$m_B\left(z\right)=\int_S\left\{\left[x_Bp_{yB}-n_Bp_{xB}+x_Bn_B\left(\partial p_{zB}/\partial z\right)\right]+\left[p_{xw}H_4-n_wp_{yw}\left(d^2H_4/dy^2\right)+n_w\left(\partial p_{zw}/\partial z\right)H_4\right]\right\}ds \tag{3.28}$$

3.7. Field equations and boundary conditions

From Eqs. (3.19)-(3.21), and (3.27), by substituting into Eq. (3.18), and performing integrations by parts, one obtains a coupled system governing the longitudinal-transverse response of the beam

$$\begin{bmatrix} P_{11}(\mathscr{D}) & P_{12}(\mathscr{D}) & P_{13}(\mathscr{D}) \\ P_{21}(\mathscr{D}) & P_{22}(\mathscr{D}) & P_{23}(\mathscr{D}) \\ P_{31}(\mathscr{D}) & P_{32}(\mathscr{D}) & P_{33}(\mathscr{D}) \end{bmatrix}_{3\times3} \begin{Bmatrix} w_T \\ w_B \\ v \end{Bmatrix}_{3\times1} = \begin{Bmatrix} q_{zT} \\ q_{zB} \\ q_y \end{Bmatrix}_{3\times1} \tag{3.29}$$

in which $\mathscr{D}$ denotes the differential operator and $P_{11} - P_{33}$ are defined as

$$P_{11}(\mathscr{D}) = -E\left(A_T + \frac{A_w}{4} + \frac{I_{xxw}}{h^2}\right)\mathscr{D}^2 + \frac{GA_w}{h^2} \quad , \quad P_{12}(\mathscr{D}) = P_{21}(\mathscr{D}) = -E\left(\frac{A_w}{4} - \frac{I_{xxw}}{h^2}\right)\mathscr{D}^2 - \frac{GA_w}{h^2}$$

$$P_{13}(\mathscr{D}) = P_{31}(\mathscr{D}) = -\frac{GA_w}{h}\mathscr{D} \quad , \quad P_{22}(\mathscr{D}) = -E\left(A_B + \frac{A_w}{4} + \frac{I_{xxw}}{h^2}\right)\mathscr{D}^2 + \frac{GA_w}{h^2},$$

$$P_{23}(\mathscr{D}) = P_{32}(\mathscr{D}) = \frac{GA_w}{h}\mathscr{D} \quad , \quad P_{33}(\mathscr{D}) = -E\left(I_{xxT} + I_{xxB}\right)\mathscr{D}^4 + GA_w\mathscr{D}^2$$

Also, one recovers the following possible boundary conditions for the problem.

$$\left[-Ew_T'\left(A_T + \frac{A_W}{4} + \frac{I_{xxW}}{h^2}\right) - Ew_B'\left(\frac{A_W}{4} - \frac{I_{xxW}}{h^2}\right) - \overline{N}_T\right]\delta w_T\Big|_0^L = 0$$

$$\left[-Ew_T'\left(\frac{A_W}{4} - \frac{I_{xxW}}{h^2}\right) - Ew_B'\left(A_B + \frac{A_W}{4} + \frac{I_{xxW}}{h^2}\right) - \overline{N}_B\right]\delta w_B\Big|_0^L = 0$$

$$\left[-\frac{GA_W}{h}\left(hv' + w_B - w_T\right) + Ev'''\left(I_{xxT} + I_{xxB}\right) - \overline{V}_y\right]\delta v\Big|_0^L = 0 \tag{3.30a-d}$$

$$\left[-Ev''\left(I_{xxT} + I_{xxB}\right) - \left(\overline{M}_{xT} + \overline{M}_{xB}\right)\right]\delta v'\Big|_0^L = 0$$

Likewise, one obtains the following system which describes the lateral-torsional response of the member

$$\begin{bmatrix} Q_{11}(\mathscr{D}) & Q_{12}(\mathscr{D}) & Q_{13}(\mathscr{D}) & Q_{14}(\mathscr{D}) \\ Q_{21}(\mathscr{D}) & Q_{22}(\mathscr{D}) & Q_{23}(\mathscr{D}) & Q_{24}(\mathscr{D}) \\ Q_{31}(\mathscr{D}) & Q_{32}(\mathscr{D}) & Q_{33}(\mathscr{D}) & Q_{34}(\mathscr{D}) \\ Q_{41}(\mathscr{D}) & Q_{42}(\mathscr{D}) & Q_{34}(\mathscr{D}) & Q_{44}(\mathscr{D}) \end{bmatrix} \begin{Bmatrix} u_T \\ \theta_T \\ u_B \\ \theta_B \end{Bmatrix} = \begin{Bmatrix} q_{xT} \\ m_T \\ q_{xB} \\ m_B \end{Bmatrix} \tag{3.31}$$

where the differential operators $Q_{11} - Q_{44}$ are defined as

$$Q_{11}(\mathscr{D}) = \left[EI_{yyT} + \frac{13Dh}{35}\right]\mathscr{D}^4 - \frac{12D}{5h}\mathscr{D}^2 + \frac{12D}{h^3}$$

$$Q_{12}(\mathscr{D}) = Q_{21}(\mathscr{D}) = \frac{11Dh^2}{210}\mathscr{D}^4 - \frac{D}{5}\mathscr{D}^2 + \frac{6D}{h^2}$$

$$Q_{22}(\mathscr{D}) = \left[EI_{\omega\omega T} + \frac{h^3 D}{105}\right]\mathscr{D}^4 - \left[GJ_T + \frac{4Dh}{15}\right]\mathscr{D}^2 + \frac{4D}{h}$$

$$Q_{13}(\mathscr{D}) = Q_{31}(\mathscr{D}) = \frac{9Dh}{70}\mathscr{D}^4 + \frac{36D}{15h}\mathscr{D}^2 - \frac{12D}{h^3}$$

$$Q_{23}(\mathscr{D}) = Q_{32}(\mathscr{D}) = \frac{13Dh^2}{420}\mathscr{D}^4 + \frac{D}{5}\mathscr{D}^2 - \frac{6D}{h^2}$$

$$Q_{14}(\mathscr{D}) = Q_{41}(\mathscr{D}) = \frac{-13Dh^2}{420}\mathscr{D}^4 - \frac{D}{5}\mathscr{D}^2 + \frac{6D}{h^2}$$

$$Q_{24}(\mathscr{D}) = Q_{42}(\mathscr{D}) = -\frac{h^3 D}{140}\mathscr{D}^4 + \frac{Dh}{15}\mathscr{D}^2 + \frac{2D}{h}$$

$$Q_{34}(\mathscr{D}) = Q_{43}(\mathscr{D}) = \frac{-11Dh^2}{210}\mathscr{D}^4 + \frac{D}{5}\mathscr{D}^2 - \frac{6D}{h^2}$$

$$Q_{33}(\mathscr{D}) = \left[EI_{yyB} + \frac{13Dh}{35}\right]\mathscr{D}^4 - \frac{36D}{15h}\mathscr{D}^2 + \frac{12D}{h^3}$$

$$Q_{44}(\mathscr{D}) = \left[EI_{\omega\omega B} + \frac{Dh^3}{105}\right]\mathscr{D}^4 - \left[GJ_B\mathscr{D}^2 + \frac{4Dh}{15}\right]\mathscr{D}^2 + \frac{4D}{h}$$

The associated boundary conditions are

$$\left[-\left(EI_{yyT} + \frac{13h}{35}D\right)u_T''' - \frac{D}{420}\left(22h^2\theta_T''' + 54hu_B''' - 13h^2\theta_B'''\right)\right.$$
$$\left. + \frac{D}{30h}(2-\nu)\left(36u_T' + 3h\theta_T' - 36u_B' + 3h\theta_B'\right) - \overline{V}_{xT}\delta u_T\right]_0^L = 0$$

$$\left[-\left(EI_{yyB} + \frac{13h}{35}D\right)u_B''' - \frac{D}{420}\left(54hu_T''' + 13h^2\theta_T''' - 22h^2\theta_B'''\right)\right.$$
$$\left. + \frac{D}{30h}(2-\nu)\left(-36u_T' - 3h\theta_T' + 36u_B' - 3h\theta_B'\right) - \overline{V}_{xB}\right]\delta u_B\Big|_0^L = 0$$

$$\left[\left(EI_{yyT}+\frac{13h}{35}D\right)u_T''+\frac{D}{420}\left(22h^2\theta_T''+54hu_B''-13h^2\theta_B''\right)\right.$$
$$\left.+\frac{D\nu}{30h}\left(-36u_T-3h\theta_T+36u_B-3h\theta_B\right)-\overline{M}_{yT}\right]\delta u_T'\Bigg|_0^L=0$$

$$\left[\left(EI_{yyB}+\frac{13h}{35}D\right)u_B''+\frac{D}{420}\left(54hu_T''+13h^2\theta_T''-22h^2\theta_B''\right)\right.$$
$$\left.+\frac{D\nu}{30h}\left(36u_T+3h\theta_T-36u_B+3h\theta_B\right)-\overline{M}_{yB}\right]\delta u_B'\Bigg|_0^L=0$$

$$\left[-\left(EI_{\omega\omega T}+\frac{h^3}{105}D\right)\theta_T'''-\frac{D}{420}\left(22h^2u_T'''+13h^2u_B'''-3h^3\theta_B'''\right)\right.$$
$$\left.+\frac{D\nu}{30h}(2-\nu)\left(3hu_T'+4h^2\theta_T'-3hu_B'-h^2\theta_B'\right)+GJ_T\theta_T'-\overline{T}_T\right]\delta\theta_T\Bigg|_0^L=0$$

$$\left[-\left(EI_{\omega\omega B}+\frac{h^3}{105}D\right)\theta_B'''-\frac{D}{420}\left(-13h^2u_T'''-3h^3\theta_T'''-22h^2u_B'''\right)\right.$$
$$\left.+\frac{D\nu}{30h}(2-\nu)\left(3hu_T'-h^2\theta_T'-3hu_B'+4h^2\theta_B'\right)+GJ_B\theta_B'-\overline{T}_B\right]\delta\theta_B\Bigg|_0^L=0$$

$$\left[\left(EI_{\omega\omega T}+\frac{h^3}{105}D\right)\theta_T''+\frac{D}{420}\left(22h^2u_T''+13h^2u_B''-3h^3\theta_B''\right)\right.$$
$$\left.+\frac{D\nu}{30h}\left(-3hu_T-4h^2\theta_T+3hu_B+h^2\theta_B\right)-\overline{B}_T\right]\delta\theta_T'\Bigg|_0^L=0$$

$$\left[\left(EI_{\omega\omega B}+\frac{h^3}{105}D\right)\theta_B''+\frac{D}{420}\left(-13h^2u_T''-3h^3\theta_T''-22h^2u_B''\right)\right.$$
$$\left.+\frac{D\nu}{30h}\left(-3hu_T+h^2\theta_T+3hu_B-4h^2\theta_B\right)-\overline{B}_B\right]\delta\theta_B'\Bigg|_0^L=0$$

(3.32)a-h

3.8. Closed form solution

The total solution is the sum of the homogeneous solution, obtained by setting the right hand sides of Eqs. (3.29) and (3.31) to zero, and the load dependent particular integrals. In the following, the homogeneous solution for the longitudinal-transverse response is provided (Section 3.8.1) and for the torsional flexural response in Section 3.8.2, and the particular solution for general tractions is provided in Section 3.8.3.

3.8.1. Homogenous solution for the longitudinal-transverse response

For the longitudinal-transverse response, the displacements are assumed to take the exponential form

$$\left\langle w_{Th}(z), w_{Bh}(z), v_h(z)\right\rangle^T = C_i \left\langle \phi \right\rangle_i^T e^{c_i z} \tag{3.33}$$

in which $\left\langle \phi \right\rangle_i^T = \left\langle \overline{A_i}, \overline{B_i}, \overline{C_i}\right\rangle^T$. From Eq. (3.33) by substituting into Eq. (3.29), one obtains

$$\left([p_4]c_i^4 + [p_2]c_i^2 + [p_1]c_i + [p_0]\right)_{4\times 4}\{\phi_i\}_{4\times 1} = \{0\}_{4\times 1} \tag{3.34}$$

in which,

$$[p_0] = \frac{GA_w}{h^2}\begin{bmatrix} 1 & -1 & 0 \\ -1 & 1 & 0 \\ 0 & 0 & 0 \end{bmatrix}, \qquad [p_1] = \frac{GA_w}{h}\begin{bmatrix} 0 & 0 & -1 \\ 0 & 0 & 1 \\ -1 & 1 & 0 \end{bmatrix}, \qquad [p_4] = \begin{bmatrix} 0 & 0 & 0 \\ 0 & 0 & 0 \\ 0 & 0 & -E\left(I_{xxT} + I_{xxB}\right) \end{bmatrix}$$

$$[p_2] = \begin{bmatrix} -E\left(A_T + A_w/4 + I_{xxw}/h^2\right) & -E\left(A_w/4 - I_{xxw}/h^2\right) & 0 \\ -E\left(A_w/4 - I_{xxw}/h^2\right) & -E\left(A_B + A_w/4 + I_{xxw}/h^2\right) & 0 \\ 0 & 0 & GA_w \end{bmatrix}$$

The polynomial eigen-value problem in Eq. (3.34) can be converted to the equivalent linearized eigen-value problem

$$\left\{\left[\begin{array}{c:c:c:c} [0] & [p_2] & [p_1] & [p_0] \\ \hdashline -[I_3] & [0] & [0] & [0] \\ \hdashline [0] & -[I_3] & [0] & [0] \\ \hdashline [0] & [0] & -[I_3] & [0] \end{array}\right] + c_i \left[\begin{array}{c:c:c:c} [p_4] & [0] & [0] & [0] \\ \hdashline [I_3] & [0] & [0] & [0] \\ \hdashline [0] & [I_3] & [0] & [0] \\ \hdashline [0] & [0] & [I_3] & [0] \end{array}\right]\right\}_{12\times 12} \left\{\begin{array}{c} \{\phi\}_i \\ \hdashline c_i\{\phi\}_i \\ \hdashline c_i^2\{\phi\}_i \\ \hdashline c_i^3\{\phi\}_i \end{array}\right\}_{12\times 1} = \{0\}_{16\times 1} \tag{3.35}$$

where $\left[I_3\right]$ denotes the 3×3 identity matrix. The solution of Eq. (3.35) is solved for the 12 eigen-pairs (c_i , $\{\phi\}_i$). Only eight of the 12 eigen-values are finite. These consist of two distinct roots c_1 and c_2 and six zero roots. Thus, the solution takes the form,

$$\begin{Bmatrix} w_{Th}(z) \\ w_{Bh}(z) \\ v_h(z) \end{Bmatrix} = \sum_{i=1}^{2} C_i e^{c_i z} \begin{Bmatrix} \bar{A}_i \\ \bar{B}_i \\ \bar{C}_i \end{Bmatrix} + \sum_{i=3}^{8} C_i z^{i-3} \begin{Bmatrix} \bar{A}_i \\ \bar{B}_i \\ \bar{C}_i \end{Bmatrix}_i \tag{3.36}$$

From Eq. (3.36), by back-substitution into Eq. (3.29), one recovers 18 equations of which 12 are independent. Constants $\bar{A}_3 ... \bar{A}_6, \bar{B}_3, \bar{C}_3$ are set to unity and the remaining constants $\bar{A}_i, \bar{B}_i, \bar{C}_i$ are determined from the 12 independent equations, yielding the solution

$$\begin{Bmatrix} w_{Th}(z) \\ w_{Bh}(z) \\ v_h(z) \end{Bmatrix} = \left[\left[\Phi_e(z)\right]_{3\times2} \quad \left[\Phi_p(z)\right]_{3\times6} \right] \{C\}_{8\times1} \tag{3.37}$$

in which $\langle C \rangle^T_{8\times1} = \langle C_1 \quad C_2 \quad .... \quad C_8 \rangle$ is a vector of integration constants to be determined from the boundary conditions of the problem. Matrix $\left[\Phi_e(z)\right] = \left[\{\phi_1\}_{3\times1} e^{c_1 z} \quad \{\phi_2\}_{3\times1} e^{c_2 z} \right]$ consists of the eigen-vectors $\{\phi_1\}, \{\phi_2\}$ corresponding to the two distinct roots c_1 and c_2 obtained by solving Eq. (3.35), respectively multiplied by the exponential functions $e^{c_1 z}, e^{c_2 z}$, and

$$\left[\Phi_p(z)\right] = \left[\begin{array}{c:c:c:c:c:c} 1 & z & z^2 + \alpha_1 z^4 & z^3 + \alpha_2 z^5 & 0 & 0 \\ 0 & z & \alpha_4 z^2 + \alpha_1 z^4 & \alpha_3 z + \alpha_4 z^3 + \alpha_2 z^5 & 1 & 0 \\ \alpha_5 z & 0 & \alpha_6 z + \alpha_8 z^3 & \alpha_7 z^2 + \alpha_9 z^4 & -\alpha_5 z & 1 \end{array} \right] \tag{3.38}$$

in which

$$\alpha_1 = \frac{\left(P_6^2 - P_3P_7\right)\left(P_1 + 2P_4 + P_2\right)}{12P_3\left(P_1 + P_4\right)\left(P_2 + P_4\right)}, \alpha_2 = -\frac{\left(P_6^2 - P_3P_7\right)\left(P_1 + P_2 + 2P_4\right)}{20P_3\left(P_4 + P_2\right)^2}$$

$$\alpha_3 = -6\frac{\left[P_1P_5P_6^2 \ - P_3^2P_4^2 + 2P_4P_5P_6^2 + P_1P_2P_3^2 + P_2P_4P_6^2\right]}{P_3\left(P_2 + P_4\right)\left(P_6^2 - P_3P_7\right)}, \alpha_4 = -\frac{P_1 + P_4}{P_2 + P_4}, \alpha_5 = -\frac{P_7}{P_6},$$

$$\alpha_6 = 2P_4\frac{\left(P_1 + P_4\right)}{P_6\left(P_4 + P_2\right)} - \frac{2P_1}{P_6}, \alpha_7 = -3P_6\frac{P_5P_7\left(P_1 + 2P_4 + P_2\right) - P_3\left(P_4^2 - P_1P_2\right)}{P_3\left(P_4 + P_2\right)\left(P_6^2 - P_3P_7\right)}$$

$$\alpha_8 = -P_6\frac{\left(P_1 + 2P_4 + P_2\right)}{3P_3\left(P_4 + P_2\right)}, \alpha_9 = -P_6\frac{\left(P_1 + 2P_4 + P_2\right)}{4P_3\left(P_4 + P_2\right)}$$

and $P_1 - P_7$ are defined as

$$P_1 = -E\left(A_T + \frac{A_w}{4} + \frac{I_{xxw}}{h^2}\right), P_2 = -E\left(A_B + \frac{A_w}{4} + \frac{I_{xxw}}{h^2}\right), P_3 = GA_w, P_4 = -E\left(\frac{A_w}{4} - \frac{I_{xxw}}{h^2}\right)$$

$$P_5 = -E\left(I_{xxT} + I_{xxB}\right), P_6 = -\frac{GA_w}{h}, P_7 = \frac{GA_w}{h^2}$$

3.8.2. Homogenous lateral-torsional response

For the lateral-torsional response, the displacements are assumed to take the exponential form

$$\left\langle u_{Th}(z), \theta_{Th}(z), u_{Bh}(z), \theta_{Bh}(z)\right\rangle^T = D_i \left\langle \psi\right\rangle_i^T e^{d_i z} \qquad (3.39)$$

in which $\left\langle \psi\right\rangle_i^T = \left\langle \overline{\overline{A_i}}, \overline{\overline{B_i}}, \overline{\overline{C_i}}, \overline{\overline{D_i}}\right\rangle^T$. From Eq. (3.39) by substituting into Eq. (3.31), one obtains

$$\left(\left[q_2\right]d_i^4 + \left[q_1\right]d_i^2 + \left[q_0\right]\right)_{4\times4}\left\{\psi_i\right\}_{4\times1} = \left\{0\right\}_{4\times1} \qquad (3.40)$$

in which,

$$\left[q_0\right] = \frac{2D}{h^3}\begin{bmatrix} 6 & 3h & -6 & 3h \\ 3h & 2h^2 & -3h & h^2 \\ -6 & -3h & 6 & -3h \\ 3h & h^2 & -3h & 2h^2 \end{bmatrix}, \left[q_1\right] = \frac{D}{5h}\begin{bmatrix} -12 & -h & 12 & -h \\ -h & -5hGJ_T/D - 4h^2/3 & h & h^2/3 \\ 12 & h & -12 & h \\ -h & h^2/3 & h & -5hGJ_T/D - 4h^2/3 \end{bmatrix}$$

$$\left[q_2\right] = \begin{bmatrix} EI_{yyT} + 13Dh/35 & 11Dh^2/210 & 9Dh/70 & -13Dh^2/420 \\ 11Dh^2/210 & EI_{\omega\omega T} + Dh^3/105 & 13Dh^2/420 & -Dh^3/420 \\ 9Dh/70 & 13Dh^2/420 & EI_{yyB} + 13Dh/35 & -11Dh^2/210 \\ -13Dh^2/420 & -Dh^3/420 & -11Dh^2/210 & EI_{\omega\omega B} + Dh^3/105 \end{bmatrix}$$

The polynomial eigen-value problem in Eq. (3.34) is then converted to the equivalent linearized eigen-value problem

$$\left\{\begin{bmatrix}[q_1] & [q_0]\\ -[I_4] & [0]\end{bmatrix}_{8\times8} + m_j\begin{bmatrix}[q_2] & [0]\\ [I_4] & [0]\end{bmatrix}_{8\times8}\right\}\begin{Bmatrix}\{\psi\}_i\\ m_j\{\psi\}_i\end{Bmatrix}_{8\times1} = \{0\}_{8\times1} \tag{3.41}$$

in which, $m_j = d_i^2$ and $[I_4]$ denotes the 4×4 identity matrix. Equation (3.41) is solved for the eight eigen-pairs ($m_j, \{\psi\}_j$, $j=1...8$), resulting in 16 eigen-pairs $\left(d_i = \pm\sqrt{m_j}, \{\psi_i\}\right)$, $\quad i=1...16$. Ten out of the 16 eigen-values, $i=1...10$ are observed to be distinct while the remaining six roots $i=11...16$ are observed to vanish. The solution thus takes the form

$$\begin{Bmatrix}u_{Th}(z)\\ \theta_{Th}(z)\\ u_{Bh}(z)\\ \theta_{Bh}(z)\end{Bmatrix} = \sum_{i=1}^{10} D_i e^{d_i z}\begin{Bmatrix}\overline{\overline{A}}_i\\ \overline{\overline{B}}_i\\ \overline{\overline{C}}_i\\ \overline{\overline{D}}_i\end{Bmatrix} + \sum_{i=11}^{16} D_i z^{i-11}\begin{Bmatrix}\overline{\overline{A}}_i\\ \overline{\overline{B}}_i\\ \overline{\overline{C}}_i\\ \overline{\overline{D}}_i\end{Bmatrix} = \left[\left[\Psi_e(z)\right]_{4\times10} \quad \left[\Psi_p(z)\right]_{4\times6}\right]\{D\}_{16\times1} \tag{3.42}$$

In the right hand side of Eq. (3.42), $\langle D\rangle^T_{16\times1} = \langle D_i \quad D_2 \quad .... \quad D_{16}\rangle^T$ is a vector of integration constants to be determined from the boundary conditions and matrix $\left[\Psi_e(z)\right] = \left[\{\psi_1\}_{4\times1}e^{d_1 z} \;\vdots\; \{\psi_2\}_{4\times1}e^{d_2 z} \;\vdots\; ... \;\vdots\; \{\psi_{10}\}_{4\times1}e^{d_{10} z}\right]$ consists of eigen-vectors $\{\psi_1\}$ to $\{\psi_{10}\}$ corresponding to the distinct roots d_1 - d_{10} obtained by solving Eq. (3.41), respectively, multiplied by the exponential functions $e^{d_1 z}$ to $e^{d_{10} z}$. The procedure for obtaining matrix $\left[\Psi_p(z)\right]_{4\times6}$ is provided in Appendix A.

3.8.3. **Particular solution**

Given general member tractions, the line loads $q_{zT}, q_{zB}, q_y, q_{xT}, q_{xB}, m_T, m_B$ can be determined from Eq. (3.28). These are then expanded as Fourier Series in terms of the longitudinal coordinate, i.e.,

$$\begin{aligned}&\langle q_{zT} \quad q_{zB} \quad q_y \quad q_{xT} \quad m_T \quad q_{xB} \quad m_B\rangle = \\ &\sum_{n=1}^{+\infty}\left\langle \cos\left(\frac{n\pi z}{L}\right) \quad \sin\left(\frac{n\pi z}{L}\right)\right\rangle_{1\times2}\left[\{\bar{q}_{zT}\}_n \quad \{\bar{q}_{zB}\}_n \quad \{\bar{q}_y\}_n \quad \{\bar{q}_{xT}\}_n \quad \{\bar{m}_T\}_n \quad \{\bar{q}_{xB}\}_n \quad \{\bar{m}_B\}_n\right]_{2\times7}\end{aligned} \tag{3.43}$$

where the Fourier coefficients $\left[\left\{\bar{q}_{zT}\right\}_n \quad \left\{\bar{q}_{zB}\right\}_n \quad \left\{\bar{q}_y\right\}_n \quad \left\{\bar{q}_{xT}\right\}_n \quad \left\{\bar{m}_T\right\}_n \quad \left\{\bar{q}_{xB}\right\}_n \quad \left\{\bar{m}_B\right\}_n\right]_{2\times 7}$ are determined from

$$\begin{aligned}&\left[\left\{\bar{q}_{zT}\right\}_n \quad \left\{\bar{q}_{zB}\right\}_n \quad \left\{\bar{q}_y\right\}_n \quad \left\{\bar{q}_{xT}\right\}_n \quad \left\{\bar{m}_T\right\}_n \quad \left\{\bar{q}_{xB}\right\}_n \quad \left\{\bar{m}_B\right\}_n\right]_{2\times 7}\\ &\quad =\int_0^L \begin{Bmatrix}\cos\left(n\pi z/L\right)\\ \sin\left(n\pi z/L\right)\end{Bmatrix}\left\langle q_{zT} \quad q_{zB} \quad q_y \quad q_{xT} \quad m_T \quad q_{xB} \quad m_B\right\rangle_{1\times 7}^T dz\end{aligned} \tag{3.44}$$

From Eq. (3.43), by substituting into the right hand sides of Equilibrium Equations (3.29) and (3.31), one can express the particular solution $\left\langle w_{Tp}(z), w_{Bp}(z), v_p(z), u_{Tp}(z), \theta_{Tp}(z), u_{Bp}(z), \theta_{Bp}(z)\right\rangle^T$ in the form

$$\begin{aligned}&\left\langle w_{Tp}(z), w_{Bp}(z), v_p(z), u_{Tp}(z), \theta_{Tp}(z), u_{Bp}(z), \theta_{Bp}(z)\right\rangle^T =\\ &\sum_{n=1}^{\infty}\left\langle \left\{S_1\right\}_n, \left\{S_2\right\}_n, \left\{S_3\right\}_n, \left\{S_4\right\}_n, \left\{S_5\right\}_n, \left\{S_6\right\}_n, \left\{S_7\right\}_n\right\rangle_{7\times 2}^T \left\langle \cos\left(\frac{n\pi z}{L}\right) \quad \sin\left(\frac{n\pi z}{L}\right)\right\rangle_{2\times 1}^T\end{aligned} \tag{3.45}$$

where the unknown displacement constants $\left\{S_i\right\}_n, i=1\ldots 7$ are expressed (Appendix B) in terms of the Fourier load terms $\left[\left\{\bar{q}_{zT}\right\}_n \quad \left\{\bar{q}_{zB}\right\}_n \quad \left\{\bar{q}_y\right\}_n \quad \left\{\bar{q}_{xT}\right\}_n \quad \left\{\bar{m}_T\right\}_n \quad \left\{\bar{q}_{xB}\right\}_n \quad \left\{\bar{m}_B\right\}_n\right]_{2\times 7}$.

3.9. Numerical examples

In order to assess the results based on the present solution, several numerical examples are solved based on the present theory and comparisons are compared to shell FEA under Abaqus/CAE, the Euler-Bernoulli beam solution, the Timoshenko beam solution, and the Vlasov theory, where applicable. In all examples, a mono-symmetric WRF1000x340 steel section is considered (Fig. 3-5) with $E = 200,000 MPa, \nu = 0.3$.

The commercial software Abaqus 6.11-1 is utilized to develop a 3D shell FEA model. The model is based on the S4R shell element, which has four nodes with six degrees of freedom per node of which five are independent. The element adopts reduced integration to avoid shear locking.

3.9.1. Example 1: Longitudinal-transverse response

A cantilever is subjected to a transverse force *P*=1,000 kN acting on the tip, Fig. 3-5 (i.e., the beam is loaded and is deforming in the plane of the web). The cantilever span is assumed to vary up to 6.00 m. For each span, the tip displacement is predicted through (a) the conventional Euler-Bernoulli beam theory which does not capture shear deformation v_{E-B}, (b) through the shear-deformable Timoshenko Theory, v_T, (c) the present theory, and (d) the shell finite element S4R in Abaqus and the results are compared in Fig. 3-5. For the shown beam, the transverse displacement v_{EB} as predicted by the Euler-Bernoulli theory is $v_{EB} = P\left(3Lz^2 - z^3\right)/6EI_x$. Under the Timoshenko theory, the displacement is $v_T = P\left(3Lz^2 - z^3\right)/6EI_x + Pz/GAK_{sx}$ where the shear correction factor is obtained as from

$$K_{sx} = \left[\left(A/I^2\right)\int_s \left(Q_x^2(s)/t(s)\right)ds\right]^{-1} = 0.23$$ (e.g.,Iyer (2005)).

In the Abaqus model, 40 elements are taken along the web height, 11 along the top half flange and six elements along the bottom half flange. Forty elements per meter are taken along the longitudinal direction. For a span of 4.00m, this corresponds to 71,040 degrees of freedom. This compares to seven active degrees of freedom used to obtain the closed form solution within the present study.

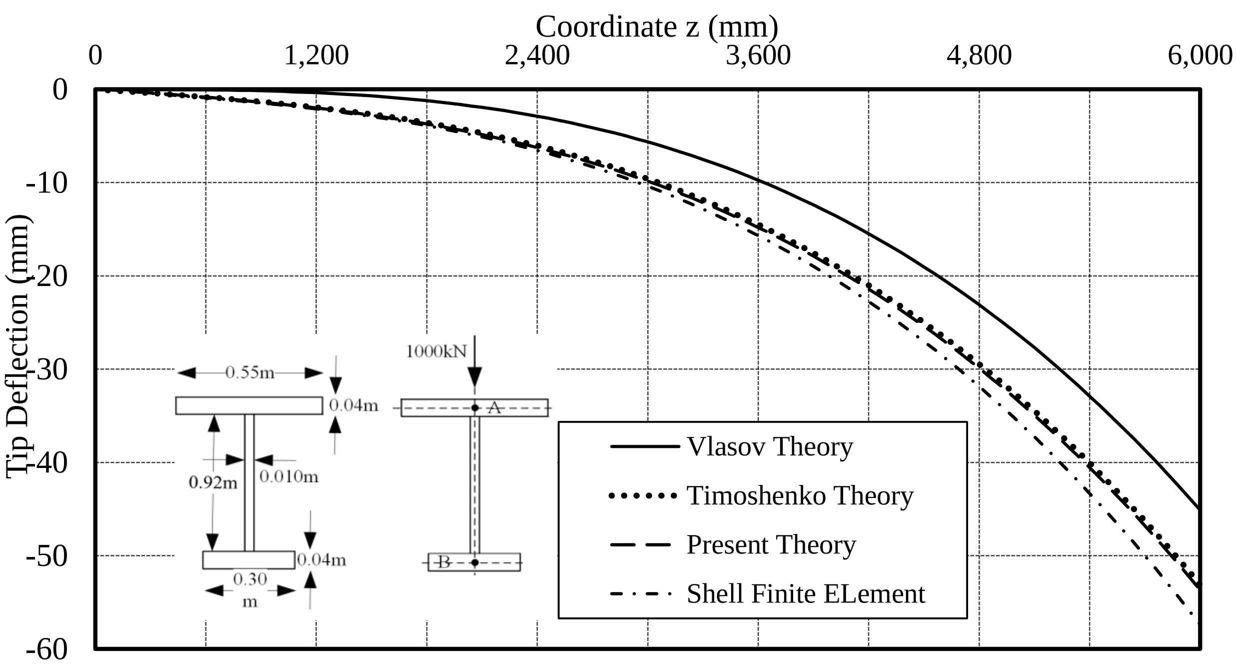

Fig. 3-5. Tip deflection for transversely loaded beams

In the shell finite element analysis, the average of the vertical displacements at points A and B are displayed. A summary of the tip displacement results is provided in Table 3-2 for a 4.00 m span beam. The present theory is shown to agree within 4.5% with the Abaqus solution, in very close agreement with the Timoshenko beam solution. The difference between the present theory and Abaqus is attributed to the fact, that unlike the shell solution, the present theory does not account for the compressibility of the web in the vertical direction under the vertical load. The Euler Bernoulli beam solution provides significantly lower displacement predictions than all three other solutions, since it does not capture shear deformation effects, which are significant for such a deep beam.

Table 3-2 Vertical displacement at the tip of 4.00 m span cantilever

Method of Analysis	Vertical Displacement (mm)	Percentage difference relative to Abaqus solution
Abaqus-S4R shell solution	20.1	-
Present theory	19.2	4.5%
Timoshenko beam	19.1	5.2%
Euler-Bernoulli beam	13.6	35.3%

3.9.2. Example 2: Cantilever under torsion

A 4.00 m span cantilever is subjected to two parallel and opposite 20 kN forces (Fig. 3-6a) inducing a 19.2 kNm twisting moment. It is required to determine the angle of twist along the beam under Vlasov theory, the present study and shell finite element for each span. The Abaqus mesh is taken identical to that of Example 1.

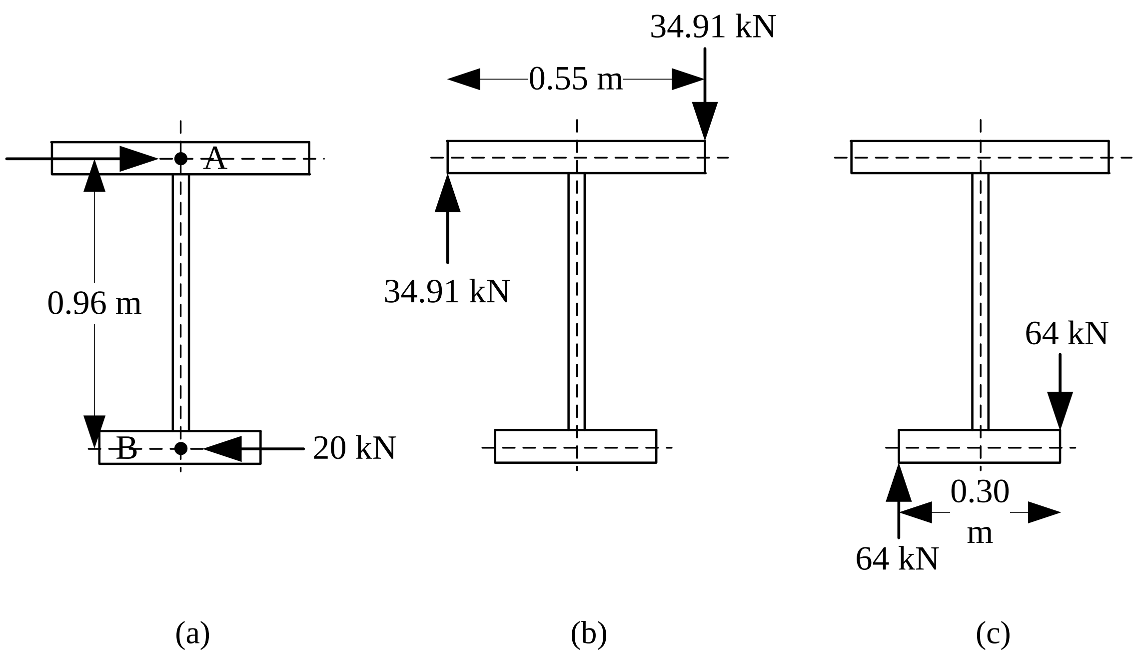

Fig. 3-6. Three scenarios for applying a twisting moment 19.2 kNm; a) Case a-Examples 2 and 3, b) Case b-Example 3, and c) Case c-Example 3

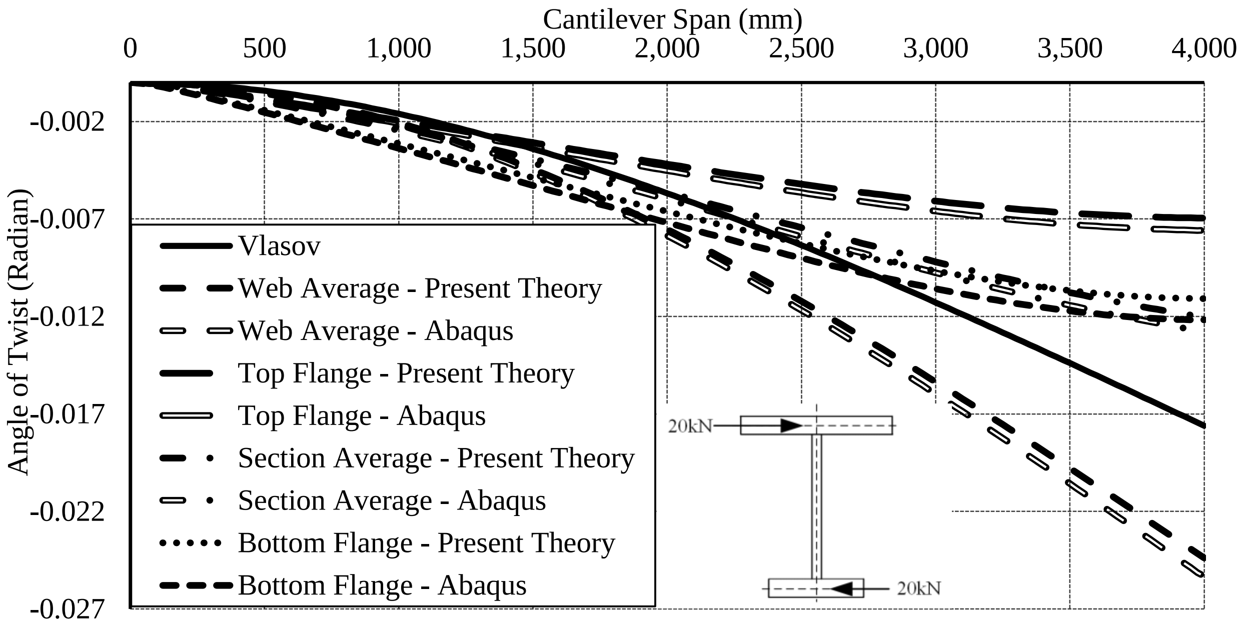

Fig. 3-7. Angles of twist along the cantilever span

For a solution which captures distortion, such as the present theory, or such as the Abaqus shell FEA, each point of the cross-section has a distinct angle of twist. Thus, it is convenient, when comparing against the Vlasov theory, to define an area-weighted average angle for the angle of twist $\bar{\theta}_w$ and $\bar{\theta}_s$ for the web and for the entire cross-section respectively, i.e.,

$$\bar{\theta}_w(z) = \frac{1}{A_W}\int_{A_w} \theta(s,z)\,dA, \qquad \bar{\theta}_s(z) = \frac{1}{A}\int_{A} \theta(s,z)\,dA \tag{3.46}$$

When evaluating the average angle of twist based on the present theory $\bar{\theta}_{th}$, the integral terms in Eqs. (3.46) are explicitly determined from the known distortional functions, while for the FEA model, the average angle of twist $\bar{\theta}_{FEA}$, is computed numerically. Fig. 3-7 shows that the angles of twist as predicted by the present theory are in very good agreement with those predicted by the Abaqus model. This is the case for both flanges, the average angle of twist of the web, and that of the cross-section as defined in Eqs. (3.46). For a span of 4.00m, the web average angle of twist as predicted by the present theory is $2.44\times10^{-2}\,rad$ while that predicted by Abaqus is $2.53\times10^{-2}\,rad$ corresponding to a 3.56% difference. The section average angle of twist by the present theory is $1.20\times10^{-2}\,rad$ which compares to $1.27\times10^{-2}\,rad$ based on Abaqus, corresponding to a 5.51% difference.

It is worthwhile to note that, close to the cantilever root, the Vlasov theory predicts a lower angle compared to the average angle of twist as predicted by the present theory and Abaqus. In contrast, at the tip, the Vlasov theory predicts a higher angle of twist that is significantly higher than that of the average angle of twist as predicted by the present theory. It is also of interest to note that near the tip, the average angle of twist for the web is significantly higher than that based on the Vlasov theory. In contrast the angles of twist of the flanges happen to be smaller than the angle of twist as predicted by the Vlasov theory.

3.9.3. **Example 3: Cantilever under various types of twisting moments**

A 3.00 m span cantilever (WRF1000x340) is subjected to a 19.2 kNm twisting moments at the tip using three different loading schemes as shown in Fig. 3-6a-c. In Case (a), two horizontal forces are applied at the web to flange junction, while in Cases (b) and (c) vertical loads are applied to the top and bottom flange as shown. Within the Vlasov theory, the solution for all three loading scenarios yields identical results. This is due to facts that all three loading scenarios yield the same equivalent twisting moment, $T = 19.2kNm$, which is conjugate to the same angle of twist, $\theta(L)$, in all cases.

Under the present theory (in Case (a)), the conjugate of term $\delta u_T(L)$ as given in Eq. (3.32)a is set equal to $V_{xT} = 20kN$, i.e.,

$$\left[-\left(EI_{yyT} + \frac{13hD}{35}\right)u_T''' - \frac{D}{420}\left(22h^2\theta_T''' + 54hu_B''' - 13h^2\theta_B'''\right) + \frac{D}{30h}(2-\nu)\left(36u_T' + 3h\theta_T' - 36u_B' + 3h\theta_B'\right)\right]_L = V_{xT}$$

Also, the conjugate of term $\delta u_B(L)$ as given in Eq. (32.b) is set to $V_{xB} = -20kN$, i.e.,

$$\left[-\left(EI_{yyB} + \frac{13hD}{35}\right)u_B''' - \frac{D}{420}\left(54hu_T''' + 13h^2\theta_T''' - 22h^2\theta_B'''\right) + \frac{D}{30h}(2-\nu)\left(-36u_T' - 3h\theta_T' + 36u_B' - 3h\theta_B'\right)\right]_L = V_{xB}$$

In Case (b), the conjugate term of $\delta\theta_T(L)$ in Eq. (33. e) is set $T_T = 19.2kNm$, i.e.,

$$\left[-\left(EI_{\omega\omega T} + \frac{h^3}{105}D\right)\theta_T''' - \frac{D}{420}\left(22h^2u_T''' + 13h^2u_B''' - 3h^3\theta_B'''\right)\right.$$
$$\left. + \frac{D\nu}{30h}(2-\nu)\left(3hu_T' + 4h^2\theta_T' - 3hu_B' - h^2\theta_B'\right) + GJ_T\theta_T'\right] = T_T$$

In Case (c), the conjugate term of $\delta\theta_B(L)$ in Eq. (33. f) is set to $T_B = 19.2kNm$, i.e.,

$$\left[-\left(EI_{\omega\omega T}+\frac{h^3}{105}D\right)\theta_T''''-\frac{D}{420}\left(22h^2u_T''''+13h^2u_B''''-3h^3\theta_B''''\right)\right.$$
$$\left.+\frac{D\nu}{30h}(2-\nu)\left(3hu_T'+4h^2\theta_T'-3hu_B'-h^2\theta_B'\right)+GJ_T\theta_T'\right]=T_B$$

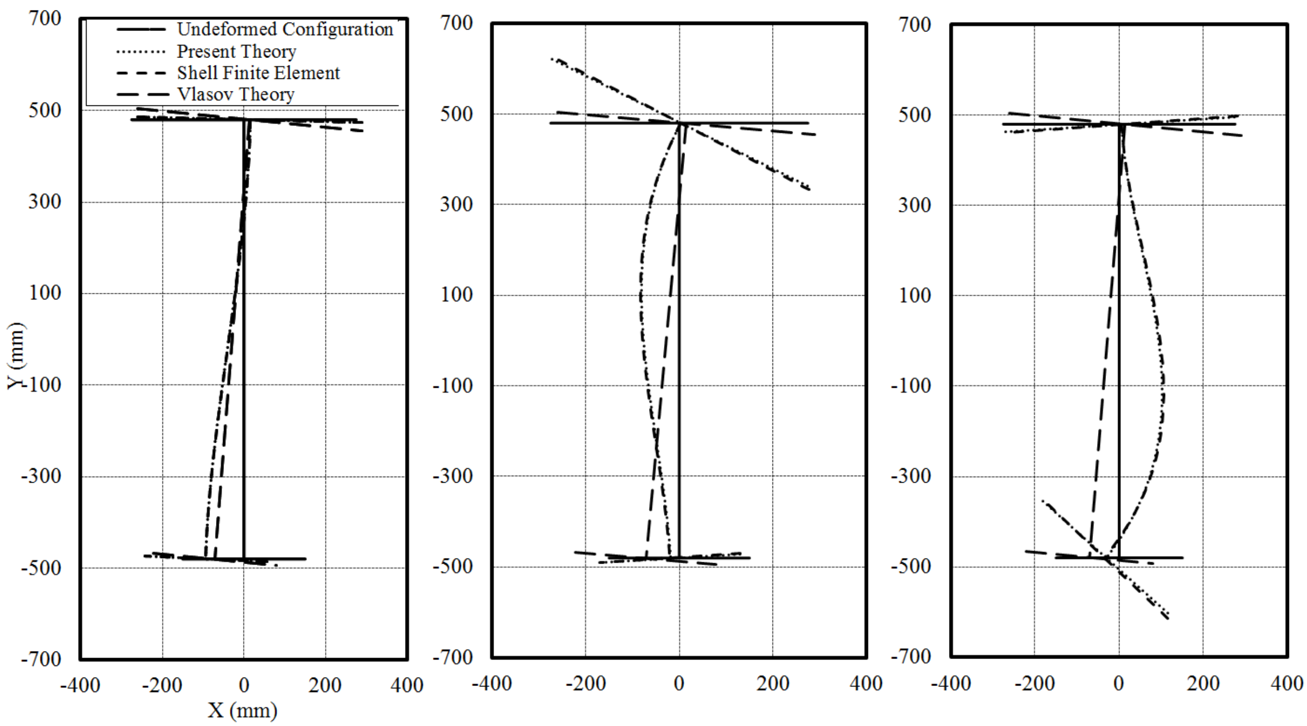

(a) (b) (c)

Fig. 3-8. Cross section deformed configuration at the tip for cases (a), (b) and (c), (Displacement amplification factor=10)

Figure 8 provides the deformed configuration of the cross section at the cantilever tip for all loading scenarios. In Case (a), where torsion is induced by horizontal forces, the twisting action is predominantly resisted by the flexural action of both flanges about the y axis, as well as the flexural resistance of the web about the *z* axis. In contrast, in Cases (b) and (c), torsion is induced by vertical forces, and are predominantly resisted by the twisting resistance of the top flange (in Case b) and the bottom flange (in Case c), as well as the flexural resistance of the web about the *z* axis. Given that the flexural resistance of the flanges about the y axis are significantly higher than their twisting resistance, it is evident that the twisting moment applied under Case (a) induces less distortion than Cases (b) and (c). Also, since the top flange is larger than the bottom flange, the distortional deformation in case (b) is smaller than that of Case (c).

3.9.4. **Example 4: Cantilever beam with restrained top flange**

A 3.0 m span cantilever (cross-section is identical to that of previous examples) is fully restrained by a continuous lateral and torsional support along the top flange. The beam is subjected to a concentrated 40 kN lateral load acting at the cantilever tip, applied at the bottom flange. The S4R shell mesh adopted in Abaqus is similar to that of Example 1. A total number of 120 elements are taken along the longitudinal direction, corresponding to 53,280 degrees of freedom. Within the present theory, the problem is solved by setting $\theta_T(z)=0, u_T(z)=0$, in Eq. (3.31), yielding two coupled equations in the remaining two displacement fields $\theta_B(z), u_B(z)$.

Fig. 3-9 shows the deformed shape of the cross section at the tip as predicted by both studies. Excellent agreement is obtained between the present solution and Abaqus. It is of interest to note that under the Vlasov theory, the solution would yield zero displacements and angle of twist given the continuous lateral and twist restraint and given that the theory does not capture distortion.

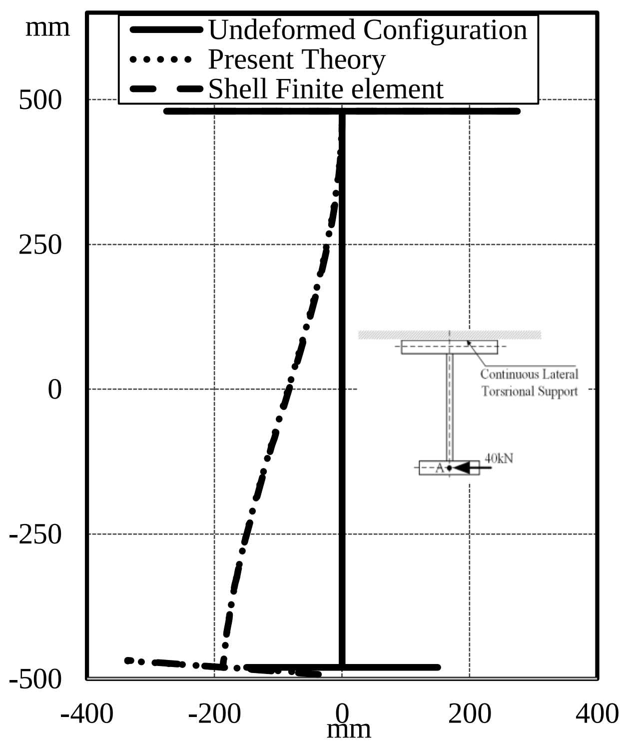

Fig. 3-9. Deformed shape of the cross section at the tip with restrained top flange, (Displacement amplification factor=10)

3.9.5. Example 5: Cantilever under transverse uniform distributed load

A 4.00m span cantilever (WRF1000x340) is subject to 50 kN/m uniform line load applied at an eccentricity $x_0 = s_0 = 0.20\,m$ from the web to flange junction (Fig. 3-10). To obtain the particular solution for the problem, the tractions corresponding to the line load can be expressed as $p_y(s, n=0, z) = 50\bar{\delta}(s-0.20)\ kN/m^2$, where $\bar{\delta}$ denotes the Dirac delta function, which has been adopted to apply localized tractions at the load line of application $s = 0.2\,m$. This is then substituted into Eqs. (3.28), yielding a vertical line load $q_y(z) = 50\,kN/m$ and top flange distributed twisting moments $m_T(z) = 10\,kN/m$. The procedure described under Section 3.8.3 is then implemented. A convergence study indicated that (n=35) Fourier terms are needed to represent the loads. Additional terms were observed not to change the results within three significant digits. The displacements and angles of twist at the tip of the cantilever are provided in Table 3-3.

Table 3-3 Displacements and angles of twist at the tip of the cantilever

Displacements (mm/Rad)	u_T (mm)	θ_T (rad)	u_B (mm)	θ_B (rad)	w_T (mm)	w_B (mm)	v (mm)
Present Theory	-1.10	-0.0589	6.78	0.0103	-0.123	0.198	1.56
3D Shell FEA	-1.13	-0.0610	6.97	0.0110	-0.125	0.193	1.54
Difference %	2.6	3.4	2.9	6.3	1.6	2.5	1.3

The deformed configuration of the cantilever tip is shown in Fig. 3-10. Overlaid on the same plot is the deformed configuration as obtained from Abaqus. The lateral displacements of both flanges and the transverse displacement of the beam are provided in Fig. 3-11. Fig. 3-12 shows the angles of twist at both flanges. Excellent agreement between the predictions of the present theory and Abaqus is observed for all displacements.

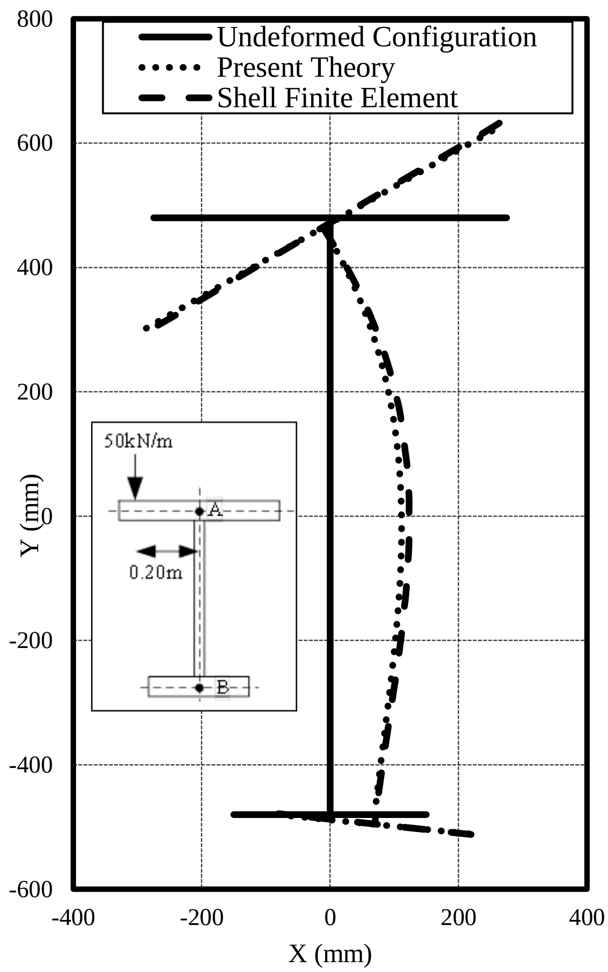

Fig. 3-10 Deformed configuration for cantilever subject to line load

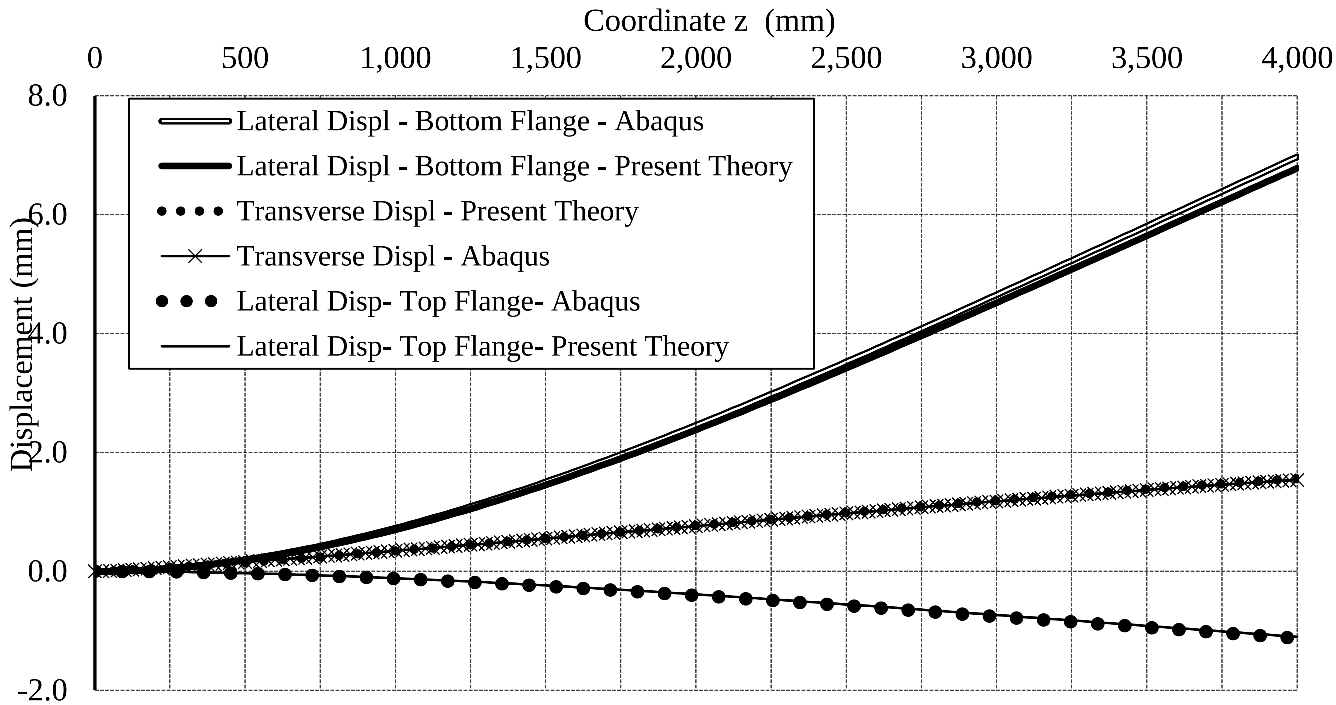

Fig. 3-11 Lateral displacements of top and bottom flanges and beam transvers displacement

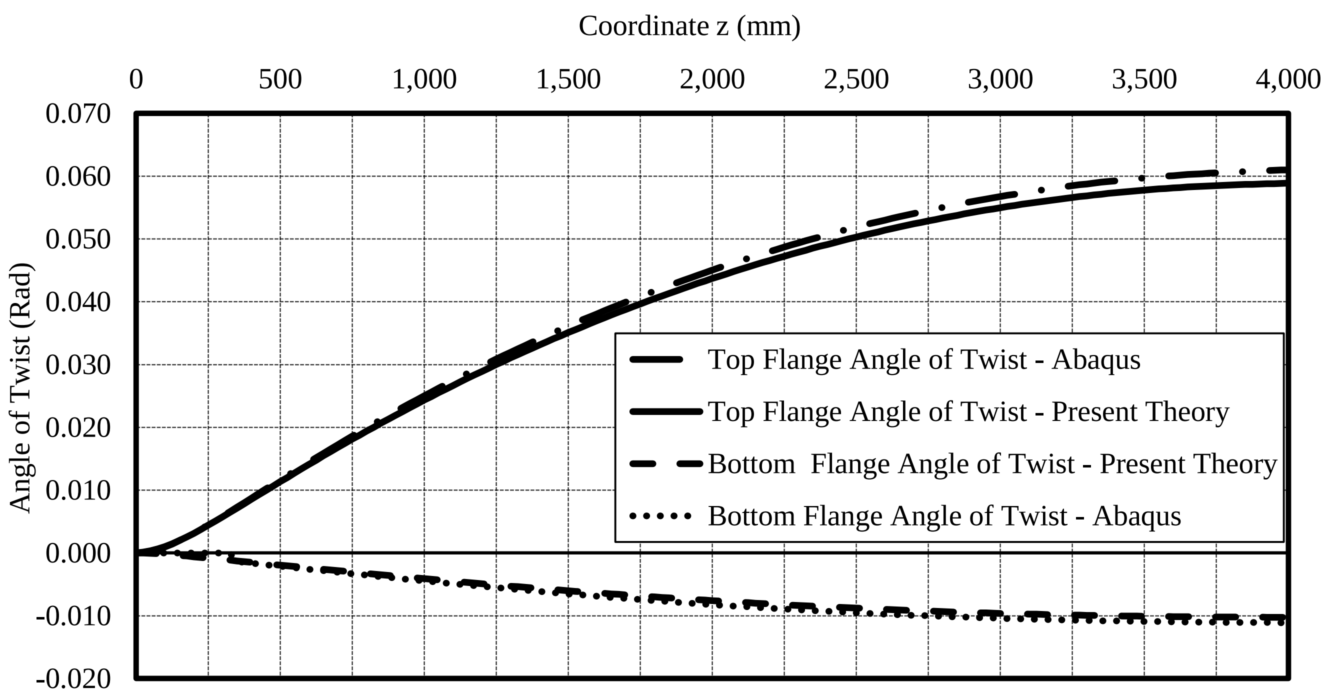

Fig. 3-12 Angles of twist of top and bottom flanges

3.10. **Summary and conclusions**

1. A new theory was developed for the analysis of mono-symmetric wide flange steel beams which incorporates web distortional effects, shear deformation effects in the web, as well as local and global warping effects.
2. The theory leads to two sets of coupled differential equations of equilibrium describing the longitudinal-transverse and lateral-torsional responses through seven displacement fields. The theory also provides the possible boundary conditions associated with the field equations.
3. General closed form solutions for the coupled equations were then developed of the resulting field equations.
4. The theory was applied to solve problems involving longitudinal-transverse responses, torsion, a beam with one flange restrained and a beam under eccentric line loads. Results were compared to those based on the Timoshenko beam theory, the Vlasov thin-walled beam theory, and 3D Shell finite element modeled in Abaqus. The results are shown to agree well with Abaqus FEA results with very few degrees of freedom.
5. The theory provides insight on the torsional behaviour of steel sections and the way it is influenced by distortional effects. Unlike the conventional Vlasov theory, the present theory shows that the response of a beam greatly depends upon the type of twisting moments applied to a section. All conclusions are confirmed by shell FEA predictions.
6. A cantilever under twisting moments is observed to generally exhibit distinct angles of twist at the top and bottom flange. The angles of twist at the tip are typically less than those predicted by the Vlasov theory. However, the average angle of twist of the web is typically larger than that predicted by the Vlasov theory.
7. For the problems investigated, the average angle of twist for the whole section was shown to be larger than that of the Vlasov theory near the cantilever root, but typically smaller at the cantilever tip.
8. The formulation lends itself naturally to model continuous lateral and/or constraints at any of the flanges to simulate cases, for instance, where one of the flanges is connected to a concrete slab while capturing the distortional response of the web and the lateral and torsional response of the unconnected flange.

3.11. **Appendix A**

This appendix provides the homogeneous solution for the torsional-flexural response. From Eq. (3.42) by setting constants $\overline{\overline{A}}_{11}...\overline{\overline{A}}_{16}=1.0$ and substituting the polynomial component of the solution

$$\begin{Bmatrix} u_{Th}(z) \\ \theta_{Th}(z) \\ u_{Bh}(z) \\ \theta_{Bh}(z) \end{Bmatrix}_p = \sum_{i=11}^{16} D_i z^{i-11} \begin{Bmatrix} 1 \\ \overline{\overline{B}}_i \\ \overline{\overline{C}}_i \\ \overline{\overline{D}}_i \end{Bmatrix} \tag{3.47}$$

into Equations (3.31), one recovers 24 equations of which 18 are independent. The remaining constants $\overline{\overline{B}}_i, \overline{\overline{C}}_i, \overline{\overline{D}}_i \quad (i=11..16)$ are determined from the 18 independent equations through

$$\left[\left[C_a\right]_{18\times 6} \;\vdots\; \left[C_j\right]_{18\times 18} \right] \begin{Bmatrix} \left\{\overline{\overline{A}}\right\}_{6\times 1} \\ \left\{\overline{\overline{J}}\right\}_{18\times 1} \end{Bmatrix} = \{0\}_{24\times 1} \tag{3.48}$$

in which $\left\langle \overline{\overline{A}} \right\rangle^T_{1\times 6} = \left\langle \overline{\overline{A}}_{11} \quad \overline{\overline{A}}_{12} \quad ... \quad \overline{\overline{A}}_{16} \right\rangle = \langle 1 \quad 1 \quad 1 \quad 1 \quad 1 \quad 1 \rangle$, $\left\langle \overline{\overline{J}} \right\rangle_{1\times 18} = \left\langle \left\langle \overline{\overline{B}} \right\rangle^T_{1\times 6} \quad \left\langle \overline{\overline{C}} \right\rangle^T_{1\times 6} \quad \left\langle \overline{\overline{D}} \right\rangle^T_{1\times 6} \right\rangle$, $\left\langle \overline{\overline{B}} \right\rangle^T_{1\times 6} = \left\langle \overline{\overline{B}}_{11} \quad \overline{\overline{B}}_{12} \quad ... \quad \overline{\overline{B}}_{16} \right\rangle$, $\left\langle \overline{\overline{C}} \right\rangle^T_{1\times 6} = \left\langle \overline{\overline{C}}_{11} \quad \overline{\overline{C}}_{12} \quad ... \quad \overline{\overline{C}}_{16} \right\rangle$ and $\left\langle \overline{\overline{D}} \right\rangle^T_{1\times 6} = \left\langle \overline{\overline{D}}_{11} \quad \overline{\overline{D}}_{12} \quad ... \quad \overline{\overline{D}}_{16} \right\rangle$. The entries of matrices $\left[C_a\right]$ and $\left[C_j\right]$ depend upon the section and material properties. The non-zero entries of matrix $\left[C_a\right]_{18\times 6}$ are

$$C_{a(1,1)} = C_{a(3,1)} = C_{a(4,2)} = C_{a(6,2)} = C_{a(8,3)} = C_{a(9,3)} = C_{a(11,4)} = C_{a(12,4)} = C_{a(14,5)} = C_{a(15,5)} = C_{a(17,6)} = C_{a(18,6)} = \frac{6D}{h^2}$$

$$C_{a(2,1)} = C_{a(5,2)} = -C_{a(7,3)} = -C_{a(10,4)} = -C_{a(13,5)} = -C_{a(16,6)} = -\frac{12D}{h^3}$$

$$C_{a(7,1)} = -\frac{48D}{h}, C_{a(10,2)} = -\frac{144D}{5h}, C_{a(13,3)} = -\frac{72D}{5h}, C_{a(16,4)} = -\frac{24D}{5h}$$

$$C_{a(8,1)} = C_{a(9,1)} = -4D, C_{a(11,2)} = C_{a(12,2)} = -\frac{12D}{5}, C_{a(15,3)} = C_{a(16,3)} = -\frac{6D}{5}$$

$$C_{a(17,4)} = C_{a(18,4)} = -\frac{2D}{5}, C_{a(13,1)} = 120EI_{yyT} + \frac{312hD}{7}, C_{a(16,2)} = 24EI_{yyT} + \frac{312hD}{35}$$

$$C_{a(14,1)} = \frac{44h^2D}{7}, C_{a(17,2)} = \frac{44h^2D}{35}, C_{a(15,1)} = \frac{-26h^2D}{7}, C_{a(18,2)} = \frac{-26h^2D}{35}$$

Also, the non-zero entries of matrix $\left[C_j\right]_{18\times 18}$ are

$$C_{j(1,7)} = C_{j(2,1)} = C_{j(2,13)} = C_{j(3,7)} = C_{j(4,8)} = C_{j(5,2)} = C_{j(5,14)} = C_{j(6,8)} = -C_{j(7,3)} = -C_{j(7,15)} = -\frac{6D}{h^2}$$

$$C_{j(8,9)} = C_{j(9,9)} = -C_{j(10,4)} = -C_{j(10,16)} = C_{j(11,10)} = C_{j(12,10)} = -C_{j(13,5)} = -C_{j(13,17)} = -\frac{6D}{h^2}$$

$$C_{j(14,11)} = C_{j(15,11)} = -C_{j(16,6)} = -C_{j(16,18)} = C_{j(17,12)} = C_{j(18,12)} = -\frac{6D}{h^2}$$

$$C_{j(2,7)} = C_{j(5,8)} = -C_{j(7,9)} = -C_{j(10,10)} = -C_{j(14,11)} = -C_{j(17,12)} = \frac{12D}{h^3}$$

$$C_{j(8,1)} = -20GJ_T - \frac{16hD}{3}, C_{j(11,2)} = -12GJ_T - \frac{16hD}{5}, C_{j(14,3)} = -6GJ_T - \frac{8hD}{5}, C_{j(17,4)} = -2GJ_T - \frac{8hD}{15}$$

$$C_{j(7,7)} = \frac{48D}{h}, C_{j(10,8)} = \frac{144D}{5h}, C_{j(13,9)} = \frac{72D}{5h}, C_{j(16,10)} = \frac{24D}{5h}$$

$$C_{j(7,1)} = C_{j(7,13)} = -C_{j(8,7)} = -C_{j(9,7)} = -4D, C_{j(10,2)} = C_{j(10,14)} = -C_{j(11,8)} = -C_{j(12,8)} = -\frac{12D}{5}$$

$$C_{j(13,3)} = C_{j(13,15)} = -C_{j(14,9)} = -C_{j(15,9)} = -\frac{6D}{5}, C_{j(16,4)} = C_{j(16,16)} = -C_{j(17,10)} = -C_{j(18,10)} = -\frac{2D}{5}$$

$$C_{j(8,13)} = C_{j(9,1)} = \frac{4Dh}{3}, C_{j(11,14)} = C_{j(12,2)} = \frac{4Dh}{5}, C_{j(14,15)} = C_{j(15,3)} = \frac{2Dh}{5}, C_{j(17,16)} = C_{j(18,4)} = \frac{2Dh}{15}$$

$$C_{j(13,1)} = \frac{44h^2D}{7}, C_{j(16,2)} = \frac{44h^2D}{35}, C_{j(13,13)} = \frac{-26h^2D}{7}, C_{j(16,14)} = \frac{-26h^2D}{35}, C_{j(9,13)} = -20GJ_B - \frac{16hD}{3}$$

$$C_{j(12,14)} = -12GJ_B - \frac{16hD}{5}, C_{j(15,15)} = -6GJ_B - \frac{8hD}{5}, C_{j(18,16)} = -2GJ_B - \frac{8hD}{15}, C_{j(14,13)} = C_{j(15,1)} = -\frac{6Dh^3}{7}$$

$$C_{j(1,1)} = C_{j(4,2)} = C_{j(6,14)} = C_{j(8,3)} = C_{j(9,15)} = C_{j(11,4)} = C_{j(12,16)} = C_{j(14,5)} = C_{j(15,17)} = C_{j(17,6)} = C_{j(18,18)} = \frac{4D}{h}$$

$$C_{j(17,14)} = C_{j(17,14)} = -\frac{6Dh^3}{35}, C_{j(15,7)} = -\frac{44h^2D}{7}, C_{j(18,8)} = -\frac{44h^2D}{35}, C_{j(13,7)} = \frac{108hD}{7}, C_{j(16,8)} = \frac{108hD}{35}$$

$$C_{j(1,13)} = C_{j(3,1)} = C_{j(4,14)} = C_{j(6,2)} = C_{j(8,15)} = C_{j(9,3)} = C_{j(11,16)} = C_{j(12,4)} = C_{j(14,17)} = \ldots$$
$$C_{j(15,5)} = C_{j(17,18)} = C_{j(18,6)} = \frac{2D}{h}$$

$$C_{j(3,13)} = EI_{\omega\omega B} + \frac{4h^3D}{420}, C_{j(15,13)} = 120EI_{\omega\omega B} + \frac{8h^3D}{7}, C_{j(18,14)} = 24EI_{\omega\omega B} + \frac{8h^3D}{35}$$

$$C_{j(14,1)} = 120EI_{\omega\omega T} + \frac{8h^3D}{7}, C_{j(17,2)} = -\frac{8h^3D}{35}, C_{j(14,7)} = -\frac{8h^3D}{7}, C_{j(17,8)} = -\frac{8h^3D}{35}$$

Solving Eq. (3.48) for $\left\{\overline{\overline{J}}\right\}$, one obtains,

$$\left\{\overline{\overline{J}}\right\}_{18\times1} = -\left[C_j\right]^{-1}_{18\times18}\left[C_a\right]_{18\times6}\left\{\overline{\overline{A}}\right\}_{6\times1} \tag{3.49}$$

From Eq. (3.49), the vectors of constants $\left\{\overline{\overline{B}}\right\}\left\{\overline{\overline{C}}\right\}$ and $\left\{\overline{\overline{D}}\right\}$ are expressed as

$$\begin{aligned}
\left\{\overline{\overline{B}}\right\}_{6\times1} &= \left[\overline{J}_b\right]_{6\times6}\left\{\overline{\overline{A}}\right\}_{6\times1} = -\left[I_1\right]_{6\times18}\left[C_j\right]^{-1}_{18\times18}\left[C_a\right]_{18\times6}\left\{\overline{\overline{A}}\right\}_{6\times1}\\
\left\{\overline{\overline{C}}\right\}_{6\times1} &= -\left[I_2\right]_{6\times18}\left[C_j\right]^{-1}_{18\times18}\left[C_a\right]_{18\times6}\left\{\overline{\overline{A}}\right\}_{6\times1}\\
\left\{\overline{\overline{D}}\right\}_{6\times1} &= -\left[I_3\right]_{6\times18}\left[C_j\right]^{-1}_{18\times18}\left[C_a\right]_{18\times6}\left\{\overline{\overline{A}}\right\}_{6\times1}
\end{aligned} \tag{3.50}$$

in which

$$\left[I_1\right]_{6\times18} = \left[\left[I\right]_{6\times6} \;\vdots\; \left[0\right]_{6\times6} \;\vdots\; \left[0\right]_{6\times6}\right], \left[I_2\right]_{6\times18} = \left[\left[0\right]_{6\times6} \;\vdots\; \left[I\right]_{6\times6} \;\vdots\; \left[0\right]_{6\times6}\right], \left[I_3\right]_{6\times18} = \left[\left[0\right]_{6\times6} \;\vdots\; \left[0\right]_{6\times6} \;\vdots\; \left[I\right]_{6\times6}\right]$$

From Eq. (3.50), by substituting into Eq. (3.47), one obtains matrix $\left[\Psi_p\left(z\right)\right]$ in Eq. (3.42) which relates the polynomial displacement components $\left\langle u_T\left(z\right) \quad \theta_T\left(z\right) \quad u_B\left(z\right) \quad \theta_B\left(z\right)\right\rangle^T_p$ to the integration constant vector $\left\langle D\right\rangle^T_{6\times1} = \left\langle D_{11} \quad D_{12} \quad .... \quad D_{16}\right\rangle^T$ as

$$\left[\Psi_p\left(z\right)\right] = \begin{bmatrix}
\left[P\left(z\right)\right]_{6\times6}\\
\hdashline
-\left(\left[I_1\right]_{6\times18}\left[C_j\right]^{-1}_{18\times18}\left[C_a\right]_{18\times6}\left\{\overline{\overline{A}}\right\}_{6\times1}\right)^T\left[P\left(z\right)\right]_{6\times6}\\
\hdashline
-\left(\left[I_2\right]_{6\times18}\left[C_j\right]^{-1}_{18\times18}\left[C_a\right]_{18\times6}\left\{\overline{\overline{A}}\right\}_{6\times1}\right)^T\left[P\left(z\right)\right]_{6\times6}\\
\hdashline
-\left(\left[I_3\right]_{6\times18}\left[C_j\right]^{-1}_{18\times18}\left[C_a\right]_{18\times6}\left\{\overline{\overline{A}}\right\}_{6\times1}\right)^T\left[P\left(z\right)\right]_{6\times6}
\end{bmatrix} \tag{3.51}$$

and $\left[P\left(z\right)\right]_{6\times6} = Diag\left(1, z, ...z^5\right)$

3.12. **Appendix B**

From Eqs. (3.43) and (3.45) by substituting into Eqs.(3.29) and (3.31), and differentiating with respect to Z, one obtains two systems of equations,

$$\left(\begin{bmatrix}\bar{P}_{11} & \bar{P}_{12} & 0\\ \bar{P}_{21} & \bar{P}_{22} & 0\\ 0 & 0 & \bar{P}_{33}\end{bmatrix}\begin{Bmatrix}S_{1c}\\ S_{2c}\\ S_{3c}\end{Bmatrix}+\begin{bmatrix}0 & 0 & \bar{P}_{13}\\ 0 & 0 & \bar{P}_{23}\\ \bar{P}_{31} & \bar{P}_{32} & 0\end{bmatrix}\begin{Bmatrix}S_{1s}\\ S_{2s}\\ S_{3s}\end{Bmatrix}-\begin{Bmatrix}\bar{q}_{zT-c}\\ \bar{q}_{zB-c}\\ \bar{q}_{y-c}\end{Bmatrix}\right)_n \cos\left(\frac{n\pi z}{L}\right)$$
$$+\left(\begin{bmatrix}\bar{P}_{11} & \bar{P}_{12} & 0\\ \bar{P}_{21} & \bar{P}_{22} & 0\\ 0 & 0 & \bar{P}_{33}\end{bmatrix}\begin{Bmatrix}S_{1s}\\ S_{2s}\\ S_{3s}\end{Bmatrix}+\begin{bmatrix}0 & 0 & -\bar{P}_{13}\\ 0 & 0 & -\bar{P}_{23}\\ -\bar{P}_{31} & -\bar{P}_{32} & 0\end{bmatrix}\begin{Bmatrix}S_{1c}\\ S_{2c}\\ S_{3c}\end{Bmatrix}-\begin{Bmatrix}\bar{q}_{zT-s}\\ \bar{q}_{zB-s}\\ \bar{q}_{y-s}\end{Bmatrix}\right)_n \sin\left(\frac{n\pi z}{L}\right)=\begin{Bmatrix}0\\0\\0\end{Bmatrix}\; n=1,2..\infty \tag{3.1}$$

where the following constants have been defined.

$$\bar{P}_{11}=+E\left(A_T+\frac{A_w}{4}+\frac{I_{xxw}}{h^2}\right)\left(\frac{n\pi}{L}\right)^2+\frac{GA_w}{h^2}\quad,\quad \bar{P}_{12}=\bar{P}_{21}=E\left(\frac{A_w}{4}-\frac{I_{xxw}}{h^2}\right)\left(\frac{n\pi}{L}\right)^2-\frac{GA_w}{h^2}$$

$$\bar{P}_{13}=\bar{P}_{31}=-\frac{GA_w}{h}\left(\frac{n\pi}{L}\right)\quad,\quad \bar{P}_{22}=E\left(A_B+\frac{A_w}{4}+\frac{I_{xxw}}{h^2}\right)\left(\frac{n\pi}{L}\right)^2+\frac{GA_w}{h^2}$$

$$\bar{P}_{23}=\bar{P}_{32}=\frac{GA_w}{h}\left(\frac{n\pi}{L}\right)\quad,\quad \bar{P}_{33}=-E\left(I_{xxT}+I_{xxB}\right)\left(\frac{n\pi}{L}\right)^4-GA_w\left(\frac{n\pi}{L}\right)^2$$

For a given mode n, by setting the coefficients of $\cos(n\pi z/L)$ and $\sin(n\pi z/L)$ to zero, one recovers six equations in the unknowns $(S_{1c},S_{2c},S_{3c},S_{1s},S_{2s},S_{3s})_n$ in terms of the load terms $\langle \bar{q}_{zT-c},\bar{q}_{zB-c},\bar{q}_{y-c},\bar{q}_{zT-s},\bar{q}_{zB-s},\bar{q}_{y-s}\rangle_n$. The resulting system of equations is then solved for $(S_{1c},S_{2c},S_{3c},S_{1s},S_{2s},S_{3s})_n$.

Also, for the torsional-flexural response, one has

$$\left(\begin{bmatrix}\bar{Q}_{11} & \bar{Q}_{12} & \bar{Q}_{13} & \bar{Q}_{14}\\ \bar{Q}_{21} & \bar{Q}_{22} & \bar{Q}_{23} & \bar{Q}_{24}\\ \bar{Q}_{31} & \bar{Q}_{32} & \bar{Q}_{33} & \bar{Q}_{34}\\ \bar{Q}_{41} & \bar{Q}_{42} & \bar{Q}_{34} & \bar{Q}_{44}\end{bmatrix}\begin{Bmatrix}S_{1c}\\ S_{2c}\\ S_{3c}\\ S_{4c}\end{Bmatrix}-\begin{Bmatrix}\bar{q}_{xT-c}\\ \bar{m}_{T-c}\\ \bar{q}_{xB-c}\\ \bar{m}_{B-c}\end{Bmatrix}\right)_n \cos\left(\frac{n\pi z}{L}\right)$$
$$+\left(\begin{bmatrix}\bar{Q}_{11} & \bar{Q}_{12} & \bar{Q}_{13} & \bar{Q}_{14}\\ \bar{Q}_{21} & \bar{Q}_{22} & \bar{Q}_{23} & \bar{Q}_{24}\\ \bar{Q}_{31} & \bar{Q}_{32} & \bar{Q}_{33} & \bar{Q}_{34}\\ \bar{Q}_{41} & \bar{Q}_{42} & \bar{Q}_{34} & \bar{Q}_{44}\end{bmatrix}\begin{Bmatrix}S_{1s}\\ S_{2s}\\ S_{3s}\\ S_{4s}\end{Bmatrix}-\begin{Bmatrix}\bar{q}_{xT-s}\\ \bar{m}_{T-s}\\ \bar{q}_{xB-s}\\ \bar{m}_{B-s}\end{Bmatrix}\right)_n \sin\left(\frac{n\pi z}{L}\right)=\begin{Bmatrix}0\\0\\0\end{Bmatrix}\; n=1,2..\infty \tag{3.2}$$

where

$$\bar{Q}_{11} = \left[EI_{yyT} + \frac{13Dh}{35}\right]\left(\frac{n\pi}{L}\right)^4 + \frac{12D}{5h}\left(\frac{n\pi}{L}\right)^2 + \frac{12D}{h^3}$$

$$\bar{Q}_{12} = Q_{21} = \frac{11Dh^2}{210}\left(\frac{n\pi}{L}\right)^4 + \frac{D}{5}\left(\frac{n\pi}{L}\right)^2 + \frac{6D}{h^2}$$

$$\bar{Q}_{22} = \left[EI_{\omega\omega T} + \frac{h^3 D}{105}\right]\left(\frac{n\pi}{L}\right)^4 + \left[GJ_T + \frac{4Dh}{15}\right]\left(\frac{n\pi}{L}\right)^2 + \frac{4D}{h} \quad \bar{Q}_{23} = \bar{Q}_{32} = \frac{13Dh^2}{420}\left(\frac{n\pi}{L}\right)^4 - \frac{D}{5}\left(\frac{n\pi}{L}\right)^2 - \frac{6D}{h^2}$$

$$\bar{Q}_{13} = \bar{Q}_{31} = \frac{9Dh}{70}\left(\frac{n\pi}{L}\right)^4 - \frac{36D}{15h}\left(\frac{n\pi}{L}\right)^2 - \frac{12D}{h^3} \qquad \bar{Q}_{14} = \bar{Q}_{41} = \frac{-13Dh^2}{420}\left(\frac{n\pi}{L}\right)^4 + \frac{D}{5}\left(\frac{n\pi}{L}\right)^2 + \frac{6D}{h^2}$$

$$\bar{Q}_{24} = \bar{Q}_{42} = -\frac{h^3 D}{140}\left(\frac{n\pi}{L}\right)^4 - \frac{Dh}{15}\left(\frac{n\pi}{L}\right)^2 + \frac{2D}{h}$$

$$\bar{Q}_{34} = \bar{Q}_{43} = \frac{-11Dh^2}{210}\left(\frac{n\pi}{L}\right)^4 - \frac{D}{5}\left(\frac{n\pi}{L}\right)^2 - \frac{6D}{h^2}$$

$$\bar{Q}_{33} = \left[EI_{yyB} + \frac{13Dh}{35}\right]\left(\frac{n\pi}{L}\right)^4 + \frac{36D}{15h}\left(\frac{n\pi}{L}\right)^2 + \frac{12D}{h^3}$$

$$\bar{Q}_{44} = \left[EI_{\omega\omega B} + \frac{Dh^3}{105}\right]\left(\frac{n\pi}{L}\right)^4 + \left[GJ_B\mathscr{D}^2 + \frac{4Dh}{15}\right]\left(\frac{n\pi}{L}\right)^2 + \frac{4D}{h}$$

Again, for a given mode n, by setting the coefficients of $\cos(n\pi z/L)$ and $\sin(n\pi z/L)$ to zero, one recovers eight equations in the unknowns $\left(S_{1c}, S_{2c}, S_{3c}, S_{4c}, S_{1s}, S_{2s}, S_{3s}, S_{4s}\right)_n$ in terms of the load terms $\left\langle \bar{q}_{xT-c}, \bar{m}_{T-c}, \bar{q}_{xB-c}, \bar{m}_{B-c}, \bar{q}_{xT-s}, \bar{m}_{T-s}, \bar{q}_{xB-s}, \bar{m}_{B-s} \right\rangle_n$ The resulting system of equations is then solved for $\left(S_{1c}, S_{2c}, S_{3c}, S_{4c}, S_{1s}, S_{2s}, S_{3s}, S_{4s}\right)_n$.

3.13. **List of symbols**

Subscripts T, B, W, M and P denote the correspondence to Top and Bottom flanges and the Web or Membrane and Plate bending action respectively.

$\gamma_{xzB}, \gamma_{yzB}, \gamma_{xyB}, \gamma_{xzT}, \gamma_{yzT}, \gamma_{xyT}$	Shear strain of the xz, yz, xy plane
$\gamma_{yzM}, \gamma_{yzP}$	Web strain in the yz plane
ε_{yP}	Normal strain of the web along the *y* direction
ε_z	Total normal strain along the *z* direction

$\varepsilon_{zB}, \varepsilon_{zT}, \varepsilon_{zM}, \varepsilon_{zP}$	Normal strain along the *z* direction
θ_B, θ_T	Angle of twist at the flange to web junction
ν	Poisson's ratio
Π	Total energy of the system
$\overline{\sigma}_{zz}$	Normal tractions along z-axis acting at member ends
σ_{yP}	Normal stress of the web due to plate bending, along the *y* direction
$\sigma_{zB}, \sigma_{zT}, \sigma_{zM}, \sigma_{zP}$	Total normal stress in the web and the flanges along the *z* direction
$\overline{\tau}_{zx}, \overline{\tau}_{zy}$	Shear tractions along *x* and *y* axes acting at member ends
$\tau_{xzB}, \tau_{xzT}, \tau_{yzM}, \tau_{yzP}$	Shear stresses
$\{\Phi_e\}, \{\Psi_e\}$	The exponential components of the homogenous solution
$\{\Phi_p\}, \{\Psi_p\}$	The polynomial components of the homogenous solution
$\langle\phi\rangle_i^T, \langle\psi\rangle_i^T$	The i^{th} eigenvector of the Generalized Eigenvalue Problem
A_B, A_T, A_W	Cross sectional areas
$\overline{B}_B, \overline{B}_T$	Bimoments at member ends
b_B, b_T	Flange widths
c_i	Eigenvalues of the linearized eigen value arising from longitudinal-transverse response equations
$\mathscr{D}$	Differential Operator
D	Flexural rigidity of the web
D_i	Integration constants arising in the lateral-torsional response
d_i	Eigenvalues of the linearized eigen-value problem arising from the lateral-torsional response equations
E	Modulus of elasticity
G	Shear modulus
$H_1(y) \sim H_4(y)$	Cubic shape functions

$H_5(y), H_6(y)$	Linear shape functions
h	Height of the cross section, measured along the flanges centerline
$[I_3],[I_4]$	Identity matrices of the size 3×3 and 4×4
$I_{\omega\omega B}, I_{\omega\omega T}$	Local warping constant of the bottom and top flanges
$I_{xxB}, I_{xxT}, I_{xxW}, I_{yyB}, I_{yyT}$	Moment of inertia about x and y axes
I_{xyB}, I_{xyT}	Product moment of inertia
J_B, J_T	Polar moment of inertia
L	Beam span
$\overline{N}_B, \overline{N}_T$	End axial forces applied on bottom and top flanges
$\overline{M}_{xB}, \overline{M}_{yB}, \overline{M}_{xT}, \overline{M}_{yT}$	End bending moments induced by tractions about x and y axes
$m_B(z), m_T(z)$	Distributed twisting moment
n_B, n_T, n_w	Normal component of local coordinate system
P_{ij}	Components of the DEs coefficient matrix due to longitudinal-transverse response
$[p_i] \quad i=1,\ldots,4$	DEs coefficient matrix of the ith order for longitudinal-transverse response
Q_{ij}	Components of the differential equation coefficient for lateral-torsional response
$[q_i] \quad i=0,1,\ 2$	DEs coefficient matrix of the i^{th} order of lateral-torsional response
$q_{xB}(z), q_{xT}(z)$	Lateral distributed load, along *z* axis
$q_y(z)$	Transverse distributed load, along *z* axis
$q_{zB}(z), q_{zT}(z)$	Longitudinal distributed load, along *z* axis
$S_{xB}, S_{xT}, S_{yB}, S_{yT}$	First moment of area about the *x* and *y* axes
$\overline{T}_B, \overline{T}_T$	Twisting moments at the end of the beam

t_B, t_T, t_W	Thickness of the flanges and the web
U_B, U_T, U_{WM}, U_{WP}	Internal strain energy
u_B, u_T	Lateral displacements at the flange centroid
$\bar{u}_B, \bar{u}_T, \bar{u}_w$	Lateral displacements of a point offset the middle surface
V	Total potential energy gained by the loads
V_1, V_2	Load potential energy due to end tractions and member tractions
$\bar{V}_{xB}, \bar{V}_{xT}$	Lateral shear forces at the end induced by tractions
$\bar{V}_y$	Transverse shear force at the end induced by tractions
v	Transverse displacement on the middle surface
$\bar{v}_T, \bar{v}_B$	Transverse displacements of a point offset the middle surface
$\bar{v}_w$	Total transverse generalized displacement of the web
$\bar{v}_{wP}$	Transverse displacement of the web due to plate bending behaviour
w_B, w_T	Longitudinal displacements at flange centroid
$\bar{w}_B, \bar{w}_T, \bar{w}_w$	Longitudinal displacements for a point offset from the middle surface
$\bar{w}_{wP}$	Longitudinal displacements of the web due to plate bending action relative to a point on the middle surface

3.14. References

Ádány, S., and Schafer, B. W. (2008). "A full modal decomposition of thin-walled, single-branched open cross-section members via the constrained finite strip method." *Journal of Constructional Steel Research*, 64(1), 12-29.

American Institute of Steel Construction (2005). "Specification for structural steel buildings." AISC, Chicago, IL.

Andreassen, M. J., and Jönsson, J. (2012). "Distortional solutions for loaded semi-discretized thin-walled beams." *Thin-Walled Structures*, 50(1), 116-127.

Bradford, and Ronagh (1997). "Generalized Elastic Buckling of Restrained I-Beams by FEM." *Journal of Structural Engineering*, 123(12), 1631-1637.

Bradford, M. A. (1985). "Distortional buckling of monosymmetric I-beams." *Journal of Constructional Steel Research*, 5(2), 123-136.

Bradford, M. A. (1986). "Inelastic distortional buckling of I-beams." *Computers & Structures*, 24(6), 923-933.

Bradford, M. A. (1988a). "Buckling of elastically restrained beams with web distortions." *Thin-Walled Structures*, 6(4), 287-304.

Bradford, M. A. (1990b). "Stability of mono-symmetric beam-columns with thin webs." *Journal of Constructional Steel Research*, 15(4), 323-339.

Bradford, M. A. (1992a). "Buckling of doubly-symmetric cantilevers with slender webs." *Engineering Structures*, 14(5), 327-334.

Bradford, M. A. (1992b). "Lateral-Distortional buckling of steel I—Section members." *Journal of Constructional Steel Research*, 23(1–3), 97-116.

Bradford, M. A., and Ronagh, H. R. (1997). "Generalized Elastic Buckling of Restrained I-beams by FEM." *Journal of Structural Engineering*, 123(12), 1631-1637.

Bradford, M. A., and Trahair, N. S. (1981). "Distortional Buckling of I-Beams." *Journal of the Structural Division, ASCE*, 107(2), 355-370.

Bradford, M. A., and Trahair, N. S. (1982). "Distortional buckling of thin-web beam-columns." *Engineering Structures*, 4(1), 2-10.

Chen, W. E. I., and Ye, J. (2010). "ELASTIC LATERAL AND RESTRAINED DISTORTIONAL BUCKLING OF DOUBLY SYMMETRIC I-BEAMS." *International Journal of Structural Stability and Dynamics*, 10(05), 983-1016.

Davies, J. M., and Leach, P. (1994). "First-order generalised beam theory." *Journal of Constructional Steel Research*, 31(2-3), 187-220.

Dekker, N. W., and Kemp, A. R. (1998). "A simplified distortional buckling model for doubly symmetrical I-sections." *Canadian Journal of Civil Engineering*, 25(4), 718-727.

European Committee for Standardization (CEN). (2003). "Eurocode 3: Design of steel structures Part 1-1: General rules and rules for buildings."Brussels, Belgium.

Gjelsvik, A. (1981). *The theory of thin walled bars / Atle Gjelsvik*, Wiley, New York, NY, USA.

Gonçalves, R., Ritto-Corrêa, M., and Camotim, D. (2010). "A new approach to the calculation of cross-section deformation modes in the framework of generalized beam theory." *Comput Mech*, 46(5), 759-781.

Hancock, G. J. (1978). "Local, Distortional, and Lateral Buckling of I-Beams." *Journal of the Structural Division*, 104(11), 1787-1798.

Hancock, G. J., Bradford, M. A., and Trahair, N. S. (1980). "Web distortion and flexural-torsional buckling." *Journal of the Structural Division, ASCE*, 106(7), 1557-1571.

Hughes, O., and Ma, M. (1996a). "Lateral Distortional Buckling of Monosymmetric Beams under Point Load." *Journal of Engineering Mechanics*, 122(10), 1022-1029.

Iyer, H. (2005). "The Effects of Shear Deformation in Rectangular and Wide Flange Sections." Master of Science, Virginia Polytechnic Institute and State, Blacksburg, Virginia.

Johnson, C. P., and Will, K. M. (1974). "Beam Buckling by Finite Element Procedure." *Journal of the Structural Division*, 100(3), 669-685.

Jönsson, J. (1998). "Determination of shear stresses, warping functions and section properties of thin-walled beams using finite elements." *Computers & Structures*, 68(4), 393-410.

Jönsson, J. (1999a). "Distortional theory of thin-walled beams." *Thin-Walled Structures*, 33(4), 269-303.

Jönsson, J. (1999b). "Distortional warping functions and shear distributions in thin-walled beams." *Thin-Walled Structures*, 33(4), 245-268.

Jönsson, J., and Andreassen, M. J. (2011). "Distortional eigenmodes and homogeneous solutions for semi-discretized thin-walled beams." *Thin-Walled Structures*, 49(6), 691-707.

Kalkan, I., and Buyukkaragoz, A. (2012). "A numerical and analytical study on distortional buckling of doubly-symmetric steel I-beams." *Journal of Constructional Steel Research*, 70(0), 289-297.

Ma, M., and Hughes, O. (1996b). "Lateral distortional buckling of monosymmetric I-beams under distributed vertical load." *Thin-Walled Structures*, 26(2), 123-145.

Ng, M. L.-H., and Ronagh, H. R. (2004). "An Analytical Solution for the Elastic Lateral-Distortional Buckling of I-section Beams." *Advances in Structural Engineering*, 7(2), 189-200

Pi, Y., and Trahair, N. (2000). "Distortion and Warping at Beam Supports." *Journal of Structural Engineering*, 126(11), 1279-1287.

Rajasekaran, S., and Murray, D. W. (1973). "Coupled Local Buckling in Wide-Flange Beam-Columns." *Journal of the Structural Division*, 99(6), 1003-1023.

Rendek, S., and Baláž, I. (2004). "Distortion of thin-walled beams." *Thin-Walled Structures*, 42(2), 255-277.
Roberts, T. M., and Jhita, P. S. (1983b). "Lateral, local and distortional buckling of I-beams." *Thin-Walled Structures*, 1(4), 289-308.
Saadé, K., Warzée, G., and Espion, B. (2006). "Modeling distortional shear in thin-walled elastic beams." *Thin-Walled Structures*, 44(7), 808-821.
Samanta, A., and Kumar, A. (2006b). "Distortional buckling in monosymmetric I-beams." *Thin-Walled Structures*, 44(1), 51-56.
Samanta, A., and Kumar, A. (2008). "Distortional buckling in braced-cantilever I-beams." *Thin-Walled Structures*, 46(6), 637-645.
Schardt, R. (1989). *Verallgemeinerte Technische Biegetheorie(Generalized BeamTheory)*, Springer Verlag, Berlin,.
Standards Association of Australia (1998). "AS 4100 steel structures."Sydney, Australia.
Timoshenko, S. P. (1921). "On the correction for shear of the differential Equation for transverse vibration of prismatic beams." *Philosophical Magazine* 41, 744-746.
Vlasov, V. Z. (1961). *Thin walled elastic beams*, Israel Program for Scientific Translations, Jerusalem, Israel. Available from Office of Technical Services, US Department of Commerce,Washington, D.C.
Vrcelj, Z., and Bradford, M. A. (2006a). "Elastic distortional buckling of continuously restrained I-section beam–columns." *Journal of Constructional Steel Research*, 62(3), 223-230.
Wang, C. M., Chin, C. K., and Kitipornchai, S. (1991). "Parametric study on distortional buckling of monosymmetric beam-columns." *Journal of Constructional Steel Research*, 18(2), 89-110.
Zirakian, T. (2008). "Elastic distortional buckling of doubly symmetric I-shaped flexural members with slender webs." *Thin-Walled Structures*, 46(5), 466-475.

Chapter 4

Distortional Theory for the Analysis of Wide Flange Steel Beams –Finite Element Formulation[a]

4.1. Abstract

Two finite element formulations are developed for the general distortional analysis of beams with monosymmetric sections. In the first formulation, cubic and linear Hermitian polynomials are adopted to interpolate the nodal displacements; whereas in the second formulation, shape functions that exactly satisfy the governing field equations were used. Because the distortional lateral-torsional and the longitudinal-transverse responses are fully uncoupled, separate finite elements were developed for both types of behaviors. A comparison with other finite element solutions and a recently developed distortional theory established the validity of the present formulations. A study was then performed on the stability and convergence characteristics of both elements. The new elements were then adopted to solve linearly static analysis of simple beams and beams with overhangs. The formulation is shown to reliably capture the difference in behavior between stiffened and unstiffened beams

Authors Keywords: Thin-Walled Beam, Distortion, Torsion, Warping, Coupling, Finite element

[a] Pezeshky, P., and Mohareb, M. (2015). "Finite-Element Formulations for the Distortional Analysis of Wide Flange Steel Beams." *Journal of Engineering Mechanics*, 04015071.

4.2. Introduction and Literature Review

Classical theories (Vlasov (1961), Gjelsvik (1981)) associate with four principal modes of deformation (i.e. Axial, biaxial bending and torsion). However, beams with slender web are shown to deform significantly in a distortional mode (e.g., Rajasekaran and Murray (1973), Hancock et al. (1980), Bradford and Trahair (1981),Wang et al. (1991) and Hassan and Mohareb (2012)). Schardt (1994) developed a generalized beam theory (GBT) in which distortion is introduced as the fifth mode of deformation orthogonalized to the other modes. Subsequently, Davies and Leach (1994) provided closed form and finite difference solutions and determined the relevant sectional properties and warping functions based on the GBT approach. Jönsson (1998), Jönsson (1999a) and Jönsson (1999b) characterized distortion in a manner consistent with the way torsion is treated in thin-walled beam theories. He developed a linear finite element to formulate torsional and distortional warping functions and shear stresses for open and closed sections. Saadé et al. (2006) developed a finite element using the orthogonality condition between distortional modes and other classical modes of deformation. Their kinematics are identical to those of the Vlasov theory (Vlasov 1961), except that they introduced a distortional center for each segment of the cross section. Jönsson and Andreassen (2011) extended the GBT approach and developed a finite element to relate the displacements within the cross section to nodal displacement using Hermitian polynomials. In their work, longitudinal displacements are approximated through polynomial interpolations while the distortional displacements are characterized through exponential interpolations. Andreassen and Jönsson (2012), then extended their work to account for distributed loads. A recent study (Pezeshky and Mohareb 2014) developed a distortional theory for wide flange cross sections. Unlike the treatments adopted in GBT solutions, the orthogonality conditions were relaxed and the resulting coupled differential equations (DEs) were exactly solved for the general loading.

In addition to the various studies related to static distortional analysis summarized in the previous section, a series of distortional buckling studies were developed by various researchers. This includes the work of Rajasekaran and Murray (1973), Johnson and Will (1974),(Bradford and Trahair 1981; 1982) ,(Bradford 1985; 1986; 1992a; 1992b), Chin et al. (1992), Ronagh and Bradford (1994), Bradford and Ronagh (1997), who developed finite element solutions for a variety of boundary and loading conditions. A common feature among these studies is the use of cubic displacement functions in the longitudinal direction . In other studies, trigonometric functions were adopted to characterize the displacement fields as a function of the longitudinal coordinate. This includes the work of Hancock et al. (1980), Roberts and Jhita (1983b), Bradford (1988a) and (1990b), Wang et al. (1991), Hughes and Ma (1996a), Ma and Hughes (1996b), Ng and Ronagh (2004), Vrcelj and Bradford (2006a).

In the above studies, web distortion was assumed to have a cubic distribution except for the study of Johnson and Will (1974) who adopted a quadratic polynomial, and (Hughes and Ma 1996a; Ma and Hughes 1996b) who used a quintic polynomial to characterize web distortion.

Parametric studies on distortional buckling analysis were provided in the work of Dekker and Kemp (1998), Samanta and Kumar (2006b), Kumar and Samanta (2006c), White and Jung (2007), Zirakian and Showkati (2007), Samanta and Kumar (2008), Zirakian (2008), Trahair (2009) and Kalkan and Buyukkaragoz (2012). A comparative summary between the features, methodologies and approaches of above studies is provided in Pezeshky and Mohareb (2014).

While the study in Pezeshky and Mohareb (2014) provides closed form solution for beams suitable for the analysis of single span beams, for multiple span beams, the imposition of boundary and continuity conditions can be tedious. Thus, the current study generalizes the solution for multiple span beams by developing two finite element (FEs) formulations which capture distortion.

4.3. Statement of the problem

A beam with slender web and thick flanges is assumed to be subjected to general member loading. General loadings are defined through member tractions $p_z(s,n,z)$, $p_y(s,n,z)$ and $p_x(s,n,z)$ in longitudinal, transverse, and lateral directions, respectively. Member tractions will be transformed into nodal forces later through shape functions.

The width of top flange is b_T and that of bottom flange is b_B. The height of the section, defined as the distance between the centrelines of top and bottom flanges, is denoted h and the thicknesses of top and bottom flanges and the web are denoted as t_T, t_B and t_W, respectively, (Fig. 3-1). As a convention, subscripts T denote parameters pertaining to the top flange and subscripts B denote parameters relating to the bottom flange. A global right handed coordinate and three local coordinates are assigned to top and bottom flanges and the web. The components of the local coordinates are shown in Fig. 4-1. The tangential components of local coordinates in the top flange, bottom flange, and web ($s = x_T$, $s = x_B$ and $s = y_W$) are defined along the middle surface of section and are measured from the centroid of each component.

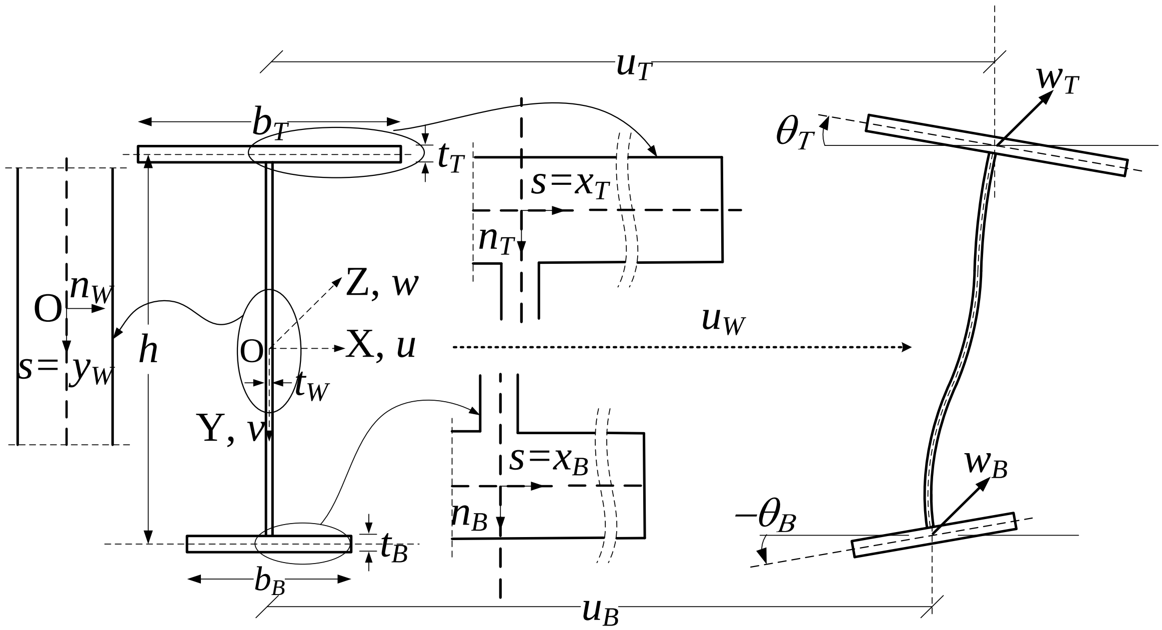

Fig. 4-1. Cross section dimensions, global and local coordinates

4.4. Assumptions and Kinematics

Strains and rotations are assumed small. The material is homogeneous, linearly elastic and isotropic and thus obeys Hooke's law. The formulation is restricted to prismatic open thin-walled members. Kinematics assumptions are identical to those of presented in Pezeshky and Mohareb (2014). The flanges deform as a Gjelsvik beam while the web behaves as a thin plate in bending action and deforms as a Timoshenko beam in membrane deformation. In Fig. 3-1, it is shown that top flange moves laterally through u_T and twists about Z axis through angle of twist θ_T. In a similar manner, u_B represents the lateral displacement and θ_B denotes the angle of twist of bottom flange. Longitudinal displacement of the section is described based on the longitudinal displacement of top and bottom flanges through w_T and w_B. The transverse displacement, v, is assumed constant in the plane of the cross section and varies along the longitudinal direction. Distortion of the web, u_W, is introduced through a cubic Hermitian function, i.e.,

$$u_W\left(y,z\right)=L_1\left(y\right)u_T\left(z\right)+L_2\left(y\right)\theta_T\left(z\right)+L_3\left(y\right)u_B\left(z\right)+L_4\left(y\right)\theta_B\left(z\right) \tag{4.1}$$

in which,

$$L_1(y)=\frac{1}{2}-\frac{3y}{2h}+\frac{2y^3}{h^3}\ ,\qquad L_2(y)=\frac{h}{8}-\frac{y}{4}-\frac{y^2}{2h}+\frac{y^3}{h^2}$$
$$L_3(y)=\frac{1}{2}+\frac{3y}{2h}-\frac{2y^3}{h^3},\qquad L_4(y)=-\frac{h}{8}-\frac{y}{4}+\frac{y^2}{2h}+\frac{y^3}{h^2} \tag{4.2}$$

Likewise, longitudinal displacement of the web, w_W , is defined through linear polynomials, i.e.,

$$w_W(y,z)=L_5(y)w_T(z)+L_6(y)w_B(z) \tag{4.3}$$

in which

$$L_5(y)=\left(\frac{1}{2}-\frac{y}{h}\right),\ L_6(y)=\left(\frac{1}{2}+\frac{y}{h}\right) \tag{4.4}$$

4.5. **Energy Formulation**

Total potential energy, Π, consists of the internal strain energy of both flanges and the web U and the potential energy V gained by the external loads, i.e.

$$\Pi=U_T+U_B+U_w-V \tag{4.5}$$

In Eq. (3.18), the internal strain energy in the top flange U_T , the bottom flange U_B , and the web U_W are given by

$$U_T=\frac{1}{2}\int_z\int_{A_T}\left(E\varepsilon_{zT}{}^2+G\gamma_{xzT}{}^2\right)dAdz$$
$$U_B=\frac{1}{2}\int_z\int_{A_B}\left(E\varepsilon_{zB}{}^2+G\gamma_{xzB}{}^2\right)dAdz \tag{4.6}$$
$$U_W=\frac{1}{2}\int_z\int_{A_W}\left(E\varepsilon_{zM}{}^2+G\gamma_{yzM}{}^2\right)dAdz+\int_z\int_{A_W}\frac{E}{2(1-\nu^2)}\left[\varepsilon_{zP}^2+\varepsilon_{yP}^2+2\nu\varepsilon_{zP}\varepsilon_{yP}+(1-\nu)\gamma_{yzP}^2\right]dAdz$$

in which E and G are elastic and shear moduli, ε and γ are normal and shear strains, ν is Poisson's ratio, subscript M denotes the strain related to membrane action and subscript P denotes that of plate bending terms of the web strain. Also the load potential energy V is given by

$$V=\int_z\int_s\left(p_x\overline{u}+p_y\overline{v}+p_z\overline{w}\right)dsdz \tag{4.7}$$

where $\bar{u}(s,n,z), \bar{v}(s,n,z)$ and $\bar{w}(s,n,z)$ are the displacements at any point (s,n,z). By substituting strain-displacement relations, expressed in Pezeshky and Mohareb (2014), into Eqs. (3.19) one obtains expressions for total potential energy in terms of the seven displacements, i.e.,

$$U_T = U_{T1} + U_{T2} = \frac{1}{2}\int_L \left(EA_T w_T'^2 + EI_{xxT} v_T''^2 \right) dz + \frac{1}{2}\int_L \left(EI_{yyT} u_T''^2 + EI_{\omega\omega T} \theta_T''^2 + GJ_T \theta_T'^2 \right) dz \tag{4.8}$$

where ‘ ′ ’ denotes differentiation w.r.t z. In Eq. (4.8), internal strain energy U_T was subdivided into two components. The first component U_{T1} relates to the longitudinal transverse response (i.e., is a functional of w_T, v and their derivatives) and the second component U_{T2} relates to the lateral torsional response (i.e., is a functional of $u_T, \theta_T, u_B, \theta_B$ and their derivatives). As a convention, subscript ‘1’ denotes parameters related to longitudinal-transverse response and subscript ‘2’ denotes the parameters of the lateral-torsional response. In a similar manner, the remaining energy expressions are subdivided into longitudinal-transverse and lateral-torsional components, i.e.,

$$U_B = U_{B1} + U_{B2} = \frac{1}{2}\int_L \left(EA_B w_B'^2 + EI_{xxB} v_B''^2 \right) dz + \frac{1}{2}\int_L \left(EI_{yyB} u_B''^2 + EI_{\omega\omega B} \theta_B''^2 + GJ_B \theta_B'^2 \right) dz$$

$$\begin{aligned} U_W = U_{W1} + U_{W2} = \frac{1}{2}\int_L \Big\{ & E\Big[(A_W/4)\left(w_T'(z) + w_B'(z) \right)^2 + \left(I_{xxW}/h^2 \right)\left(w_T'(z) - w_B'(z) \right)^2 \Big] \\ & + \left(GA_W/h^2 \right)\Big[\left(w_T(z) - w_B(z) \right)^2 + h^2 v'^2(z) + 2hv'\left(w_T(z) - w_B(z) \right) \Big] \Big\} dz \\ & + \frac{D}{2}\iint_A \left[\left(\frac{\partial^2 u_W}{\partial z^2} \right)^2 + \left(\frac{\partial^2 u_W}{\partial y^2} \right)^2 + 2\nu \left(\frac{\partial^2 u_W}{\partial z^2} \right)\left(\frac{\partial^2 u_W}{\partial y^2} \right) + 2(1-\nu)\left(\frac{\partial^2 u_W}{\partial z \partial y} \right)^2 \right] dA \end{aligned}$$

$$V = V_1 + V_2 = \int_L \left[q_y v(z) + q_{zT} w_T(z) + q_{zB} w_B(z) \right] dz + \int_L \left[q_{xT} u_T(z) + q_{xB} u_B(z) + m_T \theta_T(z) + m_B \theta_B(z) \right] dz \tag{4.9}$$

in which, the following cross-sectional properties have been defined

$$\left(A_T, I_{xxT}, I_{yyT}, I_{\omega\omega T}, J_T \right) = \int_{A_T} \left(1, n_T^2, x_T^2, n_T^2 x_T^2, 4n_T^2 \right) dA_T = \left(b_T t_T, b_T t_T^3/12, b_T^3 t_T/12, b_T^3 t_T^3/144, b_T t_T^3/3 \right)$$

$$\left(A_B, I_{xxB}, I_{yyB}, I_{\omega\omega B}, J_B \right) = \int_{A_B} \left(1, n_B^2, x_B^2, n_B^2 x_B^2, 4n_B^2 \right) dA_B = \left(b_B t_B, b_B t_B^3/12, b_B^3 t_B/12, b_B^3 t_B^3/144, b_B t_B^3/3 \right).$$

$D = Et_W{}^3 \big/ 12\left(1-\nu^2\right)$,

$$\left(A_W, I_{xxW}\right) = \int_{A_w} \left(1, y^2\right) dA_W = \left\{t_W\left[h-0.5\left(t_T+t_B\right)\right],\quad t_W\left[h-0.5\left(t_T+t_B\right)\right]^3 \big/ 12\right\}$$

Also, the following equivalent line loads arise

$$q_{zT}(z) = \int_S \left(p_{zT} + p_{zW} L_5\right) ds, \quad q_{zB}(z) = \int_S \left(p_{zB} + p_{zW} L_6\right) ds$$

$$q_y(z) = \int_S \left\{\left[p_{yT} + n_T\left(\partial p_{zT}/\partial z\right)\right] + \left[p_{yB} + n_B\left(\partial p_{zB}/\partial z\right)\right] + \left(p_{yW}\right)\right\} ds$$

$$q_{xT}(z) = \int_S \left\{\left[p_{xT} + x_T\left(\partial p_{zT}/\partial z\right)\right] + \left[p_{xW} L_1 - n_W p_{yW}\left(dL_1/dy\right) + n_W\left(\partial p_{zW}/\partial z\right) L_1\right]\right\} ds$$

$$q_{xB}(z) = \int_S \left\{\left[p_{xB} + x_B\left(\partial p_{zB}/\partial z\right)\right] + \left[p_{xW} L_3 - n_W p_{yW}\left(dL_3/dy\right) + n_W\left(\partial p_{zW}/\partial z\right) L_3\right]\right\} ds$$

$$m_T(z) = \int_S \left\{\left[x_T p_{yT} - n_T p_{xT} + x_T n_T\left(\partial p_{zT}/\partial z\right)\right] + \left[p_{xW} L_2 - n_W p_{yW}\left(d^2 L_2/dy^2\right) + n_W\left(\partial p_{zW}/\partial z\right) L_2\right]\right\} ds$$

$$m_B(z) = \int_S \left\{\left[x_B p_{yB} - n_B p_{xB} + x_B n_B\left(\partial p_{zB}/\partial z\right)\right] + \left[p_{xW} L_4 - n_W p_{yW}\left(d^2 L_4/dy^2\right) + n_W\left(\partial p_{zW}/\partial z\right) L_4\right]\right\} ds$$

where, $\left(p_x, p_y, p_z\right)_{T,B,W}$ are the member tractions across the top and bottom flanges and the web.

Hence, the total potential energy of the system can be expressed as

$$\Pi = \Pi_1\left(w_T, w_T', w_B, w_B', v, v', v''\right) + \Pi_2\left(u_T, u_T', u_T'', \theta_T, \theta_T', \theta_T'', u_B, u_B', u_B'', \theta_B, \theta_B', \theta_B''\right) \tag{4.10}$$

where Π_1 is the total potential energy related to the longitudinal-transverse response and Π_2 denotes the total potential energy related the lateral-transverse response. It is noted that the two sets of argument functions of functionals Π_1 and Π_2 are mutually exclusive. This allows a separate treatment for each in the following finite element formulations

4.6. Finite Element Formulation 1- Based on Polynomial Interpolation (FE1)

Functional Π_1 leads to a finite element for the longitudinal transverse response while functional Π_2 leads to a finite element for the lateral torsional response. For the longitudinal transverse response, a two-node finite element is taken with four degrees of freedom (DOFs) per node, i.e., a total of eight DOFs, (Fig. 4-2a). The element is developed under section Longitudinal-transverse response. For the lateral torsional response, a two node finite element with eight degrees of freedom per node, i.e. a total of 16 DOFs is introduced, (Fig. 4-2b). This element is presented under section Lateral-torsional response.

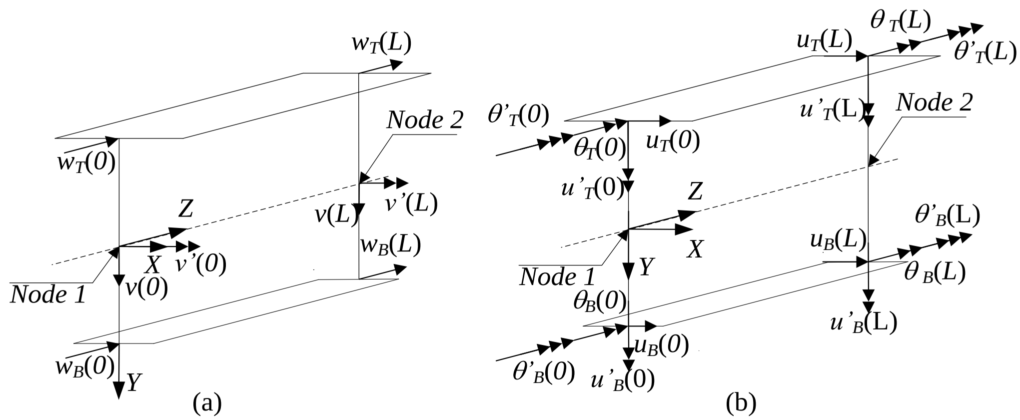

Fig. 4-2. Degrees of freedom of a) longitudinal-transverse element b) lateral torsional element

4.6.1. Longitudinal-transverse response

4.6.1.1. Displacement fields in terms of Nodal Displacement

The displacement fields are related to the vector of nodal displacements interpolated through linear and cubic Hermitian polynomials, i.e.

$$w_T(z) = \langle N(z)\rangle_{1\times2}^T \{\bar{w}_T\}_{2\times1}, w_B(z) = \langle N(z)\rangle_{1\times2}^T \{\bar{w}_B\}_{2\times1}, v(z) = \langle H_1(z)\rangle_{1\times2}^T \{\bar{v}\}_{4\times1} \tag{4.11}$$

in which the displacement shape functions are expressed as,

$$\langle N(z)\rangle_{1\times2}^T = \langle 1 - z/L \quad z/L\rangle$$
$$\langle H_1(z)\rangle_{1\times4}^T = \left\langle 1 - 3(z/L)^2 + 2(z/L)^3 \;\vdots\; -z\left[1-(z/L)\right]^2 \;\vdots\; 3(z/L)^2 - 2(z/L)^3 \;\vdots\; -L\left[(z/L)^3 - (z/L)^2\right]\right\rangle \tag{4.12}$$

and the vector of nodal displacements is defined as

$$\langle \Delta_1\rangle_{1\times8}^T = \left\langle \langle \bar{w}_T\rangle_{1\times2}^T \;\vdots\; \langle \bar{w}_b\rangle_{1\times2}^T \;\vdots\; \langle \bar{v}\rangle_{1\times4}^T \right\rangle \tag{4.13}$$

where,

$$\langle \bar{w}_T\rangle_{1\times2}^T = \langle w_T(0) \quad w_T(L)\rangle \quad , \qquad \langle \bar{w}_B\rangle_{1\times2}^T = \langle w_B(0) \quad w_B(L)\rangle$$
$$\langle \bar{v}_T\rangle_{1\times4}^T = \langle v(0) \quad v'(0) \quad v(L) \quad v'(L)\rangle \tag{4.14}$$

From Eq. (4.11), by substituting into Eqs. (4.8) and (4.9), one obtains

$$U_{T1} = \frac{1}{2}\left(\left\langle \bar{w}_T \right\rangle_{1\times 2}^T \left[K_1\right]_{2\times 2} \left\{\bar{w}_T\right\}_{2\times 1} + \left\langle \bar{v} \right\rangle_{1\times 4}^T \left[K_2\right]_{4\times 4} \left\{\bar{v}\right\}_{4\times 1}\right)$$

$$U_{B1} = \frac{1}{2}\left(\left\langle \bar{w}_B \right\rangle_{1\times 2}^T \left[K_3\right]_{2\times 2} \left\{\bar{w}_B\right\}_{2\times 1} + \left\langle \bar{v} \right\rangle_{1\times 4}^T \left[K_4\right]_{4\times 4} \left\{\bar{v}\right\}_{4\times 1}\right)$$

$$\begin{aligned} U_{W1} = \frac{1}{2}\Big\{ & \left\langle \bar{w}_T \right\rangle_{1\times 2}^T \left[K_5\right]_{2\times 2} \left\{\bar{w}_T\right\}_{2\times 1} + \left\langle \bar{w}_B \right\rangle_{1\times 2}^T \left[K_5\right]_{2\times 2} \left\{\bar{w}_B\right\}_{2\times 1} + 2\left\langle \bar{w}_T \right\rangle_{1\times 2}^T \left[K_5\right]_{2\times 2} \left\{\bar{w}_B\right\}_{2\times 1} \\ & + \left\langle \bar{w}_T \right\rangle_{1\times 2}^T \left[K_6\right]_{2\times 2} \left\{\bar{w}_T\right\}_{2\times 1} + \left\langle \bar{w}_B \right\rangle_{1\times 2}^T \left[K_6\right]_{2\times 2} \left\{\bar{w}_B\right\}_{2\times 1} - 2\left\langle \bar{w}_T \right\rangle_{1\times 2}^T \left[K_6\right]_{2\times 2} \left\{\bar{w}_B\right\}_{2\times 1} \\ & + \left\langle \bar{w}_T \right\rangle_{1\times 2}^T \left[K_7\right]_{2\times 2} \left\{\bar{w}_T\right\}_{2\times 1} + \left\langle \bar{w}_B \right\rangle_{1\times 2}^T \left[K_7\right]_{2\times 2} \left\{\bar{w}_B\right\}_{2\times 1} - 2\left\langle \bar{w}_T \right\rangle_{1\times 2}^T \left[K_7\right]_{2\times 2} \left\{\bar{w}_B\right\}_{2\times 1} \\ & + \left\langle \bar{v} \right\rangle_{1\times 4}^T \left[K_8\right]_{4\times 4} \left\{\bar{v}\right\}_{4\times 1} - 2\left\langle \bar{v} \right\rangle_{1\times 4}^T \left[K_9\right]_{4\times 2} \left\{\bar{w}_T\right\}_{2\times 1} + 2\left\langle \bar{v} \right\rangle_{1\times 4}^T \left[K_9\right]_{4\times 2} \left\{\bar{w}_B\right\}_{2\times 1}\Big\} \end{aligned}$$

$$V_1 = \left\langle Q_{zT} \right\rangle_{1\times 2}^T \left\{\bar{w}_T\right\}_{2\times 1} + \left\langle Q_{zB} \right\rangle_{1\times 2}^T \left\{\bar{w}_B\right\}_{2\times 1} + \left\langle Q_y \right\rangle_{1\times 4}^T \left\{\bar{v}\right\}_{4\times 1}$$

in which,

$$\left[K_1\right]_{2\times 2} = EA_T \int_z \left\{N'(z)\right\}\left\langle N'(z)\right\rangle^T dz$$

$$\left[K_2\right]_{4\times 4} = EI_{xxT} \int_z \left\{H_1''(z)\right\}\left\langle H_1''(z)\right\rangle^T dz$$

$$\left[K_3\right]_{2\times 2} = EA_B \int_z \left\{N'(z)\right\}\left\langle N'(z)\right\rangle^T dz$$

$$\left[K_4\right]_{4\times 4} = EI_{xxB} \int_z \left\{H_1''(z)\right\}\left\langle H_1''(z)\right\rangle^T dz$$

$$\left[K_5\right]_{2\times 2} = EA_W/4 \int_z \left\{N'(z)\right\}\left\langle N'(z)\right\rangle^T dz$$

$$\left[K_6\right]_{2\times 2} = EI_{xxW}/h^2 \int_z \left\{N'(z)\right\}\left\langle N'(z)\right\rangle^T dz$$

$$\left[K_7\right]_{2\times 2} = GA_W/h^2 \int_z \left\{N(z)\right\}\left\langle N(z)\right\rangle^T dz$$

$$\left[K_8\right]_{4\times 4} = GA_W \int_z \left\{H_1'(z)\right\}\left\langle H_1'(z)\right\rangle^T dz$$

$$\left[K_9\right]_{4\times 2} = GA_W/h \int_z \left\{H_1'(z)\right\}\left\langle N(z)\right\rangle^T dz$$

and

$$\left\langle Q_{zT}\right\rangle_{1\times 2} = q_{zT}\int_z \left\langle N(z)\right\rangle_{1\times 2}^T dz \quad , \quad \left\langle Q_{zB}\right\rangle_{1\times 2} = q_{zB}\int_z \left\langle N(z)\right\rangle_{1\times 2}^T dz \, , \quad \left\langle Q_y\right\rangle_{1\times 4} = q_y\int_z \left\langle H_1(z)\right\rangle_{1\times 4}^T dz \tag{4.15}$$

4.6.1.2. **Equilibrium Conditions**

By taking the first variation of total potential energy and setting it equal to zero, one obtains the stationary condition, i.e.

$$\delta\pi = \delta\{\Delta_1\}\left(\left[\bar{K}_1\right]\{\Delta_1\} - \{Q_1\}\right) = 0 \tag{4.16}$$

in which,

$$\left[\bar{K}_1\right]_{8\times8} = \left[\begin{array}{c:c:c} \left([K_1]+[K_5]+[K_7]+[K_9]\right)_{2\times2} & \left([K_6]-[K_8]-[K_{10}]\right)_{2\times2} & [K_{12}]_{2\times4} \\ \hdashline \left([K_6]-[K_8]-[K_{10}]\right)_{2\times2} & \left([K_3]+[K_5]+[K_7]+[K_9]\right)_{2\times2} & -[K_{13}]_{2\times4} \\ \hdashline [K_{12}]^T_{4\times2} & -[K_{13}]^T_{4\times2} & \left([K_2]+[K_4]+[K_{11}]\right)_{4\times4} \end{array}\right] \tag{4.17}$$

$\langle Q_1\rangle^T_{1\times8} = \left\langle \langle Q_{zT}\rangle_{1\times2} \;\vdots\; \langle Q_{zB}\rangle_{1\times2} \;\vdots\; \langle Q_y\rangle_{1\times4} \right\rangle$, and one recalls that $\{\Delta_1\}$ has been defined in Eq. (4.13)

4.6.2. **Lateral-torsional response**

4.6.2.1. **Displacement fields in terms of Nodal Displacement**

In a similar manner, displacement fields of lateral torsional response are interpolated through Hermitian polynomials, i.e.

$$\begin{aligned} u_T(z) &= \langle H_2(z)\rangle^T_{1\times4}\{\bar{u}_T\}_{4\times1}, \theta_T(z) = \langle H_2(z)\rangle^T_{1\times4}\{\bar{\theta}_T\}_{4\times1} \\ u_B(z) &= \langle H_2(z)\rangle^T_{1\times4}\{\bar{u}_B\}_{4\times1}, \theta_B(z) = \langle H_2(z)\rangle^T_{1\times4}\{\bar{\theta}_B\}_{4\times1} \end{aligned} \tag{4.18}$$

in which

$$\langle \Delta_2\rangle^T_{1\times16} = \left\langle \langle \bar{u}_T\rangle^T_{1\times4} \;\vdots\; \langle \bar{\theta}_T\rangle^T_{1\times4} \;\vdots\; \langle \bar{u}_B\rangle^T_{1\times4} \;\vdots\; \langle \bar{\theta}_B\rangle^T_{1\times4} \right\rangle \tag{4.19}$$

where,

$$\begin{aligned} \langle \bar{u}_T\rangle^T_{1\times4} &= \langle u_T(0) \quad u'_T(0) \quad u_T(L) \quad u'_T(L)\rangle \\ \langle \bar{u}_B\rangle^T_{1\times4} &= \langle u_B(0) \quad u'_B(0) \quad u_B(L) \quad u'_B(L)\rangle \\ \langle \bar{\theta}_T\rangle^T_{1\times4} &= \langle \theta_T(0) \quad \theta'_T(0) \quad \theta_T(L) \quad \theta'_T(L)\rangle \\ \langle \bar{\theta}_B\rangle^T_{1\times4} &= \langle \theta_B(0) \quad \theta'_B(0) \quad \theta_B(L) \quad \theta'_B(L)\rangle \end{aligned} \tag{4.20}$$

Shape function $\langle H_2(z)\rangle^T$ is nearly identical to $\langle H_1(z)\rangle^T$ with a difference in sign in the second and fourth terms, i.e.

$$\left\langle H_2(z)\right\rangle^T = \left\langle 1-3(z/L)^2+2(z/L)^3 \;\vdots\; z\left[1-(z/L)\right]^2 \;\vdots\; 3(z/L)^2-2(z/L)^3 \;\vdots\; L\left[(z/L)^3-(z/L)^2\right]\right\rangle \tag{4.21}$$

From Eq. (4.18) by substituting into Eqs. (4.8) and (4.9), lateral torsional components of total potential energy are expressed in terms of nodal displacements, i.e.

$$U_{T2} = \frac{1}{2}\left(\left\langle \bar{u}_T\right\rangle^T \left[K_{10}\right]\left\{\bar{u}_T\right\} + \left\langle \bar{\theta}_T\right\rangle^T \left[K_{11}\right]\left\{\bar{\theta}_T\right\} + \left\langle \bar{\theta}_T\right\rangle^T \left[K_{12}\right]\left\{\bar{\theta}_T\right\}\right)$$

$$U_{B2} = \frac{1}{2}\left(\left\langle \bar{u}_B\right\rangle^T \left[K_{13}\right]\left\{\bar{u}_B\right\} + \left\langle \bar{\theta}_B\right\rangle^T \left[K_{14}\right]\left\{\bar{\theta}_B\right\} + \left\langle \bar{\theta}_B\right\rangle^T \left[K_{15}\right]\left\{\bar{\theta}_B\right\}\right)$$

$$U_{W2} = \frac{1}{2}\left[\left\langle \Delta_2\right\rangle^T \left[K_{16}\right]\left\{\Delta_2\right\} + \left\langle \Delta_2\right\rangle^T \left[K_{17}\right]\left\{\Delta_2\right\} + \left\langle \Delta_2\right\rangle^T \left[K_{18}\right]\left\{\Delta_2\right\} + \left\langle \Delta_2\right\rangle^T \left[K_{19}\right]\left\{\Delta_2\right\}\right]$$

$$V_2 = Q_{xT}\left\{\bar{u}_T\right\} + Q_{xB}\left\{\bar{u}_B\right\} + M_T\left\{\bar{\theta}_T\right\} + M_B\left\{\bar{\theta}_B\right\}$$

in which,

$$\left[K_{10}\right]_{4\times4} = EI_{yyT}\int_z \left\{H_2''(z)\right\}\left\langle H_2''(z)\right\rangle^T dz$$

$$\left[K_{11}\right]_{4\times4} = EI_{\omega\omega T}\int_z \left\{H_2''(z)\right\}\left\langle H_2''(z)\right\rangle^T dz$$

$$\left[K_{12}\right]_{4\times4} = GJ_T\int_z \left\{H_2'(z)\right\}\left\langle H_2'(z)\right\rangle^T dz$$

$$\left[K_{13}\right]_{4\times4} = EI_{yyB}\int_z \left\{H_2''(z)\right\}\left\langle H_2''(z)\right\rangle^T dz$$

$$\left[K_{14}\right]_{4\times4} = EI_{\omega\omega B}\int_z \left\{H_2''(z)\right\}\left\langle H_2''(z)\right\rangle^T dz$$

$$\left[K_{15}\right]_{4\times4} = GJ_B\int_z \left\{H_2'(z)\right\}\left\langle H_2'(z)\right\rangle^T dz$$

$$\left[K_{16}\right]_{16\times16} = \int_z \left[L_{N_{WP}}(z)\right]''^T \left[A_{WP1}\right]\left[L_{N_{WP}}(z)\right]'' dz$$

$$\left[K_{17}\right]_{16\times16} = \int_z \left[L_{N_{WP}}(z)\right]^T \left[A_{WP2}\right]\left[L_{N_{WP}}(z)\right] dz$$

$$\left[K_{18}\right]_{16\times16} = \int_z \left[L_{N_{WP}}(z)\right]'^T \left[A_{WP3}\right]\left[L_{N_{WP}}(z)\right]' dz$$

$$\left[K_{19}\right]_{16\times16} = \int_z \left[L_{N_{WP}}(z)\right]'^T \left[A_{WP4}\right]\left[L_{N_{WP}}(z)\right]' dz$$

$$\left\langle Q_{xT}\right\rangle_{1\times4} = q_{xT}\int_z \left\langle H_2(z)\right\rangle dz \quad , \quad \left\langle Q_{xB}\right\rangle_{1\times4} = q_{xB}\int_z \left\langle H_2(z)\right\rangle dz$$

$$\left\langle M_T\right\rangle_{1\times4} = m_T\int_z \left\langle H_2(z)\right\rangle dz \quad , \quad \left\langle M_B\right\rangle_{1\times4} = m_B\int_z \left\langle H_2(z)\right\rangle dz$$

where,

$$[A_{WP1}]_{4\times4}=\frac{D}{420}\begin{bmatrix}156h & 22h^2 & 54h & -13h^2\\ 22h^2 & 4h^3 & 13h^2 & -3h^3\\ 54h & 13h^2 & 156h & -22h^2\\ -13h^2 & -3h^3 & -22h^2 & 4h^3\end{bmatrix},[A_{WP2}]_{4\times4}=\frac{D}{12h^3}\begin{bmatrix}144 & 72h & -144 & 72h\\ 72h & 48h^2 & -72h & 24h^2\\ -144 & -72h & 144 & -72h\\ 72h & 24h^2 & -72h & 48h^2\end{bmatrix}$$

$$[A_{WP3}]_{4\times4}=\frac{D\nu}{30h}\begin{bmatrix}-36 & -3h & 36 & -3h\\ -3h & -4h^2 & 3h & h^2\\ 36 & 3h & -36 & 3h\\ -3h & h^2 & 3h & -4h^2\end{bmatrix},[A_{WP4}]_{4\times4}=\frac{D(1-\nu)}{15h}\begin{bmatrix}36 & 3h & -36 & 3h\\ 3h & 4h^2 & -3h & -h^2\\ -36 & -3h & 36 & -3h\\ 3h & -h^2 & -3h & 4h^2\end{bmatrix}$$

$$\left[L_{N_{WP}}\right]_{4\times16}=\left[\begin{array}{c:c:c:c}\langle H_2(z)\rangle^T_{1\times4} & 0 & 0 & 0\\ \hdashline 0 & \langle H_2(z)\rangle^T_{1\times4} & 0 & 0\\ \hdashline 0 & 0 & \langle H_2(z)\rangle^T_{1\times4} & 0\\ \hdashline 0 & 0 & 0 & \langle H_2(z)\rangle^T_{1\times4}\end{array}\right]$$

4.6.2.2. **Equilibrium Conditions**

By taking the first variation of total potential energy and setting it equal to zero, one obtains the stationary condition

$$\delta\pi=\delta\{\Delta_2\}\left(\left[\bar{K}_2\right]\{\Delta_2\}-\{Q_2\}\right)=0 \tag{4.22}$$

in which,

$$\left[\bar{K}_2\right]_{16\times16}=\left[\bar{\bar{K}}_2\right]_{16\times16}+[K_{16}]_{16\times16}+[K_{17}]_{16\times16}+[K_{18}]_{16\times16}+[K_{19}]_{16\times16} \tag{4.23}$$

and $\left[\bar{\bar{K}}_2\right]$ is a diagonal block matrix, defined by

$$\left[\bar{\bar{K}}_2\right]=Diag\left([K_{10}],[K_{11}]+[K_{12}],[K_{13}],[K_{14}]+[K_{15}]\right) \tag{4.24}$$

In Eq. (4.22), the energy equivalent load vector $\langle Q_2\rangle^T$ is defined as,

$$\langle Q_2\rangle^T_{1\times16}=\left\langle\langle Q_{xT}\rangle_{1\times4}\quad\langle M_T\rangle_{1\times4}\quad\langle Q_{xB}\rangle_{1\times4}\quad\langle M_B\rangle_{1\times4}\right\rangle \tag{4.25}$$

4.7. **Finite Element Formulation 2- Based on Exact Shape Functions (FE2)**

In this section, a finite element based on the closed form solution is devised. In a recent study, Pezeshky and Mohareb (2014) formulated the governing equations for the problem yielding two sets of coupled differential equations. The first set governs the longitudinal-transverse response and takes the form

$$\begin{bmatrix} P_{11}(\mathscr{D}) & P_{12}(\mathscr{D}) & P_{13}(\mathscr{D}) \\ P_{21}(\mathscr{D}) & P_{22}(\mathscr{D}) & P_{23}(\mathscr{D}) \\ P_{31}(\mathscr{D}) & P_{32}(\mathscr{D}) & P_{33}(\mathscr{D}) \end{bmatrix}_{3\times3} \begin{Bmatrix} w_T \\ w_B \\ v \end{Bmatrix}_{3\times1} = \begin{Bmatrix} q_{zT} \\ q_{zB} \\ q_y \end{Bmatrix}_{3\times1} \tag{4.26}$$

in which $\mathscr{D}$ denotes the differential operator and $P_{11} - P_{33}$ are defined as

$$P_{11}(\mathscr{D}) = -E\left(A_T + \frac{A_w}{4} + \frac{I_{xxw}}{h^2}\right)\mathscr{D}^2 + \frac{GA_w}{h^2} \quad , \quad P_{12}(\mathscr{D}) = P_{21}(\mathscr{D}) = -E\left(\frac{A_w}{4} - \frac{I_{xxw}}{h^2}\right)\mathscr{D}^2 - \frac{GA_w}{h^2}$$

$$P_{13}(\mathscr{D}) = P_{31}(\mathscr{D}) = -\frac{GA_w}{h}\mathscr{D} \quad , \quad P_{22}(\mathscr{D}) = -E\left(A_B + \frac{A_w}{4} + \frac{I_{xxw}}{h^2}\right)\mathscr{D}^2 + \frac{GA_w}{h^2},$$

$$P_{23}(\mathscr{D}) = P_{32}(\mathscr{D}) = \frac{GA_w}{h}\mathscr{D} \quad , \quad P_{33}(\mathscr{D}) = -E\left(I_{xxT} + I_{xxB}\right)\mathscr{D}^4 + GA_w\mathscr{D}^2$$

The second set of DEs governs the lateral-torsional response including distortional effects and takes the form

$$\begin{bmatrix} Q_{11}(\mathscr{D}) & Q_{12}(\mathscr{D}) & Q_{13}(\mathscr{D}) & Q_{14}(\mathscr{D}) \\ Q_{21}(\mathscr{D}) & Q_{22}(\mathscr{D}) & Q_{23}(\mathscr{D}) & Q_{24}(\mathscr{D}) \\ Q_{31}(\mathscr{D}) & Q_{32}(\mathscr{D}) & Q_{33}(\mathscr{D}) & Q_{34}(\mathscr{D}) \\ Q_{41}(\mathscr{D}) & Q_{42}(\mathscr{D}) & Q_{34}(\mathscr{D}) & Q_{44}(\mathscr{D}) \end{bmatrix} \begin{Bmatrix} u_T \\ \theta_T \\ u_B \\ \theta_B \end{Bmatrix} = \begin{Bmatrix} q_{xT} \\ m_T \\ q_{xB} \\ m_B \end{Bmatrix} \tag{4.27}$$

where the differential operators $Q_{11} - Q_{44}$ are defined as

$$Q_{11}(\mathscr{D}) = \left[EI_{yyT} + \frac{13Dh}{35}\right]\mathscr{D}^4 - \frac{12D}{5h}\mathscr{D}^2 + \frac{12D}{h^3}$$

$$Q_{12}(\mathscr{D}) = Q_{21}(\mathscr{D}) = \frac{11Dh^2}{210}\mathscr{D}^4 - \frac{D}{5}\mathscr{D}^2 + \frac{6D}{h^2}$$

$$Q_{22}(\mathscr{D}) = \left[EI_{\omega\omega T} + \frac{h^3 D}{105}\right]\mathscr{D}^4 - \left[GJ_T + \frac{4Dh}{15}\right]\mathscr{D}^2 + \frac{4D}{h}$$

$$Q_{13}(\mathscr{D}) = Q_{31}(\mathscr{D}) = \frac{9Dh}{70}\mathscr{D}^4 + \frac{36D}{15h}\mathscr{D}^2 - \frac{12D}{h^3}$$

$$Q_{23}(\mathscr{D}) = Q_{32}(\mathscr{D}) = \frac{13Dh^2}{420}\mathscr{D}^4 + \frac{D}{5}\mathscr{D}^2 - \frac{6D}{h^2}$$

$$Q_{14}(\mathscr{D}) = Q_{41}(\mathscr{D}) = \frac{-13Dh^2}{420}\mathscr{D}^4 - \frac{D}{5}\mathscr{D}^2 + \frac{6D}{h^2}$$

$$Q_{24}\left(\mathscr{D}\right)=Q_{42}\left(\mathscr{D}\right)=-\frac{h^3D}{140}\mathscr{D}^4+\frac{Dh}{15}\mathscr{D}^2+\frac{2D}{h}$$

$$Q_{34}\left(\mathscr{D}\right)=Q_{43}\left(\mathscr{D}\right)=\frac{-11Dh^2}{210}\mathscr{D}^4+\frac{D}{5}\mathscr{D}^2-\frac{6D}{h^2}$$

$$Q_{33}\left(\mathscr{D}\right)=\left[EI_{yyB}+\frac{13Dh}{35}\right]\mathscr{D}^4-\frac{36D}{15h}\mathscr{D}^2+\frac{12D}{h^3}$$

$$Q_{44}\left(\mathscr{D}\right)=\left[EI_{\omega\omega B}+\frac{Dh^3}{105}\right]\mathscr{D}^4-\left[GJ_B\mathscr{D}^2+\frac{4Dh}{15}\right]\mathscr{D}^2+\frac{4D}{h}$$

The closed form solution has been obtained and displacement fields are expressed as

$$\begin{Bmatrix} w_T(z) \\ w_B(z) \\ v(z) \end{Bmatrix}=\left[\Phi(z)\right]_{3\times 8}\{C\}_{8\times 1}=\begin{bmatrix} \left\langle \Phi_{w_T}(z)\right\rangle_{1\times 8} \\ \left\langle \Phi_{w_B}(z)\right\rangle_{1\times 8} \\ \left\langle \Phi_{v}(z)\right\rangle_{1\times 8} \end{bmatrix}\{C\}_{8\times 1} \tag{4.28}$$

and

$$\begin{Bmatrix} u_T(z) \\ \theta_T(z) \\ u_B(z) \\ \theta_B(z) \end{Bmatrix}=\left[\Psi(z)\right]_{4\times 16}\{B\}_{16\times 1}=\begin{bmatrix} \left\langle \Psi_{u_T}(z)\right\rangle_{1\times 16} \\ \left\langle \Psi_{\theta_T}(z)\right\rangle_{1\times 16} \\ \left\langle \Psi_{u_B}(z)\right\rangle_{1\times 16} \\ \left\langle \Psi_{\theta_B}(z)\right\rangle_{1\times 16} \end{bmatrix}\{B\}_{16\times 1} \tag{4.29}$$

in which $\left[\Phi(z)\right]$ and $\left[\Psi(z)\right]$ are the solution functions of the system of equations (3.29) and (3.31) as provided in Pezeshky and Mohareb (2014), $\langle B\rangle^T_{16\times 1}=\langle B_i \quad B_2 \quad .... \quad B_{16}\rangle^T$ and $\langle C\rangle^T_{8\times 1}=\langle C_1 \quad C_2 \quad .... \quad C_8\rangle$ are vectors of integration constants to be determined from the boundary conditions. In a manner similar to FE1 formulation, two separate finite elements are developed for a) the longitudinal-transverse response and b) the lateral-torsional response.

4.7.1. **Longitudinal-transverse response**

4.7.1.1. **Displacement fields in terms of Nodal Displacement**

The continuous displacement fields are related to the nodal displacements shown in Fig. 4-2a. Rather than using the polynomial interpolation scheme adopted in the FE1 formulation, the closed form solution provided in Eqs. (4.28) is used to develop shape functions which satisfy the equilibrium equations. The nodal displacements $\{\bar{w}_T\},\{\bar{w}_B\},\{\bar{v}\}$ are related to the vector of constants $\{C\}$ through

$$\begin{Bmatrix} \{\bar{w}_T\}_{2\times1} \\ \{\bar{w}_B\}_{2\times1} \\ \{\bar{v}\}_{4\times1} \end{Bmatrix}_{8\times1} = \begin{bmatrix} [E_1]_{2\times8} \\ [E_2]_{2\times8} \\ [E_3]_{4\times8} \end{bmatrix}_{8\times8} \{C\}_{8\times1} = \left[\bar{E}\right]_{8\times8}\{C\}_{8\times1} \tag{4.30}$$

in which sub-matrices $[E_i],\quad i=1,2,3$ are defined as

$$[E_1]_{2\times8} = \left[\{\Phi_{w_T}(0)\}_{8\times1}^T \;\vdots\; \{\Phi_{w_T}(L)\}_{8\times1}^T\right]_{2\times8}^T$$

$$[E_2]_{2\times8} = \left[\{\Phi_{w_B}(0)\}_{8\times1}^T \;\vdots\; \{\Phi_{w_B}(L)\}_{8\times1}^T\right]_{2\times8}^T$$

$$[E_3]_{4\times8} = \left[\{\Phi_{v}(0)\}_{8\times1}^T \;\vdots\; \{\Phi'_{v}(0)\}_{8\times1}^T \;\vdots\; \{\Phi_{v}(L)\}_{8\times1}^T \;\vdots\; \{\Phi'_{v}(L)\}_{8\times1}^T\right]_{4\times8}^T$$

Equation (4.30) is solved for the vector of integration constants $\{C\}$ and substituted into Eq. (4.28) , yielding

$$\begin{Bmatrix} w_T(z) \\ w_B(z) \\ v(z) \end{Bmatrix}_{3\times1} = \left[\bar{A}(z)\right]_{3\times8} \begin{Bmatrix} \{\bar{w}_T\}_{2\times1} \\ \{\bar{w}_B\}_{2\times1} \\ \{\bar{v}\}_{4\times1} \end{Bmatrix}_{8\times1} = \begin{bmatrix} \langle \bar{A}_{w_T}(z)\rangle_{1\times8}^T \\ \langle \bar{A}_{w_B}(z)\rangle_{1\times8}^T \\ \langle \bar{A}_{v}(z)\rangle_{1\times8}^T \end{bmatrix} \begin{Bmatrix} \{\bar{w}_T\} \\ \{\bar{w}_B\} \\ \{\bar{v}\} \end{Bmatrix} = \begin{bmatrix} \langle \Phi_{w_T}(z)\rangle_{1\times8} \\ \langle \Phi_{w_B}(z)\rangle_{1\times8} \\ \langle \Phi_{v}(z)\rangle_{1\times8} \end{bmatrix} \left[\bar{E}\right]_{8\times8}^{-1} \begin{Bmatrix} \{\bar{w}_T\} \\ \{\bar{w}_B\} \\ \{\bar{v}\} \end{Bmatrix} \tag{4.31}$$

where the matrix of shape functions $\left[\bar{A}(z)\right] = \left[\Phi(z)\right]_{3\times8}\left[\bar{E}\right]_{8\times8}^{-1}$ has been defined. From Eq. (4.31), by substituting into the total potential energy equations (4.9), one obtains, i.e.,

$$U_{T1} = \frac{1}{2}\langle\Delta_1\rangle_{1\times8}^T\left([K_1]_{8\times8} + [K_2]_{8\times8}\right)\{\Delta_1\}_{8\times1}$$

$$U_{B1} = \frac{1}{2}\langle\Delta_1\rangle_{1\times8}^T\left([K_3]_{8\times8} + [K_4]_{8\times8}\right)\{\Delta_1\}_{8\times1}$$

$$\begin{aligned} U_{W1} = \frac{1}{2}\langle\Delta_1\rangle_{1\times8}^T \{ & [K_5]_{8\times8} + [K_6]_{8\times8} + 2[K_7]_{8\times8} + [K_8]_{8\times8} + [K_9]_{8\times8} - 2[K_{10}]_{8\times8} \\ & + [K_{11}]_{8\times8} + [K_{12}]_{8\times8} - 2[K_{13}]_{8\times8} + [K_{14}]_{8\times8} - 2[K_{15}]_{8\times8} + 2[K_{16}]_{8\times8}\}\{\Delta_1\}_{8\times1} \end{aligned}$$

$$V_1 = \langle Q_{zT}\rangle_{1\times8}^T\{\Delta_1\}_{8\times1} + \langle Q_{zB}\rangle_{1\times8}^T\{\Delta_1\}_{8\times1} + \langle Q_y\rangle_{1\times8}^T\{\Delta_1\}_{8\times1}$$

in which,

$$[K_1]_{8\times8} = EA_T \int_z \{\bar{A}'_{w_T}(z)\}\langle\bar{A}'_{w_T}(z)\rangle^T dz$$

$$[K_2]_{8\times8} = EI_{xxT} \int_z \{\bar{A}''_V(z)\}\langle\bar{A}''_V(z)\rangle^T dz$$

$$[K_3]_{8\times8} = EA_B \int_z \{\bar{A}'_{w_B}(z)\}\langle\bar{A}'_{w_B}(z)\rangle^T dz$$

$$[K_4]_{8\times8} = EI_{xxB} \int_z \{\bar{A}''_V(z)\}\langle\bar{A}''_V(z)\rangle^T dz$$

$$[K_5]_{8\times8} = EA_W/4 \int_z \{\bar{A}'_{w_T}(z)\}\langle\bar{A}'_{w_T}(z)\rangle^T dz$$

$$[K_6]_{8\times8} = EA_W/4 \int_z \{\bar{A}'_{w_B}(z)\}\langle\bar{A}'_{w_B}(z)\rangle^T dz$$

$$[K_7]_{8\times8} = EA_W/4 \int_z \{\bar{A}'_{w_T}(z)\}\langle\bar{A}'_{w_B}(z)\rangle^T dz$$

$$[K_8]_{8\times8} = EI_{xxW}/h^2 \int_z \{\bar{A}'_{w_T}(z)\}\langle\bar{A}'_{w_T}(z)\rangle^T dz$$

$$[K_9]_{8\times8} = EI_{xxW}/h^2 \int_z \{\bar{A}'_{w_B}(z)\}\langle\bar{A}'_{w_B}(z)\rangle^T dz$$

$$[K_{10}]_{8\times8} = EI_{xxW}/h^2 \int_z \{\bar{A}'_{w_T}(z)\}\langle\bar{A}'_{w_B}(z)\rangle^T dz$$

$$[K_{11}]_{8\times8} = GA_W/h^2 \int_z \{\bar{A}_{w_T}(z)\}\langle\bar{A}_{w_T}(z)\rangle^T dz$$

$$[K_{12}]_{8\times8} = GA_W/h^2 \int_z \{\bar{A}_{w_B}(z)\}\langle\bar{A}_{w_B}(z)\rangle^T dz$$

$$[K_{13}]_{8\times8} = GA_W/h^2 \int_z \{\bar{A}_{w_T}(z)\}\langle\bar{A}_{w_B}(z)\rangle^T dz$$

$$[K_{14}]_{8\times8} = GA_W \int_z \{\bar{A}'_V(z)\}\langle\bar{A}'_V(z)\rangle^T dz$$

$$[K_{15}]_{8\times8} = GA_W/h \int_z \{\bar{A}'_V(z)\}\langle\bar{A}_{w_T}(z)\rangle^T dz$$

$$[K_{16}]_{8\times8} = GA_W/h \int_z \{\bar{A}'_V(z)\}\langle\bar{A}_{w_B}(z)\rangle^T dz$$

and

$$\langle Q_{zT}\rangle_{1\times8} = q_{zT} \int_z \langle\bar{A}_{w_T}(z)\rangle dz \quad , \quad \langle Q_{zB}\rangle_{1\times8} = q_{zB} \int_z \langle\bar{A}_{w_B}(z)\rangle dz \quad , \qquad \langle Q_y\rangle_{1\times8} = q_y \int_z \langle\bar{A}_V(z)\rangle dz \tag{4.32}$$

4.7.1.2. **Equilibrium Conditions**

In a similar manner to equilibrium conditions of FE1, the equilibrium equation (4.16) is obtained and stiffness matrix and vector of nodal forces are introduced as,

$$\left[\bar{K}_1\right]_{8\times 8} = \sum_{i=1}^{16}\left[K_i\right] \tag{4.33}$$

$\left\langle Q_1\right\rangle^T_{1\times 8} = \left\langle \left\langle Q_{zT}\right\rangle_{1\times 8} + \left\langle Q_{zB}\right\rangle_{1\times 8} + \left\langle Q_y\right\rangle_{1\times 8}\right\rangle$, and one recalls that $\left\{\Delta_1\right\}$ has been defined in Eq. (4.13)

4.7.2. **Lateral torsional response**

4.7.2.1. **Displacement fields in terms of Nodal Displacement**

In a manner similar to the previous section, the continuous displacement fields are related to the nodal displacements shown in Fig. 4-2b. The closed form solution provided in Eqs. (4.29) is used to develop shape functions which satisfy the equilibrium equations. The nodal displacements $\left\{\bar{u}_T\right\},\left\{\bar{\theta}_T\right\},\left\{\bar{u}_B\right\},\left\{\bar{\theta}_B\right\}$ are related to the vector of constants $\left\{B\right\}$ through

$$\begin{Bmatrix} \left\{\bar{u}_T\right\} \\ \left\{\bar{\theta}_T\right\} \\ \left\{\bar{u}_B\right\} \\ \left\{\bar{\theta}_B\right\} \end{Bmatrix}_{16\times 1} = \begin{bmatrix} \left[E_4\right] \\ \left[E_5\right] \\ \left[E_6\right] \\ \left[E_7\right] \end{bmatrix}_{16\times 16} \left\{B\right\}_{16\times 1} = \left[\bar{\bar{E}}\right]_{16\times 16}\left\{B\right\}_{16\times 1} \tag{4.34}$$

in which sub-matrices $\left[E_i\right],\quad i = 4...7$ have been defined

$$\begin{aligned}
\left[E_4\right]_{4\times 16} &= \left[\left\{\Psi_{u_T}(0)\right\}^T_{16\times 1} \;\vdots\; \left\{\Psi'_{u_T}(0)\right\}^T_{16\times 1} \;\vdots\; \left\{\Psi_{u_T}(L)\right\}^T_{16\times 1} \;\vdots\; \left\{\Psi'_{u_T}(L)\right\}^T_{16\times 1}\right]^T_{4\times 16} \\
\left[E_5\right]_{4\times 16} &= \left[\left\{\Psi_{\theta_T}(0)\right\}^T_{16\times 1} \;\vdots\; \left\{\Psi'_{\theta_T}(0)\right\}^T_{16\times 1} \;\vdots\; \left\{\Psi_{\theta_T}(L)\right\}^T_{16\times 1} \;\vdots\; \left\{\Psi'_{\theta_T}(L)\right\}^T_{16\times 1}\right]^T_{4\times 16} \\
\left[E_6\right]_{4\times 16} &= \left[\left\{\Psi_{u_B}(0)\right\}^T_{16\times 1} \;\vdots\; \left\{\Psi'_{u_B}(0)\right\}^T_{16\times 1} \;\vdots\; \left\{\Psi_{u_B}(L)\right\}^T_{16\times 1} \;\vdots\; \left\{\Psi'_{u_B}(L)\right\}^T_{16\times 1}\right]^T_{4\times 16} \\
\left[E_7\right]_{4\times 16} &= \left[\left\{\Psi_{\theta_B}(0)\right\}^T_{16\times 1} \;\vdots\; \left\{\Psi'_{\theta_B}(0)\right\}^T_{16\times 1} \;\vdots\; \left\{\Psi_{\theta_B}(L)\right\}^T_{16\times 1} \;\vdots\; \left\{\Psi'_{\theta_B}(L)\right\}^T_{16\times 1}\right]^T_{4\times 16}
\end{aligned} \tag{4.35}$$

Solving Eq. (4.34) for $\left\{B\right\}$ and substituting into Eq. (4.29), the displacement fields are rewritten as,

$$\begin{Bmatrix} u_T(z) \\ \theta_T(z) \\ u_B(z) \\ \theta_B(z) \end{Bmatrix}_{4\times1} = \left[\bar{\bar{A}}(z)\right]_{4\times16} \begin{Bmatrix} \{\bar{u}_T\} \\ \{\bar{\theta}_T\} \\ \{\bar{u}_B\} \\ \{\bar{\theta}_B\} \end{Bmatrix}_{16\times1} = \begin{bmatrix} \left\langle \bar{\bar{A}}_{u_T}(z) \right\rangle_{1\times16} \\ \left\langle \bar{\bar{A}}_{\theta_T}(z) \right\rangle_{1\times16} \\ \left\langle \bar{\bar{A}}_{u_B}(z) \right\rangle_{1\times16} \\ \left\langle \bar{\bar{A}}_{\theta_B}(z) \right\rangle_{1\times16} \end{bmatrix} \begin{Bmatrix} \{\bar{u}_T\} \\ \{\bar{\theta}_T\} \\ \{\bar{u}_B\} \\ \{\bar{\theta}_B\} \end{Bmatrix} = \begin{bmatrix} \left\langle \Psi_{u_T}(z) \right\rangle_{1\times16} \\ \left\langle \Psi_{\theta_T}(z) \right\rangle_{1\times16} \\ \left\langle \Psi_{u_B}(z) \right\rangle_{1\times16} \\ \left\langle \Psi_{\theta_B}(z) \right\rangle_{1\times16} \end{bmatrix}_{4\times16} \left[\bar{\bar{E}}\right]^{-1}_{16\times16} \begin{Bmatrix} \{\bar{u}_T\} \\ \{\bar{\theta}_T\} \\ \{\bar{u}_B\} \\ \{\bar{\theta}_B\} \end{Bmatrix}$$

(4.36)

where $\left[\bar{\bar{A}}(z)\right]^{T}_{4\times16} = \left[\Psi(z)\right]_{4\times16}\left[\bar{\bar{E}}\right]^{-1}_{16\times16}$. By substituting Eq. (4.36) into the total potential energy Eqs. (4.9) , one obtains

$$U_{T2} = \frac{1}{2}\langle\Delta_2\rangle^{T}_{1\times16}\left(\left[K_{17}\right]+\left[K_{18}\right]+\left[K_{19}\right]\right)\{\Delta_2\}_{16\times1}$$

$$U_{B2} = \frac{1}{2}\langle\Delta_2\rangle^{T}_{1\times16}\left(\left[K_{20}\right]+\left[K_{21}\right]+\left[K_{22}\right]\right)\{\Delta_2\}_{16\times1}$$

$$U_{W2} = \frac{1}{2}\langle\Delta_2\rangle^{T}_{1\times16}\left[\left[K_{16}\right]+\left[K_{17}\right]+\left[K_{18}\right]+\left[K_{19}\right]\right]\{\Delta_2\}_{16\times1}$$

$$V_2 = Q_{xT}\{\Delta_2\} + Q_{xB}\{\Delta_2\} + M_T\{\Delta_2\} + M_B\{\Delta_2\}$$

in which,

$$\left[K_{17}\right]_{16\times16} = EI_{yyT}\int_z \left\{\bar{\bar{A}}''_{u_T}(z)\right\}\left\langle \bar{\bar{A}}''_{u_T}(z)\right\rangle^T dz$$

$$\left[K_{18}\right]_{16\times16} = EI_{\omega\omega T}\int_z \left\{\bar{\bar{A}}''_{\theta_T}(z)\right\}\left\langle \bar{\bar{A}}''_{\theta_T}(z)\right\rangle^T dz$$

$$\left[K_{19}\right]_{16\times16} = GJ_T\int_z \left\{\bar{\bar{A}}'_{\theta_T}\right\}\left\langle \bar{\bar{A}}'_{\theta_T}(z)\right\rangle^T dz$$

$$\left[K_{20}\right]_{16\times16} = EI_{yyB}\int_z \left\{\bar{\bar{A}}''_{u_B}(z)\right\}\left\langle \bar{\bar{A}}''_{u_B}(z)\right\rangle^T dz$$

$$\left[K_{21}\right]_{16\times16} = EI_{\omega\omega B}\int_z \left\{\bar{\bar{A}}''_{\theta_B}(z)\right\}\left\langle \bar{\bar{A}}''_{\theta_B}(z)\right\rangle^T dz$$

$$\left[K_{22}\right]_{16\times16} = GJ_B\int_z \left\{\bar{\bar{A}}'_{\theta_B}\right\}\left\langle \bar{\bar{A}}'_{\theta_B}(z)\right\rangle^T dz$$

$$\left[K_{23}\right]_{16\times16} = \int_z \left[\bar{\bar{A}}(z)\right]''^T \left[A_{WP1}\right]\left[\bar{\bar{A}}(z)\right]'' dz$$

$$\left[K_{24}\right]_{16\times16} = \int_z \left[\bar{\bar{A}}(z)\right]^T \left[A_{WP2}\right]\left[\bar{\bar{A}}(z)\right] dz$$

$$\left[K_{25}\right]_{16\times16} = \int_z \left[\bar{\bar{A}}(z)\right]''^T \left[A_{WP3}\right]\left[\bar{\bar{A}}(z)\right] dz$$

$$\left[K_{26}\right]_{16\times16} = \int_z \left[\bar{\bar{A}}(z)\right]'^T \left[A_{WP4}\right]\left[\bar{\bar{A}}(z)\right]' dz$$

$$\left\langle Q_{xT}\right\rangle_{1\times16} = q_{xT}\int_z \left\langle \bar{\bar{A}}_{u_T}(z)\right\rangle dz \quad , \quad \left\langle Q_{xB}\right\rangle_{1\times16} = q_{xB}\int_z \left\langle \bar{\bar{A}}_{u_B}(z)\right\rangle dz$$

$$\left\langle M_T\right\rangle_{1\times16} = m_T\int_z \left\langle \bar{\bar{A}}_{\theta_T}(z)\right\rangle dz \quad , \quad \left\langle M_B\right\rangle_{1\times16} = m_B\int_z \left\langle \bar{\bar{A}}_{\theta_B}(z)\right\rangle dz$$

where,

$$\left[A_{WP1}\right]_{4\times4} = \frac{D}{420}\begin{bmatrix} 156h & 22h^2 & 54h & -13h^2 \\ 22h^2 & 4h^3 & 13h^2 & -3h^3 \\ 54h & 13h^2 & 156h & -22h^2 \\ -13h^2 & -3h^3 & -22h^2 & 4h^3 \end{bmatrix}, \left[A_{WP2}\right]_{4\times4} = \frac{D}{12h^3}\begin{bmatrix} 144 & 72h & -144 & 72h \\ 72h & 48h^2 & -72h & 24h^2 \\ -144 & -72h & 144 & -72h \\ 72h & 24h^2 & -72h & 48h^2 \end{bmatrix}$$

$$\left[A_{WP3}\right]_{4\times4} = \frac{D\nu}{30h}\begin{bmatrix} -36 & -3h & 36 & -3h \\ -3h & -4h^2 & 3h & h^2 \\ 36 & 3h & -36 & 3h \\ -3h & h^2 & 3h & -4h^2 \end{bmatrix}, \left[A_{WP4}\right]_{4\times4} = \frac{D(1-\nu)}{15h}\begin{bmatrix} 36 & 3h & -36 & 3h \\ 3h & 4h^2 & -3h & -h^2 \\ -36 & -3h & 36 & -3h \\ 3h & -h^2 & -3h & 4h^2 \end{bmatrix}$$

4.7.2.2. **Equilibrium Conditions**

The equilibrium condition is evoked and the equilibrium equation (4.22) is obtained. Hence stiffness matrix and vector of nodal forces are introduced as,

$$\left[\bar{K}_2\right]_{16\times16} = \sum_{i=17}^{26}\left[K_i\right] \tag{4.37}$$

In Eq. (4.22), the energy equivalent load vector $\langle Q_2 \rangle^T$ is defined as,

$\langle Q_2 \rangle^T_{1\times16} = \left\langle \langle Q_{xT} \rangle_{1\times16} + \langle M_T \rangle_{1\times16} + \langle Q_{xB} \rangle_{1\times16} + \langle M_B \rangle_{1\times16} \right\rangle$, and one recalls that $\{\Delta_2\}$ has been defined in Eq. (4.19).

4.8. **Numerical Examples**

In this section, two newly developed finite elements are observed through numerical examples and results are compared to closed form expressions (Pezeshky and Mohareb (2014)). In all examples, a mono-symmetric WRF1000x340 steel section is considered with $E = 200,000\,MPa, \nu = 0.3$, (Fig. 4-3).

4.8.1. **Example 1: Cantilever under transverse loading**

A cantilever in which its span varies up to six meters is subjected to a concentrated transverse force applied at the tip (Point A), Fig. 4-3. Tip deflection is observed for various spans using two FEs and closed form solution (Fig. 4-3).

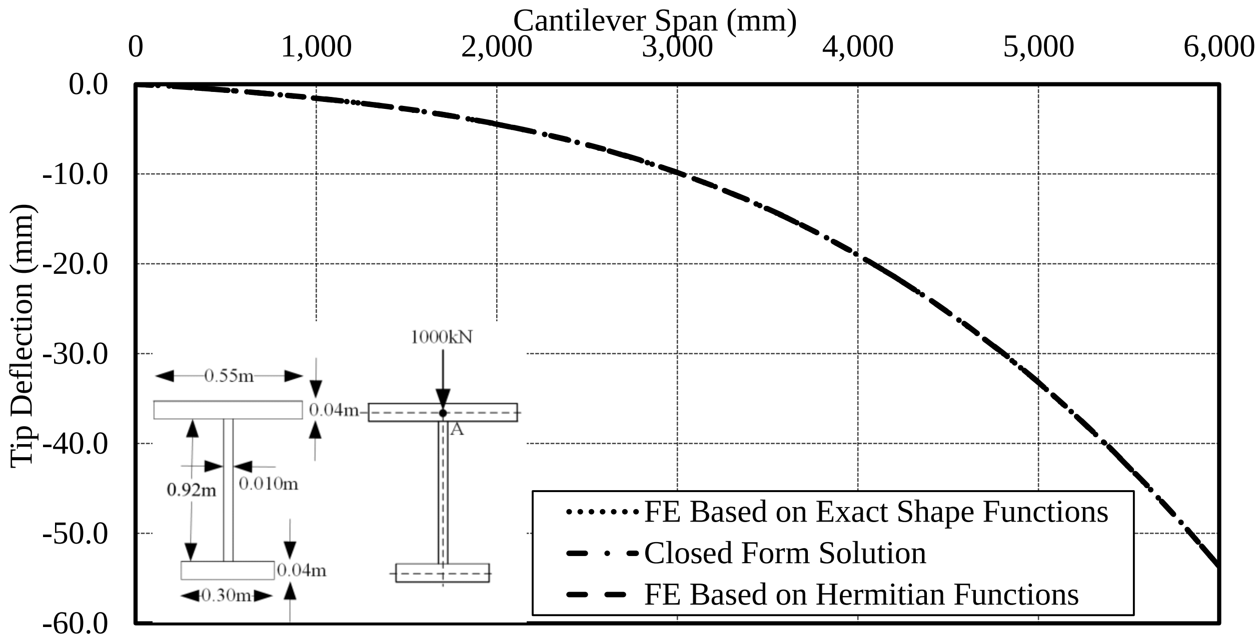

Fig. 4-3. Tip deflection under concentrated transverse force

Result obtained from both finite elements shows excellent agreements with the closed form solution.

4.8.2. **Example 2: Mesh Sensitivity Analysis**

A 12.00m span cantilever is subjected to two parallel 20 kN forces as show in Fig. 4-4. The problem is solved twice; once based on FE1 element and another time based on the FE2 element. For comparison, the problem is also solved based on the closed form solution provided in Pezeshky and Mohareb (2014).

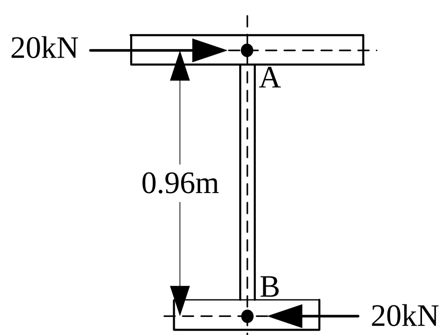

Fig. 4-4. Cantilever subjected to parallel forces

Table 4-1 provides the lateral displacements at generators A and B (Fig. 4-4) and angles of twists for the top and bottom flanges at the cantilever tip. The percentage difference (PD) from the closed form solution is also provided after each displacement field. The FE2 element based on the exact interpolation scheme was expected to yield a solution in exact agreement with the closed form solution. Thus, a solution based on a single 12m element was attempted but was found unsuccessful as matrix $\left[\bar{\bar{E}}\right]_{16\times16}$ was non-invertible. Several runs were then conducted while increasing the number of FE2 elements attempted, thus reducing the element span L. All attempts where $L > 1.5m$ were observed to fail in inverting matrix $\left[\bar{\bar{E}}\right]_{16\times16}$. The reasons for the numerical difficulties are discussed in Appendix A. In contrast, for all cases where the condition $L \le 1.5m$ was met, the FE2 solution was observed to be in perfect agreement with the closed form solution. The problem was also solved using several FE1 element meshes (ranging from a single element to 60 elements). Unlike the FE2 element, The FE1 solutions were found to be unconditionally stable. However, they involved discretization errors. The solution based on eight FE1 elements involved a discretization error of less than 0.40%. In this respect, the FE2 solution which involved no discretization error provided slightly superior results while adopting the same number of degrees of freedom.

Table 4-1. Mesh sensitivity analysis

Solution	N.O. of Elements	Top Flange				Bottom Flange			
		Lateral Displacement		Angle of Twist		Lateral Displacement		Angle of Twist	
		Magnitude (mm)	P.D.[1] %	Magnitude (rad)	P.D. %	Magnitude (mm)	P.D. %	Magnitude (rad)	P.D. %
FE2	8	23.37	0.0000	-0.1117	0.0000	-143.9	0.0000	-0.1363	0.0000
FE1	1	22.76	-2.589	-0.1078	-3.483	-140.2	-2.589	-0.1333	-2.165
	2	23.00	-1.596	-0.1095	-2.003	-141.6	-1.596	-0.1342	-1.531
	3	23.15	-0.9236	-0.1104	-1.2096	-142.6	-0.9235	-0.1350	-0.9359
	4	23.23	-0.6079	-0.1108	-0.8161	-143.1	-0.6079	-0.1354	-0.6376
	5	23.27	-0.4357	-0.1111	-0.5911	-143.3	-0.4357	-0.1356	-0.4660
	6	23.29	-0.3294	-0.1112	-0.4483	-143.5	-0.3294	-0.1358	-0.3567
	8	23.32	-0.2075	-0.1114	-0.2818	-143.6	-0.2075	-0.1359	-0.2282

	12	23.35	-0.1015	-0.1116	-0.1358	-143.8	-0.1015	-0.1361	-0.1138
	15	23.35	-0.0656	-0.1116	-0.0867	-143.9	-0.0656	-0.1361	-0.0745
	24	23.36	-0.0231	-0.1117	-0.0295	-143.9	-0.0231	-0.1362	-0.0270
	60	23.37	-0.0017	-0.1117	-0.0020	-143.9	-0.0146	-0.1362	-0.0021

P.D.[1]: Percentage Difference with closed form solution (Pezeshky and Mohareb (2014)).

4.8.3. Example 3: Beam with Overhangs under Torsion

A 6.00m span beam with one 1.5m overhang at both ends is subjected to a 5 kN/m lateral uniform distributed load acting at top flange, (Fig. 4-5a-b). The beam is laterally and torsionally supported at the bottom flange by two columns through lateral braces (not shown) and through the weak axis bending action of the supporting column (assumed to be large enough in this example to provide full fixity). Two cases are considered. These are (a) no stiffeners at the column to beam junction (Fig. 4-5a) keeping the top flange free to translate laterally, and (b) a pair of stiffeners at each flange (Fig. 4-5.b), providing a lateral restraint to the top flange at the column locations. It is required to analyze the beam using FE1 and compare the results against those obtained from 3D shell FEA in Abaqus. The model consists of 12 finite elements, i.e., 13 nodes with eight degrees of freedom per node corresponding to a total number of 104 DOFs. In the Abaqus model, 40 elements are taken along the web height, 11 along the top half flange width and six elements along the bottom half flange, respectively, and 240 elements were taken in the longitudinal direction. For a span of 6.00m, this corresponds to 108,450 degrees of freedom. In both models, the columns are idealized as point supports (Fig. 4-6a-b)

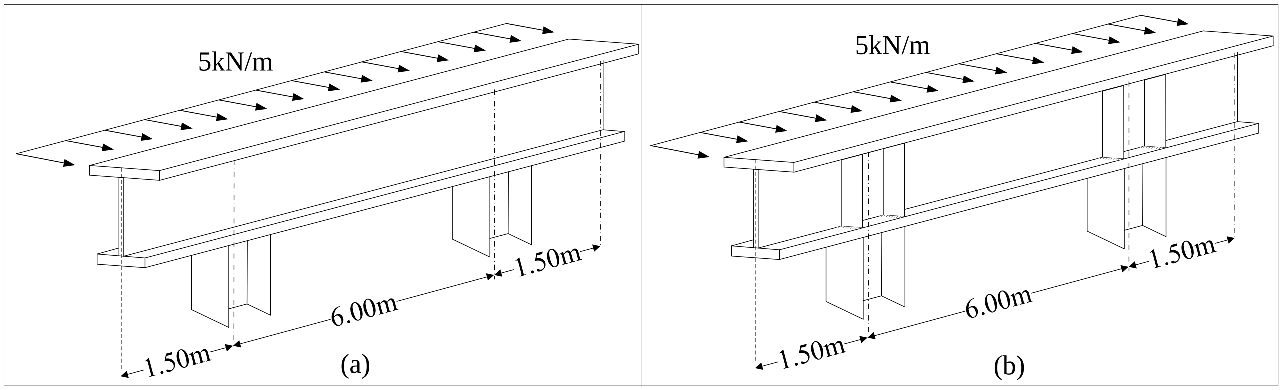

Fig. 4-5. Multi-span beam, a) No Stiffeners provided b) Pair of stiffeners provided

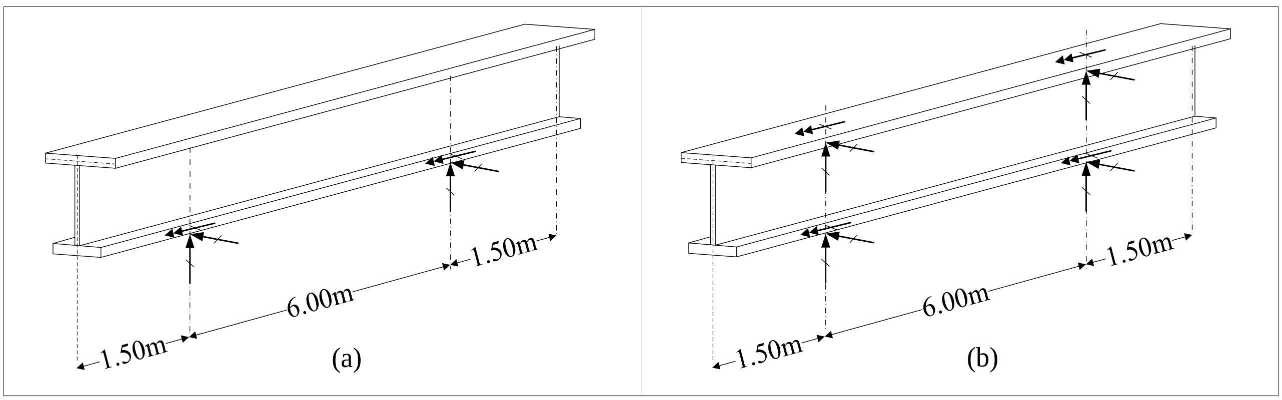

Fig. 4-6. Point supports at beam-column junction, a) no stiffeners provided b) stiffeners provided.

The lateral displacement of the top and bottom flanges along the span are shown in Fig. 4-7 and the twist diagrams are shown in Fig. 4-8. The results obtained from the FE1 solution are in excellent aggreement with those extracted from the shell FE in Abaqus. For the case without stiffeners, the lateral displacement of the top flange is significantly larger than that of the bottom flange. Also, the average angle of twist of the top flange is an order of magnitude greater than the average angle of twist of bottom flange (Fig. 4-8), suggesting significant distortion in the section.

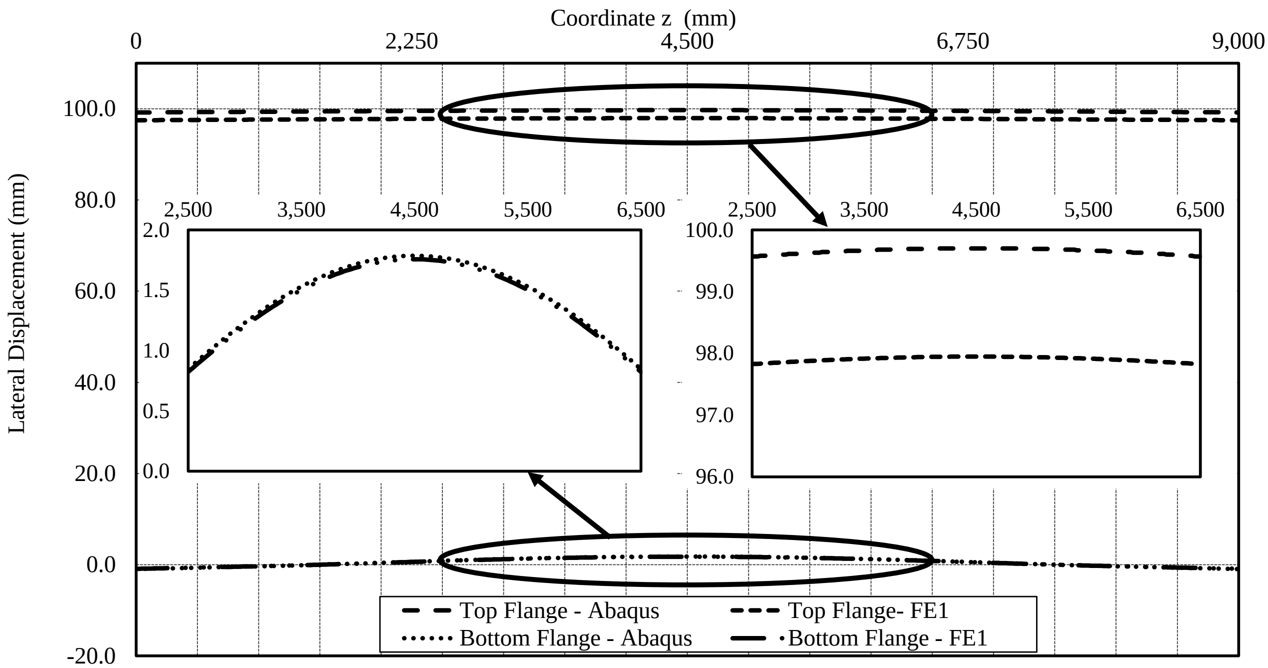

Fig. 4-7. Comparison of Lateral displacements along top and bottom flanges (mm)

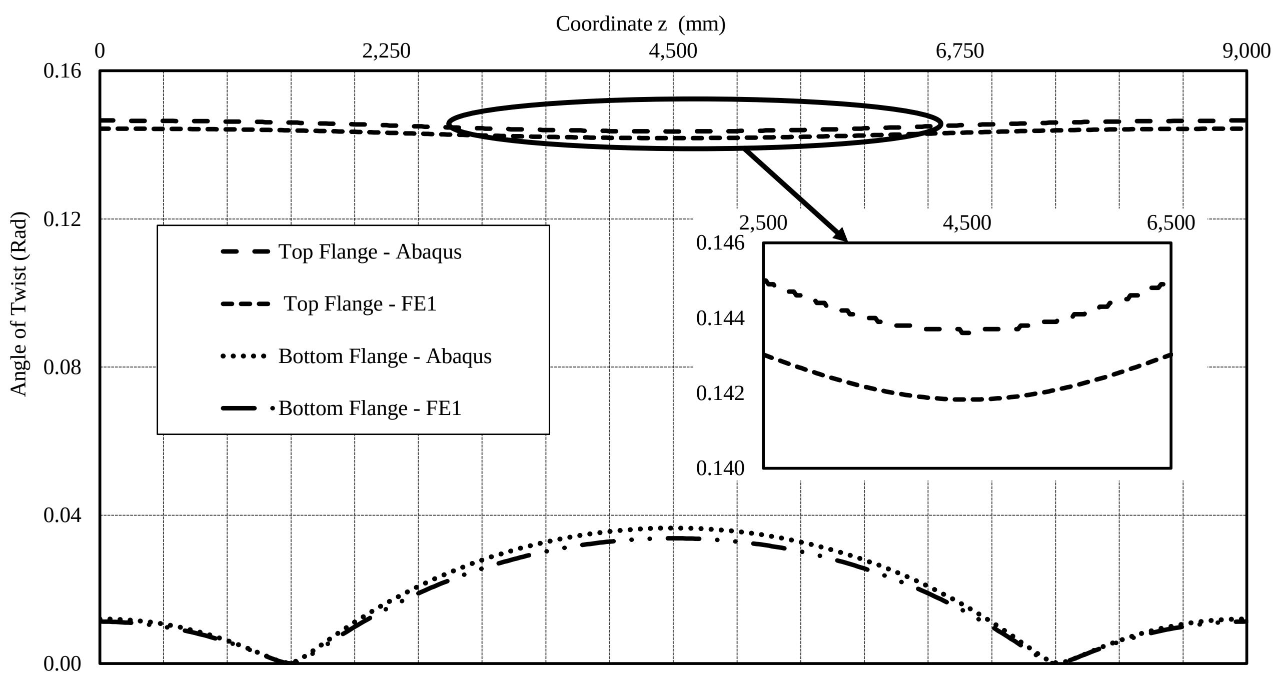

Fig. 4-8. Angle of twist of top and bottom flanges under Hermitian FE and Abaqus (mm)

For the stiffened case, the lateral displacements are shown in Fig. 4-9 and the angles of twist in Fig. 4-10. It is shown that the presence of stiffeners make the lateral displacement and angle of twist of the top flange nearly only slightly larger than those of the bottom flange. This is a natural of the fact that the uniform load is directly applied to the top flange.

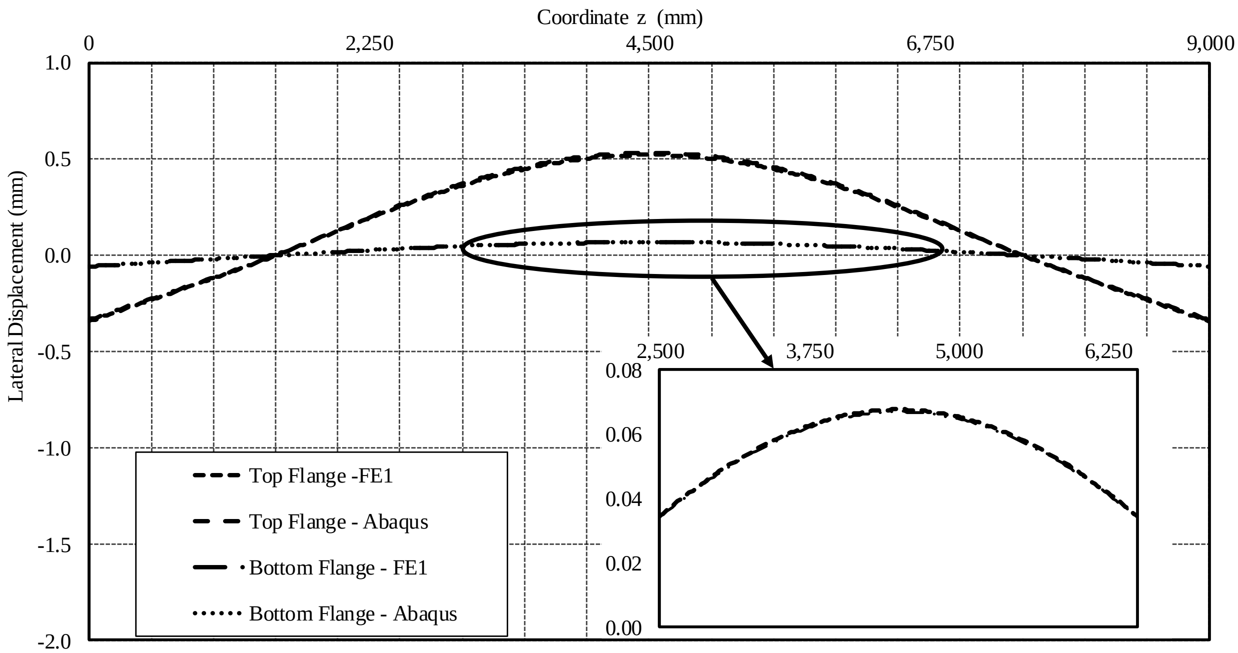

Fig. 4-9. Lateral displacement of top and bottom flanges of stiffened beam

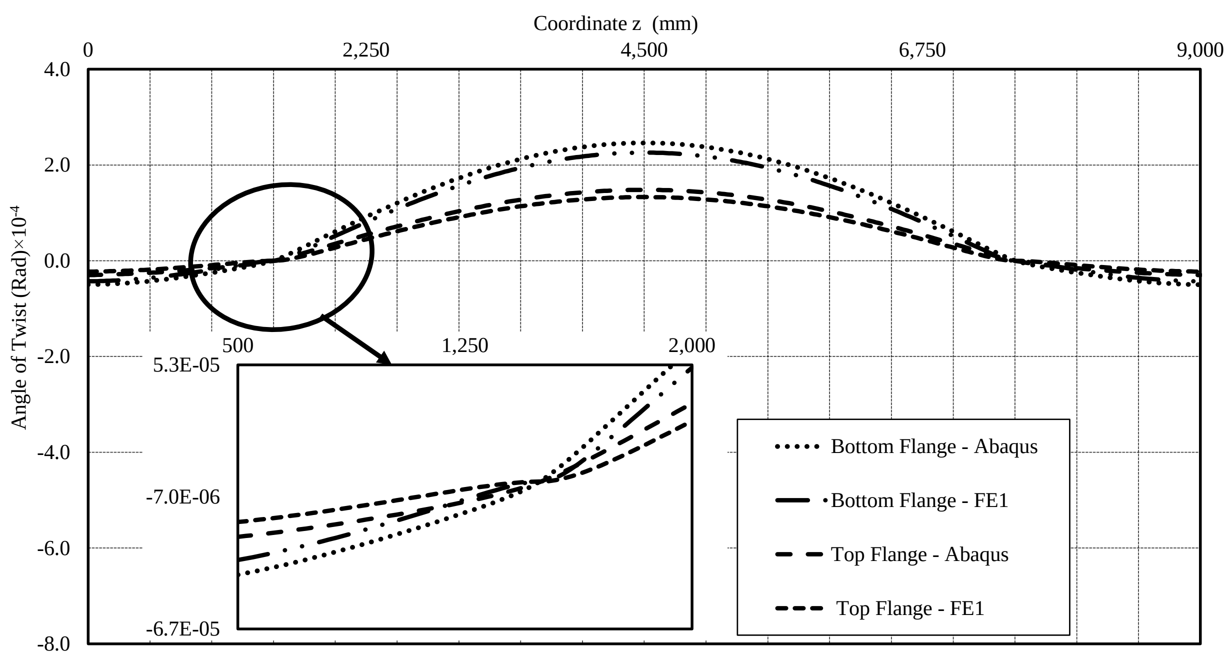

Fig. 4-10. Angle of twist of top and bottom flanges of stiffened beam

The example shows that the additon of stiffeners is particularly effective in reducing distortion in the beam by extending the point of lateral restraint at the column to beam junction to the top flange, thus reducing the difference in lateral displacements/twists of both flanges. The present finite element formulation is also shown to be successful in quantifying the distortion for both cases with and without stiffeners.

4.9. Summary and Conclusion

1- Two finite elements were developed for the distortional analysis of wide flange steel sections. Both FEs are applicable to the beams with general type of loading and supports. The first element is based on Hermitian polynomial shape function while the second element is based on exact shape functions resulting from closed form solutions of the governing differential equations.
2- The lateral-torsional response was observed to be fully uncoupled from the longitudinal-transverse response, which allowed the developing of separate solution for both types of responses.
3- Numerical examples were solved to demonstrate applicability of the finite elements to general form of beam problems (involving general traction loads, and beams with overhangs)
4- Solutions based on the FE1 element were observed to be unconditionally stable while involving a discretization error. The discretization error was observed to decrease with finer mesh. In contrast FE2 was shown not to involve a discretization error and yields results in perfect agreement as long as the element length taken is smaller than a threshold value.
5- The effect of stiffeners was observed for lateral displacement and angle of twist of top and bottom flanges.

4.10. Appendix A- Closed form solution for lateral torsional response

For the lateral-torsional response, the displacements are assumed to take the exponential form

$$\left\langle u_{Th}(z), \theta_{Th}(z), u_{Bh}(z), \theta_{Bh}(z)\right\rangle^T = D_i \left\langle \psi \right\rangle_i^T e^{d_i z} \tag{4.38}$$

in which $\left\langle \psi \right\rangle_i^T = \left\langle \overline{\overline{A}}_i, \overline{\overline{B}}_i, \overline{\overline{C}}_i, \overline{\overline{D}}_i \right\rangle^T$. From Eq. (4.38) by substituting into Eq. (3.31), one obtains

$$\left(\left[q_2\right] d_i^4 + \left[q_1\right] d_i^2 + \left[q_0\right]\right)_{4\times4} \left\{\psi_i\right\}_{4\times1} = \left\{0\right\}_{4\times1} \tag{4.39}$$

in which,

$$[q_0] = \frac{2D}{h^3}\begin{bmatrix} 6 & 3h & -6 & 3h \\ 3h & 2h^2 & -3h & h^2 \\ -6 & -3h & 6 & -3h \\ 3h & h^2 & -3h & 2h^2 \end{bmatrix}$$

$$[q_1] = \frac{D}{5h}\begin{bmatrix} -12 & -h & 12 & -h \\ -h & -5hGJ_T/D - 4h^2/3 & h & h^2/3 \\ 12 & h & -12 & h \\ -h & h^2/3 & h & -5hGJ_T/D - 4h^2/3 \end{bmatrix}$$

$$[q_2] = \begin{bmatrix} EI_{yyT} + 13Dh/35 & 11Dh^2/210 & 9Dh/70 & -13Dh^2/420 \\ 11Dh^2/210 & EI_{\omega\omega T} + Dh^3/105 & 13Dh^2/420 & -Dh^3/420 \\ 9Dh/70 & 13Dh^2/420 & EI_{yyB} + 13Dh/35 & -11Dh^2/210 \\ -13Dh^2/420 & -Dh^3/420 & -11Dh^2/210 & EI_{\omega\omega B} + Dh^3/105 \end{bmatrix} \tag{4.40}$$

The above system of equations is solved for the eigen-pairs ($m_j, \{\psi\}_j$, $j = 1...8$), resulting in 16 eigen-pairs $\left(d_i = \pm\sqrt{m_j}, \{\psi_i\}\right)$, $i = 1...16$. Ten out of the 16 eigen-values, $i = 1...10$ are observed to be a) distinct, and b) either complex or real, while the remaining six roots $i = 11...16$ are observed to vanish. The solution thus takes the form,

$$\begin{Bmatrix} u_{Th}(z) \\ \theta_{Th}(z) \\ u_{Bh}(z) \\ \theta_{Bh}(z) \end{Bmatrix} = \sum_{i=1}^{10} D_i e^{d_i z}\begin{Bmatrix} \overline{\overline{A_i}} \\ \overline{\overline{B_i}} \\ \overline{\overline{C_i}} \\ \overline{\overline{D_i}} \end{Bmatrix} + \sum_{i=11}^{16} D_i z^{i-11}\begin{Bmatrix} \overline{\overline{A_i}} \\ \overline{\overline{B_i}} \\ \overline{\overline{C_i}} \\ \overline{\overline{D_i}} \end{Bmatrix} = \left[\left[\Psi_e(z)\right]_{4\times10} \quad \left[\Psi_p(z)\right]_{4\times6}\right]\{D\}_{16\times1} \tag{4.41}$$

In the right hand side of (4.41), $\langle D\rangle^T_{16\times1} = \langle D_i \quad D_2 \quad .... \quad D_{16}\rangle^T$ is a vector of integration constants. The procedure for obtaining matrix $\left[\Psi_p(z)\right]_{4\times6}$ is provided in Pezeshky and Mohareb (2014) and matrix $\left[\Psi_e(z)\right]$ is defined as

$$\left[\Psi_e(z)\right]_{4\times10} = \left[\{\psi_1\}_{4\times1} e^{d_1 z} \;\vdots\; \{\psi_2\}_{4\times1} e^{d_2 z} \;\vdots\; ... \;\vdots\; \{\psi_{10}\}_{4\times1} e^{d_{10} z}\right] \tag{4.42}$$

which consists of eigen-vectors $\{\psi_1\}$ to $\{\psi_{10}\}$ corresponding to the distinct roots d_1 - d_{10} obtained by solving Eq. (4.39), multiplied by the exponential functions $e^{d_1 z}$ to $e^{d_{10} z}$, respectively. The eigen-values are sorted in descending order of the complex norm so that $\|d_1\| > \|d_2\| > ....\|d_{10}\|$.When the largest eigenvalue d_1 of the system has a large magnitude, the entries of matrix in Eq. (4.42) are such that $\left[\Psi_e(z)\right]_{4\times10}\,\{\psi_1\}_{4\times1}e^{d_1L} >> \{\psi_{10}\}_{4\times1}e^{d_{10}L} = \{\psi_{10}\}_{4\times1}e^{-d_1L}$ signifying that some of the entries of the matrix will be orders of magnitude apart. The large difference in the entries of matrix $\left[\Psi_e(z)\right]_{4\times10}$, leads to similar differences in matrix $\left[\Psi(z)\right]_{4\times16}$ in Eq. (4.41), $\left\langle\Psi_{u_T}(z)\right\rangle_{1\times16}$, $\left\langle\Psi_{\theta_T}(z)\right\rangle_{1\times16}$, $\left\langle\Psi_{u_B}(z)\right\rangle_{1\times16}$, $\left\langle\Psi_{\theta_B}(z)\right\rangle_{1\times16}$ in Eq. (4.36), leading to numerical difficulties when inverting matrix $\left[\bar{\bar{E}}\right]_{16\times16}$ in Eq. (4.34). Thus, to guarantee that matrix $\left[\bar{\bar{E}}\right]_{16\times16}$ is numerically invertible, a threshold value ε needs to be enforced such that $d_1L \le \varepsilon$. The magnitude of d_1 is dependent solely on sectional properties as evidenced by Eq. (4.39) and defined in Eq. (4.40) . This places the restriction $L \le \varepsilon/d_1$ on the maximum length of element to be used. For the present problem, the value ε =21 was obtained through numeric experimentation.

4.11. Notations

The following symbols are used in this paper:

A_B, A_T, A_W	Cross sectional areas
$\{B\}$	Vector of integration constants of lateral-torsional system
b_B, b_T	Flange widths
$\{C\}$	Vector of integration constants of longitudinal-transverse system
$\mathscr{D}$	Differential Operator
D	Flexural rigidity of the web
E	Modulus of elasticity
G	Shear modulus
$H_1(z)$	Cubic shape functions

$N(z)$	Linear shape functions
h	Height of the cross section, measured along the flanges centerline
$I_{\omega\omega B}, I_{\omega\omega T}$	Local warping constant of the bottom and top flanges
$I_{xxB}, I_{xxT}, I_{xxW}, I_{yyB}, I_{yyT}$	Moment of inertia about x and y axes
I_{xyB}, I_{xyT}	Product moment of inertia
J_B, J_T	Polar moment of inertia
$[K_i]$	Stiffness sub-matrices
$[\bar{K}_1]$	Global stiffness matrix pertains to longitudinal-transverse response
$[\bar{K}_2]$	Global stiffness matrix pertains to lateral-torsional response
L	Beam span
$L_1(z) - L_4(z)$	Cubic interpolation functions
$L_5(z) - L_6(z)$	Linear interpolation functions
m_B, m_T	Distributed twisting moment
n_B, n_T, n_w	Normal component of local coordinate system
P_{ij}	Components of the DEs coefficient matrix due to longitudinal-transverse response
$(p_x, p_y, p_z)_{T,B,W}$	member tractions across the top and bottom flanges and the web
Q_{ij}	Components of the differential equation coefficient for lateral-torsional response
$\{Q_{zT}\}, \{Q_{zB}\}, \{Q_y\}$	Vector of nodal forces of longitudinal-transverse system
$\{Q_{xT}\}, \{Q_{xB}\}, \{M_T\}, \{M_B\}$	Vector of nodal forces of lateral-torsional system
$q_{xB}(z), q_{xT}(z)$	Lateral distributed load, along z axis
$q_y(z)$	Transverse distributed load, along z axis

$q_{zB}(z), q_{zT}(z)$	Longitudinal distributed load, along *z* axis
$S_{xB}, S_{xT}, S_{yB}, S_{yT}$	First moment of area about the *x* and *y* axes
t_B, t_T, t_W	Thickness of the flanges and the web
U_B, U_T, U_{WM}, U_{WP}	Internal strain energy
u_B, u_T	Lateral displacements at the flange centroid
$\bar{u}_B, \bar{u}_T$	Nodal lateral displacements of bottom and top flanges
V	Total potential energy gained by the loads
V_1, V_2	Load potential energy due to end tractions and member tractions
v	Transverse displacement of the web middle surface
$\bar{v}$	Nodal transverse displacement
w_B, w_T	Longitudinal displacements at flange centroid
$\bar{w}_B, \bar{w}_T$	Nodal longitudinal displacement of bottom and top flanges
$\gamma_{xzB}, \gamma_{xzT}$	Shear strain of the xz, yz, xy plane
$\gamma_{yzM}, \gamma_{yzP}$	Web strain in the yz plane
ε_{yP}	Normal strain of the web along the *y* direction
$\varepsilon_{zB}, \varepsilon_{zT}, \varepsilon_{zM}, \varepsilon_{zP}$	Normal strain along the *z* direction
θ_B, θ_T	Angle of twist at the flange to web junction
$\bar{\theta}_B, \bar{\theta}_T$	Nodal angle of twist of bottom and top flanges
ν	Poisson's ratio
Π	Total energy of the system
$\left\{\Phi_{w_T}\right\}, \left\{\Phi_{w_B}\right\}, \left\{\Phi_v\right\}$	The solution functions of longitudinal-transverse system
$\left\{\Psi_{u_T}\right\}, \left\{\Psi_{\theta_T}\right\}, \left\{\Psi_{u_B}\right\}, \left\{\Psi_{\theta_B}\right\}$	The solution functions of lateral-torsional system

4.12. **Subscripts**

T, B, W, M and P = correspond to the top and bottom flanges and the web or membrane and plate bending action, respectively.

4.13. **References**

Andreassen, M. J., and Jönsson, J. (2012). "Distortional solutions for loaded semi-discretized thin-walled beams." *Thin-Walled Structures*, 50(1), 116-127.

Bradford, and Ronagh (1997). "Generalized Elastic Buckling of Restrained I-Beams by FEM." *Journal of Structural Engineering*, 123(12), 1631-1637.

Bradford, M. A. (1985). "Distortional buckling of monosymmetric I-beams." *Journal of Constructional Steel Research*, 5(2), 123-136.

Bradford, M. A. (1986). "Inelastic distortional buckling of I-beams." *Computers & Structures*, 24(6), 923-933.

Bradford, M. A. (1988a). "Buckling of elastically restrained beams with web distortions." *Thin-Walled Structures*, 6(4), 287-304.

Bradford, M. A. (1990b). "Stability of mono-symmetric beam-columns with thin webs." *Journal of Constructional Steel Research*, 15(4), 323-339.

Bradford, M. A. (1992a). "Buckling of doubly-symmetric cantilevers with slender webs." *Engineering Structures*, 14(5), 327-334.

Bradford, M. A. (1992b). "Lateral-Distortional buckling of steel I—Section members." *Journal of Constructional Steel Research*, 23(1–3), 97-116.

Bradford, M. A., and Trahair, N. S. (1981). "Distortional Buckling of I-Beams." *Journal of the Structural Division, ASCE*, 107(2), 355-370.

Bradford, M. A., and Trahair, N. S. (1982). "Distortional buckling of thin-web beam-columns." *Engineering Structures*, 4(1), 2-10.

Chin, C. K., Al-Bermani, F. G. A., and Kitipornchai, S. (1992). "Stability of thin-walled members having arbitrary flange shape and flexible web." *Engineering Structures*, 14(2), 121-132.

Davies, J. M., and Leach, P. (1994). "First-order generalised beam theory." *Journal of Constructional Steel Research*, 31(2-3), 187-220.

Dekker, N. W., and Kemp, A. R. (1998). "A simplified distortional buckling model for doubly symmetrical I-sections." *Canadian Journal of Civil Engineering*, 25(4), 718-727.

Gjelsvik, A. (1981). *The theory of thin walled bars / Atle Gjelsvik*, Wiley, New York, NY, USA.

Hancock, G. J., Bradford, M. A., and Trahair, N. S. (1980). "Web distortion and flexural-torsional buckling." *Journal of the Structural Division, ASCE*, 106(7), 1557-1571.

Hassan, R., and Mohareb, M. (2012). "Distortional lateral torsional buckling analysis for beams of wide flange cross-sections." *3rd International Structural Specialty Conference*Edmonton, Alberta.

Hughes, O., and Ma, M. (1996a). "Lateral Distortional Buckling of Monosymmetric Beams under Point Load." *Journal of Engineering Mechanics*, 122(10), 1022-1029.

Johnson, C. P., and Will, K. M. (1974). "Beam Buckling by Finite Element Procedure." *Journal of the Structural Division*, 100(3), 669-685.

Jönsson, J. (1998). "Determination of shear stresses, warping functions and section properties of thin-walled beams using finite elements." *Computers & Structures*, 68(4), 393-410.

Jönsson, J. (1999a). "Distortional theory of thin-walled beams." *Thin-Walled Structures*, 33(4), 269-303.

Jönsson, J. (1999b). "Distortional warping functions and shear distributions in thin-walled beams." *Thin-Walled Structures*, 33(4), 245-268.

Jönsson, J., and Andreassen, M. J. (2011). "Distortional eigenmodes and homogeneous solutions for semi-discretized thin-walled beams." *Thin-Walled Structures*, 49(6), 691-707.

Kalkan, I., and Buyukkaragoz, A. (2012). "A numerical and analytical study on distortional buckling of doubly-symmetric steel I-beams." *Journal of Constructional Steel Research*, 70(0), 289-297.

Kumar, A., and Samanta, A. (2006c). "Distortional buckling in monosymmetric I-beams: Reverse-curvature bending." *Thin-Walled Structures*, 44(7), 721-725.

Ma, M., and Hughes, O. (1996b). "Lateral distortional buckling of monosymmetric I-beams under distributed vertical load." *Thin-Walled Structures*, 26(2), 123-145.

Ng, M. L.-H., and Ronagh, H. R. (2004). "An Analytical Solution for the Elastic Lateral-Distortional Buckling of I-section Beams." *Advances in Structural Engineering*, 7(2), 189-200

Pezeshky, P., and Mohareb, M. (2014). "Distortional theory for the analysis of wide flange steel beams." *Engineering Structures*, 75, 181-196.

Pezeshky, P., and Mohareb, M. (2014). "Distortional Theory for the Analysis of Wide Flange Steel Beams –Finite Element Formulation." *J. Eng. Mech*, Under Review.

Pezeshky, P., and Mohareb, M. (2014). "Distortional Theory for the Analysis of Wide Flange Steel Beams." *Engineering Structures*, Accepted on May 2014.

Rajasekaran, S., and Murray, D. W. (1973). "Coupled Local Buckling in Wide-Flange Beam-Columns." *Journal of the Structural Division*, 99(6), 1003-1023.

Roberts, T. M., and Jhita, P. S. (1983b). "Lateral, local and distortional buckling of I-beams." *Thin-Walled Structures*, 1(4), 289-308.

Ronagh, H. R., and Bradford, M. A. (1994). "Some notes on finite element buckling formulations for beams." *Computers & Structures*, 52(6), 1119-1126.

Saadé, K., Warzée, G., and Espion, B. (2006). "Modeling distortional shear in thin-walled elastic beams." *Thin-Walled Structures*, 44(7), 808-821.

Samanta, A., and Kumar, A. (2006b). "Distortional buckling in monosymmetric I-beams." *Thin-Walled Structures*, 44(1), 51-56.

Samanta, A., and Kumar, A. (2008). "Distortional buckling in braced-cantilever I-beams." *Thin-Walled Structures*, 46(6), 637-645.

Schardt, R. (1994). "Generalized beam theory—an adequate method for coupled stability problems." *Thin-Walled Structures*, 19(2–4), 161-180.

Trahair, N. S. (2009). "Lateral–distortional buckling of monorails." *Engineering Structures*, 31(12), 2873-2879.

Vlasov, V. Z. (1961). *Thin walled elastic beams*, Israel Program for Scientific Translations, Jerusalem, Israel. Available from Office of Technical Services, US Department of Commerce,Washington, D.C.

Vrcelj, Z., and Bradford, M. A. (2006a). "Elastic distortional buckling of continuously restrained I-section beam–columns." *Journal of Constructional Steel Research*, 62(3), 223-230.

Wang, C. M., Chin, C. K., and Kitipornchai, S. (1991). "Parametric study on distortional buckling of monosymmetric beam-columns." *Journal of Constructional Steel Research*, 18(2), 89-110.

White, D. W., and Jung, S.-K. (2007). "Effect of web distortion on the buckling strength of noncomposite discretely-braced steel I-section members." *Engineering Structures*, 29(8), 1872-1888.

Zirakian, T. (2008). "Elastic distortional buckling of doubly symmetric I-shaped flexural members with slender webs." *Thin-Walled Structures*, 46(5), 466-475.

Zirakian, T., and Showkati, H. (2007). "Experiments on Distortional Buckling of I-Beams." *Journal of Structural Engineering*, 133(7), 1009-1017.

Chapter 5

Geometric nonlinear analysis of shear-deformable beam-columns

5.1. Introduction and motivation

Distortional effects in beam-columns with wide flange cross-sections subjected to strong axis moments and compressive forces are known to be significant in beams with slender deep webs. The accurate characterization of the distortional lateral torsional buckling strength of such members entails two aspects. The first aspect is to develop a geometrically nonlinear pre-buckling analysis that captures the interaction between axial forces and strong axis moments. Given that the theory sought is aimed to be applicable for members with deep cross-sections, shear deformation is expected to have a significant effect on member pre-buckling response. The present chapter develops a shear deformable geometrically non-linear formulation for the pre-buckling analysis of beam-columns. The second aspect of the solution is to develop a distortional lateral torsional buckling theory and will be the focus of Chapter 6.

5.2. Statement of the problem

Given a prismatic deep member with a wide flange doubly symmetric section subjected to a transverse line load $q_y(z)$ (Fig. 5-1a) whose line of action is defined by the curve $y_{qy}(z)$ from the section centroid and a longitudinal line load $q_z(z)$ whose line of action is defined by the curve $y_{qz}(z)$ from the section centroid, it is required to develop a finite element formulation to perform a geometric nonlinear analysis.

5.3. Geometry and coordinates

The cross-section flange width is b and its thickness is t. The web height is denoted h and is defined as the distance between middle surfaces of both flanges and t_w denotes the web thickness. A global right handed $OXYZ$ coordinate system is introduced with origin O located at web mid-height as shown in Fig. 5-1a.

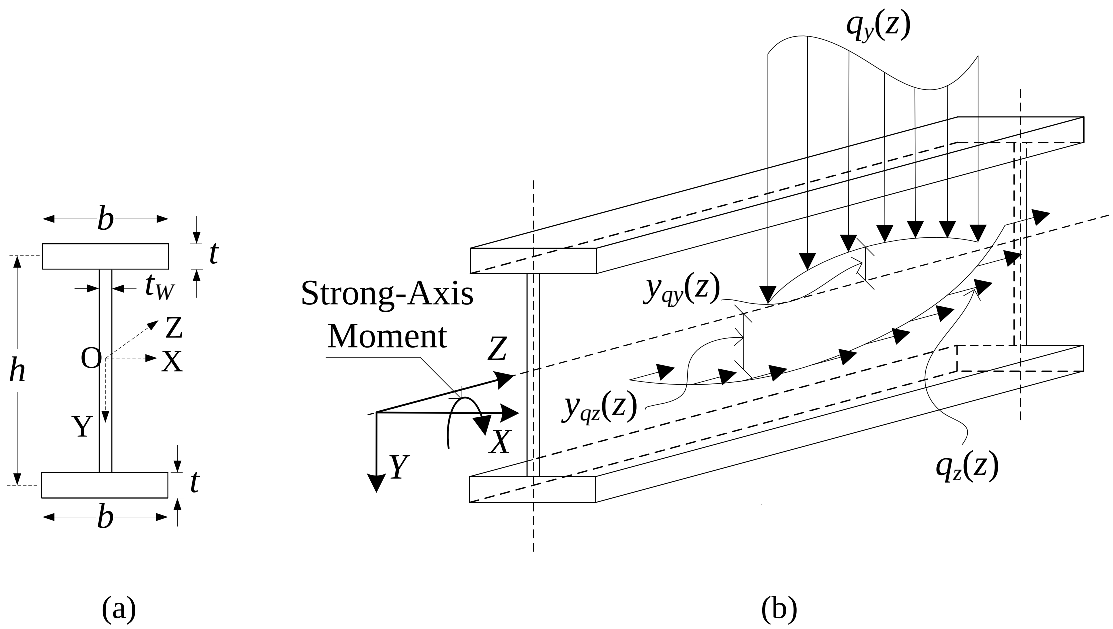

Fig. 5-1. a) Cross section dimensions b) Loading scheme

5.4. Assumptions and kinematics

(1) The material is homogeneous, linearly elastic, isotropic, and obeys Hooke's law.

(2) When characterizing the normal strains, the nonlinear strain terms that characterize rotations are retained in the formulation. However, the nonlinear strain terms involving the longitudinal displacement are neglected given their relatively smaller effect compared to those of linear strain contribution.

(3) Given that the analysis is aimed at beams with deep cross-sections, shear deformation effects are captured by adopting kinematics consistent with the Timoshenko beam-column. A given section of the beam is assumed to behave as a rigid disk undergoing transverse displacement component $v(z)$ and longitudinal displacement $w(z)$ and both defined at the section centroid (Fig. 5-2a)

(4) Also, the section undergoes a rotation $\theta_x(z)$ about the x axis that is different from the beam centreline slope $v'(z)$, i.e., $v'(z) \neq \theta_x(z)$ (Fig. 5-2b). As a result, the longitudinal displacement $\bar{w}(y,z)$ at any point in the cross-section z is given by

$$\bar{w}(z) = w(z) + y\theta_x(z) \tag{5.1}$$

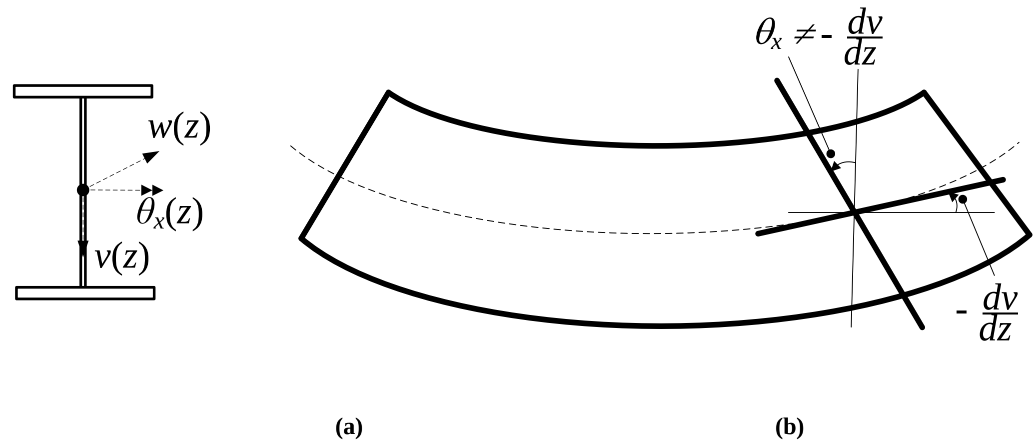

Fig. 5-2 a) Displacements field of the beam b) shear deformations within the plane of the web

5.5. Formulation

Based on the kinematic equation in Eq. (5.1), the longitudinal strain ε and shear strain γ can be expressed as

$$\varepsilon = \frac{\partial \bar{w}}{\partial z} + \frac{1}{2}\left(\frac{\partial \bar{v}}{\partial z}\right)^2 = w'(z) + y\theta_x'(z) + \frac{1}{2}\left[v'^2(z) + \left(w'(z) + y\theta_x'(z)\right)^2\right]$$
$$\gamma = \frac{\partial \bar{w}}{\partial y} + \frac{\partial \bar{v}}{\partial z} + \left[\frac{\partial \bar{w}}{\partial z}\frac{\partial \bar{w}}{\partial y} + \frac{\partial \bar{v}}{\partial z}\frac{\partial \bar{v}}{\partial y}\right] = \theta_x(z) + v'(z) + \left[\theta_x(z) w'(z)\right] \quad (5.2)\text{a-b}$$

Chajes and Churchill (1987) proposed three methods to characterize the non-linear force-deformation relationship for Euler-Bernoulli beam a) the linear incremental method b) the non-linear incremental method and c) the direct method. The present work adapts the second methodology to the Timoshenko-Beam kinematics. An incremental stiffness matrix is required to obtain the relationship between an increment change in deformation and corresponding incremental change in stress resultants. It is assumed that ε_0 is the axial strain within an element at the beginning of the incremental step. As a convention, strains, displacements and forces with subscript “0” denote that field variables at the beginning of the increment while field variables with subscript “a” denote the change of increment fields from the beginning to the end of increment “a”. The change of total potential energy, $\Delta\Pi_a$, is the sum of the change in the internal strain energy ΔU_a and in the potential energy ΔV_a gained by the external loads in the current incremental step (i.e., in going from strains ε_0, γ_0 to strain $\varepsilon_0 + \varepsilon_a$ and $\gamma_0 + \gamma_a$ is

$$\Delta\Pi_a = \Delta U_a + \Delta V_a \tag{5.3}$$

where the change in the internal strain energy ΔU_a is expressed as

$$\begin{aligned}\Delta U_a &= \int_z \int_A \int_{\varepsilon_0}^{\varepsilon_0+\varepsilon_a} (\sigma d\varepsilon)\, dAdz + \int_z \int_A \int_{\gamma_0}^{\gamma_0+\gamma_a} (\tau d\gamma)\, dAdz \\ &= \int_z \int_A \sigma_0 \varepsilon_a dAdz + \int_z \int_A \tau_0 \gamma_a dAdz + \frac{E}{2}\int_z \int_A \varepsilon_a^2 dAdz + \frac{G}{2}\int_z \int_A \gamma_a^2 dAdz\end{aligned} \tag{5.4}$$

where E and G are elastic and shear moduli. Knowing that $\sigma_0 = E\varepsilon_0, \tau_0 = G\gamma_0$, one express the stresses in terms of stress resultants, i.e.

$$\begin{aligned}\sigma_0 &= \frac{P_0}{A} + \frac{M_0}{I_x} y \\ \tau_0 &= \frac{V_0 Q_x}{I_x t_w}\end{aligned} \tag{5.5}$$

From Eqs. (5.2) and (5.5) by substituting into Eq. (5.4), the change of internal strain energy at the increment (a) is rewritten as

$$\begin{aligned}\Delta U_a &= \int_z \int_A \sigma_0 \left\{ w'(z) + y\theta_x'(z) + \frac{1}{2}\left[v'^2(z) + \left(w'(z) + y\theta_x'(z) \right)^2 \right] \right\}_a dAdz \\ &+ \int_z \int_A \tau_0 \left[\theta_x(z) + v'(z) + \theta_x(z) w'(z) \right]_a dz \\ &+ \frac{E}{2}\int_z \int_A \left\{ w'(z) + y\theta_x'(z) + \frac{1}{2}\left[v'^2(z) + \left(w'(z) + y\theta_x'(z) \right)^2 \right] \right\}_a^2 dAdz \\ &+ \frac{G}{2}\int_z \int_A \left[\theta_x(z) + v'(z) + \theta_x(z) w'(z) \right]_a^2 dAdz\end{aligned}$$

For a doubly wide flange section, the shear stresses can be approximated as $\tau_a = V/A_w$ where A_w is the area of the web. By performing the integrals w.r.t. the area A, one obtains

$$\begin{aligned}\Delta U_a &= \int_z P_0 \left\{ w' + \frac{1}{2}\left[v'^2 + w'^2 \right] \right\}_a dz + \int_z M_0 \left(\theta_x' + w'\theta_x' \right)_a dz \\ &+ \int_z V_0 \left[\theta_x(z) + v'(z) + \theta_x(z) w'(z) \right]_a dz \\ &+ \frac{E}{2}\int_z \left(I_x \theta_x'^2 + Aw'^2 + \frac{1}{4}v'^4 + \frac{1}{2} I_x v'^2 \theta_x'^2 + w'\left[A\left(v'^2 + w'^2 \right) + I_x \theta_x'^2 \right] + 2 I_x \theta_x' w' \theta_x' \right)_a dz \\ &+ \frac{GA}{2}\int_z \left(\theta_x^2 + v'^2 + 2\theta_x v' + \theta_x^2 w'^2 + 2\theta_x^2 w' + 2v'\theta_x w' \right)_a dz\end{aligned} \tag{5.6}$$

where the cross-sectional properties $A=\int_A dA, I_x=\int_A y^2 dA$ have been defined. The axial and shear forces and bending moments within the members are related to the nodal forces $f_0=\left(P_1,V_2,M_1,P_2,V_2,M_2\right)_0$ using linear interpolation, i.e.

$$\begin{aligned}
P_0(z)&=\langle -(1-z/L) \quad -z/L\rangle \begin{Bmatrix} P_{1-0} \\ P_{2-0} \end{Bmatrix}, \\
V_0(z)&=\langle 1-z/L \quad -z/L\rangle \begin{Bmatrix} V_{1-0} \\ V_{2-0} \end{Bmatrix}, \\
M_0(z)&=\langle 1-z/L \quad -z/L\rangle \begin{Bmatrix} M_{1-0} \\ M_{2-0} \end{Bmatrix}
\end{aligned} \tag{5.7}$$

The total load potential energy V_a at the load step 'a' is given by

$$\Delta V_a=\int_z \left\{\left[p_{y(0)}(z)+p_{y(a)}(z)\right]v_a(z)+\left[p_{z(0)}(z)+p_{z(a)}(z)\right]\left[w_a(z)+y_{Pz}(z)\theta_{x(a)}(z)\right]\right\}dz \tag{5.8}$$

where $v_a(z)$ is the change of transverse displacement in increment "a" and $w_a\left(y_{Pz}(z),z\right)$ is the change of longitudinal displacement at the centroid in increment "a", $\left(p_{y(0)},p_{z(0)}\right)$ are the accumulated line loads at the beginning of increment "a" and $\left(p_{y(a)},p_{z(a)}\right)$ are the incremental line loads of increment "a" acting on the web.

5.6. Finite element formulation

A two-node finite element is developed with three degrees of freedom (DOFs) per node (Fig. 5-3a). The corresponding stress resultants are also shown in Fig. 5-3b.

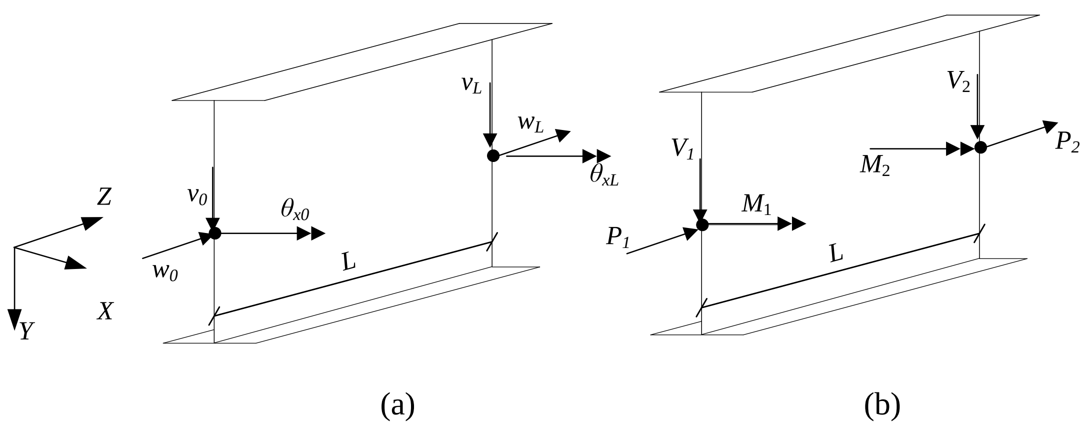

Fig. 5-3. Two-node finite element, a) degrees of freedom b) stress resultants

The displacement fields are related to the vector of nodal displacements using linear approximation for longitudinal displacement w_a, i.e.

$$w_a(z) = \mathbf{N}(z)^{\mathbf{T}}_{\mathbf{1\times6}}\,\hat{\mathbf{d}}_{\mathbf{a(6\times1)}} \tag{5.9}$$

where $\mathbf{N}(z)^{\mathbf{T}}_{\mathbf{1\times6}} = \langle 1-z/L \quad z/L \mid \mathbf{0}_{\mathbf{1\times4}} \rangle$ is a vector of linear interpolation functions and $\hat{\mathbf{d}}^{\mathbf{T}}_{\mathbf{a(1\times6)}} = \langle w(0) \quad w(L) \mid v(0) \quad \theta_x(0) \quad v(L) \quad \theta_x(L) \rangle$ is the vector of nodal displacements. To avoid shear locking , the transverse displacement v and angle of rotation θ are also interpolated using the shape functions based on the exact solution of Timoshenko beam in the absence of geometric nonlinear effects (Friedman and Kosmatka (1993)), i.e.

$$\begin{aligned} v_a(z) &= \mathbf{T}(z)^{\mathbf{T}}_{\mathbf{1\times6}}\,\hat{\mathbf{d}}_{\mathbf{a6\times1}} \\ \theta_{x-a}(z) &= \mathbf{S}(z)^{\mathbf{T}}_{\mathbf{1\times6}}\,\hat{\mathbf{d}}_{\mathbf{a6\times1}} \end{aligned} \tag{5.10}$$

in which the shape functions are expressed as

$$\begin{aligned} \mathbf{T}(z)_{\mathbf{6\times1}} &= \frac{1}{L^3(1+\alpha)} \begin{Bmatrix} \mathbf{0}_{\mathbf{2\times1}} \\ \hdashline 2z^3 - 3z^2 L - \alpha z l^2 + (1+\alpha) l^3 \\ z^3 L - 2z^2(1+0.25\alpha)L^2 + (1+0.5)zL^3 \\ -2z^3 + 3z^2 L + \alpha z L^2 \\ z^3 L + z^2(0.5\alpha - 1)L^2 - 0.5 z\alpha L^3 \end{Bmatrix} \\ \mathbf{S}(z)_{\mathbf{6\times1}} &= \frac{1}{L^3(1+\alpha)} \begin{Bmatrix} \mathbf{0}_{\mathbf{2\times1}} \\ \hdashline 6z^2 - 6zL \\ 3z^2 L - 4z(1+0.25\alpha)L^2 + (1+\alpha)L^3 \\ -6z^2 + 6zL \\ 3z^2 L + 2z(0.5\alpha - 1)L^2 \end{Bmatrix} \end{aligned} \tag{5.11}$$

and $\alpha = 12EI/(L^2 GA_w)$.

5.6.1. Total potential energy in terms of nodal displacement

From Eqs. (5.7) and (5.9)-(5.11), by substituting into Eq. (5.6), one obtains

$$\Delta U_a = \mathbf{F_z}\hat{\mathbf{d}}_{\mathbf{a}} + \mathbf{F_y}\hat{\mathbf{d}}_{\mathbf{a}} + \mathbf{M_x}\hat{\mathbf{d}}_{\mathbf{a}} + \frac{1}{2}\hat{\mathbf{d}}^{\mathbf{T}}_{\mathbf{a}}\left(\mathbf{K_E} + \mathbf{K_G} + \mathbf{K_D}\right)\hat{\mathbf{d}}_{\mathbf{a}} \tag{5.12}$$

where

where $\mathbf{K_E}$ is element elastic stiffness matrix, $\mathbf{K_G}$ is the element geometric stiffness matrix which captures the softening effect of axial force on the stiffness of the structure $\mathbf{K_{D-a}}$ is the element displacement stiffness matrix which captures the weakening effect of displacement changes (i.e., longitudinal, transverse and rotations) on the stiffness of the structure defined as

$$\mathbf{K}_{\mathbf{E}(6\times6)} = \mathbf{k}_1 + \mathbf{k}_2 + \mathbf{k}_3 + \mathbf{k}_4 + \mathbf{k}_5$$

$$\mathbf{K}_{\mathbf{G}(6\times6)} = \mathbf{k}_{\mathbf{g1}} + \mathbf{k}_{\mathbf{g2}} + \mathbf{k}_{\mathbf{g3}} + \mathbf{k}_{\mathbf{g4}}$$

$$\mathbf{K}_{\mathbf{D\text{-}a}(6\times6)} = \left(\mathbf{k}_{\mathbf{D1}} + \mathbf{k}_{\mathbf{D2}} + \mathbf{k}_{\mathbf{D3}} + \mathbf{k}_{\mathbf{D4}} + \mathbf{k}_{\mathbf{D5}} + \mathbf{k}_{\mathbf{D6}}\right)_{\mathbf{a}}$$

and

$$\mathbf{F}_{\mathbf{z}(1\times6)} = \int_0^L \left[-P_1\left(1-z/L\right) + P_2\left(z/L\right)\right]\mathbf{N}^{\mathbf{T}}_{,z\mathbf{1}\times\mathbf{6}}dz$$

$$\mathbf{F}_{\mathbf{y}(1\times6)} = \frac{A}{A_w}\int_0^L \left[V_1\left(1-z/L\right) - V_2\left(z/L\right)\right]\left(-\mathbf{S}^{\mathbf{T}}_{\mathbf{1}\times\mathbf{6}} + \mathbf{T}^{\mathbf{T}}_{,z\mathbf{1}\times\mathbf{6}}\right)dz$$

$$\mathbf{M}_{\mathbf{x}(1\times6)} = -\int_0^L \left[M_1\left(1-z/L\right) - M_2\left(z/L\right)\right]\mathbf{S}^{\mathbf{T}}_{,z\mathbf{1}\times\mathbf{6}}dz$$

Also, elastic stiffness sub-matrices $\mathbf{k}_1 - \mathbf{k}_5$, geometric stiffness sub-matrices $\mathbf{k}_{\mathbf{g1}} - \mathbf{k}_{\mathbf{g4}}$ and displacement stiffness sub-matrices $\left(\mathbf{k}_{\mathbf{D1}} - \mathbf{k}_{\mathbf{D6}}\right)_{\mathbf{a}}$ are defined as

$$\mathbf{k}_{\mathbf{1}(6\times6)} = EA\int_z \mathbf{N}_{,z\mathbf{6}\times\mathbf{1}}\mathbf{N}'^{\mathbf{T}}_{,z\mathbf{1}\times\mathbf{6}}dz$$

$$\mathbf{k}_{\mathbf{2}(6\times6)} = EI_x\int_z \mathbf{S}_{,z\mathbf{6}\times\mathbf{1}}\mathbf{S}^{\mathbf{T}}_{,z\mathbf{1}\times\mathbf{6}}dz$$

$$\mathbf{k}_{\mathbf{3}(6\times6)} = GA\int_z \mathbf{S}_{\mathbf{6}\times\mathbf{1}}\mathbf{S}^{\mathbf{T}}_{\mathbf{1}\times\mathbf{6}}dz$$

$$\mathbf{k}_{\mathbf{4}(6\times6)} = GA\int_z \mathbf{T}_{,z\mathbf{6}\times\mathbf{1}}\mathbf{T}^{\mathbf{T}}_{,z\mathbf{1}\times\mathbf{6}}dz$$

$$\mathbf{k}_{\mathbf{5}(6\times6)} = 2GA\int_z \mathbf{S}_{\mathbf{6}\times\mathbf{1}}\mathbf{T}^{\mathbf{T}}_{,z\mathbf{1}\times\mathbf{6}}dz$$

$$\mathbf{k}_{\mathbf{g1}(6\times6)} = \int_0^L \left[-P_{1-0}\left(1-z/L\right) + P_{2-0}\left(z/L\right)\right]\mathbf{T}_{,z\mathbf{6}\times\mathbf{1}}\mathbf{T}^{\mathbf{T}}_{,z\mathbf{1}\times\mathbf{6}}dz$$

$$\mathbf{k}_{\mathbf{g2}(6\times6)} = \int_0^L \left[-P_{1-0}\left(1-z/L\right) + P_{2-0}\left(z/L\right)\right]\mathbf{N}_{,z\mathbf{6}\times\mathbf{1}}\mathbf{N}^{\mathbf{T}}_{,z\mathbf{1}\times\mathbf{6}}dz$$

$$\mathbf{k}_{\mathbf{g3}(6\times6)} = 2\int_0^L \left[M_{1-0}\left(1-z/L\right) - M_{2-0}\left(z/L\right)\right]\mathbf{N}_{,z\mathbf{6}\times\mathbf{1}}\mathbf{S}^{\mathbf{T}}_{,z\mathbf{1}\times\mathbf{6}}dz$$

$$\mathbf{k}_{\mathbf{g4}(6\times6)} = 2\frac{A}{A_w}\int_0^L \left[V_{1-0}\left(1-z/L\right) - V_{2-0}\left(z/L\right)\right]\mathbf{N}_{,z\mathbf{6}\times\mathbf{1}}\mathbf{S}^{\mathbf{T}}_{\mathbf{1}\times\mathbf{6}}dz$$

$$\mathbf{k}_{\mathbf{D1\text{-}a}(\mathbf{6\times6})} = \frac{3}{2}EA\int_{\mathbf{z}}\mathbf{T}_{,z(\mathbf{6\times1})}\mathbf{N}^{\mathbf{T}}_{,z(\mathbf{1\times6})}\hat{\mathbf{d}}_{\mathbf{a}(\mathbf{6\times1})}\mathbf{T}^{\mathbf{T}}_{,z(\mathbf{1\times6})}\mathbf{dz}$$

$$\mathbf{k}_{\mathbf{D2\text{-}a}(\mathbf{6\times6})} = \frac{3}{2}EA\int_{z}\mathbf{N}_{,z(\mathbf{6\times1})}\mathbf{N}^{\mathbf{T}}_{,z(\mathbf{1\times6})}\hat{\mathbf{d}}_{\mathbf{a}(\mathbf{6\times1})}\mathbf{N}^{\mathbf{T}}_{,z(\mathbf{1\times6})}dz$$

$$\mathbf{k}_{\mathbf{D3\text{-}a}(\mathbf{6\times6})} = \frac{9}{2}EI_x\int_{\mathbf{z}}\mathbf{S}^{\mathbf{T}}_{,z(\mathbf{6\times1})}\mathbf{N}^{\mathbf{T}}_{,z(\mathbf{1\times6})}\hat{\mathbf{d}}_{\mathbf{a}(\mathbf{6\times1})}\mathbf{S}^{\mathbf{T}}_{\mathbf{1\times6}}\mathbf{dz}$$

$$\mathbf{k}_{\mathbf{D4\text{-}a}(\mathbf{6\times6})} = 3GA\int_{\mathbf{z}}\left(\mathbf{S}_{(\mathbf{6\times1})} + \mathbf{T}_{,z(\mathbf{6\times1})}\right)\mathbf{N}^{\mathbf{T}}_{,z(\mathbf{1\times6})}\hat{\mathbf{d}}_{\mathbf{a}(\mathbf{6\times1})}\mathbf{S}^{\mathbf{T}}_{\mathbf{1\times6}}\mathbf{dz}$$

$$\mathbf{k}_{\mathbf{D5\text{-}a}(\mathbf{6\times6})} = \frac{EA}{2}\int_{\mathbf{z}}\mathbf{T}_{,z(\mathbf{6\times1})}\left(\mathbf{T}_{,z(\mathbf{1\times6})}\hat{\mathbf{d}}_{\mathbf{a}(\mathbf{6\times1})}\right)^2\mathbf{T}^{\mathbf{T}}_{,z(\mathbf{1\times6})}\mathbf{dz}$$

$$\mathbf{k}_{\mathbf{D6\text{-}a}(\mathbf{6\times6})} = 2GA\int_{\mathbf{z}}\mathbf{S}_{(\mathbf{6\times1})}\left(\mathbf{N}_{,z(\mathbf{1\times6})}\hat{\mathbf{d}}_{\mathbf{a}(\mathbf{6\times1})}\right)^2\mathbf{S}^{\mathbf{T}}_{(\mathbf{1\times6})}\mathbf{dz}$$

$$\mathbf{k}_{\mathbf{D7\text{-}a}(\mathbf{6\times6})} = EI_x\int_{\mathbf{z}}\mathbf{T}_{,z(\mathbf{6\times1})}\left(\mathbf{S}_{,z(\mathbf{1\times6})}\hat{\mathbf{d}}_{\mathbf{a}(\mathbf{6\times1})}\right)^2\mathbf{T}^{\mathbf{T}}_{,z(\mathbf{1\times6})}\mathbf{dz}$$

Also, the energy equivalent force vectors are rewritten using Eq. (5.8) as

$$\Delta V_a = \mathbf{Q}^{\mathbf{T}}_{\mathbf{z}}\hat{\mathbf{w}}_a + \left(\mathbf{R}^{\mathbf{T}}_{\mathbf{x}} + \mathbf{Q}^{\mathbf{T}}_{\mathbf{y}}\right)\hat{\mathbf{v}}_a$$

where

$$\begin{aligned}
\mathbf{Q}_{\mathbf{z}(\mathbf{1\times6})} &= \int_z\left[p_{y(0)}(z) + p_{y(a)}(z)\right]\mathbf{N}(\mathbf{z})^{\mathbf{T}}_{\mathbf{1\times6}}\,dz \\
\mathbf{R}_{\mathbf{x}(\mathbf{1\times6})} &= \int_z\left[p_{y(0)}(z) + p_{y(a)}(z)\right]\mathbf{S}(\mathbf{z})^{\mathbf{T}}_{\mathbf{1\times6}}\,dz \\
\mathbf{Q}_{\mathbf{y}(\mathbf{1\times6})} &= \int_z\left[p_{y(0)}(z) + p_{y(a)}(z)\right]\mathbf{T}(\mathbf{z})^{\mathbf{T}}_{\mathbf{1\times6}}\,dz
\end{aligned} \tag{5.13}$$

5.6.2. Discretized equilibrium conditions

By evoking the stationarity condition, $\delta\Pi_a = 0$ one obtains the stationary condition, i.e.

$$\mathbf{K}_{\mathbf{T-a}}\hat{\mathbf{d}}_{\mathbf{a}} + \mathbf{Q} = 0 \tag{5.14}$$

in which the tangent stiffness matrix $\mathbf{K}_{\mathbf{T\text{-}a}}$ is defined as

$$\mathbf{K}_{\mathbf{T-a}(\mathbf{6\times6})} = \mathbf{K}_{\mathbf{E}(\mathbf{6\times6})} + \mathbf{K}_{\mathbf{G}(\mathbf{6\times6})} + \mathbf{K}_{\mathbf{D-a}(\mathbf{6\times6})} \tag{5.15}$$

and the nodal force equivalent vector $\mathbf{Q}^{\mathbf{T}}$ takes the form

$$\mathbf{Q}^{\mathbf{T}}_{\mathbf{1\times6}} = \left\langle\left(\mathbf{Q}_{\mathbf{z}} + \mathbf{F}_{\mathbf{z}}\right)_{(\mathbf{1\times2})} \;\vdots\; \left(\mathbf{R}_{\mathbf{x}} + \mathbf{Q}_{\mathbf{y}} + \mathbf{F}_{\mathbf{y}} + \mathbf{M}_{\mathbf{x}}\right)_{(\mathbf{1\times4})}\right\rangle_{\mathbf{a}}$$

One recalls that $\mathbf{d_a}$ is the nodal displacements defined in Eq. (5.9).

5.7. Coordinate transformations

In Eq. (4.16), the element stiffness matrix is expressed in local coordinates. In a structure consisting of several members, each member has a distinct orientation. Thus, a global coordinate system is selected and all element local coordinates are related to the global coordinate system. The element nodal displacements $\hat{\boldsymbol{\psi}}_\mathbf{a}$ associated to the global coordinate system (Y, Z) can be related to the element nodal displacements $\hat{\mathbf{d}}$ in the local coordinate system (y, z) through

$$\hat{\mathbf{d}}_\mathbf{a} = \mathbf{T}_e \hat{\boldsymbol{\psi}}_\mathbf{a} \tag{5.16}$$

where matrix $\mathbf{T}_{\mathbf{e}6\times6}$ is the transformation matrix obtained as

$$\mathbf{T}_{\mathbf{e}6\times6} = \left[\begin{array}{c:c} \mathbf{T}^*_{e3\times3} & \mathbf{0} \\ \hdashline \mathbf{0} & \mathbf{T}^*_{e3\times3} \end{array}\right] \tag{5.17}$$

in which the matrix of direction cosines $\left[\mathbf{T}^*_e\right]_{3\times3}$ which relates the global directions (Y, Z) to the local directions (y, z) of the member is given by

$$\left[\mathbf{T}^*_e\right]_{3\times3} = \begin{bmatrix} l & m & 0 \\ -m & l & 0 \\ 0 & 0 & 1 \end{bmatrix}_e \tag{5.18}$$

and

$$l = \cos(z, Z), \; m = \cos(z, Y) \tag{5.19}$$

Hence, one transforms the element tangent stiffness matric $\mathbf{k}_{\mathbf{T\text{-}a}}$ in Eq. (5.15) to the global tangent stiffness matrix $\mathbf{K}_{\mathbf{T\text{-}a}}$, i.e.

$$\mathbf{K}_{\mathbf{T\text{-}a}} = \mathbf{T}_e^{\mathbf{T}} \mathbf{k}_{\mathbf{T\text{-}a}} \mathbf{T}_e \tag{5.20}$$

5.8. Details of the iterative technique

In order to perform the incremental nonlinear analysis, based on Appendix IV of Chajes and Churchill (1987), the nodal force vector for the structure is divided into increments. For a given load increment, the equilibrium condition is iteratively achieved. The solution proceeds by applying the incremental force vector $\mathbf{Q_a}$ (i.e., load step) and involves the following steps:

1- The element elastic stiffness matrix in the un-deformed configuration $\mathbf{k_E}$ is formed for each element. As a convention, lower case letters denote that the variables pertaining to the element and all capitalized letters denote variables related to the structure.

2- The element geometric stiffness matrix $\mathbf{k_G}$ is formed in the presence of internal forces $\mathbf{f}_0$ defined in Eqs(5.7).

3- The total element stiffness matrices are then formed using the equation $\mathbf{k_{T\text{-}a}} = \mathbf{k_E} + \mathbf{k_G}$

4- Transform the element stiffness matrix $\mathbf{k_{T\text{-}a}}$ from local to global coordinates using $\mathbf{T_e}$ and assemble element contributions to form the tangent stiffness matrix $\mathbf{K_{T\text{-}a}}$ for the structure

5- Initialize the iteration number $i : i = 0$ and set $\mathbf{Q}_{\mathbf{a}(i)} = \mathbf{Q_a}$.

6- Increase the iteration number by one $i = i + 1$. The equilibrium condition $\mathbf{K}_{\mathbf{T\text{-}a}(i-1)}\hat{\boldsymbol{\psi}}_i = \mathbf{Q}_{\mathbf{a}(i-1)}$ is solved for the vector of incremental nodal displacement $\hat{\boldsymbol{\psi}}_i$ of the structure.

7- Add the displacement contributions of all iterations i=1 through n, $\hat{\boldsymbol{\psi}}_{\mathbf{a(i)}} = \sum_{n=1}^{i} \hat{\boldsymbol{\psi}}_i$

8- For each element, given its transformation matrix $\mathbf{T_e}$ (Section 5.7) and its incremental nodal displacement vector $\hat{\mathbf{d}}_\mathbf{a}$, form the displacement stiffness matrix $\mathbf{k_{D\text{-}a}}$.

9- For each element, given its incremental nodal displacement vector $\hat{\mathbf{d}}_\mathbf{a}$, calculate the corresponding incremental internal force vector $\mathbf{f_a} = \mathbf{k_{T\text{-}a}}\hat{\mathbf{d}}_\mathbf{a}$.

10- Form the element tangent stiffness matrix $\mathbf{k_{T\text{-}a}}$ in local coordinates based on the relation $\mathbf{k_{T\text{-}a}} = \mathbf{k_E} + \mathbf{k_G} + \mathbf{k_{D\text{-}a}}$

11- The global tangent stiffness matrix $(\mathbf{K_{T\text{-}a}})_i$ is obtained using the transformation in Eq. (5.20)

12- Calculate the imbalance nodal force vector $\mathbf{Q}_{\mathbf{a}(i)}$ from the equation $(\mathbf{K_{T\text{-}a}})_i\, \hat{\boldsymbol{\psi}}_{\mathbf{a}(i)} = \mathbf{Q_a} - \mathbf{Q}_{\mathbf{a}(i)}$

13- Repeat steps 6 to 13 until the imbalance nodal force vector $\mathbf{Q}_{\mathbf{a}(i)}$ becomes negligible.

14- Update the total nodal displacement vector through the addition $\hat{\boldsymbol{\psi}} = \hat{\boldsymbol{\psi}} + \hat{\boldsymbol{\psi}}_{\mathbf{a}}$ and update the total stress resultant vector $\mathbf{f} = \mathbf{f} + \mathbf{f}_{\mathbf{a}}$.

15- Return to step 2 for the next load increment.

5.9. Numerical examples

5.9.1. Example 1: Long-span simply supported member

A 8.0m span simply supported member (Fig. 5-4) with a W250x45 cross-section (geometric parameters are provided in Fig. 5-4), is subjected to an increasing transverse point load $V = \alpha 180 kN$ acting at mid-span, and an axial point load $H = \alpha 1800 kN$ acting at the end $z = L$ where α is increamentally increased by ramping α from 0.0 to 1.0. The corresponding midspan transverse displacement is sought using six types of analyses; a) a non-shear deformable Euler-Bernoulli-type linear analysis b) a linear analysis capturing shear deformation effects (i.e. Timoshenko beam), c) geometric non-linear analysis for an Euler-Bernoulli (non-shear deformable) based on the formulation of Chajes and Churchill (1987), d) a geometric non-linear analysis including shear deformation effects as developed in the current study, e) a geometric non-linear analysis based on shear deformable B31 beam elements in the Abaqus library. The direct method has been used to trace the equilibrium path using load control with automatic incrementation. The last solution (f) is based on the shear deformable SAP2000 beam element using the “P-Delta plus Large Displacement” type of analysis. Again, load control with automatic incrementation has been used to trace the non-linear equilibrium path. In all six analyses, 26 elements were taken to model the 8m span of the member. As expected, the non-shear deformable linear Euler-Bernouilli beam solution (a) is observed to have a slightly stiffer respsonse than that of the shear deformable linear Timoshenko beam solution (b). The effect of shear deformation in this case is rather minor given that the span to dept ratio of the member is large. A similar observation is made when comparing the results of the nonlinear non-shear deformable linear Euler-Bernouilli beam solution (c) and the shear deformable Timoshenko beam solution (d). The results of the three nonlinear solutions (d-f) for the present formulation, SAP2000, and Abaqus exhibit very close agreement, suggesting the validity of the present solution and the correctness of the implementation.

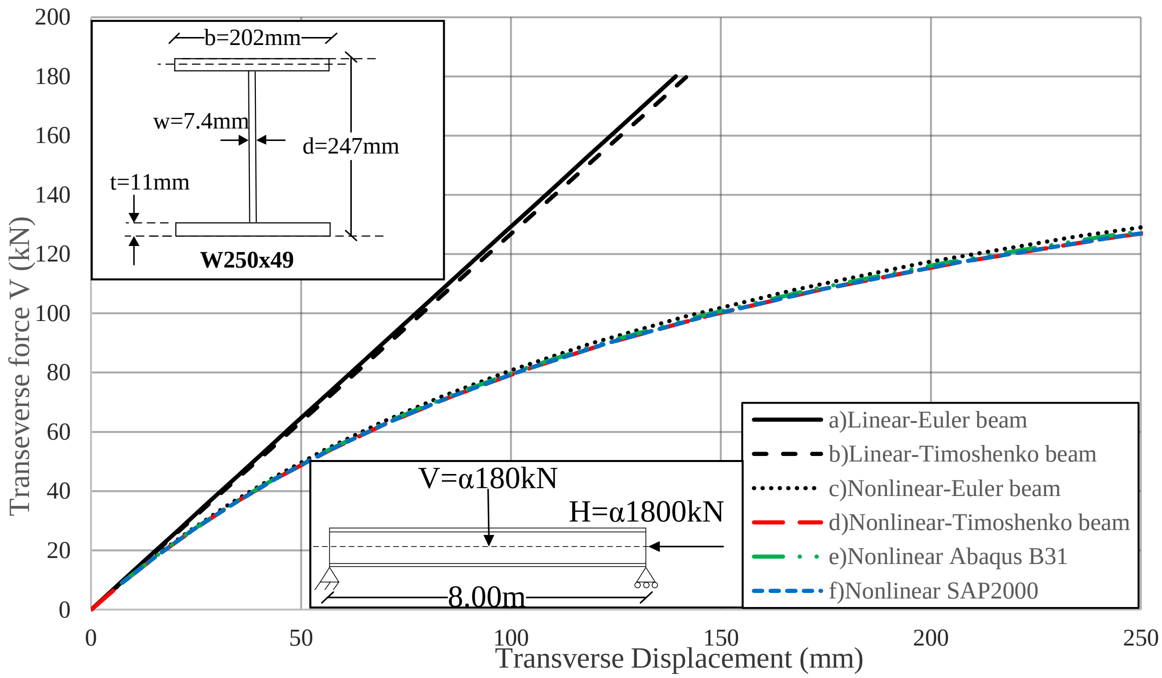

Fig. 5-4 Force-displacement diagram for a simply supported beam under transverse load acting at the mid-span and axial force acting the end

5.9.2. **Example 2: Short span cantilever**

A 1.5m span cantilever beam with a W310x39 cross-section (geometric parameters are provided in Fig. 5-5) is subjected to a transverse point load $V = \alpha 1,500kN$ acting at mid-span and an axial point load $H = \alpha 15,000kN$ acting at the end $z = L$. The force-displacement relations based on the four types of analyses (a-d) described in Example 1 are depicted in Fig. 5-5. As expected, for the short span cantilever, the shear deformation effect is observed to become more significant as evidenced by the significant difference between solutions (b) and (a), and between solutions (d) and (c). The large displacement differences observed between analyses (d) and (c) throughout the pre-buckling analysis will be shown to influence the bifurcation point in some cases in Chapter 6.

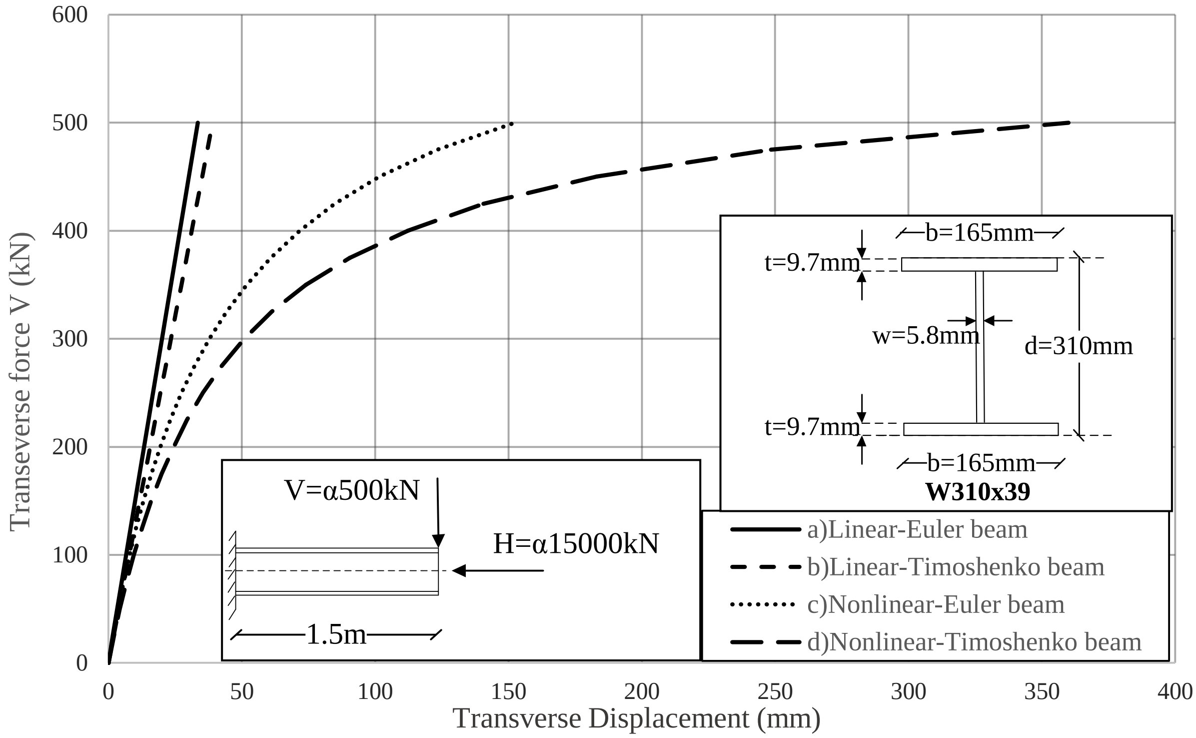

Fig. 5-5 Force-displacement diagram for a cantilever beam under transverse and axial loads acting at the tip

5.10. References

Chajes, A., and Churchill, J. (1987). "Nonlinear Frame Analysis by Finite Element Methods." *Journal of Structural Engineering*, 113(6), 1221-1235.

CSI. 2011. SAP2000, version 15.0.1.Computers and structures, Inc., Berkeley.

Friedman, Z., and Kosmatka, J. B. (1993). "An improved two-node timoshenko beam finite element." *Computers & Structures*, 47(3), 473-481.

SIMULIA. 2011a. Abaqus/CAE Analysis, version 6.11-1Dassault Systemes.

SIMULIA. 2011b. Abaqus/CAE User's Manual, version 6.11-1Dassault Systemes.

Chapter 6

Lateral torsional buckling of wide flange sections including distortional and pre-buckling effects

6.1. Abstract

The present study develops a unified lateral torsional buckling finite element formulation for the analysis of beams with wide flange doubly symmetric cross-sections. The solution captures several non-conventional features. These include the softening effect due to web distortion, the stiffening effect induced by pre-buckling deformations, the pre-buckling nonlinear interaction between strong axis moments and axial forces, the contribution of pre-buckling shear deformation effects within the plane of the web, the destabilizing effects due to transverse loads being offset from the shear centre, and the presence of transverse stiffeners on web distortion. Within the framework of the present theory, it is possible to evoke or suppress any combination of the features and thus isolate the individual contribution of each effect or quantify the combined contributions of multiple effects on the member lateral torsional capacity. The new solution is then applied to investigate the influence of the ratios of beam span-to-depth, flange width-to-thickness, web height-to-thickness, and flange width-to-web height on the lateral torsional buckling strength of simply supported beams and cantilevers. Comparisons with conventional lateral torsional buckling solutions that omit distortional and pre-buckling effects quantify the influence of distortional and/or pre-buckling deformation effects. The theory is also used to investigate the influence of P-delta effects of beam-columns subjected to transverse and axial forces on their lateral torsional buckling resistance. The theory is used to investigate the load height effect relative to the shear centre. Comparisons are made with load height effects as predicted by non-distortional buckling theories. The solution is adopted to quantify the beneficial effect of transverse stiffeners in controlling/suppressing web distortion in beams and increasing their buckling resistance.

Keywords: Lateral torsional buckling, finite element, distortion, pre-buckling deformation, geometric non-linear analysis, beam-columns, load height effect, shear deformation, plate girders

6.2. Introduction and motivation

Lateral torsional buckling solutions for beams with wide-flange cross-sections are commonly based on the Vlasov thin-walled beam kinematic assumption that, throughout buckling, a given cross-section moves within its own plane laterally and undergoes twisting rotation as a rigid disk (Fig. 6-1a) as it displaces from the position of buckling onset to the buckled configuration. The Vlasov assumption neglects possible distortional deformations of the web within the plane of the cross-section (Fig. 6-1b) and thus over-predicts the critical lateral torsional buckling capacity. While distortional effects may be small in some cases, past studies (Section 6.3.1) have shown that distortional effects gain significance in beams with slender webs, stocky flanges, and/or shorter spans. In such situations, the omission of web distortion leads to grossly over-estimating the lateral torsional buckling capacity of the member.

Also, while all conventional lateral torsional buckling solutions and commercial finite element software account for the pre-buckling stresses induced in the member in going from the un-deformed configuration to the position of buckling onset, most solutions omit the associated pre-buckling deformation and curvature, by assuming that the member is approximately straight at the onset of buckling. Past studies (Section 6.3.2) have shown that pre-buckling deformations induce a beneficial stiffening effect, i.e., the omission of pre-buckling deformation leads to under-predicting the lateral torsional buckling capacity of members.

As discussed in Section 6.3.1, some lateral torsional buckling solutions have captured the web distortion effects alone while others (Section 6.3.2) have accounted for pre-buckling deformation effects alone. To the authors' knowledge, no solutions have captured the combined effects of web distortion and pre-buckling deformation. The subject is thus the focus of the present study. The present study thus develops a unified lateral torsional buckling solution that captures multiple effects including (1) web distortion and (2) pre-buckling deformation (PBD), (3) pre-buckling interaction effects between axial loads and strong-axis bending including P-delta effects through a geometric non-linear analysis, (4) pre-buckling shear-deformation effects, and (5) the destabilizing effects due to load offset from the shear centre. While, by default, the present solution captures all effects combined, methodologies were developed to suppress/evoke any combination of features as needed.

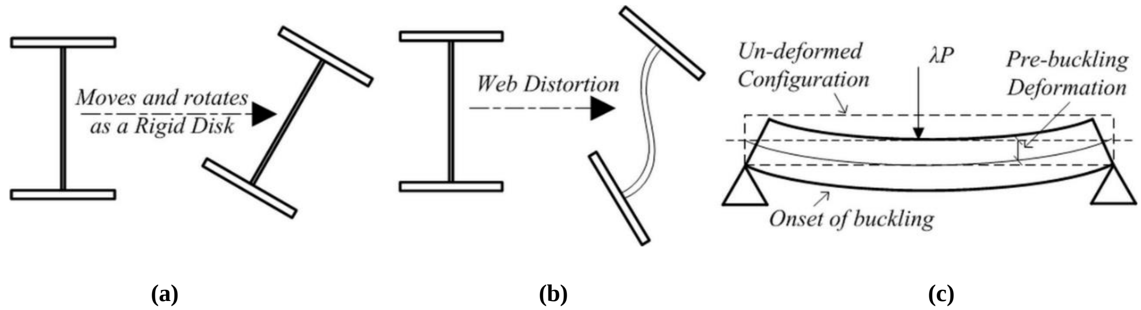

Fig. 6-1 a) Classical LTB kinematics b) distortion lateral torsional buckling c) beam configuration onset of buckling incorporating PBD effect

6.3. Literature review

A distinctive feature of the present study is that it combines the effect of distortion and pre-buckling deformation effects. Thus, within the large number of lateral torsional buckling studies, the present review places emphasis on those that incorporate distortional effects, followed by those that incorporate pre-buckling deformation effects.

6.3.1. Distortional buckling effect:

Distortional buckling solutions for I-sections were developed using finite strip method (Hancock (1978)) and an energy solution (Hancock et al. (1980)). Finite element solutions were developed by Bradford and Trahair (1981) who formulated a 12 degree of freedom (DOF) element and Bradford and Trahair (1982) who developed a 16 DOF element. Distortional buckling solutions were developed for mono-symmetric beams (Bradford (1985)), inelastic buckling of I-beams (Bradford 1986), and mono-symmetric I-beams with continuous elastic lateral restrain (Bradford (1988a). Further research was conducted on buckling of tee sections using finite strip and energy solution (Bradford (1988b), buckling of tee sections using plate finite element analysis (Bradford (1990a), mono-symmetric beam-columns (Bradford (1990b), and doubly-symmetric cantilevers (Bradford (1992a). The effect of rotational and translational restraints in I-beams were investigated in (Bradford (1992b) and Ronagh and Bradford (1994)), beams laterally restrained at one flange (Bradford and Ronagh (1997)), tee cantilevers (Bradford (1999)),and I-beam columns with continuous elastic restraint (Vrcelj and Bradford (2006a)).

Roberts and Jhita (1983b) investigated local instability of the I-beams and developed energy solutions that capture the distortion of the web. Wang et al. (1991) conducted a parametric study to investigate the effect of web distortion on the buckling of simply supported members with mono-symmetric I-sections subjected to uniform moment and axial forces. Chin et al. (1992)

developed a super-element with 16 buckling DOFs that captures web distortion. The distortional buckling of beams with mono-symmetric sections was investigated under point loads (Hughes and Ma (1996a) and under uniformly distributed loads (Ma and Hughes (1996b)). In both studies, web deformations were approximated by quintic polynomials along the height. Dekker and Kemp (1998) devised a simplified distortional model based on continuous springs, to model the stiffness of the web and the flanges. Pi and Trahair (2000) devised an approximate distortional buckling solution based on torsional and warping rigidities that characterize web distortion. Ng and Ronagh (2004) developed a finite element based on Fourier series in longitudinal direction and cubic functions along the height. Using shell finite element modeling in Abaqus, web distortion effects on distortional lateral torsional buckling (LTB) moments were investigated for simply supported beams (Samanta and Kumar (2006b)) and cantilevers (Kumar and Samanta (2006c)).
Experimental investigations of the distortional buckling were conducted for castellated I-beams (Zirakian and Showkati (2006d)) and for I-beams subjected to mid-span loading with lateral bracing at the compression flange (Zirakian and Showkati (2007)). Samanta and Kumar (2008) investigated the effect of lateral braces on the distortional buckling of I-beam cantilevers. Trahair (2009) numerically investigated the distortional buckling of monorails with loads applied at the bottom flange and characterized the effect of web stiffeners and flange torsional stiffeners on the critical moments. Chen and Ye (2010) developed an energy-based solution for lateral distortional buckling of simply supported beams under transverse distributed load using the Ritz method. Kalkan and Buyukkaragoz (2012) characterized the reduction of torsional and warping rigidities of beams due to web distortion. Pezeshky and Mohareb (2014) developed a distortional theory for the analysis of beams with mono-symmetric sections and developed two finite element solutions (Pezeshky and Mohareb (2015)). Hassan and Mohareb (2015) conducted a shell based distortional buckling analysis for beams with cleat end connections. Among the above studies, only the work of Hancock et al. (1980), Bradford and Trahair (1981), Bradford and Trahair (1982), Bradford (1990b) and Vrcelj and Bradford (2006a) incorporated the effect of axial loads.

6.3.2. **Pre-buckling deformation effect:**

A limited number of studies investigated the effect of pre-buckling deformations on the buckling capacity of thin-walled beams. Such studies are first reviewed followed by the few studies that investigated the effect of pre-buckling deformations in plates.

Clark and Knoll (1958) investigated the effect of pre-buckling deformation on lateral buckling strength of the beam columns. Trahair and Woolcock (1973) developed an energy-based solution for simply supported beams and cantilevers. Anderson and Trahair (1972) derived the differential equations of neutral stability for the lateral torsional buckling of beams and developed numerical solutions for various boundary conditions and loading cases. Roberts and Azizian (1983a) developed a finite element that captures PBD effects. Roberts and Jhita (1983b) derived a critical moment expression for simply supported beams. The solution captures the magnifying influence of axial forces on pre-buckling deflections and curvatures. Pi et al. (1992a) developed energy expressions for lateral buckling analysis of doubly symmetric thin-walled beams including PBD effects and provided comparisons with the classical solution. Based on variational approach, Pi and Trahair (1992b) derived the LTB equilibrium equations for I beam-columns including PBD effects and developed a finite element formulation. In a companion paper, Pi and Trahair (1992c) compared their numerical results against those based on classical LTB solutions. Machado and Cortínez (2005) developed an energy solution for simply supported composite beams including PBD and shear deformation effects. The study investigated the effect of PBD on cantilevers under tip point load. Andrade and Camotim (2004) derived the governing differential equations and boundary conditions for lateral torsional buckling of prismatic and tapered thin-walled open beams. Energy solutions were provided for simply supported beams and cantilevers with tapered members. Mohri and Potier-Ferry (2006) formulated analytical LTB solutions for simply supported beams that capture PBD effects. Erkmen and Attard (2011) investigated the LTB of the thin-walled beams including the combined effect of shear deformation and PBD. Mohri et al. (2012) investigated the effect of PBD on lateral torsional buckling of mono-symmetric beams. Analytical solutions were provided for simply supported beams and comparisons were provided against classical and finite element predictions. Among the above studies, the work of Roberts and Azizian (1983a) Pi and Trahair (1992b) Pi and Trahair (1992c) Mohri and Potier-Ferry (2006) Erkmen and Attard (2011) accounted for the load height effect.

The effect of pre-buckling deformations on the buckling capacity of plates was investigated in Ziegler (1983c) who formulated a buckling theory for plates subjected to in-plane forces. The study accounted for the effects of shear deformation and in-plane PBD and showed that both effects are of the same order of magnitude. Based on Trefftz criterion, Wang et al. (1992d) developed an elastic buckling solution that accounts for PBD effects for rectangular plates under in-plane stresses. The study indicated that PBD effects are significant for plates with large thickness to span ratios. Xiang et al. (1993) investigated the effects of PBD on the buckling strength of thick plates under various boundary conditions based on Rayleigh-Ritz type solution. Hong et al. (1993a) developed an analytical buckling solution for circular Mindlin plates under uniform radial compressive stresses, which included the second order terms of in plane strains. The stationarity conditions of the total potential energy lead to two coupled differential equations of equilibrium, which were explicitly solved for various boundary conditions. Hong et al. (1993b) developed closed form and approximate critical stress solutions and compared the results against analytical solutions. The study investigated second order in-plane displacement and PBD effects. Liew et al. (1996) investigated the effects of PBD on laminated plates. The governing equations were formulated by evoking the stationarity conditions of the total potential energy and a closed form buckling Navier-type solution was developed for simply supported boundary conditions. The effect of PBD was shown to be the same order of magnitude as the shear effect for various loading scenarios, boundary conditions and plate aspect ratios.

6.4. Statement of the problem

A prismatic member with a doubly symmetric wide flange cross section (Fig. 6-2a) has flanges of width b and thickness t. Web height is h and its thickness is w. The beam is subjected to a combination of loads applied within the $x=0$ plane, consisting of a) A transverse line load $q_y(z)$ whose line of action is defined by the curve $y_{qy}(z)$ from the web mid-height. $q_y(z)$ induces strong-axis pre-buckling bending moments, and b) Longitudinal line load $q_z(z)$ whose line of action is defined by the curve $y_{qz}(z)$ from the web mid-height. Load $q_z(z)$ induces axial forces accompanied by strong-axis moments (in addition to induced in (a)) resulting from the product of the longitudinal force $q_z(z)$ by the eccentricity $y_{qz}(z)$ (Fig. 6-2)b.

The un-deformed configuration of the member is depicted as Stage 1 in Fig. 6-3. Under reference loads $q_y(z)$, $q_z(z)$ the member cross-section is assumed to move to Stage 2 where the web mid-height is assumed to undergo a pre-buckling transverse displacement $v_p(z)$. Also, owing to strong axis bending of the web and associated longitudinal displacements, both flanges undergo longitudinal displacements $w_{Tp}(z)$ and $w_{Bp}(z)$. As a convention, subscript *'T'* denotes quantities related to the top flange while '*B*' denotes quantities related to the bottom flange. Displacement fields $v_p(z)$, $w_{Tp}(z)$ and $w_{Bp}(z)$ are determined from pre-buckling equilibrium considerations. As a matter of convention, all field variables (e.g., displacements, strains, stresses or stress resultants) induced in the pre-buckling stage (i.e., in going from Stage 1 to Stage 2) are denoted by subscript '*p*' . The reference loads in Stage 2 are then assumed to increase by a factor λ . Two possible analysis scenarios are then considered in the present solution:

<u>a) Nonlinear pre-buckling analysis:</u> Given second order effects, when loads are magnified by factor λ , i.e., take the values λq_y, λq_z the associated pre-buckling displacements increase in a nonlinear fashion, i.e., the pre-buckling displacements are $w_{Tp}(\lambda, z), w_{Bp}(\lambda, z)$ and $v_p(\lambda, z)$ are to be determined from a geometrically nonlinear pre-buckling analysis. When the load factor λ attains a critical value (Stage 3 in Fig. 6-3), the system attains the state of onset of buckling and the member has a tendency to buckle laterally, with no further increase in loading, to the buckled configuration (Stage 4). Once an equilibrium configuration has been determined on the non-linear pre-buckling path, the stability of the system is checked. If the system is found in stable equilibrium, the load factor is incremented, and a new pre-buckling position on the primary equilibrium path is sought and the procedure is repeated until a neutral state of equilibrium is detected, at which the system is deemed to have buckled at the load level $\lambda = \lambda_{cr}$

<u>b) Linear pre-buckling analysis:</u> In cases where the nonlinear pre-buckling load-displacement effects are negligible, one can assume that as the reference loads are magnified to attain λq_y and λq_z the corresponding pre-buckling displacements are also linearly magnified i.e., $v_p(\lambda, z) = \lambda v_p(z), w_{Tp}(\lambda, z) = \lambda w_{Tp}(z)$ and $w_{Bp}(\lambda, z) = \lambda w_{Bp}(z)$. In such a case, the critical load multiplier $\lambda = \lambda_{cr}$ can be obtained directly by solving the resulting eigenvalue solution.

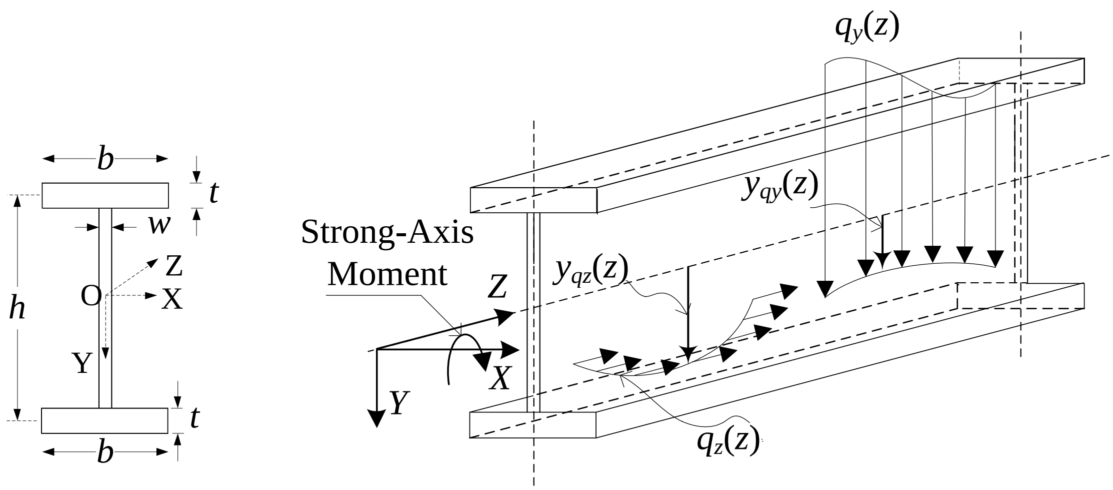

Fig. 6-2 a) Cross section dimensions b) Loading scheme pre-buckling analysis

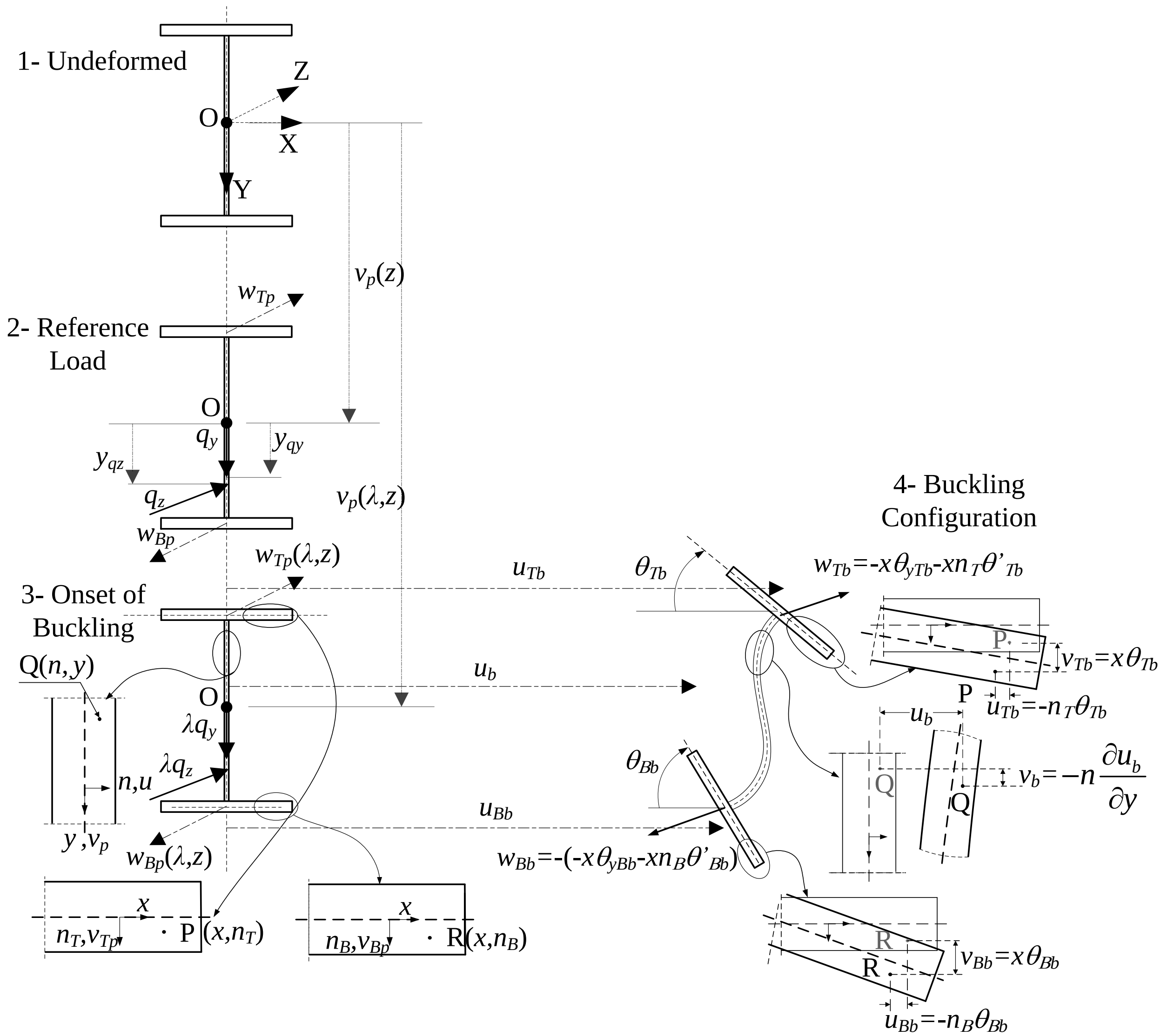

Fig. 6-3 Stages of Deformation

6.4.1. **Assumptions**

The formulation is restricted to prismatic members. Material is assumed linearly elastic, homogeneous and isotropic. A right-handed coordinate system is adopted in which the origin 'O' lies on web mid-height. A local right-handed coordinate system is also assigned to each of the flanges and the web. Points P, R and Q within the top flange, bottom flange, and web, respectively, are offset from the middle surface and have local coordinates (x, n_T) , (x, n_B) and (n, y) .The assumptions related to the pre-buckling analysis (Stage 1-3) are:

1- Web compressibility in the transverse direction is negligible, i.e. $v_p(y,z) = v_p(z)$

2- The nonlinear strain terms are retained, i.e. a geometrically nonlinear analysis is performed in the pre-buckling stage.

3- Throughout pre-buckling, the longitudinal displacement of the web is assumed to follow a linear distribution across the height.

The assumptions related to the buckling analysis (Stage 3-4) are;

4- The flanges are assumed to undergo local warping according to the kinematics of the Gjelsvik theory (Gjelsvik (1981).

5- The web is assumed to undergo biaxial bending as a plate. Hence, the displacement $u_b(y,z)$ out of the plane of the web is a function of coordinates y and z.

6.4.2. **Kinematics**

Throughout buckling, the flange centroids undergo lateral displacements $u_{Tb}(y,z)$,$u_{Bb}(y,z)$, angles of twist θ_{Tb},θ_{Bb} and weak axis angles of rotation $u'_{Tb}(z)$,$u'_{Bb}(z)$. As a result, a point offset by a distance x and n_T from the top flange centroid undergoes displacements $u_{Tb}(n_T,z)$ and $v_b(x,z)$. The flanges are assumed to undergo local warping deformations according (Gjelsvik 1981). Thus, a point offset by distances x and n from the flange centroids undergo longitudinal displacements $w_{Tb}(n,x,z)$ and $w_{Bb}(n,x,z)$.

Throughout buckling, the web is assumed to deform as a Kirchhoff plate. Hence, a point with coordinates (y,z) within the web plane moves out of the plane of the web by a displacement $u_b(y,z)$. Also, a generic point originally offset from the middle surface of the web by a distance n undergoes a transverse displacement $v_b(n,y,z)$ depicted in Fig. 6-3 and a longitudinal displacement $w_b(n,y,z)$. As a convention, all field variables induced in the buckling stage (i.e., in going from Stage 3 to Stage 4 in Fig. 6-3) are denoted by subscript *‘b’*.

6.4.3. Pre-buckling Analysis

6.4.3.1. Finite element formulation

A two-noded shear deformable beam element (i.e., the Timoshenko beam) with three DOFs per node (i.e. the transverse displacement v_p, the longitudinal displacement w_p and the angle of rotation θ_{xp}) is developed for pre-buckling analysis (Fig. 6-4). In order to derive the stiffness and geometric matrices and fixed end moment vector for the sought beam element, the shape functions in (Friedman and Kosmatka (1993) were adopted. As shown in Fig. 6-4, stress resultants P_1, V_1, M_1, P_2, V_2 and M_2 denote the axial and shear forces and the bending moments at both ends of the element.

In the pre-buckling stage, two types of analysis are implemented; a) Linear and b) nonlinear incremental geometric analysis. In the linear analysis, the equilibrium conditions of the beam take the form $\mathbf{K_E u_p = F}$, where $\mathbf{K_E}$ is elastic stiffness matrix, $\mathbf{u_p}$ is the nodal displacement vector, and $\mathbf{F}$ is the nodal force vector. In the nonlinear geometric incremental analysis, the equilibrium condition takes the form $\mathbf{K_{Tp} \Delta u_p} = \left(\mathbf{K_E} + \mathbf{K_G} + \mathbf{K_D}\right)\mathbf{\Delta u_p} = \mathbf{\Delta F}$ (Chajes and Churchill 1987) where $\mathbf{K_{Tp}}$ is the tangent stiffness matrix , matrix $\mathbf{K_G}$ captures the effect of geometric changes and presence of axial force within the member and matrix $\mathbf{K_D}$ captures the effect of displacement changes on the tangent stiffness matrix. The details of the formulation were provided in Chapter 5. The total displacements $\mathbf{u_p}$ is obtained by summing the displacement increments $\mathbf{\Delta u_p}$ computed for each load increment $\mathbf{\Delta F}$. The underlying geometrically nonlinear analysis has been implemented based on the (Chajes and Churchill 1987)) modified for the presence of shear deformation by using the shape functions in (Friedman and Kosmatka 1993). It is noted that suppressing pre-buckling shear deformation effects (for instance to investigate the effect of pre-pre-buckling shear deformation on buckling strength as will be shown later on) can be achieved by replacing the Timoshenko stiffness matrices by the conventional Euler-Bernoulli stiffness matrices.

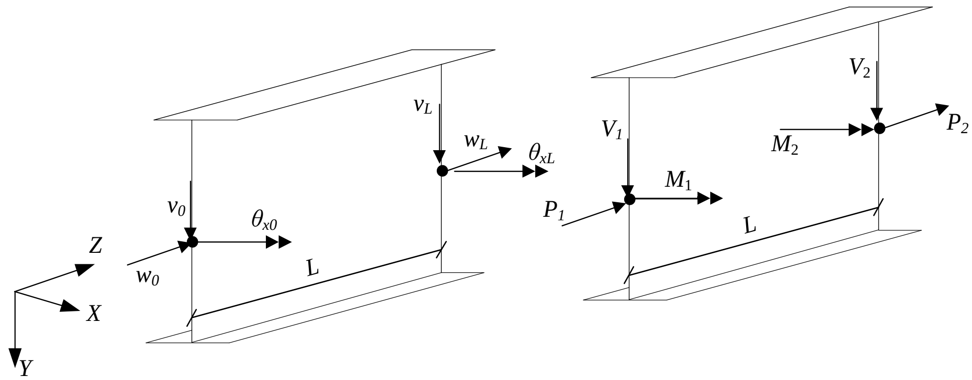

Fig. 6-4 Two-node shear deformable element a) degrees of freedom b) nodal forces

6.4.3.2. **Expressions of pre-buckling stresses in terms of stress resultants**

The normal stresses are related to the pre-buckling moments N_p, M_p through

$$\sigma_{zp}(y,z) = \frac{N_p(z)}{A} + \frac{M_p(z)}{I_x}(y) \qquad -h/2 < y < h/2$$

$$\sigma_{zTp}(z) \approx \frac{N_p(z)}{A} + \left(-\frac{h}{2}\right)\frac{M_p(z)}{I_x} \qquad y = -h/2 \qquad \text{(6.1)a-c}$$

$$\sigma_{zBp}(z) \approx \frac{N_p(z)}{A} + \left(\frac{h}{2}\right)\frac{M_p(z)}{I_x} \qquad y = h/2$$

where A the cross is section arear and I_x is the strong axis moment of inertia. Also, the shear stresses are related to the pre-buckling shear stress V_p through

$$\tau_{yzp}(y,z) = \frac{V_p(z)Q_x(y)}{I_x w} \qquad \text{(6.2)}$$

and $Q_x(y)$ is the first moment of inertia about the *x*-axis. The shear stresses in the flanges is assumed to have a negligible contribution.

6.4.3.3. **Expressions for pre-buckling displacements**

The internal force-displacement relations of a shear deformable beam (Friedman and Kosmatka (1993)) arise from the boundary condition terms and take the form

$$\begin{aligned} M_p(z) &= -EI_x\theta'_{xp}(z) \\ V_p(z) &= GAv'_p(z) + GA\theta_{xp}(z) \end{aligned} \qquad \text{(6.3)a-b}$$

Bending moments $M_p(z)$ can be approximately related to end stress resultants M_{p1} and M_{p2} through linear interpolation, i.e., $M_p(z) = -(1-z/L)M_{p1} + (z/L)M_{p2}$. By substitution into Eq. (6.3)a, and integrating both sides of Eq. (6.3) w.r.t z from zero to *z*, one obtains the expression for angle of rotation $\theta_{xp}(z)$, i.e.

$$\theta_{xp}(z) = -\frac{1}{EI_x}\int_0^z \left[-M_{p1}\left(1-\frac{z}{L}\right) + M_{p2}\left(\frac{z}{L}\right)\right]dz = -\frac{1}{EI_x}\left[-M_{p1}z + \frac{1}{2}\left(\frac{M_{p1}}{L} + M_{p2}\right)z^2\right] + \theta_{xp}(0) \quad (6.4)$$

The shear force within the element is also related to the end shear forced V_{p1} and V_{p2} linearly i.e.,

$$V_p(z) = -(1-z/L)V_{p1} + (z/L)V_{p2} \quad (6.5)$$

From Eqs. (6.4)-(6.5) by substituting into Eq. (6.3)b, one obtains the derivative of transverse displacement $v_p'(z)$ expressed in terms of stress resultants, i.e.

$$v_p'(z) = -\theta_{xp}(z) + \frac{V(z)}{GA} = \frac{1}{EI_x}\left[-M_{p1}z + \frac{1}{2}\left(\frac{M_{p1}}{L} + M_{p2}\right)z^2\right] - \theta_{xp}(0) + \frac{1}{GA}\left[V_{p1}\left(1-\frac{z}{L}\right) - V_{p2}\left(\frac{z}{L}\right)\right] \quad (6.6)$$

The longitudinal displacement due to normal forces is obtained as

$$w_p'(z) = \frac{1}{EA}N_p(z) \quad (6.7)$$

The normal force within the element $N_p(z)$ can be expressed in terms of end nodal forces using linear interpolation, i.e. $N_p(z) \approx -(1-z/L)N_{p1} + (z/L)N_{p2}$. By substituting into Eq. (6.7) and integrating w.r.t Z , one obtains the longitudinal displacement due to normal force, i.e.

$$w_p(z) = \frac{1}{EA}\left[-\left(z - z^2/2L\right)N_{p1} + \left(z^2/2L\right)N_{p2}\right] + w_p(0)$$

The longitudinal displacement at the top and bottom flanges are then expressed due to bending moments and normal forces, i.e.

$$w_{Tp}(z) = -\theta_{xp}(z) \times \frac{h}{2} + w_p(z)$$
$$= -\left\{ -\frac{1}{EI_x}\left[-M_{p1}z + \frac{1}{2}\left(\frac{M_{p1}}{L} + M_{p2}\right)z^2 \right] + \theta_{xp}(0) \right\} \times \frac{h}{2} + \frac{1}{EA}\left[-\left(z - z^2/2L\right)N_{p1} + \left(z^2/2L\right)N_{p2} \right] + w_p(0)$$
$$w_{Bp}(z) = \theta_{xp}(z) \times \frac{h}{2} + w_p(z)$$
$$= \left\{ -\frac{1}{EI_x}\left[-M_{p1}z + \frac{1}{2}\left(\frac{M_{p1}}{L} + M_{p2}\right)z^2 \right] + \theta_{xp}(0) \right\} \times \frac{h}{2} + \frac{1}{EA}\left[-\left(z - z^2/2L\right)N_{p1} + \left(z^2/2L\right)N_{p2} \right] + w_p(0)$$

(6.8)a-b

6.4.4. Expressions for buckling displacements

6.4.4.1. Displacements for a generic point within the flanges

Each flange is treated as a separate beam with a rectangular cross-section that follows a modified form of the Gjelsvik beam kinematics (Gjelsvik 1981) to account for (a) moderate rotation effects including pre-buckling deformation and (b) pre-buckling shear deformation effects. Pi et al. (1992a) provided expressions for the displacement fields of a generic point within an I-beam cross-section following the Vlasov kinematics (Vlasov 1961) in terms of the transverse and lateral displacements at the shear centre, the longitudinal displacement at the centroid, and the angle of twist. The study of Pi et al. (1992) accounts for moderate rotations and includes pre-buckling deformation effects. The present study starts with the expression Pi et al. (1992) while introducing the following modifications:

(a)While the study of Pi et al. (1992) focused on I-shaped cross-sections with significant global warping and negligible local warping effects, in the present theory, when treating each flange as a separate beam with a rectangular cross-section, the global warping function vanishes when the pole of the flange is taken to coincide at the flange centroid. Thus, the global warping sectorial term ω in Pi et al. (1992) is replaced by the local warping term as given in Gjelsvik (1981) (i.e., xn where n denotes the normal distance from flange mid-surface).

(b) The study of Pi et al. (1992) considers the pre-buckling response of a beam to follow the kinematics of the conventional Euler-Bernouilli beam where the pre-buckling angle of rotation for the cross-section is equal to that of the beam axis. In contrast, the present theory adopts pre-Timoshenko buckling kinematics whereby the pre-buckling angle of rotation of the cross-section

θ_{xp} is assumed to be distinct from the rotation of the beam axis v'_p . The necessary modifications were made to the expression by Pi al. (1992) where applicable.

(c) When relating the longitudinal displacements within the flanges to the pre-buckling rotation, the expression v'_p in Pi et al. (1992) is replaced by the term $\pm\theta_{xp}\left(h/2\right)$, and

(d)Rather than using the degrees of freedom w_p, θ_{xp} as in Pi et al. (1992), the present formulation adopts the alternative degrees of freedom w_{Tp}, w_{Bp} as per the transformation relation in (6.8)a-b.

The total displacement fields (from Configurations 1 to 4) $\hat{u}_T\left(x,n_T,z\right), \hat{v}_T\left(x,n_T,z\right), \hat{w}_T\left(x,n_T,z\right)$ for a generic point $\left(x,n_T,z\right)$ within the top flange are thus expressed in terms of the pre-buckling displacement fields $v_p\left(z\right), \theta_{xp}\left(z\right)$ and buckling displacement fields $u_{Tb}\left(z\right), \theta_{Tb}\left(z\right)$ as

$$
\begin{aligned}
\hat{u}_T\left(x,n_T,z\right) = u_{Tb}\left(z\right) - n_T\theta_{Tb}\left(z\right) + \Big\langle & -\frac{1}{2}x\left[u'^2_{Tb}\left(z\right)+\theta^2_{Tb}\left(z\right)-u'_{Tb}\left(z\right)\theta_{xp}\left(\lambda,z\right)\theta_{Tb}\left(z\right)\right] \\
& -\frac{1}{2}\left[\frac{h}{2}u'_{Tb}\left(z\right)\theta_{xp}\left(\lambda,z\right)+n_T u'^2_{Tb}\left(z\right)\theta_{Tb}\left(z\right)\right] \\
& -xu'_{Tb}\left(z\right)\left\{n_T\theta'_{Tb}\left(z\right)+\frac{h}{4}\left[u''_{Tb}\left(z\right)\theta_{xp}\left(\lambda,z\right)-u'_{Tb}\left(z\right)\theta'_{xp}\left(\lambda,z\right)\right]\right\}\Big\rangle
\end{aligned}
$$

$$
\begin{aligned}
\hat{v}_T\left(x,n_T,z\right) = v_p\left(\lambda,z\right) + x\theta_{Tb}\left(z\right) + \Big\langle & -\frac{1}{2}x\left[-u'_{Tb}\left(z\right)\theta_{xp}\left(\lambda,z\right)+\theta^2_{xp}\left(\lambda,z\right)\theta_{Tb}\left(z\right)\right] \\
& -\frac{1}{2}\left[-\frac{h}{2}\theta^2_{xp}\left(\lambda,z\right)+n_T\theta^2_{Tb}\left(z\right)-\frac{h}{2}u'_{Tb}\left(z\right)\theta_{xp}\left(\lambda,z\right)\theta_{Tb}\left(z\right)\right] \\
& -\frac{h}{2}x\theta_{xp}\left(\lambda,z\right)\left\{\theta'_{Tb}\left(z\right)-\frac{1}{2}\left[u''_{Tb}\left(z\right)\theta_{xp}\left(\lambda,z\right)-u'_{Tb}\left(z\right)\theta'_{xp}\left(\lambda,z\right)\right]\right\}\Big\rangle
\end{aligned}
$$

$$
\begin{aligned}
\hat{w}_T\left(x,n_T,z\right) = & \left[w_{Tp}\left(\lambda,z\right)-xu'_{Tb}\left(z\right)+n_T\theta_{xp}\left(\lambda,z\right)-xn_T\theta'_{Tb}\left(z\right)\right] \\
& +\Big\langle x\left[\theta_{xp}\left(\lambda,z\right)\theta_{Tb}\left(z\right)+\frac{1}{2}u'_{Tb}\left(z\right)\theta^2_{Tb}\left(z\right)\right]+n_T u'_T\left(z\right)\theta_{Tb}\left(z\right)+\frac{h}{4}\theta_{xp}\left(\lambda,z\right)\theta^2_{Tb}\left(z\right) \\
& +\frac{h}{4}x\left\{u'_T\left(z\right)\theta'_{xp}\left(\lambda,z\right)-u''_T\left(z\right)\theta_{xp}\left(\lambda,z\right)+\frac{1}{2}\left[u''_{Tb}\left(z\right)\theta_{xp}\left(\lambda,z\right)-u'_{Tb}\left(z\right)\theta'_{xp}\left(\lambda,z\right)\right]\left[\theta^2_{xp}\left(\lambda,z\right)+u'^2_{Tb}\left(z\right)\right]\right\} \\
& -\frac{1}{2}\theta'_{Tb}\left(z\right)\left[\frac{h}{2}x\theta^2_{xp}\left(\lambda,z\right)-xn_T u'^2_{Tb}\left(z\right)\right]\Big\rangle
\end{aligned}
$$

(6.9)a-c

Similar equations are written for the bottom flange displacements by replacing subscripts T with B and replacing $y = h/2$ with $y = -h/2$ where applicable, yielding

$$\begin{aligned}
\hat{u}_B(x,n_B,z) = u_{Bb}(z) - n_B\theta_{Bb}(z) + \Big\langle -\frac{1}{2}x\left[u'^2_{Bb}(z) + \theta^2_{Bb}(z) - u'_{Bb}(z)\theta_{xp}(\lambda,z)\theta_{Bb}(z)\right] \\
-\frac{1}{2}\left[-\frac{h}{2}u'_{Bb}(z)\theta_{xp}(\lambda,z) + n_B u'^2_{Bb}(z)\theta_{Bb}(z)\right] \\
-xu'_{Bb}(z)\left\{n_B u'_{Bb}(z)\theta'_{Bb}(z) - \frac{h}{4}\left[u''_{Bb}(z)\theta_{xp}(\lambda,z) - u'_{Bb}(z)\theta'_{xp}(\lambda,z)\right]\right\}\Big\rangle
\end{aligned}$$

$$\begin{aligned}
\hat{v}_B(x,n_B,z) = v_p(\lambda,z) + x\theta_{Bb}(z) + \Big\langle -\frac{1}{2}x\left[-u'_{Bb}(z)\theta_{xp}(\lambda,z) + \theta^2_{xp}(\lambda,z)\theta_{Bb}(z)\right] \\
-\frac{1}{2}\left[\frac{h}{2}\theta^2_{xp}(\lambda,z) + n_B\theta^2_{Tb}(z) + \frac{h}{2}u'_{Bb}(z)\theta_{xp}(\lambda,z)\theta_{Bb}(z)\right] \\
+\frac{h}{4}x\theta_{xp}(\lambda,z)\left\{n_B\theta'_{Bb}(z) - \frac{1}{2}\left[u''_{Bb}(z)\theta_{xp}(\lambda,z) - u'_{Bb}(z)\theta'_{xp}(\lambda,z)\right]\right\}\Big\rangle
\end{aligned}$$

$$\begin{aligned}
&\hat{w}_B(x,n_B,z) = \left[w_{Bp}(\lambda,z) - xu'_{Bb}(z) + n_B\theta_{xp}(\lambda,z) - xn_B\theta'_{Tb}(z)\right] \\
&+\Big\langle x\left[\theta_{xp}(\lambda,z)\theta_{Bb}(z) + \frac{1}{2}u'_{Bb}(z)\theta^2_{Bb}(z)\right] + n_B u'_B(z)\theta_{Bb}(z) - \frac{h}{4}\theta_{xp}(\lambda,z)\theta^2_{Bb}(z) \\
&-\frac{h}{4}x\left\{u'_B(z)\theta'_{xp}(\lambda,z) - u''_B(z)\theta_{xp}(\lambda,z) + \frac{1}{2}\left[u''_{Bb}(z)\theta_{xp}(\lambda,z) - u'_{Bb}(z)\theta'_{xp}(\lambda,z)\right]\left[\theta^2_{xp}(\lambda,z) + u'^2_{Bb}(z)\right]\right\} \\
&-\frac{1}{2}\theta'_{Bb}(z)\left[-\frac{h}{2}x\theta^2_{xp}(\lambda,z) - xn_B u'^2_{Bb}(z)\right]\Big\rangle
\end{aligned}$$

(6.10)a-c

6.4.4.2. **Displacements for a generic point within the web**

Throughout pre-buckling, we recall that the web is assumed to deform as a Timoshenko beam. Hence, the longitudinal displacement of the web mid-surface varies linearly along the height. Throughout buckling, we recall that the web is assumed to behave as a thin-plate. The associated longitudinal and transverse displacements are respectively given by $-n\,\partial\hat{u}_b(y,z)/\partial z$ and $-n\,\partial\hat{u}_b(y,z)/\partial y$. The total displacements are then given by adding the pre-buckling to the buckling displacements yielding

$$\hat{w}(n,y,z) = \left(\frac{1}{2} - \frac{y}{h}\right)w_{Tp}(\lambda,z) + \left(\frac{1}{2} + \frac{y}{h}\right)w_{Bp}(\lambda,z) - n\frac{\partial\hat{u}_b(y,z)}{\partial z} \tag{6.11}$$

$$\widehat{v}(n,y,z) = -n\frac{\partial \widehat{u}_b\left(y,z\right)}{\partial y} + v_p\left(\lambda, z\right) \tag{6.12}$$

6.5. Expressions for strains and stresses

In contrast to previous studies (e.g., Hancock et al. (1980), Ng and Ronagh (2009), Ádány and Schafer (2008), Andreassen and Jönsson (2012), etc) the present study retains the complete form of the second order strains.

6.5.1. Strains in the top flange

The Green Lagrange Strain tensor for the top flange is given by

$$\varepsilon_{zT} = \varepsilon_{zLT} + \varepsilon_{zNT} = \frac{\partial \widehat{w}_T}{\partial z} + \frac{1}{2}\left[\left(\frac{\partial \widehat{u}_T^{\alpha}}{\partial z}\right)^2 + \left(\frac{\partial \widehat{v}_T^{\beta}}{\partial z}\right)^2 + \left(\frac{\partial \widehat{w}_T^{\gamma}}{\partial z}\right)^2\right]$$

$$\gamma_{xzT} = \gamma_{xzLT} + \gamma_{xzNT} = \frac{\partial \widehat{w}_T}{\partial x} + \frac{\partial \widehat{u}_T}{\partial z} + \left(\frac{\partial \widehat{w}_T^{\delta}}{\partial x}\frac{\partial \widehat{w}_T^{\delta}}{\partial z} + \frac{\partial \widehat{u}_T^{\varepsilon}}{\partial x}\frac{\partial \widehat{u}_T^{\varepsilon}}{\partial z} + \frac{\partial \widehat{v}_T^{\eta}}{\partial x}\frac{\partial \widehat{v}_T^{\eta}}{\partial z}\right) \tag{6.13)a-b}$$

From Eqs. (6.9), by substituting into Eqs. (6.13), one obtains the strains within the top flange, i.e.

$$\varepsilon_{zTp} = \lambda w_{Tp}{}' + \lambda n_T \theta'_{xp} + \frac{1}{2}\lambda^2 v'^2_p$$

$$\begin{aligned}
\varepsilon_{zTb} = & -x u''_{Tb} - x n_T \theta''_{Tb} + \lambda x\left[\left(\theta_{xp} + v'_p\right)\theta'_{Tb} + \theta'_{xp}\theta_{Tb}\right] + n_T u''_T \theta_{Tb} + \lambda\frac{h}{4}\theta'_{xp}\theta^2_{Tb} + \frac{h}{2}\theta'_{Tb}\theta_{Tb}\left(\theta_{xp} + v'_p\right) \\
& + \frac{h}{4}\lambda x\left(u'_T\theta''_{xp} - u'''_T\theta_{xp} - \theta''_{Tb}\theta^2_{xp} - 2\theta'_{Tb}\theta_{xp}\theta'_{xp}\right) + \frac{h^2}{4}\theta_{xp}\theta'_{xp}\theta_{Tb}\theta'_{Tb} \\
& + \frac{1}{2}\left[\left(u'_{Tb}\right)^2 + \left(n_T\theta'_{Tb}\right)^2 + \frac{h^2}{16}\lambda^2\left(u''^2_{Tb}\theta^2_{xp} + u'^2_{Tb}\theta'^2_{xp} + 2u'_{Tb}u''_{Tb}\theta_{xp}\theta'_{xp}\right) - \lambda\frac{h}{2}u'_{Tb}\left(\theta_{xp}u''_{Tb} + \theta'_{xp}u'_{Tb}\right)\right] \\
& + \frac{1}{2}\Bigg\{\left(x\theta'_{Tb}\right)^2 + \frac{1}{4}x^2\lambda^2\left(u''^2_{Tb}\theta^2_{xp} + u'^2_{Tb}\theta'^2_{xp} + 2u''_{Tb}\theta_{xp}\theta'_{xp}u'_{Tb}\right) + x^2\frac{h^2}{4}\lambda^2\left(\theta^2_{xp}\theta''^2_{Tb} + \theta'^2_{xp}\theta'^2_{Tb} + 2\theta'_{Tb}\theta_{xp}\theta'_{xp}\theta''_{Tb}\right) \\
& + 2\lambda v'_p\left[-\frac{1}{2}\lambda x\left(-u''_{Tb}\theta_{xp} - \theta'_{xp}u'_{Tb}\right) + \lambda\frac{h}{4}\left(u''_{Tb}\theta_{xp}\theta_{Tb} + u'_{Tb}\theta'_{xp}\theta_{Tb} + u'_{Tb}\theta_{xp}\theta'_{Tb}\right) - \lambda x\frac{h}{2}\left(\theta'_{xp}\theta'_{Tb} + \theta_{xp}\theta''_{Tb}\right)\right] \\
& + 2\lambda x\theta'_{Tb}\Bigg[-\frac{1}{2}x\left(-u''_{Tb}\theta_{xp} - \theta'_{xp}u'_{Tb} + 2\theta_{Tb}\theta'_{xp}\theta_{xp} + \theta'_{Tb}\theta^2_{xp}\right) + \frac{h}{2}\theta'_{xp}\theta_{xp} \\
& + x\frac{h}{4}\theta'_{xp}\left(-2\theta'_{Tb} + u''_{Tb}\theta_{xp} - u'_{Tb}\theta'_{xp}\right) + x\frac{h}{4}\theta_{xp}\left(-2\theta''_{Tb} - u'_T\theta''_{xp} + u'''_T\theta_{xp}\right)\Bigg] \\
& - \lambda^2 x^2\frac{h}{2}\left(\theta'_{xp}\theta'_{Tb} + \theta_{xp}\theta''_{Tb}\right)\left(u''_{Tb}\theta_{xp} + \theta'_{xp}u'_{Tb}\right)\Bigg\}
\end{aligned}$$

$$\gamma_{xzTp} = 0$$

$$\gamma_{xzTb} = -2n_T\theta'_{Tb} - \frac{h}{4}\lambda\left(2u''_{Tb}\theta_{xp}\right) + \lambda\left(\left(\theta_{xp} + v'_p\right)\theta_{Tb} + \frac{1}{2}\lambda v'_p u'_T\theta_{xp}\right) + \lambda\frac{h}{4}\left(-\theta'_{Tb}\theta^2_{xp} + 2\theta_{Tb}\theta'_{xp}\theta_{xp}\right)$$
$$+\left[-u'_{Tb} - n_T\theta'_{Tb} + \lambda\theta_{xp}\theta_{Tb} + \lambda\frac{h}{4}\left(u'_T\theta'_{xp} - u''_T\theta_{xp} - \theta'_{Tb}\theta^2_{xp}\right)\right]\left(w'_{Tp} + n_T\theta'_{xp}\right) - \frac{h}{2}\lambda^2\theta'_{Tb}\theta_{xp}v'_p$$

(6.14)a-d

where all primes denote differentiation with respect to z. The internal strain energy due to shear has two components $\frac{1}{2}\int_z\int_{A_T} 2G\left(\bar{\gamma}_{xzTb}\right)^2 dAdz$ and $\int_z\int_{A_T} \tau_{xzTp}\bar{\bar{\gamma}}_{xzTb}dAdz$, where $\bar{\gamma}_{xzTb}$ and $\bar{\bar{\gamma}}_{xzTb}$ are the first and second variations of the shear strain. The mid-surface pre-buckling shear stresses in the flange are negligible (i.e. $\tau_{xzTp} = 0$), hence the term $\int_z\int_{A_T} \tau_{xzTp}\bar{\bar{\gamma}}_{xzTb}dAdz$ vanishes and the term $\bar{\bar{\gamma}}_{xzTb}$ does not contribute to the formulation.

6.5.2. **Strains in the web**

The total normal strains ε_y and ε_z an shear strain γ_{yz} the web are expressed as a sum of the linear and nonlinear components, i.e.,

$$\varepsilon_y = \varepsilon_{yL} + \varepsilon_{yN}$$
$$\varepsilon_z = \varepsilon_{zL} + \varepsilon_{zN} \qquad (6.15)\text{a-c}$$
$$\gamma_{yz} = \gamma_{yzL} + \gamma_{yzN}$$

in which the linear strains are given by

$$\varepsilon_{yL} = \frac{\partial}{\partial y}\left(\hat{v}_b\left(n,y,z\right) + \hat{v}_p\left(\lambda,z\right)\right) = -n\frac{\partial^2\hat{u}_b\left(y,z\right)}{\partial y^2}$$

$$\varepsilon_{zL} = \frac{\partial}{\partial z}\left(\hat{w}_b\left(n,y,z\right) + \hat{w}_p\left(\lambda,z\right)\right) = -n\frac{\partial^2\hat{u}_b\left(y,z\right)}{\partial z^2} + \left(\frac{1}{2} + \frac{y}{h}\right)w'_{Bp}\left(\lambda,z\right) + \left(\frac{1}{2} - \frac{y}{h}\right)w'_{Tp}\left(\lambda,z\right)$$

$$\gamma_{yzL} = \frac{\partial}{\partial y}\left(\hat{w}_b\left(n,y,z\right) + \hat{w}_p\left(\lambda,z\right)\right) + \frac{\partial}{\partial z}\left(\hat{v}_b\left(n,y,z\right) + \hat{v}_p\left(\lambda,z\right)\right)$$
$$= -2n\frac{\partial^2\hat{u}_b}{\partial y\partial z} + \frac{1}{h}\left(w_{Bp}\left(\lambda,z\right) - w_{Tp}\left(\lambda,z\right)\right) + v'_p\left(\lambda,z\right)$$

(6.16)a-c

and the nonlinear strain components are

$$\varepsilon_{yN} = \frac{1}{2}\left\{\left(\frac{\partial}{\partial y}\hat{u}_b(y,z)\right)^2 + \left[\frac{\partial}{\partial y}\left(\hat{w}_b(y,z) + \lambda\hat{w}_p(z)\right)\right]^2\right\}$$

$$= \frac{1}{2}\left[\left(\frac{\partial\hat{u}_b}{\partial y}\right)^2 + \left(-n\frac{\partial^2\hat{u}_b}{\partial y\partial z} - \frac{\lambda w_{Tp}}{h} + \frac{\lambda w_{Bp}}{h}\right)^2\right]$$

$$\varepsilon_{zN} = \frac{1}{2}\left\{\left(\frac{\partial\hat{u}_b(y,z)}{\partial z}\right)^2 + \left[\frac{\partial}{\partial z}\left(\hat{v}_b(y,z) + \lambda\hat{v}_p(z)\right)\right]^2\right\}$$

$$= \frac{1}{2}\left\{\left(\frac{\partial\hat{u}_b}{\partial z}\right)^2 + \left(-n\frac{\partial^2\hat{u}_b}{\partial y\partial z} + \lambda v_p'\right)^2\right\}$$

$$\gamma_{yzN} = \frac{\partial\hat{u}_b}{\partial y}\frac{\partial\hat{u}_b}{\partial z} + \frac{\partial}{\partial y}\left(\hat{v}_b + \lambda\hat{v}_p\right)\frac{\partial}{\partial z}\left(\hat{v}_b + \lambda\hat{v}_p\right) + \frac{\partial}{\partial y}\left(\hat{w}_b + \lambda\hat{w}_p\right)\frac{\partial}{\partial z}\left(\hat{w}_b + \lambda\hat{w}_p\right)$$

$$= \frac{\partial\hat{u}_b}{\partial y}\frac{\partial\hat{u}_b}{\partial z} + \left(-n\frac{\partial^2\hat{u}_b}{\partial y^2}\right)\left(-n\frac{\partial^2\hat{u}_b}{\partial y\partial z} + \lambda v_p'\right)$$

$$+\left(-n\frac{\partial\hat{u}_b}{\partial y\partial z} - \frac{\lambda w_{Tp}}{h} + \frac{\lambda w_{Bp}}{h}\right)\left[-n\frac{\partial^2\hat{u}_b}{\partial z^2} + \left(\frac{1}{2} - \frac{y}{h}\right)\lambda w_{Tp}' + \left(\frac{1}{2} + \frac{y}{h}\right)\lambda w_{Bp}'\right] \quad \text{(6.17)a-c}$$

6.5.3. Stress strain relations

From Hooke's law, the stresses in the top and bottom flanges are expressed as

$$\sigma_{zT} = E\varepsilon_{zT}\ ,\ \sigma_{zB} = E\varepsilon_{zB}\ ,\ \tau_{xzT} = G\gamma_{xzT}\ ,\ \tau_{xzB} = G\gamma_{xzB} \quad (6.18)$$

and those in the web are given by

$$\sigma_y = \frac{E}{1-\nu^2}\left(\varepsilon_y + \nu\varepsilon_z\right), \sigma_z = \frac{E}{1-\nu^2}\left(\varepsilon_z + \nu\varepsilon_y\right), \tau_{yz} = \frac{E}{2(1+\nu)}\gamma_{yz} \quad (6.19)$$

6.6. Variational principle

The total potential energy $\Pi = U + V$ is the sum of the internal strain energy U and the potential energy V gained by the loads. The total internal strain energy $U = U_T + U_B + U_W$ is the sum of the internal strain energies stored in the top and bottom flanges, U_T and U_B, and the web U_W. The potential energy $V = V_1 + V_2$ is the sum of the potential energy gain V_1 by the transverse loads and the potential energy gain V_2 by the axial loads i.e., $\Pi = (U_T + U_B + U_W) + (V_1 + V_2)$

6.6.1. **Internal strain energy**

6.6.1.1. **Contribution of the web**

The internal strain energy stored in the web in going from position 1 to 4 is

$$\begin{aligned} U_W &= \frac{1}{2}\int_V \left(\sigma_{zb}\varepsilon_{zb} + \sigma_{yb}\varepsilon_{yb} + \tau_{yzb}\gamma_{yzb}\right)dV + \int_V \left(\sigma_{zp}\varepsilon_{zb} + \sigma_{yp}\varepsilon_{yb} + \tau_{yzp}\gamma_{yzb}\right)dV \\ &+ \frac{1}{2}\int_V \left(\sigma_{zp}\varepsilon_{zp} + \sigma_{yp}\varepsilon_{yp} + \tau_{yzp}\gamma_{yzp}\right)dV \end{aligned} \tag{6.20}$$

From Eqs. (6.19), by substituting into Eq. (6.20), and recalling that the total stress and strains are the sum of the pre-buckling and buckling terms, one obtains

$$\begin{aligned} U_W &= \frac{E}{2(1-\nu^2)}\int_V \left[\left(\varepsilon_{zb} + \nu\varepsilon_{yb}\right)\varepsilon_{zb} + \left(\varepsilon_{yb} + \nu\varepsilon_{zb}\right)\varepsilon_{yb} + \frac{(1-\nu)}{2}\gamma_{yzb}\gamma_{yzb}\right]dV \\ &+ \int_V \left(\sigma_{zp}\varepsilon_{zb} + \sigma_{yp}\varepsilon_{yb} + \tau_{yzp}\gamma_{yzb}\right)dV \\ &+ \frac{1}{2}\int_V \left(\sigma_{zp}\varepsilon_{zp} + \sigma_{yp}\varepsilon_{yp} + \tau_{yzp}\gamma_{yzp}\right)dV \end{aligned} \tag{6.21}$$

where σ_{zp} , σ_{yp} and τ_{yzp} denote the pre-buckling stresses and ε_{zb} , ε_{yb} and γ_{yzb} denote the strains at the onset of buckling as given by

$$\begin{aligned} \varepsilon_{zb} &= -n\frac{\partial^2 \hat{u}_b}{\partial z^2} + \frac{1}{2}\left[\left(\frac{\partial \hat{u}_b}{\partial z}\right)^2 + \left(-n\frac{\partial^2 \hat{u}_b}{\partial y \partial z} + \lambda v'_p\right)^2\right] \\ \varepsilon_{yb} &= -n\frac{\partial^2 \hat{u}_b}{\partial y^2} + \frac{1}{2}\left[\left(\frac{\partial \hat{u}_b}{\partial y}\right)^2 + \left(-n\frac{\partial^2 \hat{u}_b}{\partial y \partial z} - \frac{\lambda w_{Tp}}{h} + \frac{\lambda w_{Bp}}{h}\right)^2\right] \\ \gamma_{yzb} &= -2n\frac{\partial^2 \hat{u}_b}{\partial y \partial z} + \frac{\partial \hat{u}_b}{\partial y}\frac{\partial \hat{u}_b}{\partial z} + \left(-n\frac{\partial^2 \hat{u}_b}{\partial y^2}\right)\left(-n\frac{\partial^2 \hat{u}_b}{\partial y \partial z} + \lambda v'_p\right) \\ &+ \left(-n\frac{\partial \hat{u}_b}{\partial y \partial z} - \frac{\lambda w_{Tp}}{h} + \frac{\lambda w_{Bp}}{h}\right)\left[-n\frac{\partial^2 \hat{u}_b}{\partial z^2} + \left(\frac{1}{2} - \frac{y}{h}\right)\lambda w'_{Tp} + \left(\frac{1}{2} + \frac{y}{h}\right)\lambda w'_{Bp}\right] \end{aligned} \tag{6.22)a-c}$$

Noting that the second variation of a functional $F = (1/2)\int_V \alpha_i \alpha_j dV$ of the product of two argument functions α_i, α_j is $(1/2)\overline{\overline{F}} = (1/2)\int_V \left(2\overline{\alpha}_i\overline{\alpha}_j + \overline{\overline{\alpha}}_i\alpha_j + \alpha_i\overline{\overline{\alpha}}_j\right)dV$ where a single bar ‘ $^-$ ’ denotes the first variation of the argument function with respect to buckling displacements and the double-bar ‘ $=$ ’ denotes the second variation, the second variation of total strain energy of the web (Eq. (6.23)) is found to be

$$\bar{\bar{U}}_W = \frac{E}{(1-\nu^2)}\int_V \left[\left(\bar{\varepsilon}_{zb}\right)^2 + \left(\bar{\varepsilon}_{yb}\right)^2 + 2\nu\bar{\varepsilon}_{zb}\bar{\varepsilon}_{yb} + \frac{1}{2}(1-\nu)\left(\bar{\gamma}_{yzb}\right)^2 \right] dV + \int_V \left(\sigma_{zp}\bar{\bar{\varepsilon}}_{zb} + \sigma_{yp}\bar{\bar{\varepsilon}}_{yb} + \tau_{yzp}\bar{\bar{\gamma}}_{yzb}\right) dV \tag{6.23}$$

where

$$\bar{\varepsilon}_{zb} = -n\frac{\partial^2 \bar{\bar{u}}_b}{\partial z^2} - \lambda n \frac{\partial^2 \bar{\bar{u}}_b}{\partial y \partial z} v'_p$$

$$\bar{\varepsilon}_{yb} = -n\frac{\partial^2 \bar{\bar{u}}_b}{\partial y^2} - n\lambda \frac{\partial^2 \bar{\bar{u}}_b}{\partial y \partial z}\left(-\frac{w_{Tp}}{h} + \frac{w_{Bp}}{h}\right)$$

$$\bar{\gamma}_{yzb} = -2n\frac{\partial^2 \bar{\bar{u}}_b}{\partial y \partial z} + \left(-\lambda n \frac{\partial^2 \bar{\bar{u}}_b}{\partial y^2} v'_p\right) + \left(-n\lambda \frac{\partial \bar{\bar{u}}_b}{\partial y \partial z}\right)\left[\left(\frac{1}{2} - \frac{y}{h}\right) w'_{Tp} + \left(\frac{1}{2} + \frac{y}{h}\right) w'_{Bp}\right]$$
$$+\lambda\left(-\frac{w_{Tp}}{h} + \frac{w_{Bp}}{h}\right)\left[-n\frac{\partial^2 \bar{\bar{u}}_b}{\partial z^2}\right]$$

$$\bar{\bar{\varepsilon}}_{zb} = \left[\left(\frac{\partial \bar{\bar{u}}_b}{\partial z}\right)^2 + \left(n\frac{\partial^2 \bar{\bar{u}}_b}{\partial y \partial z}\right)^2\right]$$

$$\bar{\bar{\varepsilon}}_{yb} = \left(\frac{\partial \bar{\bar{u}}_b}{\partial y}\right)^2 + \left(n\frac{\partial^2 \bar{\bar{u}}_b}{\partial y \partial z}\right)^2$$

$$\bar{\bar{\gamma}}_{yzb} = 2\frac{\partial \bar{\bar{u}}_b}{\partial y}\frac{\partial \bar{\bar{u}}_b}{\partial z} + 2n^2\left(\frac{\partial^2 \bar{\bar{u}}_b}{\partial y \partial z}\frac{\partial^2 \bar{\bar{u}}_b}{\partial y^2} + \frac{\partial^2 \bar{\bar{u}}_b}{\partial y \partial z}\frac{\partial^2 \bar{\bar{u}}_b}{\partial z^2}\right) \tag{6.24a-f}$$

From Eq. (6.24) by substituting into Eq. (6.23), one obtains

$$
\begin{aligned}
\bar{\bar{U}}_W &= \frac{E}{(1-\nu^2)}\times \\
&\int_V \Bigg\{ \left(n\bar{\bar{u}}_{b,zz}\right)^2 + \left(n\bar{\bar{u}}_{b,yy}\right)^2 + 2\nu n^2 \bar{\bar{u}}_{b,zz}\bar{\bar{u}}_{b,yy} + \frac{(1-\nu)}{2}\left(2n\bar{\bar{u}}_{b,yz}\right)^2 \\
&+\left(\lambda n\bar{\bar{u}}_{b,yz}v'_p\right)^2 + 2\lambda n^2\bar{\bar{u}}_{b,zz}\bar{\bar{u}}_{b,yz}v'_p + 1/h^2\left[n\lambda\bar{\bar{u}}_{b,yz}\left(-w_{Tp}+w_{Bp}\right)\right]^2 + 2n^2\lambda\bar{\bar{u}}_{b,yy}\bar{\bar{u}}_{b,yz}\left(-w_{Tp}+w_{Bp}\right)/h \\
&+2\nu n^2\left[\lambda\bar{\bar{u}}_{b,zz}\bar{\bar{u}}_{b,yz}\left(-w_{Tp}+w_{Bp}\right)/h + \lambda\bar{\bar{u}}_{b,yy}\bar{\bar{u}}_{b,yz}v'_p + \lambda^2\bar{\bar{u}}_{b,yz}\,\bar{\bar{u}}_{b,yz}v'_p\left(-w_{Tp}+w_{Bp}\right)/h\right] \\
&+\frac{(1-\nu)}{2}\Bigg\langle \left(n\lambda\bar{\bar{u}}^{\psi}_{b,yy}v'^{\psi}\right)^2 + \left\{n\lambda\bar{\bar{u}}_{b,yz}\left[\left(\frac{1}{2}-\frac{y}{h}\right)w'_{Tp} + \left(\frac{1}{2}+\frac{y}{h}\right)w'_{Bp}\right]\right\}^2 + \left[n\lambda\bar{\bar{u}}_{b,zz}\left(-\frac{w_{Tp}}{h}+\frac{w_{Bp}}{h}\right)\right]^2 \\
&+4n^2\lambda\bar{\bar{u}}_{b,yz}\left\{\bar{\bar{u}}_{b,yy}v'_p + \bar{\bar{u}}_{b,yz}\left[\left(\frac{1}{2}-\frac{y}{h}\right)w'_{Tp} + \left(\frac{1}{2}+\frac{y}{h}\right)w'_{Bp}\right] + \bar{\bar{u}}_{b,zz}\left(-\frac{w_{Tp}}{h}+\frac{w_{Bp}}{h}\right)\right\} \\
&+2n^2\lambda^2\bar{\bar{u}}_{b,yy}v'_p\left[\bar{\bar{u}}_{b,yz}\left[\left(\frac{1}{2}-\frac{y}{h}\right)w'_{Tp} + \left(\frac{1}{2}+\frac{y}{h}\right)w'_{Bp}\right] + \bar{\bar{u}}_{b,zz}\left(-\frac{w_{Tp}}{h}+\frac{w_{Bp}}{h}\right)\right] \\
&+2n^2\lambda^2\bar{\bar{u}}_{b,yz}\bar{\bar{u}}_{b,zz}\left[\left(\frac{1}{2}-\frac{y}{h}\right)w'_{Tp} + \left(\frac{1}{2}+\frac{y}{h}\right)w'_{Bp}\right]\left(-\frac{w_{Tp}}{h}+\frac{w_{Bp}}{h}\right)\Bigg\rangle dV \\
&+\lambda\int_V \left\{\sigma_{zp}\left(\bar{\bar{u}}^2_{b,z} + n^2\bar{\bar{u}}^2_{b,yz}\right) + 2\tau_{yzp}\left[\bar{\bar{u}}_{b,y}\bar{\bar{u}}_{b,z} + n^2\left(\frac{\partial^2\bar{\bar{u}}_b}{\partial y\partial z}\frac{\partial^2\bar{\bar{u}}_b}{\partial y^2} + \frac{\partial^2\bar{\bar{u}}_b}{\partial y\partial z}\frac{\partial^2\bar{\bar{u}}_b}{\partial z^2}\right)\right]\right\} dV
\end{aligned}
\tag{6.25}
$$

By performing integrations over the thickness, Eq. (6.25) takes the form

$$\bar{\bar{U}}_W = D\int_z\int_y \Big\{ \left(\bar{\bar{u}}_{b,zz}\right)^2 + \left(\bar{\bar{u}}_{b,yy}\right)^2 + 2\nu\bar{\bar{u}}_{b,zz}\bar{\bar{u}}_{b,yy} + 2\left(1-\nu\right)\left(\bar{\bar{u}}_{b,yz}\right)^2$$

$$+\left(\lambda\bar{\bar{u}}_{b,yz}v_{,zp}\right)^2 + 2\lambda\bar{\bar{u}}_{b,zz}\bar{\bar{u}}_{b,yz}v_{,zp} + 1/h^2\left[\lambda\bar{\bar{u}}_{b,yz}\left(-w_{Tp}+w_{Bp}\right)\right]^2 + 2\lambda\bar{\bar{u}}_{b,yy}\bar{\bar{u}}_{b,yz}\left(-w_{Tp}+w_{Bp}\right)/h$$

$$+2\nu\left[\lambda\bar{\bar{u}}_{b,zz}\bar{\bar{u}}_{b,yz}\left(-w_{Tp}+w_{Bp}\right)/h + \lambda\bar{\bar{u}}_{b,yy}\bar{\bar{u}}_{b,yz}v_{,zp} + \lambda^2\bar{\bar{u}}_{b,yz}\bar{\bar{u}}_{b,yz}v_{,zp}\left(-w_{Tp}+w_{Bp}\right)/h\right]$$

$$+\frac{\left(1-\nu\right)}{2}\Big\langle \left(\lambda\bar{\bar{u}}_{b,yy}v_{,zp}\right)^2 + \left\{\lambda\bar{\bar{u}}_{b,yz}\left[\left(\frac{1}{2}-\frac{y}{h}\right)w_{,zTp} + \left(\frac{1}{2}+\frac{y}{h}\right)w_{,zBp}\right]\right\}^2 + \left[\lambda\bar{\bar{u}}_{b,zz}\left(-\frac{w_{Tp}}{h}+\frac{w_{Bp}}{h}\right)\right]^2$$

$$+4\lambda\bar{\bar{u}}_{b,yz}\left\{\bar{\bar{u}}_{b,yy}v_{,zp} + \bar{\bar{u}}_{b,yz}\left[\left(\frac{1}{2}-\frac{y}{h}\right)w_{,zTp} + \left(\frac{1}{2}+\frac{y}{h}\right)w_{,zBp}\right] + \bar{\bar{u}}_{b,zz}\left(-\frac{w_{Tp}}{h}+\frac{w_{Bp}}{h}\right)\right\}$$

$$+2\lambda^2\bar{\bar{u}}_{b,yy}v'_p\left[\bar{\bar{u}}_{b,yz}\left[\left(\frac{1}{2}-\frac{y}{h}\right)w_{,zTp} + \left(\frac{1}{2}+\frac{y}{h}\right)w_{,zBp}\right] + \bar{\bar{u}}_{b,zz}\left(-\frac{w_{Tp}}{h}+\frac{w_{Bp}}{h}\right)\right]$$

$$+2\lambda^2\bar{\bar{u}}_{b,yz}\bar{\bar{u}}_{b,zz}\left[\left(\frac{1}{2}-\frac{y}{h}\right)w_{,zTp} + \left(\frac{1}{2}+\frac{y}{h}\right)w'_{Bp}\right]\left(-\frac{w_{Tp}}{h}+\frac{w_{Bp}}{h}\right)\Big\rangle dydz$$

$$+\lambda\int_z\int_y\left\{N_{zp}\left(\bar{\bar{u}}_{b,z}^2 + \frac{t^2}{12}\bar{\bar{u}}_{b,yz}^2\right) + N_{yzp}\left[\bar{\bar{u}}_{b,y}\bar{\bar{u}}_{b,z} + \frac{t^2}{12}\left(\frac{\partial^2\bar{\bar{u}}_b}{\partial y\partial z}\frac{\partial^2\bar{\bar{u}}_b}{\partial y^2} + \frac{\partial^2\bar{\bar{u}}_b}{\partial y\partial z}\frac{\partial^2\bar{\bar{u}}_b}{\partial z^2}\right)\right]\right\}dydz$$

(6.26)

where $D = Ew^3/12\left(1-\nu^2\right)$ $N_{zp} = \sigma_{zp}t$ and $N_{yzp} = 2\tau_{yzp}t$.

6.6.1.2. **Contributions of the Flanges**

The strain energy of the top flange is given by

$$U_T = \frac{1}{2}\int_L\int_{A_T}\left(\sigma_{zT}\varepsilon_{zT} + \tau_{xzT}\gamma_{xzT}\right)dAdz \tag{6.27}$$

and its second variation is

$$\bar{\bar{U}}_T = \frac{1}{2}\int_z\int_{A_T}\left(2E\left(\bar{\varepsilon}_{zTb}\right)^2 + 2G\left(\bar{\gamma}_{xzTb}\right)^2\right)dAdz + \int_z\int_{A_T}\left(\sigma_{zTp}\bar{\bar{\varepsilon}}_{zTb} + \tau_{xzTp}\bar{\bar{\gamma}}_{xzTb}\right)dAdz \tag{6.28}$$

where

$$\begin{aligned}
\bar{\varepsilon}_{zTb} &= -x\bar{u}''_{Tb} - xn_T\bar{\theta}''_{Tb} + \lambda x\left[\left(\theta_{xp}+v'_p\right)\bar{\theta}'_{Tb} + \theta'_{xp}\bar{\theta}_{Tb}\right] + \frac{h}{4}\lambda x\left[\bar{u}'_T\theta''_{xp} - \bar{u}'''_T\theta_{xp} - \bar{\theta}''_{Tb}\theta^2_{xp}\right] \\
&\quad + \left\{-\frac{1}{2}\lambda^2 xv'_p\left[\left(-\bar{u}''_{Tb}\theta_{xp} - \theta'_{xp}\bar{u}'_{Tb}\right) + h\left(\theta'_{xp}\bar{\theta}'_{Tb} + \theta_{xp}\bar{\theta}''_{Tb}\right)\right]\right\} \\
\bar{\gamma}_{xzTb} &= -2n_T\bar{\theta}'_{Tb} - \frac{h}{4}\lambda\left(2\bar{u}''_{Tb}\theta_{xp}\right) + \lambda\left(\theta_{xp}+v'_p\right)\bar{\theta}_{Tb} + \frac{1}{2}\lambda^2\theta_{xp}v'_p\bar{u}'_T \\
&\quad + \lambda\left\{-\bar{u}'_{Tb} - n_T\bar{\theta}'_{Tb} + \lambda\theta_{xp}\bar{\theta}_{Tb} + \lambda\frac{h}{4}\left[\bar{u}'_T\theta'_{xp} - \bar{u}''_T\theta_{xp} - \bar{\theta}'_{Tb}\theta^2_{xp}\right]\right\}\left(w'_{Tp} + n_T\theta'_{xp}\right) \\
&\quad + \lambda\frac{h}{4}\left(-\theta'_{Tb}\theta^2_{xp} + 2\theta_{Tb}\theta'_{xp}\theta_{xp}\right) - \frac{h}{2}\lambda^2\bar{\theta}'_{Tb}\theta_{xp}v'_p \\
\bar{\bar{\varepsilon}}_{zTb} &= \\
&\left[\left(\bar{u}'_{Tb}\right)^2 + \left(n_T\bar{\theta}'_{Tb}\right)^2 + \left(x\bar{\theta}'_{Tb}\right)^2\right] + \lambda\frac{h}{2}\theta'_{xp}\bar{\theta}^2_{Tb} + h\bar{\theta}'_{Tb}\bar{\theta}_{Tb}\left(\theta_{xp}+v'_p\right) \\
&\quad + \left[\frac{h^2}{16}\lambda^2\left(\bar{u}''^2_{Tb}\theta^2_{xp} + \bar{u}'^2_{Tb}\theta'^2_{xp} + 2\bar{u}'_{Tb}\bar{u}''_{Tb}\theta_{xp}\theta'_{xp}\right) - \lambda\frac{h}{2}\bar{u}'_{Tb}\left(\theta_{xp}\bar{u}''_{Tb} + \theta'_{xp}\bar{u}'_{Tb}\right)\right]\frac{h^2}{2}\left(\theta_{xp}\theta'_{xp}\bar{\theta}_{Tb}\bar{\theta}'_{Tb}\right) \\
&\quad + \left\{\frac{1}{4}x^2\lambda^2\left(\bar{u}''^2_{Tb}\theta^2_{xp} + \bar{u}'^2_{Tb}\theta'^2_{xp} + 2\bar{u}''_{Tb}\theta_{xp}\theta'_{xp}\bar{u}'_{Tb}\right) + x^2\frac{h^2}{4}\lambda^2\left(\theta^2_{xp}\bar{\theta}''^2_{Tb} + \theta'^2_{xp}\bar{\theta}'^2_{Tb} + 2\bar{\theta}'_{Tb}\theta_{xp}\theta'_{xp}\bar{\theta}''_{Tb}\right) + \right. \\
&\quad + 2\lambda v'_p\left[\lambda\frac{h}{4}\left(\bar{u}''_{Tb}\theta_{xp}\bar{\theta}_{Tb} + \bar{u}'_{Tb}\theta'_{xp}\bar{\theta}_{Tb} + \bar{u}'_{Tb}\theta_{xp}\bar{\theta}'_{Tb}\right)\right] + \lambda x^2\bar{\theta}'_{Tb}\left(\theta_{xp}\bar{u}''_{Tb} + \theta'_{xp}\bar{u}'_{Tb} - 2\bar{\theta}_{Tb}\theta'_{xp}\theta_{xp} - \bar{\theta}'_{Tb}\theta^2_{xp}\right) \\
&\quad + 2\lambda x\bar{\theta}'_{Tb}\left[+x\frac{h}{4}\theta'_{xp}\left(-2\bar{\theta}'_{Tb} + \bar{u}''_{Tb}\theta_{xp} - \bar{u}'_{Tb}\theta'_{xp}\right) + x\frac{h}{4}\theta_{xp}\left(-2\bar{\theta}''_{Tb} - \bar{u}'_T\theta''_{xp} + \bar{u}'''_T\theta_{xp}\right)\right] \\
&\quad \left. -\lambda^2x^2\frac{h}{2}\left(\theta'_{xp}\bar{\theta}'_{Tb} + \theta_{xp}\bar{\theta}''_{Tb}\right)\left(\bar{u}''_{Tb}\theta_{xp} + \theta'_{xp}\bar{u}'_{Tb}\right)\right\}
\end{aligned} \tag{6.29}$$

and σ_{zTp} and τ_{xzTp} are pre-buckling stresses within the top flange. Compatibility of displacements at the web to flange junction necessitates that the lateral displacement of the top flange is related to the lateral displacement $\hat{u}_b$ of the web through the relation $u_{Tb}(z) = \hat{u}_b(-h/2, z)$. Also, the angle of twist of the top flange θ_{Tb} is related to the first derivative of the lateral displacement of the web $\hat{u}_{b,y}$ through the relation $\theta_{Tb}(z) = -\hat{u}_{b,y}(-h/2, z)$. Hence, one rewrites Eqs. (6.29) in terms of the web displacement field as

$$
\begin{aligned}
\bar{\varepsilon}_{zTb} = \Big\{ & -x\bar{\hat{u}}_{b,zz} + xn_T\bar{\hat{u}}_{b,yzz} - \lambda x\left[\left(\theta_{xp}+v_{p,z}\right)\bar{\hat{u}}_{b,yz} + \theta_{xp,z}\bar{\hat{u}}_{b,y}\right] \\
& + \frac{h}{4}\lambda x\left[\bar{\hat{u}}_{b,z}\theta_{xp,zz} - \bar{\hat{u}}_{b,zzz}\theta_{xp} + \bar{\hat{u}}_{b,yzz}\theta_{xp}^2\right] \\
& + \frac{1}{2}\lambda^2 x v_{p,z}\left[\left(\theta_{xp}\bar{\hat{u}}_{b,zz} + \theta_{xp,z}\bar{\hat{u}}_{b,z}\right) + h\left(\theta_{xp,z}\bar{\hat{u}}_{b,yz} + \theta_{xp}\bar{\hat{u}}_{b,yzz}\right)\right]\Big\}_{y=-h/2} \\
\bar{\gamma}_{xzTb} = \Big\{ & 2n_T\bar{\hat{u}}_{b,yz} - \lambda\left(\theta_{xp}+v_{p,z}\right)\bar{\hat{u}}_{b,y} + \frac{1}{2}\lambda\theta_{xp}v_{p,z}\bar{\hat{u}}_{b,z} + \lambda\frac{h}{4}\left(\bar{\hat{u}}_{b,yz}\theta_{xp}^2 - 2\bar{\hat{u}}_{b,y}\theta_{xp,z}\theta_{xp}\right) \\
& + \lambda\left[-\bar{\hat{u}}_{b,z} + n_T\bar{\hat{u}}_{b,yz} - \lambda\theta_{xp}\bar{\hat{u}}_{b,y} + \lambda\frac{h}{4}\left(\bar{\hat{u}}_{b,z}\theta_{xp,z} - \bar{\hat{u}}_{b,zz}\theta_{xp} + \bar{\hat{u}}_{b,yz}\theta_{xp}^2\right)\right]\left(w_{Tp,z} + n_T\theta_{xp,z}\right) \\
& - \frac{h}{4}\lambda\left(2\bar{\hat{u}}_{b,zz}\theta_{xp}\right) + \frac{h}{2}\lambda^2\bar{\hat{u}}_{b,yz}\theta_{xp}v_{p,z}\Big\}_{y=-h/2} \\
\bar{\bar{\varepsilon}}_{zTb} = \Big[& \bar{\hat{u}}_{b,z}^2 + \left(n_T\bar{\hat{u}}_{b,yz}\right)^2 + \left(x\bar{\hat{u}}_{b,yz}\right)^2 + \lambda\frac{h}{2}\theta_{xp,z}\bar{\hat{u}}_{b,y}^2 + h\bar{\hat{u}}_{b,yz}\bar{\hat{u}}_{b,y}\left(\theta_{xp}+v_{p,z}\right) \\
& - \lambda x^2\bar{\hat{u}}_{b,yz}\left(\theta_{xp}\bar{\hat{u}}_{b,zz} + \theta_{xp,z}\bar{\hat{u}}_{b,z} - 2\bar{\hat{u}}_{b,y}\theta_{xp,z}\theta_{xp} - \bar{\hat{u}}_{b,yz}\theta_{xp}^2\right)\Big] + \lambda\frac{h^2}{2}\left(\theta_{xp}\theta_{xp,z}\bar{\hat{u}}_{b,y}\bar{\hat{u}}_{b,yz}\right) \\
& + \left[\frac{h^2}{16}\lambda^2\left(\bar{\hat{u}}_{b,zz}^2\theta_{xp}^2 + \bar{\hat{u}}_{b,z}^2\theta_{xp,z}^2 + 2\bar{\hat{u}}_{b,z}\bar{\hat{u}}_{b,zz}\theta_{xp}\theta_{xp,z}\right) - \lambda\frac{h}{2}\bar{\hat{u}}_{b,z}\left(\theta_{xp}\bar{\hat{u}}_{b,zz} + \theta_{xp,z}\bar{\hat{u}}_{b,z}\right)\right] \\
& + \Big\{\frac{1}{4}x^2\lambda^2\left(\bar{\hat{u}}_{b,zz}^2\theta_{xp}^2 + \bar{\hat{u}}_{b,z}^2\theta_{xp,z}^2 + 2\bar{\hat{u}}_{b,zz}\bar{\hat{u}}_{b,z}\theta_{xp}\theta_{xp,z}\right) \\
& + x^2\frac{h^2}{4}\lambda^2\left(\theta_{xp}^2\bar{\hat{u}}_{b,yzz}^2 + \theta_{xp,z}^2\bar{\hat{u}}_{b,yz}^2 + 2\bar{\hat{u}}_{b,yz}\bar{\hat{u}}_{b,yzz}\theta_{xp}\theta_{xp,z}\right) \\
& - 2\lambda v_{p,z}\left[\lambda\frac{h}{4}\left(\bar{\hat{u}}_{b,zz}\theta_{xp}\bar{\hat{u}}_{b,y} + \bar{\hat{u}}_{b,z}\theta_{xp,z}\bar{\hat{u}}_{b,y} + \bar{\hat{u}}_{b,z}\theta_{xp}\bar{\hat{u}}_{b,yz}\right)\right] \\
& - 2\lambda x\bar{\hat{u}}_{b,yz}\Big[-\frac{1}{2}x\left(-\bar{\hat{u}}_{b,zz}\theta_{xp} - \theta_{xp,z}\bar{\hat{u}}_{b,z} - 2\bar{\hat{u}}_{b,y}\theta_{xp,z}\theta_{xp} - \bar{\hat{u}}_{b,yz}\theta_{xp}^2\right) \\
& \qquad + x\frac{h}{4}\theta_{xp,z}\left(2\bar{\hat{u}}_{b,yz} + \bar{\hat{u}}_{b,zz}\theta_{xp} - \bar{\hat{u}}_{b,z}\theta_{xp,z}\right) + x\frac{h}{4}\theta_{xp}\left(2\bar{\hat{u}}_{b,yzz} - \bar{\hat{u}}_{b,z}\theta_{xp,zz} + \bar{\hat{u}}_{b,zzz}\theta_{xp}\right)\Big] \\
& - \lambda^2 x^2\frac{h}{2}\left(-\theta_{xp,z}\bar{\hat{u}}_{b,yz} - \theta_{xp}\bar{\hat{u}}_{b,yzz}\right)\left(\bar{\hat{u}}_{b,zz}\theta_{xp} + \theta_{xp,z}\bar{\hat{u}}_{b,z}\right)\Big\}_{y=-h/2}
\end{aligned}
\tag{6.30}
$$

From Eqs. (6.30) by substituting into Eq. (6.28), one obtains the second variation of total strain energy of the flange as

$$
\begin{aligned}
\bar{\bar{U}}_T = \int_z \int_{A_F} & \Bigg\{ -x\bar{\hat{u}}_{b,\mathrm{zz}} + xn_T\bar{\hat{u}}_{b,\mathrm{yzz}} - \lambda x\left[\left(\theta_{xp} + v_{p,z}\right)\bar{\hat{u}}_{b,\mathrm{yz}} + \theta_{xp,z}\bar{\hat{u}}_{b,\mathrm{y}}\right] \\
& + \frac{h}{4}\lambda x\left[\bar{\hat{u}}_{b,\mathrm{z}}\theta_{xp,zz} - \bar{\hat{u}}_{b,\mathrm{zzz}}\theta_{xp} + \bar{\hat{u}}_{b,\mathrm{yzz}}\theta_{xp}^2 + 2\bar{\hat{u}}_{b,\mathrm{yz}}\theta_{xp}\theta_{xp,z}\right] \\
& + \frac{1}{2}\lambda^2 xv_{p,z}\left[\left(\theta_{xp}\bar{\hat{u}}_{b,\mathrm{zz}} + \theta_{xp,z}\bar{\hat{u}}_{b,\mathrm{z}}\right) + h\left(\theta_{xp,z}\bar{\hat{u}}_{b,\mathrm{yz}} + \theta_{xp}\bar{\hat{u}}_{b,\mathrm{yzz}}\right)\right] - \lambda\frac{h}{2}x\bar{\hat{u}}_{b,\mathrm{yz}}\theta_{xp,z}\theta_{xp}\Bigg\}^2 \\
+ G & \Bigg\{ 2n_T\bar{\hat{u}}_{b,\mathrm{yz}} - \lambda\left(\theta_{xp} + v_{p,z}\right)\bar{\hat{u}}_{b,\mathrm{y}} + \frac{1}{2}\lambda\theta_{xp}v_{p,z}\bar{\hat{u}}_{b,\mathrm{z}} + \lambda\frac{h}{4}\left(\bar{\hat{u}}_{b,\mathrm{yz}}\theta_{xp}^2 - 2\bar{\hat{u}}_{b,\mathrm{y}}\theta_{xp,z}\theta_{xp}\right) \\
& + \lambda\left[-\bar{\hat{u}}_{b,\mathrm{z}} + n_T\bar{\hat{u}}_{b,\mathrm{yz}} - \lambda\theta_{xp}\bar{\hat{u}}_{b,\mathrm{y}} + \lambda\frac{h}{4}\left(\bar{\hat{u}}_{b,\mathrm{z}}\theta_{xp,z} - \bar{\hat{u}}_{b,\mathrm{zz}}\theta_{xp} + \bar{\hat{u}}_{b,\mathrm{yz}}\theta_{xp}^2\right)\right]\left(w_{Tp,z} + n_T\theta_{xp,z}\right) \\
& - \frac{h}{4}\lambda\left(2\bar{\hat{u}}_{b,\mathrm{zz}}\theta_{xp}\right) + \frac{h}{2}\lambda^2\bar{\hat{u}}_{b,\mathrm{yz}}\theta_{xp}v_{p,z}\Bigg\}^2_{y=-h/2} dAdz \\
+ \int_z \int_{A_F} \sigma_{zTp} & \Bigg\{\Bigg[\bar{\hat{u}}_{b,\mathrm{z}}^2 + \left(n_T\bar{\hat{u}}_{b,\mathrm{yz}}\right)^2 + \left(x\bar{\hat{u}}_{b,\mathrm{yz}}\right)^2 + \lambda\frac{h}{2}\theta_{xp,z}\bar{\hat{u}}_{b,\mathrm{y}}^2 + h\bar{\hat{u}}_{b,\mathrm{yz}}\bar{\hat{u}}_{b,\mathrm{y}}\left(\theta_{xp} + v_{p,z}\right) \\
& - \lambda x^2\bar{\hat{u}}_{b,\mathrm{yz}}\left(\theta_{xp}\bar{\hat{u}}_{b,\mathrm{zz}} + \theta_{xp,z}\bar{\hat{u}}_{b,\mathrm{z}} - 2\bar{\hat{u}}_{b,\mathrm{y}}\theta_{xp,z}\theta_{xp} - \bar{\hat{u}}_{b,\mathrm{yz}}\theta_{xp}^2\right)\Bigg] + \lambda\frac{h^2}{2}\left(\theta_{xp}\theta_{xp,z}\bar{\hat{u}}_{b,\mathrm{y}}\bar{\hat{u}}_{b,yz}\right) \\
& + \left[\frac{h^2}{16}\lambda^2\left(\bar{\hat{u}}_{b,\mathrm{zz}}^2\theta_{xp}^2 + \bar{\hat{u}}_{b,\mathrm{z}}^2\theta_{xp,z}^2 + 2\bar{\hat{u}}_{b,\mathrm{z}}\bar{\hat{u}}_{b,\mathrm{zz}}\theta_{xp}\theta_{xp,z}\right) - \lambda\frac{h}{2}\bar{\hat{u}}_{b,\mathrm{z}}\left(\theta_{xp}\bar{\hat{u}}_{b,\mathrm{zz}} + \theta_{xp,z}\bar{\hat{u}}_{b,\mathrm{z}}\right)\right] \\
& + \Bigg\{\frac{1}{4}x^2\lambda^2\left(\bar{\hat{u}}_{b,\mathrm{zz}}^2\theta_{xp}^2 + \bar{\hat{u}}_{b,\mathrm{z}}^2\theta_{xp,z}^2 + 2\bar{\hat{u}}_{b,\mathrm{zz}}\bar{\hat{u}}_{b,\mathrm{z}}\theta_{xp}\theta_{xp,z}\right) \\
& + x^2\frac{h^2}{4}\lambda^2\left(\theta_{xp}^2\bar{\hat{u}}_{b,\mathrm{yzz}}^2 + \theta_{xp,z}^2\bar{\hat{u}}_{b,\mathrm{yz}}^2 + 2\bar{\hat{u}}_{b,\mathrm{yz}}\bar{\hat{u}}_{b,\mathrm{yzz}}\theta_{xp}\theta_{xp,z}\right) \\
& - 2\lambda v_{p,z}\left[\lambda\frac{h}{4}\left(\bar{\hat{u}}_{b,\mathrm{zz}}\theta_{xp}\bar{\hat{u}}_{b,\mathrm{y}} + \bar{\hat{u}}_{b,\mathrm{z}}\theta_{xp,z}\bar{\hat{u}}_{b,\mathrm{y}} + \bar{\hat{u}}_{b,\mathrm{z}}\theta_{xp}\bar{\hat{u}}_{b,\mathrm{yz}}\right)\right] \\
& - 2\lambda x\bar{\hat{u}}_{b,\mathrm{yz}}\Bigg[-\frac{1}{2}x\left(-\bar{\hat{u}}_{b,\mathrm{zz}}\theta_{xp} - \theta_{xp,z}\bar{\hat{u}}_{b,\mathrm{z}} - 2\bar{\hat{u}}_{b,\mathrm{y}}\theta_{xp,z}\theta_{xp} - \bar{\hat{u}}_{b,\mathrm{yz}}\theta_{xp}^2\right) \\
& \qquad + x\frac{h}{4}\theta_{xp,z}\left(2\bar{\hat{u}}_{b,\mathrm{yz}} + \bar{\hat{u}}_{b,\mathrm{zz}}\theta_{xp} - \bar{\hat{u}}_{b,\mathrm{z}}\theta_{xp,z}\right) + x\frac{h}{4}\theta_{xp}\left(2\bar{\hat{u}}_{b,\mathrm{yzz}} - \bar{\hat{u}}_{b,\mathrm{z}}\theta_{xp,zz} + \bar{\hat{u}}_{b,\mathrm{zzz}}\theta_{xp}\right)\Bigg] \\
& - \lambda^2x^2\frac{h}{2}\left(-\theta_{xp,z}\bar{\hat{u}}_{b,\mathrm{yz}} - \theta_{xp}\bar{\hat{u}}_{b,\mathrm{yzz}}\right)\left(\bar{\hat{u}}_{b,\mathrm{zz}}\theta_{xp} + \theta_{xp,z}\bar{\hat{u}}_{b,\mathrm{z}}\right)\Bigg\}_{y=-h/2} dAdz
\end{aligned}
\tag{6.31}
$$

By integrating over the area of the top flange, one obtains

$$
\begin{aligned}
\bar{\bar{U}}_T = E\int_z \Big\langle & I_{yF}\left(\bar{\hat{u}}_{b,zz}\right)^2 + I_{\omega F}\left(\bar{\hat{u}}_{b,yzz}\right)^2 + I_{yF}\lambda^2\left[\theta_{xp,z}^2\bar{\hat{u}}_{b,y}^2 + \bar{\hat{u}}_{b,yz}^2\left(v_{p,z}+\theta_{xp}\right)^2 + 2\bar{\hat{u}}_{b,yz}\left(v_{p,z}+\theta_{xp}\right)\theta_{xp,z}\bar{\hat{u}}_{b,y}\right] \\
& + \frac{h^2}{16}\lambda^2 I_{yF}\left(\bar{\hat{u}}_{b,z}^2\theta_{xp,zz}^2 + \bar{\hat{u}}_{b,zzz}^2\theta_{xp}^2 - 2\theta_{xp,zz}\theta_{xp}\bar{\hat{u}}_{b,z}\bar{\hat{u}}_{b,zzz}\right) \\
& + 2\lambda I_{yF}\bar{\hat{u}}_{b,zz}\Big\{\left(\theta_{xp}+v_{p,z}\right)\bar{\hat{u}}_{b,yz} + \theta_{xp,z}\bar{\hat{u}}_{b,y} - \frac{h}{4}\left(\bar{\hat{u}}_{b,z}\theta_{xp,zz} - \bar{\hat{u}}_{b,zzz}\theta_{xp} + \bar{\hat{u}}_{b,yzz}\theta_{xp}^2\right) \\
& - \frac{1}{2}\lambda v_{p,z}\left[\left(\theta_{xp}\bar{\hat{u}}_{b,zz} + \theta_{xp,z}\bar{\hat{u}}_{b,z}\right) + h\left(\theta_{xp,z}\bar{\hat{u}}_{b,yz} + \theta_{xp}\bar{\hat{u}}_{b,yzz}\right)\right]\Big\} \\
& - \frac{h}{2}\lambda^2 I_{yF}\left[\left(\theta_{xp}+v_{p,z}\right)\bar{\hat{u}}_{b,yz} + \theta_{xp,z}\bar{\hat{u}}_{b,y}\right]\left[\bar{\hat{u}}_{b,z}\theta_{xp,zz} - \bar{\hat{u}}_{b,zzz}\theta_{xp}\right]\Big\rangle_{y=-h/2} dz \\
+ G\int_z \Big\{ & 4I_{xF}\left(\bar{\hat{u}}_{b,yz}\right)^2 + \lambda^2 A_F\left(\bar{\hat{u}}_{b,y}\right)^2\left(\theta_{xp}+v_{p,z}\right)^2 + \lambda^2\left[A_F\left(\bar{\hat{u}}_{b,z}\right)^2 + I_{xF}\left(\bar{\hat{u}}_{b,yz}\right)^2\right]w_{Tp,z}^2 \\
& + \lambda^2 I_{xF}\left[\left(\bar{\hat{u}}_{b,z}\right)^2 + \frac{3}{20}t_T^2\left(\bar{\hat{u}}_{b,yz}\right)^2\right]\theta_{xp,z}^2 + \lambda^2\frac{h^2}{4}A_F\left(\bar{\hat{u}}_{b,zz}\theta_{xp}\right)^2 \\
& + 4\lambda I_{xF}\bar{\hat{u}}_{b,yz}\left[-\bar{\hat{u}}_{b,z} - \lambda\theta_{xp}\bar{\hat{u}}_{b,y} + \lambda\frac{h}{4}\left(\bar{\hat{u}}_{b,z}\theta_{xp,z} - \bar{\hat{u}}_{b,zz}\theta_{xp}\right)\right]\theta_{xp,z} + 4\lambda I_{xF}\bar{\hat{u}}_{b,yz}^2 w_{Tp,z} \\
& - 4\lambda^2 I_{xF}\bar{\hat{u}}_{b,z}\bar{\hat{u}}_{b,yz}w_{Tp,z}\theta_{xp,z} - 2\lambda^2 A_F\bar{\hat{u}}_{b,y}\left(\theta_{xp}+v_{p,z}\right)\left[-\bar{\hat{u}}_{b,z}w_{Tp,z} + \frac{I_{xF}}{A_F}\bar{\hat{u}}_{b,yz}\theta_{xp,z} - \frac{h}{2}\bar{\hat{u}}_{b,zz}\theta_{xp}\right] \\
& - 2\lambda^2\frac{h}{2}\left[-A_F\bar{\hat{u}}_{b,z}w_{Tp,z} + I_{xF}\bar{\hat{u}}_{b,yz}\theta_{xp,z}\right]\left(\bar{\hat{u}}_{b,zz}\theta_{xp}\right)\Big\}_{y=-h/2} dz \\
+ \int_z \lambda\sigma_{zTp}\Big[& A_F\bar{\hat{u}}_{b,z}^2 + \left(I_{xF}+I_{yF}\right)\bar{\hat{u}}_{b,yz}^2 + \lambda A_F\frac{h}{2}\theta_{xp,z}\bar{\hat{u}}_{b,y}^2 + \lambda h A_F\bar{\hat{u}}_{b,yz}\bar{\hat{u}}_{b,y}\left(\theta_{xp}+v_{p,z}\right) \\
& - \lambda I_{yF}\bar{\hat{u}}_{b,yz}\left(\theta_{xp}\bar{\hat{u}}_{b,zz} + \theta_{xp,z}\bar{\hat{u}}_{b,z} - 2\bar{\hat{u}}_{b,y}\theta_{xp,z}\theta_{xp} - \bar{\hat{u}}_{b,yz}\theta_{xp}^2\right) \\
& + \frac{h^2}{16}\lambda^2\left[A_F\left(\bar{\hat{u}}_{b,zz}^2\theta_{xp}^2 + \bar{\hat{u}}_{b,z}^2\theta_{xp,z}^2 + 2\bar{\hat{u}}_{b,z}\bar{\hat{u}}_{b,zz}\theta_{xp}\theta_{xp,z}\right)\right] \\
& - \lambda\frac{h}{2}A_F\bar{\hat{u}}_{b,z}\left(\theta_{xp}\bar{\hat{u}}_{b,zz} + \theta_{xp,z}\bar{\hat{u}}_{b,z}\right) + \lambda A_F\frac{h^2}{2}\left(\theta_{xp}\theta_{xp,z}\bar{\hat{u}}_{b,y}\bar{\hat{u}}_{b,yz}\right) \\
& + \lambda^2\frac{I_{yF}}{4}\left[\left(\bar{\hat{u}}_{b,zz}^2\theta_{xp}^2 + \bar{\hat{u}}_{b,z}^2\theta_{xp,z}^2 + 2\bar{\hat{u}}_{b,zz}\bar{\hat{u}}_{b,z}\theta_{xp}\theta_{xp,z}\right) + h^2\left(\theta_{xp}^2\bar{\hat{u}}_{b,yzz}^2 + \theta_{xp,z}^2\bar{\hat{u}}_{b,yz}^2 + 2\bar{\hat{u}}_{b,yz}\bar{\hat{u}}_{b,yzz}\theta_{xp}\theta_{xp,z}\right)\right] \\
& - 2\frac{h}{4}A_F\lambda^2 v_{p,z}\left[\left(\bar{\hat{u}}_{b,zz}\theta_{xp}\bar{\hat{u}}_{b,y} + \bar{\hat{u}}_{b,z}\theta_{xp,z}\bar{\hat{u}}_{b,y} + \bar{\hat{u}}_{b,z}\theta_{xp}\bar{\hat{u}}_{b,yz}\right)\right] \\
& - 2\lambda I_{yF}\bar{\hat{u}}_{b,yz}\Big[\frac{1}{2}\left(\bar{\hat{u}}_{b,zz}\theta_{xp} + \theta_{xp,z}\bar{\hat{u}}_{b,z} + 2\bar{\hat{u}}_{b,y}\theta_{xp,z}\theta_{xp} + \bar{\hat{u}}_{b,yz}\theta_{xp}^2\right) \\
& \qquad + \frac{h}{4}\theta_{xp,z}\left(2\bar{\hat{u}}_{b,yz} + \bar{\hat{u}}_{b,zz}\theta_{xp} - \bar{\hat{u}}_{b,z}\theta_{xp,z}\right) + \frac{h}{4}\theta_{xp}\left(2\bar{\hat{u}}_{b,yzz} - \bar{\hat{u}}_{b,z}\theta_{xp,zz} + \bar{\hat{u}}_{b,zzz}\theta_{xp}\right)\Big] \\
& - \lambda^2 I_{yF}\frac{h}{2}\left(-\theta_{xp,z}\bar{\hat{u}}_{b,yz}\bar{\hat{u}}_{b,zz}\theta_{xp} - \theta_{xp,z}^2\bar{\hat{u}}_{b,yz}\bar{\hat{u}}_{b,z} - \theta_{xp}^2\bar{\hat{u}}_{b,yzz}\bar{\hat{u}}_{b,zz} - \theta_{xp}\bar{\hat{u}}_{b,yzz}\theta_{xp,z}\bar{\hat{u}}_{b,z}\right)\Big\}_{y=-h/2} dz
\end{aligned}
$$

(6.32)

where $\left(A_F, I_{xF}, I_{yF}, I_{\omega F}\right) = \int\limits_{A_F} \left(1, n_T^2, x_T^2, n_T^2 x_T^2\right) dA_F = \left(bt, bt^3/12, b^3t/12, b^3t^3/144\right)$.

Similar expressions are obtained for the bottom flange by replacing subscripts T by B and by setting $y = h/2$ instead of $y = -h/2$. One obtains

$$
\begin{aligned}
\bar{\bar{U}}_B = E\int_z \Big\langle & I_{yF}\left(\bar{\hat{u}}_{b,zz}\right)^2 + I_{\omega F}\left(\bar{\hat{u}}_{b,yzz}\right)^2 + I_{yF}\lambda^2\left[\theta_{xp,z}^2\bar{\hat{u}}_{b,y}^2 + \bar{\hat{u}}_{b,yz}^2\left(v_{p,z}+\theta_{xp}\right)^2 + 2\bar{\hat{u}}_{b,yz}\left(v_{p,z}+\theta_{xp}\right)\theta_{xp,z}\bar{\hat{u}}_{b,y}\right] \\
& + \frac{h^2}{16}\lambda^2 I_{yF}\left(\bar{\hat{u}}_{b,z}^2\theta_{xp,zz}^2 + \bar{\hat{u}}_{b,zzz}^2\theta_{xp}^2 - 2\theta_{xp,zz}\theta_{xp}\bar{\hat{u}}_{b,z}\bar{\hat{u}}_{b,zzz}\right) \\
& + 2\lambda I_{yF}\bar{\hat{u}}_{b,zz}\Big\{\left(\theta_{xp}+v_{p,z}\right)\bar{\hat{u}}_{b,yz} + \theta_{xp,z}\bar{\hat{u}}_{b,y} + \frac{h}{4}\left(\bar{\hat{u}}_{b,z}\theta_{xp,zz} - \bar{\hat{u}}_{b,zzz}\theta_{xp} + \bar{\hat{u}}_{b,yzz}\theta_{xp}^2\right) \\
& - \frac{1}{2}\lambda v_{p,z}\left[\left(\theta_{xp}\bar{\hat{u}}_{b,zz} + \theta_{xp,z}\bar{\hat{u}}_{b,z}\right) - h\left(\theta_{xp,z}\bar{\hat{u}}_{b,yz} + \theta_{xp}\bar{\hat{u}}_{b,yzz}\right)\right]\Big\} \\
& - \frac{h}{2}\lambda^2 I_{yF}\left[\left(\theta_{xp}+v_{p,z}\right)\bar{\hat{u}}_{b,yz} + \theta_{xp,z}\bar{\hat{u}}_{b,y}\right]\left[\bar{\hat{u}}_{b,z}\theta_{xp,zz} - \bar{\hat{u}}_{b,zzz}\theta_{xp}\right]\Big\rangle_{y=h/2} dz \\
+ G\int_z \Big\{ & 4I_{xF}\left(\bar{\hat{u}}_{b,yz}\right)^2 + \lambda^2 A_F\left(\bar{\hat{u}}_{b,y}\right)^2\left(\theta_{xp}+v_{p,z}\right)^2 + \lambda^2\left[A_F\left(\bar{\hat{u}}_{b,z}\right)^2 + I_{xF}\left(\bar{\hat{u}}_{b,yz}\right)^2\right]w_{Bp,z}^2 \\
& + \lambda^2 I_{xF}\left[\left(\bar{\hat{u}}_{b,z}\right)^2 + \frac{3}{20}t_T^2\left(\bar{\hat{u}}_{b,yz}\right)^2\right]\theta_{xp,z}^2 + \lambda^2\frac{h^2}{4}A_F\left(\bar{\hat{u}}_{b,zz}\theta_{xp}\right)^2 \\
& + 4\lambda I_{xF}\bar{\hat{u}}_{b,yz}\left[-\bar{\hat{u}}_{b,z} - \lambda\theta_{xp}\bar{\hat{u}}_{b,y} - \lambda\frac{h}{4}\left(\bar{\hat{u}}_{b,z}\theta_{xp,z} - \bar{\hat{u}}_{b,zz}\theta_{xp}\right)\right]\theta_{xp,z} \\
& - 2\lambda^2 A_F\bar{\hat{u}}_{b,y}\left(\theta_{xp}+v_{p,z}\right)\left[-\bar{\hat{u}}_{b,z}w_{Bp,z} + \frac{I_{xF}}{A_F}\bar{\hat{u}}_{b,yz}\theta_{xp,z} + \frac{h}{2}\bar{\hat{u}}_{b,zz}\theta_{xp}\right] + 4\lambda I_{xF}\bar{\hat{u}}_{b,yz}^2 w_{Bp,z} \\
& + 2\lambda^2\frac{h}{2}\left[-A_F\bar{\hat{u}}_{b,z}w_{Bp,z} + I_{xF}\bar{\hat{u}}_{b,yz}\theta_{xp,z}\right]\left(\bar{\hat{u}}_{b,zz}\theta_{xp}\right) - 4\lambda^2 I_{xF}\bar{\hat{u}}_{b,z}\bar{\hat{u}}_{b,yz}w_{Bp,z}\theta_{xp,z}\Big\}_{y=h/2} dz \\
+ \int_z \lambda\sigma_{zBp}\Big[& A_F\bar{\hat{u}}_{b,z}^2 + \left(I_{xF}+I_{yF}\right)\bar{\hat{u}}_{b,yz}^2 - \lambda A_F\frac{h}{2}\theta_{xp,z}\bar{\hat{u}}_{b,y}^2 - \lambda h A_F\bar{\hat{u}}_{b,yz}\bar{\hat{u}}_{b,y}\left(\theta_{xp}+v_{p,z}\right) \\
& - \lambda I_{yF}\bar{\hat{u}}_{b,yz}\left(\theta_{xp}\bar{\hat{u}}_{b,zz} + \theta_{xp,z}\bar{\hat{u}}_{b,z} - 2\bar{\hat{u}}_{b,y}\theta_{xp,z}\theta_{xp} - \bar{\hat{u}}_{b,yz}\theta_{xp}^2\right) \\
& + \frac{h^2}{16}\lambda^2\left[A_F\left(\bar{\hat{u}}_{b,zz}^2\theta_{xp}^2 + \bar{\hat{u}}_{b,z}^2\theta_{xp,z}^2 + 2\bar{\hat{u}}_{b,z}\bar{\hat{u}}_{b,zz}\theta_{xp}\theta_{xp,z}\right)\right] \\
& + \lambda\frac{h}{2}A_F\bar{\hat{u}}_{b,z}\left(\theta_{xp}\bar{\hat{u}}_{b,zz} + \theta_{xp,z}\bar{\hat{u}}_{b,z}\right) + \lambda A_F\frac{h^2}{2}\left(\theta_{xp}\theta_{xp,z}\bar{\hat{u}}_{b,y}\bar{\hat{u}}_{b,yz}\right) \\
& + \lambda^2\frac{I_{yF}}{4}\left[\left(\bar{\hat{u}}_{b,zz}^2\theta_{xp}^2 + \bar{\hat{u}}_{b,z}^2\theta_{xp,z}^2 + 2\bar{\hat{u}}_{b,zz}\bar{\hat{u}}_{b,z}\theta_{xp}\theta_{xp,z}\right) + h^2\left(\theta_{xp}^2\bar{\hat{u}}_{b,yzz}^2 + \theta_{xp,z}^2\bar{\hat{u}}_{b,yz}^2 + 2\bar{\hat{u}}_{b,yz}\bar{\hat{u}}_{b,yzz}\theta_{xp}\theta_{xp,z}\right)\right] \\
& + 2\frac{h}{4}A_F\lambda^2 v_{p,z}\left[\left(\bar{\hat{u}}_{b,zz}\theta_{xp}\bar{\hat{u}}_{b,y} + \bar{\hat{u}}_{b,z}\theta_{xp,z}\bar{\hat{u}}_{b,y} + \bar{\hat{u}}_{b,z}\theta_{xp}\bar{\hat{u}}_{b,yz}\right)\right] \\
& - 2\lambda I_{yF}\bar{\hat{u}}_{b,yz}\Big[\frac{1}{2}\left(\bar{\hat{u}}_{b,zz}\theta_{xp} + \theta_{xp,z}\bar{\hat{u}}_{b,z} + 2\bar{\hat{u}}_{b,y}\theta_{xp,z}\theta_{xp} + \bar{\hat{u}}_{b,yz}\theta_{xp}^2\right) \\
& \qquad - \frac{h}{4}\theta_{xp,z}\left(2\bar{\hat{u}}_{b,yz} + \bar{\hat{u}}_{b,zz}\theta_{xp} - \bar{\hat{u}}_{b,z}\theta_{xp,z}\right) - \frac{h}{4}\theta_{xp}\left(2\bar{\hat{u}}_{b,yzz} - \bar{\hat{u}}_{b,z}\theta_{xp,zz} + \bar{\hat{u}}_{b,zzz}\theta_{xp}\right)\Big] \\
& + \lambda^2 I_{yF}\frac{h}{2}\left(-\theta_{xp,z}\bar{\hat{u}}_{b,yz}\bar{\hat{u}}_{b,zz}\theta_{xp} - \theta_{xp,z}^2\bar{\hat{u}}_{b,yz}\bar{\hat{u}}_{b,z} - \theta_{xp}^2\bar{\hat{u}}_{b,yzz}\bar{\hat{u}}_{b,zz} - \theta_{xp}\bar{\hat{u}}_{b,yzz}\theta_{xp,z}\bar{\hat{u}}_{b,z}\right)\Big\}_{y=h/2} dz
\end{aligned}
$$

(6.33)

6.6.2. **Load potential energy**

The second variation of load potential energy $\bar{\bar{V}}$ consists of the contribution $\bar{\bar{V}}_T$ of the transverse loads and that of the axial loads $\bar{\bar{V}}_A$. While load potential energy V_A of the axial loads does not vanish and thus contributes to the pre-buckling analysis, its second variation $\bar{\bar{V}}_A$ vanishes. i.e. $\bar{\bar{V}}_A = 0$ and $\bar{\bar{V}} = \bar{\bar{V}}_T$. As the beam buckles, the vertical distance $\Delta_b(z)$ travelled by the transverse distributed load $\lambda q_y\left(y_{qy}(z), z\right)$ acting at $y_{qy}(z)$ is given by

$$\Delta_b(z) = \int_0^{y_{q_y}} \frac{1}{2}\hat{u}_{b,y}^2 dy \tag{6.34}$$

Hence, the second variation of the load potential energy in terms of buckling displacement $\bar{\hat{u}}_b(y,z)$ is

$$\bar{\bar{V}} = \int_0^{z=L} q_y(z)\Delta_b(z)dz = \int_0^{z=L} q_y(z)\left(\int_0^{y_{q_y}} \bar{\hat{u}}_{b,y}^2 dy\right)dz \tag{6.35}$$

6.7. **Finite element formulation**

6.7.1. **Interpolation scheme**

In line with past studies (e.g. (Bradford and Trahair (1982); Hancock et al. (1980)), Bradford (1985), Bradford (1992b), (Pezeshky and Mohareb 2014), (Pezeshky and Mohareb 2015)) the lateral displacement $\hat{u}_b(y,z)$ of the web middle surface can be assumed to follow a cubic Hermitian distribution along coordinate y . Along coordinate z , a cubic Hermitian distribution would also be enough express the internal strain energy of the web since no derivative orders higher than 2 appear in Eq.(6.26).

Unlike the web, third order derivatives with respect to coordinate z for displacement fields $\left(u_{b,zzz}\right)_{y=h/2}, \left(u_{b,zzz}\right)_{y=-h/2}$ of the flanges appear in Eq.(6.32)-(6.33), thus requiring C2 continuity, i.e., the displacement fields $\left(u_{b,zzz}\right)_{y=h/2}, \left(u_{b,zzz}\right)_{y=-h/2}$ need to be interpolated using quintic Hermitian polynomials in coordinate z .

However, if compatibility is to be enforced between the lateral displacement $\hat{u}_b\left(y,z\right)_{y=\pm h/2}$ at the web top and bottom, and the corresponding lateral displacement fields of the flanges $u_T\left(z\right)$, $\hat{u}_B\left(z\right)$, displacement $\hat{u}_b\left(y,z\right)_{y=\pm h/2}$ needs to follow a quintic distribution along the z coordinate. Hence, the displacement field $\hat{u}_b\left(y,z\right)$ will be interpolated using quintic Hermitian polynomial functions in coordinate z while being interpolated using cubic Hermitian polynomial functions in coordinate y .

A finite element is thus developed with two end nodes (Fig. 6-5). Each end has 10 buckling degrees of freedom (DOFs) at each end. At each node, five of the 10 degrees of freedom characterize the displacements of the top flange. These are $u_T, u'_T, u''_T, \theta_T, \theta'_T$ which respectively denote the lateral displacement, its first derivative, its second derivative, angle of twist, and its first derivate for the top flange and the remaining five degrees of freedom $u_B, u'_B, u''_B, \theta_B, \theta'_B$ characterize similar displacements for the bottom flange.

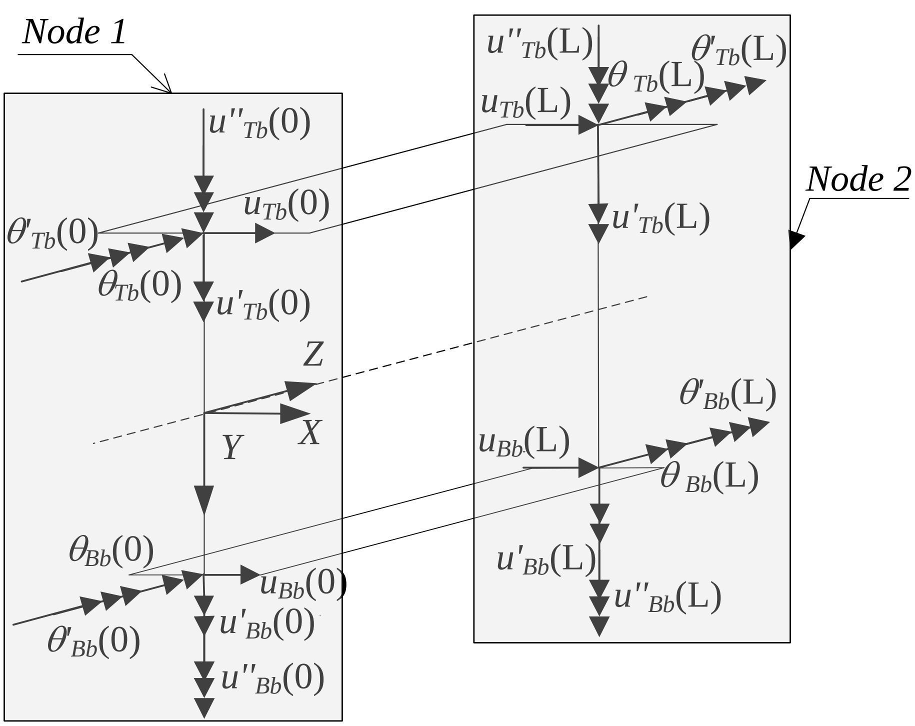

Fig. 6-5 Distortional buckling finite element with 20 DOFs

The lateral displacement $\hat{u}_b\left(y,z\right)$ of a generic point on the web middle surface is expressed in terms of the nodal displacements through

$$\hat{u}_b\left(y,z\right)=\mathbf{M}^{\mathbf{T}}_{\mathbf{1\times 20}}\left(y,\mathrm{z}\right)\hat{\mathbf{u}}_{\mathbf{b(20\times 1)}} \tag{6.36}$$

where $\mathbf{M}^{\mathbf{T}}_{\mathbf{1\times 20}}\left(y,\mathrm{z}\right)=\left\langle H_1\left(y\right)\mathbf{Q}^{\mathbf{T}}\left(z\right) \;\vdots\; H_2\left(y\right)\mathbf{N}^{\mathbf{T}}\left(z\right) \;\vdots\; H_3\left(y\right)\mathbf{Q}^{\mathbf{T}}\left(z\right) \;\vdots\; H_4\left(y\right)\mathbf{N}^{\mathbf{T}}\left(z\right)\right\rangle_{\mathbf{1}\times 20}$ is a vector of shape functions resulting from the product of cubic Hermitian functions $H_1\left(y\right)-H_4\left(y\right)$, $\mathbf{N}\left(\mathrm{z}\right)$ and the quintic shape functions $\mathbf{Q}\left(z\right)$, given by

$$H_1\left(y\right)=\frac{1}{2}-\frac{3}{2}Y+2Y^3, \qquad H_2\left(y\right)=h\left(\frac{1}{8}-\frac{1}{4}Y-\frac{1}{2}Y^2+Y^3\right)$$

$$H_3\left(y\right)=\frac{1}{2}+\frac{3}{2}Y-2Y^3, \qquad H_4\left(y\right)=-h\left(\frac{1}{8}+\frac{1}{4}Y-\frac{1}{2}Y^2-Y^3\right)$$

$$\mathbf{N}^{\mathbf{T}}_{\mathbf{1\times 4}}\left(z\right)=\left\langle 1-3Z^2+2Z^3 \quad z\left(1-Z\right)^2 \quad 3Z^2-2Z^3 \quad L\left(-Z^2+Z^3\right)\right\rangle$$

$$\mathbf{Q}^{\mathbf{T}}_{\mathbf{1\times 6}}\left(z\right)=\Big\langle 1-10Z^3+15Z^4-6Z^5 \quad L\left(Z-6Z^3+8Z^4-3Z^5\right) \quad \frac{L^2}{2}\left(Z^2-3Z^3+3Z^4-Z^5\right)$$
$$10Z^3-15Z^4+6Z^5 \quad L\left(-4Z^3+7Z^4-3Z^5\right) \quad \frac{L^2}{2}\left(3Z^3-2Z^4+Z^5\right)\Big\rangle$$

where the notation $Y=y/h$ and $Z=z/L$ has been introduced. In Eq.(6.36), $\hat{\mathbf{u}}^{\mathbf{T}}_{\mathbf{b(1\times 20)}}=\left\langle\hat{\mathbf{u}}^{\mathbf{T}}_{\mathbf{Tb}} \quad \hat{\boldsymbol{\theta}}^{\mathbf{T}}_{\mathbf{Tb}} \quad \hat{\mathbf{u}}^{\mathbf{T}}_{\mathbf{Bb}} \quad \hat{\boldsymbol{\theta}}^{\mathbf{T}}_{\mathbf{Bb}}\right\rangle$, is the vector of nodal displacements and $\hat{\mathbf{u}}^{\mathbf{T}}_{\mathbf{Tb}},\hat{\boldsymbol{\theta}}^{\mathbf{T}}_{\mathbf{Tb}},\hat{\mathbf{u}}^{\mathbf{T}}_{\mathbf{Bb}}$, $\hat{\boldsymbol{\theta}}^{\mathbf{T}}_{\mathbf{Bb}}$ are nodal displacement vectors defined by

$$\hat{\mathbf{u}}^{\mathbf{T}}_{\mathbf{Tb}}=\left\langle u_{Tb}\left(0\right) \quad u'_{Tb}\left(0\right) \quad u''_{Tb}\left(0\right) \quad u_{Tb}\left(L\right) \quad u'_{Tb}\left(L\right) \quad u''_{Tb}\left(L\right)\right\rangle ,$$
$$\hat{\boldsymbol{\theta}}^{\mathbf{T}}_{\mathbf{T}}=\left\langle \theta_{Tb}\left(0\right) \quad \theta'_{Tb}\left(0\right) \quad \theta_{Tb}\left(L\right) \quad \theta'_{Tb}\left(L\right)\right\rangle$$
$$\hat{\mathbf{u}}^{\mathbf{T}}_{\mathbf{B}}=\left\langle u_{Bb}\left(0\right) \quad u'_{Bb}\left(0\right) \quad u''_{Bb}\left(0\right) \quad u_{Bb}\left(L\right) \quad u'_{Bb}\left(L\right) \quad u''_{Bb}\left(L\right)\right\rangle ,$$
$$\hat{\boldsymbol{\theta}}^{\mathbf{T}}_{\mathbf{B}}=\left\langle \theta_{Bb}\left(0\right) \quad \theta'_{Bb}\left(0\right) \quad \theta_{Bb}\left(L\right) \quad \theta'_{Bb}\left(L\right)\right\rangle$$

6.7.2. Second variation of Internal Strain energy

From the pre-buckling stress internal force relations (Eqs. (6.4)-(6.8)), the buckling shape functions defined in Eq. (6.36), by substituting into Eq.(6.26), one can rewrite the second variation of internal strain energy of the web as

$$\bar{\bar{U}}_W = \bar{\hat{\mathbf{u}}}^{\mathbf{T}}_{\mathbf{b}(1\times 20)} \left(\mathbf{K}_{\mathbf{EW}} + \lambda \mathbf{K}_{\mathbf{G1W}} + \lambda^2 \mathbf{K}_{\mathbf{G2W}}\right)_{\mathbf{20\times 20}} \bar{\hat{\mathbf{u}}}_{\mathbf{b}(20\times 1)} \tag{6.37}$$

where $\mathbf{K}_{\mathbf{EW}}$ is the elastic stiffness matrix, $\mathbf{K}_{\mathbf{G1W}}$ is the first order geometric stiffness matrix and $\mathbf{K}_{\mathbf{G2W}}$ is the second order geometric matrix, all defined in Appendix A. Also, from Eqs. (6.4), (6.6) ,(6.8) and (6.36) by substituting into Eq. (6.32) and integrating with respect to volume, one obtains the second variation of the strain energy for the top flange as

$$\bar{\bar{U}}_T = \bar{\hat{\mathbf{u}}}^{\mathbf{T}}_{\mathbf{b}(1\times 20)} \left(\mathbf{K}_{\mathbf{ET}} + \lambda \mathbf{K}_{\mathbf{G1T}} + \lambda^2 \mathbf{K}_{\mathbf{G2T}} + \lambda^3 \mathbf{K}_{\mathbf{G3T}}\right)_{\mathbf{20\times 20}} \bar{\hat{\mathbf{u}}}_{\mathbf{b}(20\times 1)} \tag{6.38}$$

where matrices $\mathbf{K}_{\mathbf{ET}}, \mathbf{K}_{\mathbf{G1T}}, \mathbf{K}_{\mathbf{G2T}}$ and $\mathbf{K}_{\mathbf{G3T}}$ are the elastic, first order, second order, and third order geometric matrices for the top flange, as defined in Appendix B. In a similar manner, one obtains the second variation of the internal strain energy of the bottom flange as

$$\bar{\bar{U}}_B = \bar{\hat{\mathbf{u}}}^{\mathbf{T}}_{\mathbf{b}(1\times 20)} \left(\mathbf{K}_{\mathbf{EB}} + \lambda \mathbf{K}_{\mathbf{G1B}} + \lambda^2 \mathbf{K}_{\mathbf{G2B}} + \lambda^3 \mathbf{K}_{\mathbf{G3B}}\right)_{\mathbf{20\times 20}} \bar{\hat{\mathbf{u}}}_{\mathbf{b}(20\times 1)} \tag{6.39}$$

where matrices $\mathbf{K}_{\mathbf{EB}}, \mathbf{K}_{\mathbf{G1B}}, \mathbf{K}_{\mathbf{G2B}}$ and $\mathbf{K}_{\mathbf{G3B}}$ are provided in Appendix B.

6.7.2.1. Second variation of load potential

From Eq. (6.36) by substituting into Eq.(6.35) one obtains the variation of the second variation of the load potential in terms of the nodal displacements, i.e.

$$\bar{\bar{V}} = \bar{\hat{\mathbf{u}}}^{\mathbf{T}}_{\mathbf{b}} \mathbf{K}_{\mathbf{V}} \bar{\hat{\mathbf{u}}}_{\mathbf{b}} \tag{6.40}$$

where

$$\mathbf{K}_{\mathbf{V}} = \int_0^L q_y(z) \int_0^{y_{q_y}} \left[\mathbf{M}_{,y}(y,z)\mathbf{M}^{\mathbf{T}}_{,y}(y,z) + \mathbf{M}_{,y}(-h/2,z)\mathbf{M}^{\mathbf{T}}_{,y}(-h/2,z) + \mathbf{M}_{,y}(h/2,z)\mathbf{M}^{\mathbf{T}}_{,y}(h/2,z)\right] dydz \tag{6.41}$$

6.8. Kinematic constraints to supress distortion at a beam end

From Eqs. (6.37)-(6.40) one recovers the second variation of total potential energy $\bar{\bar{\Pi}}$, i.e.

$$\bar{\bar{\Pi}} = \bar{\hat{\mathbf{u}}}^{\mathbf{T}}_{\mathbf{b}} \mathbf{K}_{\mathbf{T}}(\lambda) \hat{\mathbf{u}}_{\mathbf{b}} \tag{6.42}$$

where $\mathbf{K_T}(\lambda) = \left(\mathbf{K_E} + \lambda\left(\mathbf{K_V} + \mathbf{K_{G1}}\right) + \lambda^2\mathbf{K_{G2}} + \lambda^3\mathbf{K_{G3}}\right)$. In order to capture the effect of the stiffeners on web distortion at end i (Fig. 6-6b), one needs to enforce the following kinematic constraints (e.g., Ma and Hughes (1996b) Chen and Ye (2010)).

$$\begin{aligned} &\theta_{Ti} - \theta_{Bi} = 0, && \theta'_{Ti} - \theta'_{Bi} = 0 \\ &\theta_{Ti} = \frac{u'_{Ti} - u'_{Bi}}{h}, && \theta'_{Ti} = \frac{u'_{Ti} - u'_{Bi}}{h} \end{aligned} \tag{6.43}$$

In a matrix form, one has

$$\hat{\mathbf{u}}_{\mathbf{b}i(\mathbf{10\times1})} = \mathbf{C_{10\times6}}\underset{\sim}{\hat{\mathbf{u}}}_{\mathbf{b}i(\mathbf{6\times1})} \tag{6.44}$$

where $\hat{\mathbf{u}}_{\mathbf{bi(10\times1)}} = \left\langle u_{Ti} \quad u'_{Ti} \quad u''_{Ti} \quad \theta_{Ti} \quad \theta'_{Ti} \quad u_{Bi} \quad u'_{Bi} \quad u''_{Bi} \quad \theta_{Bi} \quad \theta'_{Bi} \right\rangle_{10\times1}^{T}$ is the vector of nodal displacements at node i of the structure, $\underset{\sim}{\hat{\mathbf{u}}}_{\mathbf{b}i(\mathbf{6\times1})} = \left\langle u_{Ti} \quad u'_{Ti} \quad u''_{Ti} \quad u_{Bi} \quad u'_{Bi} \quad u''_{Bi} \right\rangle_{6\times1}^{T}$ is the reduced vector of nodal displacements after eliminating the redundant degrees of freedom through the kinematic constraints, and matrix $\mathbf{C}$ is defined as

$$\mathbf{C_{6\times10}^{T}} = \left[\begin{array}{ccc|cc|ccc|cc} 1 & & & 1/h & & & & & 1/h & \\ & 1 & & & 1/h & & & & & 1/h \\ & & 1 & & & & & & & \\ \hline & & & -1/h & & 1 & & & -1/h & \\ & & & & -1/h & & 1 & & & -1/h \\ & & & & & & & 1 & & \end{array}\right]_{6\times10}$$

The structure stiffness matrix $\mathbf{K_T}(\lambda)$ is modified to account for the kinematic relations defined in Eq. (6.44) according to the procedure presented in Appendix C, yielding

$$\bar{\bar{\Pi}} = \bar{\underset{\sim}{\hat{\mathbf{u}}}}_{\mathbf{b}}^{\mathbf{T}} \underset{\sim}{\mathbf{K}}_{\mathbf{T}}(\lambda) \bar{\underset{\sim}{\hat{\mathbf{u}}}}_{\mathbf{b}}$$

For the case of multiple stiffeners, the procedure is repeated at each section with a stiffer. In the case of non-distortional analysis, stiffener constraints are applied at all nodes.

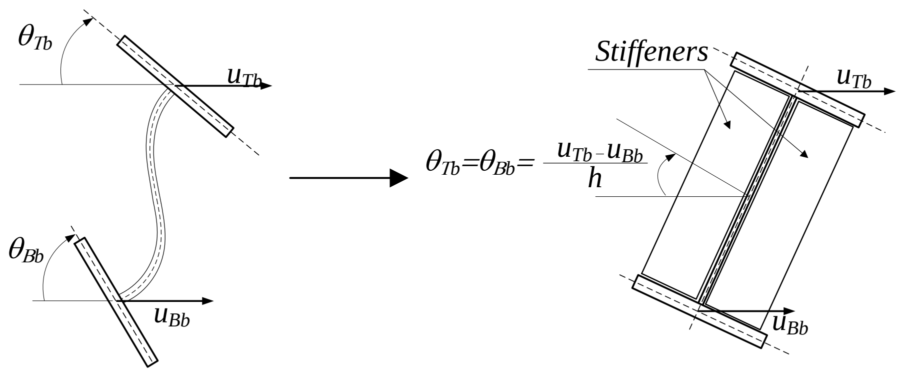

Fig. 6-6 a) Distortional element without stiffeners, b) distortional element with stiffeners

6.9. Condition of neutral stability

The condition of neutral stability is obtained by setting to zero the variation of second variation of total potential energy, i.e.

$$\delta\left(\frac{1}{2}\bar{\bar{\Pi}}\right)=\delta\left[\frac{1}{2}\left(\bar{\bar{U}}+\bar{\bar{V}}\right)\right]=\delta\frac{1}{2}\left(\bar{\bar{U}}_W+\bar{\bar{U}}_T+\bar{\bar{U}}_B+\bar{\bar{V}}\right)=0 \tag{6.45}$$

In a matrix form, one has

$$\delta\left(\frac{1}{2}\bar{\bar{\Pi}}\right)=\delta\bar{\hat{\mathbf{u}}}_{\mathbf{b}}^{\mathbf{T}}\left(\mathbf{K}_{\mathbf{E}}+\lambda\left(\mathbf{K}_{\mathbf{V}}+\mathbf{K}_{\mathbf{G}1}\right)+\lambda^2\mathbf{K}_{\mathbf{G}2}+\lambda^3\mathbf{K}_{\mathbf{G}3}\right)\hat{\mathbf{u}}_{\mathbf{b}}=\mathbf{0} \tag{6.46}$$

where the entries of the matrices $\mathbf{K_E},\mathbf{K_{G1}},\mathbf{K_{G2}},\mathbf{K_{G3}}$ are obtained from the entries of the web matrices $\mathbf{K_{EW}},\mathbf{K_{G1W}},\mathbf{K_{G2W}}$, the top flange matrices $\mathbf{K_{ET}},\mathbf{K_{G1T}},\mathbf{K_{G2T}},\mathbf{K_{G3T}}$, and the bottom flange matrices $\mathbf{K_{EB}},\mathbf{K_{G1B}},\mathbf{K_{G2B}},\mathbf{K_{G3B}}$ using the conventional assembly process.

The cubic eigen-value in equation (6.46) can be transformed to the equivalent first order right-eigenvalue problem i.e.,

$$\left(\begin{bmatrix}\mathbf{K}_{\mathbf{G}2} & \mathbf{K_{G1}}+\mathbf{K_V} & \mathbf{K_E}\\ -\mathbf{I_{20}} & \mathbf{0} & \mathbf{0}\\ & -\mathbf{I_{20}} & \mathbf{0}\end{bmatrix}+\lambda\begin{bmatrix}\mathbf{K}_{\mathbf{G}3} & \mathbf{0} & \mathbf{0}\\ & \mathbf{I_{20}} & \mathbf{0}\\ & & \mathbf{I_{20}}\end{bmatrix}\right)\begin{Bmatrix}\lambda^2\hat{\mathbf{u}}_{\mathbf{b}}\\ \lambda\hat{\mathbf{u}}_{\mathbf{b}}\\ \hat{\mathbf{u}}_{\mathbf{b}}\end{Bmatrix}=\mathbf{0}$$

where $\mathbf{I_{20}}$ is the 20×20 identity matrix.

6.10. **Types of analysis:**

6.10.1. **Pre-buckling analysis**

Throughout pre-buckling analysis, two types of solutions are possible. The first type is a linear pre-buckling analysis where the interaction effects between axial forces and strong axis bending moments are assumed negligible, or non-existent for beams with no axial forces. Such an analysis is linear. When adopted for beam columns, it will be denoted by the designation "L". When adopted for beams, it will carry no designation. In such an analysis, the corresponding critical load factor is obtained by a single-step eigen-value analysis. The second type of analysis accounts for the interaction between axial forces and strong axis bending in beam columns (or $P-\delta$ effects) by evoking the non-linear geometric analysis option. This type of analysis will be denoted by "NL". In nonlinear analysis, the response is traced incrementally. After convergence is achieved for a given increment, an eigenvalue check is then performed to detect whether a bifurcation point has been reached on the equilibrium path. Three possibilities exist: a) If $\lambda < 1$ the beam is deemed to have buckled under existing load and the reference load needs to be scaled back and a smaller load increment applied. b) If $\lambda > 1$ the beam is assumed to remain in stable equilibrium and load factor is incrementally increased, or c) If $\lambda = 1$ within a specified tolerance, the beam is deemed to have attained the sought point of buckling onset.

6.10.2. **Buckling analysis**

In the most general case, the present finite element solution captures the PBD, distortional effects and pre-buckling shear deformation effects. When all three effects are accounted for, the resulting critical moment is denoted as $M_{(D+P+S)}$. It is possible to omit pre-buckling shear deformation effects in the pre-buckling analysis by replacing the Timoshenko beam solution with the Euler Bernoulli beam formulation. The resulting critical moments will be denoted as $M_{(D+P)}$. In addition, it is also possible to suppress PBD effects by omitting the contributions of the pre-buckling geometric matrices $\mathbf{k}_{\mathbf{pg1}}$ - $\mathbf{k}_{\mathbf{pg14}}$, $\mathbf{k}_{\mathbf{PG1}}$ - $\mathbf{k}_{\mathbf{PG57}}$, $\mathbf{k}_{\mathbf{3PG1}}$ - $\mathbf{k}_{\mathbf{3PG16}}$ defined in Appendices A-B. The corresponding critical moment will be denoted as $M_{(D)}$. It is noted that shear deformation effects appear only in the pre-buckling geometric Matrices $\mathbf{k}_{\mathbf{pg1}}$ - $\mathbf{k}_{\mathbf{pg14}}$, $\mathbf{k}_{\mathbf{PG1}}$ - $\mathbf{k}_{\mathbf{PG57}}$, $\mathbf{k}_{\mathbf{3PG1}}$ - $\mathbf{k}_{\mathbf{3PG16}}$ defined in Appendices A-B. As such, irrespective of whether the pre-buckling analysis is based on a Timoshenko beam or the Euler beam, the resulting critical moment remains identical, i.e., $M_{(D)} = M_{(D+S)}$.

Conventional buckling solutions based on the finite element in Barsoum and Gallagher (1970) will be subsequently referred to as the BG element. The element is based on the thin-walled beam theory of Vlasov (1961) which omits distortion and shear deformation. The element has two nodes with four buckling DOFs per node capturing warping deformation while neglecting distortional effect, PBD effect and shear deformations within the plane of the web. A BG-type solution can be recovered from the present analysis by applying the following modifications to the present formulation:

a) supressing distortional effects by enforcing kinematic constraints described in Section 6.8 at both ends of the element

b) supressing the PBD effect by omitting the contributions of the pre-buckling geometric matrices $\mathbf{k_{pg1}}$ - $\mathbf{k_{pg14}}$, $\mathbf{k_{PG1}}$ - $\mathbf{k_{PG57}}$, $\mathbf{k_{3PG1}}$ - $\mathbf{k_{3PG16}}$ in Appendices A-B.

c) supressing shear deformation effects within the plane of the web by replacing the Timoshenko beam formulation adopted in the pre-buckling analysis by the non-shear deformable Euler-Bernoulli beam as discussed under Section 6.4.3.1.The critical moment obtained by supressing effects (a-c) will be denoted as $M_{(ND)}$. This moment is analogous to that based on the classical solution and will subsequently referenced as “classical solution”.

Under the present formulation, it is also possible to supress the effect of distortion while retaining pre-buckling and shear deformation effects, leading to a critical moment $M_{(ND+P+S)}$. Also, when shear deformation and distortional effects are supressed, the resulting critical moment will be referenced as $M_{(ND+P)}$. The above six types of solutions for a beam and the associated notation are summarized in Table 6-1. For a beam column, similar types of designation are adopted. In addition, to identify the two possible types of pre-buckling analysis, a subscript L is added to denote a linear pre-buckling analysis or NL to denote a nonlinear pre-buckling analysis.

Table 6-1Types of analysis for beam analysis

Type of analysis	Effects captured		
Designation	**Distortion**	**Pre-buckling**	**Shear deformation**
$M_{(ND)}$ **(classical)**	✗	✗	✗
$M_{(ND+P)}$	✗	✓	✗
$M_{(ND+P+S)}$	✗	✓	✓
$M_{(D)}$	✓	✗	✗
$M_{(D+P)}$	✓	✓	✗
$M_{(D+P+S)}$	✓	✓	✓

Three dimensional FEA models (Abaqus, SIMULIA (2011a)) will be conducted for verification using the S4R elements, which is a four-node element with six degrees of freedom per node of which five are independent. The element adopts reduced integration to avoid shear locking. The shell FEA is able to capture shear deformation and distortional effects. However, PBD effects are typically omitted commercial programs including Abaqus. The distortional critical moment obtained from Shell FEA is denoted as M_{FEA}.

To provide a benchmark solution to assess the validity of the present solution that incorporates PBD effects, an iterative procedure has been devised under Abaqus model to account for PBD effects, as outlined by the following steps:

1) A linearized eigen-value buckling shell analysis is conducted to obtain a critical load. Such a solution omits the pre-buckling deformation effect.

2) In order to obtain the pre-buckling transverse deflected shape of the beam, a static analysis is then conducted under the critical load obtained in Step 1.

3) A new shell analysis model is created for the curved beam configuration obtained in Step (2) and a new eigen-value linearized buckling analysis is conducted for curved beam configuration. The buckling load for the curved configuration thus obtained is higher than that based on the straight configuration obtained in Step (1).

4) Step (2) is repeated to determine the pre-buckling transverse deflected shape corresponding to the load predicted in Step (3).

5) Steps (3) and (4) are repreated until the critical load predicted in step (3) stabilizes within a specified tolerance. The distortional critical moments using above iterative approach incorporated PBD effects is denoted as M_{FEA+P}

6.11. Convergence study and contribution of higher order terms

The present section aims at (a) determining the number of elements needed to attain convergence, and (b) examining the influence of the high order buckling terms $\lambda^2\mathbf{K_{G2}}$ and $\lambda^3\mathbf{K_{G3}}$ on the predicted buckling load based on the polynomial eigenvalue problem $\left(\mathbf{K_E}+\lambda\left(\mathbf{K_V}+\mathbf{K_{G1}}\right)+\lambda^2\mathbf{K_{G2}}+\lambda^3\mathbf{K_{G3}}\right)\hat{\mathbf{u}}_\mathbf{b}=\mathbf{0}$ derived in Eq. (6.46). For each case, distortional solutions and non-distortional solutions are examined. The later type of solutions are based on the kinematic constraints discussed in Section 6.8. The cantilever problem depicted in Fig. 6-8a is examined. Cross section is $\mathrm{W}310\times 39$ and span is 2m. Fig. 6-7 depicts the critical moments as a function of the number of elements used in the analysis.

In all cases, convergence is attained when the number of elements is 25 where the predicted critical moments are found to be within less than 1% compared to the case where the number of elements taken is 35 elements.

The solutions retaining all geometric stiffness contribution is marked as “third order” and that including only the first and second order geometric stiffness matrices but omitting the term $\lambda^3\mathbf{K_{G3}}$ is marked as “second order.” The solutions with the designations M_D and $M_{(ND)}$ supressing PBD effects by omitting the contributions matrices $\lambda\mathbf{K_{G1}},\lambda^2\mathbf{K_{G2}},\lambda^3\mathbf{K_{G3}}$.

For the cantilever problem considered, the results show that the PBD effects up to the second order terms result in critical moment predictions higher by about 5-6% compared to solutions that omit pre-buckling effects. However, the difference of the second order and third order solutions is observed to be less than 1%. Whereas the second and first order geometric stiffness matrices have a stiffening effect, the contribution of the third order geometric stiffness matrix has a negligible destabilizing effect.

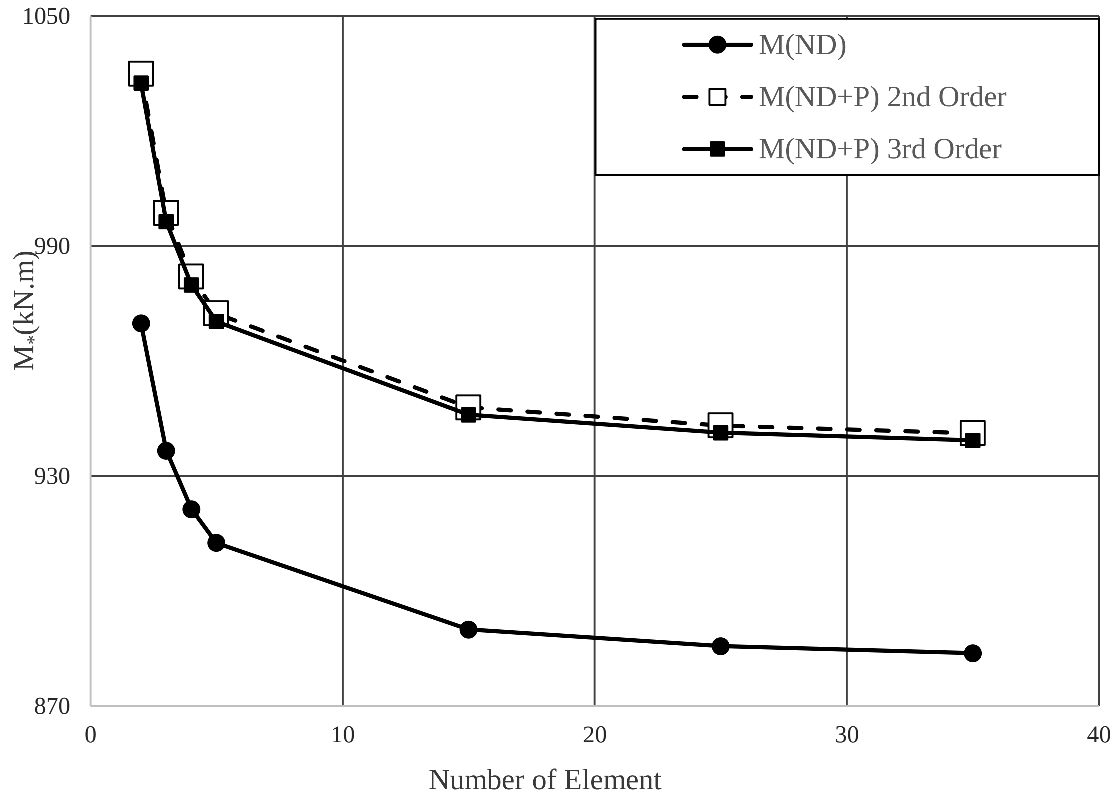

1050
990
930
870
M*(kN.m)
0
10
20
30
40
Number of Element
M(ND)
M(ND+P) 2nd Order
M(ND+P) 3rd Order

(a)

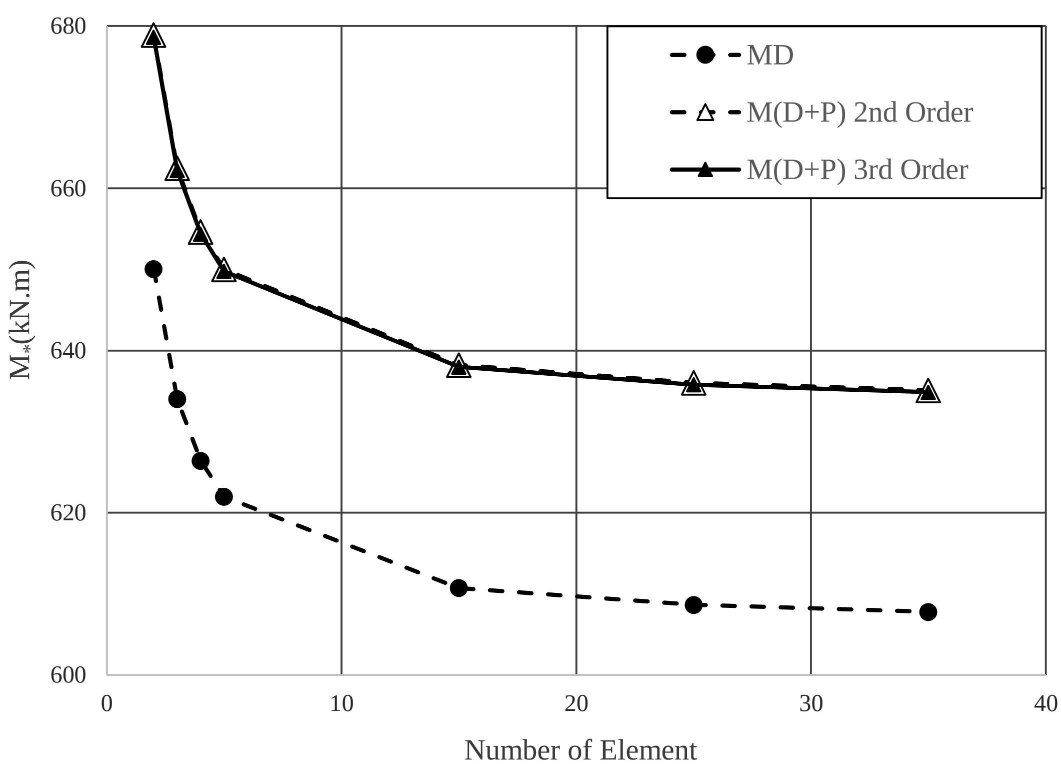

680
660
640
620
600
M*(kN.m)
0
10
20
30
40
Number of Element
MD
M(D+P) 2nd Order
M(D+P) 3rd Order

(b)

Fig. 6-7 Convergence study for cantilever problem a) Non-distortional solutions b) Distortional solutions

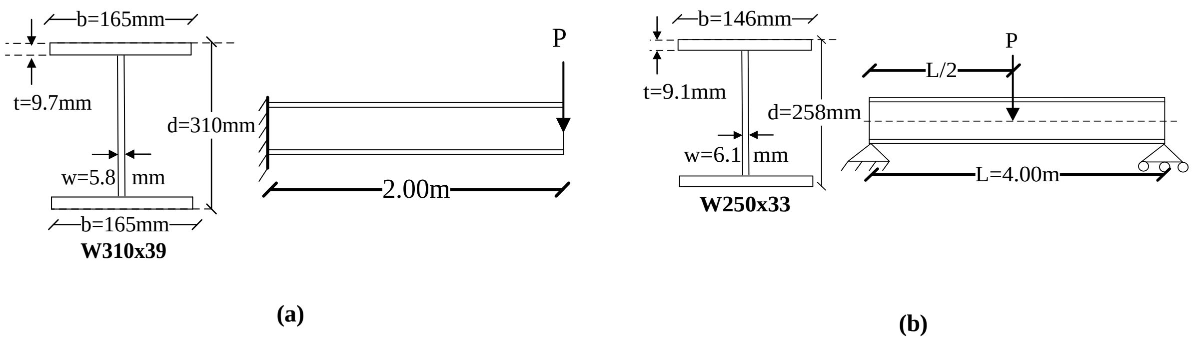

Fig. 6-8 Examples a) cantilever under tip point load b) simply supported beam under mid-span point load

6.12. Verification

The two examples in (Fig. 6-8) are examined to verify the results a) 2.00 m span cantilever with a $W310\times39$ cross section under a tip point load and a) a 4.00 m span simply supported beam with a $W250\times33$ cross section under a mid-span point load. Column 3 in Table 6-2 provides the ratio of the non-distortional critical moments $M_{(ND)}$ based on the present formulation (while applying the non-distortional kinematic constraints defined in Section 6.8) compared to those obtained based on the BG solution as1.02 and 0.99 respectively for examples (a), and (b). For Example (b), the predicted critical moment $M_{ND} = 131kNm$ in Column 2 compares well with the critical moment predicted by the critical moment expression $C_b\left(\pi/L\right)\sqrt{EI_yGJ+\left(\pi E/L\right)^2 C_wI_y}$ where C_b is a standard-dependent moment gradient factor, L is the span, I_y is the weak axis moment of inertia, J is the Saint-Venant torsional constant and C_w is the warping constant.

For example, the critical moments based on CAN-CSA S16-14 (2014), ANSI/AISC 360-16 (2016), AS/NZS 4600-05 (2005), EN-1993-1-1-05 (2005) are respectively $122kNm$, $130kNm$, $134kNm$ and $132kNm$, corresponding to respective FEA-based critical moment to standard-based critical moment ratios M_{ND}/M_{STD} of 1.07, 1.01, 0.98 and 0.99

Column 6 provides the ratio of the distortional critical moments $M_{(D)}$ based on the present solution relative to that based on the shell 3D FEA solution as 1.05 and 1.03, respectively. Column (9) provides the ratios for the distortional critical moments $M_{(D+P+S)}$ including PBD and shear deformation effects relative to those based on the iterative shell FEA procedure $M_{(FEA+P)}$ to capture the PBD effects. The ratios obtained are 1.00 and 0.98 respectively.

Table 6-2 Comparison of critical moments (kNm)

	1	2	3	4	5	6	7	8	9
	$M_{(BG)}$	$M_{(ND)}$	$M_{(ND)}/M_{(BG)}$	$M_{(FEA)}$	$M_{(D)}$	$M_{(D)}/M_{(FEA)}$	$M_{(FEA+P)}$	$M_{(D+P+S)}$	$M_{(D+P+S)}/M_{(FEA+P)}$
Example (a)	868	882	1.02	579	607	1.05	634	634	1.00
Example (b)	132	131	0.99	120	124	1.03	133	131	0.98

6.13. Numerical examples

6.13.1. Example 1-Parametric investigation: Simply supported beam under point load

It is required to investigate the effect of the dimensionless parameters L/d , b/t , d/w and b/d on the critical moments. Towards this goal, a simply supported beam is considered (Fig. 6-9a) with a reference cross-section W250x33 and subjected to a transverse point load applied at mid-span. The geometric parameters of the W250x33 section are provided in Fig. 6-9b and the corresponding reference dimensionless parameters are $L/d = 18.0$, $b/t = 16.0$, $d/w = 42.3$ and $b/d = 0.57$. Each of the dimensionless ratios L/d , b/t , d/w and b/d are varied one at a time from the reference values, while keeping the other three dimensionless parameters unchanged. Six type of critical moment solutions are provided for each run, as described in 6.10.2 and summarized in Fig. 6-9c-f. All critical moments are normalized with respect to the non-distortional critical moment M_{ND} in the absence of distortional and pre-buckling effects. Previous non-distortional theories (e.g., Trahair and Woolcock (1973), Vacharajittiphan et al. (1974), Roberts and Azizian (1983d) , Pi et al. (1992a), Machado and Cortínez (2005)), reported a ratio of critical moments including PBD effects to critical moments excluding PBD effects as $C_p = 1/\sqrt{1 - I_y/I_x}$

Thus, in order to compare the present results with past findings, overlaid on the graph is a plot for C_p . The ratio of distortional to non-distortional critical moments M_D/M_{ND} provides an indication of distortional effects on the critical moment capacity. Also shown in the figures is a plot for the ratio $C_p M_D / M_{ND}$ in order to assess whether the use of the C_p coefficient can be extended to characterize approximately the PBD effects in conjunction with distortional buckling analysis.

The plots for the M_D/M_{ND} (curve viii) indicate that distortional effects increase as d/w and b/d increase (Fig. 6-9d-f) and decrease as L/d and b/t increase (Fig. 6-9c). Distortional effects thus tend to gain significance for short span beams (i.e., with small L/d), small ratio of b/t and high ratios of d/w and b/d . The ratio $M_{(ND+P)}/M_{(ND)}$ of non-distortional moments including PBD effects to those excluding PBD effects (curve ii) provide an indication of PBD effects in the absence of distortion. The plots suggest that PBD effects slightly decrease as L/d and d/w increase but increases as b/t and b/d increase. The ratio $M_{(ND+P)}/M_{(ND)}$ as depicted by curve ii is found in excellent agreement with the pre-buckling deformation coefficient $C_p = 1/\sqrt{1-I_y/I_x}$ (curve iii in Fig. 6-9c-f) obtained in past studies.

The difference between the distortional critical moment including PBD effects $M_{(D+P)}/M_{(ND)}$ (curve vii) and the distortional critical moment excluding PBD effects $M_{(D)}/M_{(ND)}$ (curve viii), provide an indication of PBD effect in the presence of distortion. The difference between both curves suggest that PBD effects increase as L/d and b/d increase (Fig. 6-9c and f). In contrast, the ratio of critical moments $M_{(D+P)}/M_{(ND)}$ reduces as d/w and b/t increase (Fig. 6-10d-e). The PBD effect while capturing distortion (curve vii in Fig. 6-10c-f) shows excellent agreement with C_p (curve iii in Fig. 6-10c-f).

The ratio of non-distortional critical moments including shear deformation and PBD effect to non-distortional critical moments $M_{(ND+P+S)}/M_{(ND)}$ (curve i) provides an indicator of shear deformation effect on critical moments. The shear deformation effect is observed to gain significance in short span beams with small L/d and high ratio of b/d against $M_{(ND+P)}/M_{(ND)}$ (curve ii). As shown on Fig. 6-9c, the effect of shear deformation on the distortional critical moments $M_{(D+P+S)}$ is observed to be negligible as evidenced by the proximity of curves vi and vii. Thus, on Fig. 6-9d-f, curve vii was omitted as it was found to be indistinguishable from curve vi.

Reference Case

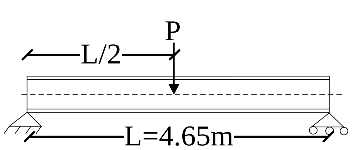

(a)

(c)

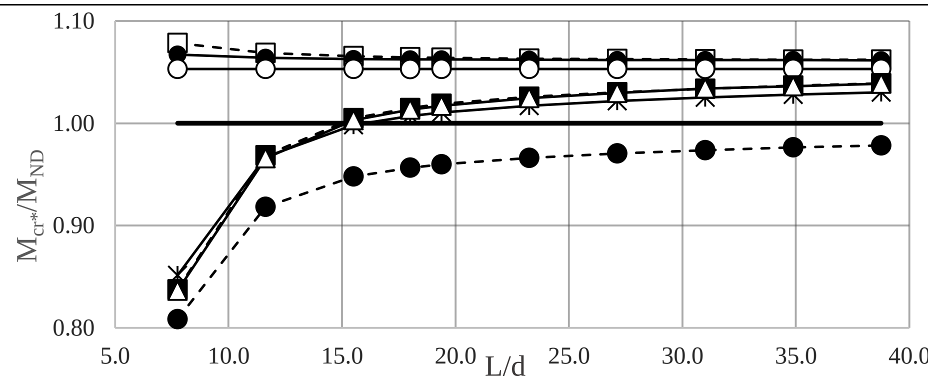

(d)

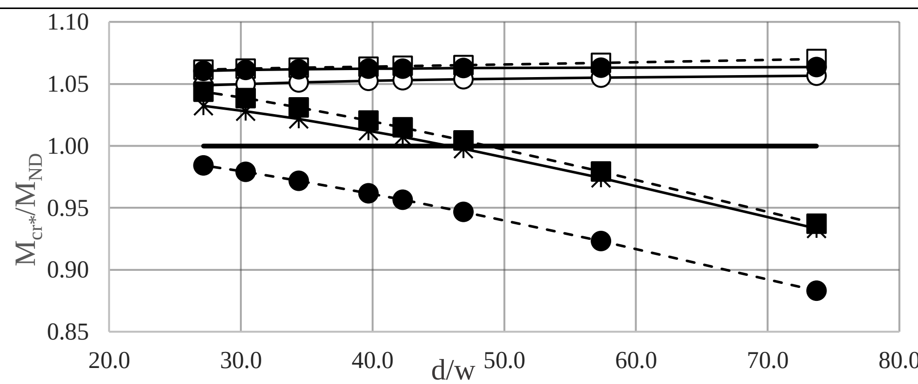

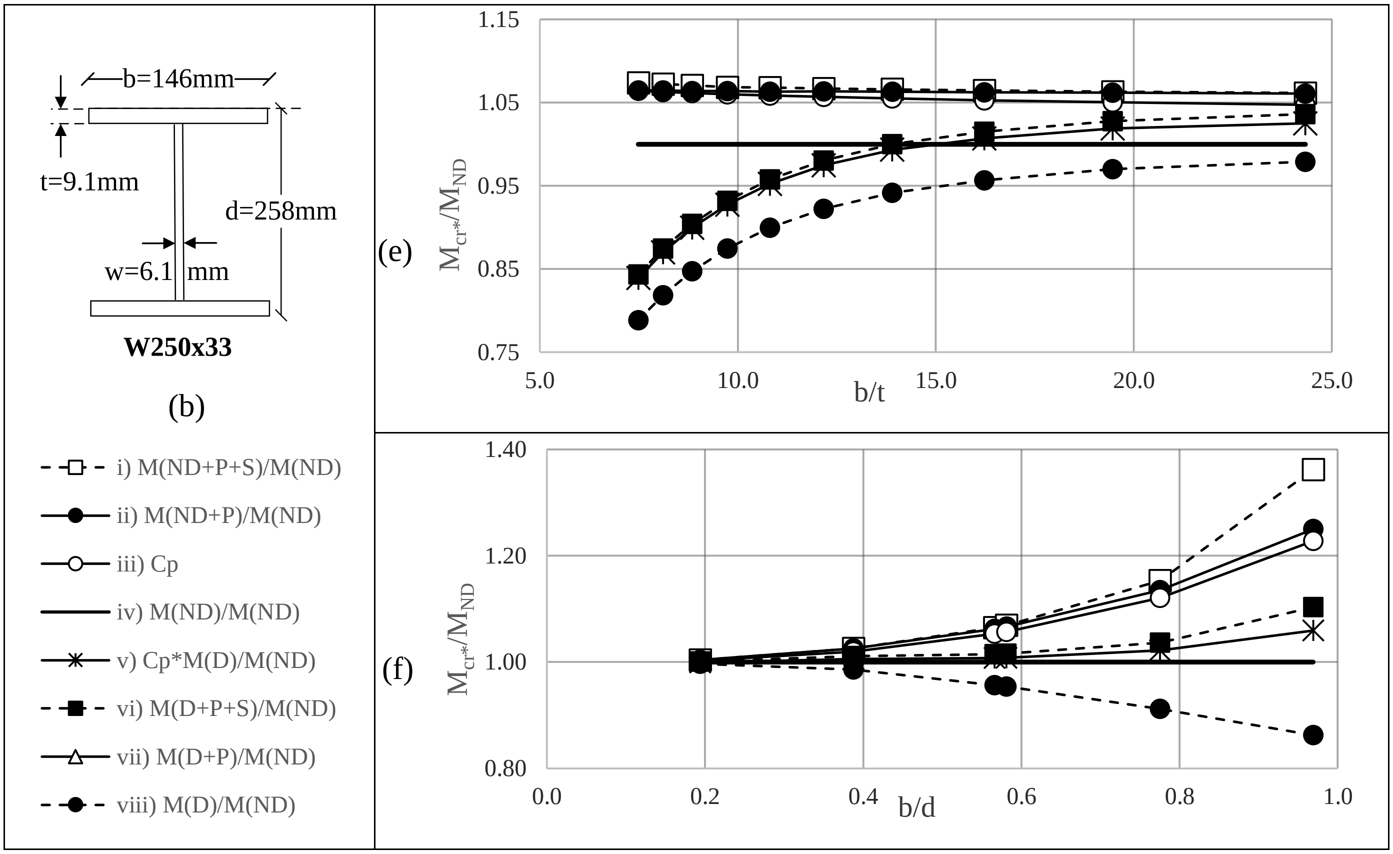

Fig. 6-9 a) Cross Section dimensions b) Loading scheme c-f) Ratio of various types of critical moments to the classical solution versus dimensionless parameters L/d , d/w , b/t and b/d

6.13.2. **Example 2-Parametric investigation: Cantilever under tip load**

It is required to extend the parametric investigation of the effect of the dimensionless parameters L/d , d/w , b/t and b/d on the critical moments of cantilevers. A cantilever with a reference W310x39 cross-section (Fig. 6-10a) is subjected to a transverse point load at the tip. The geometric parameters of the W310x39 section are provided in Fig. 6-10b and the corresponding reference dimensionless parameters are $L/d = 6.45$, $b/t = 17.0$, $d/w = 53.4$ and $b/d = 0.53$. In a manner similar to Example 1 each of the four dimensionless ratios is varied one at a time while keeping the other three dimensionless parameters unchanged, leading to plots in Fig. 6-10c-f.

The plots for M_D/M_{ND} suggest that distortional effects become less significant as L/d increases (curve viii in Fig. 6-10c) and gain significance as d/w , b/t and b/d increase (curves viii in Fig. 6-10d-f).

In the absence of distortion, the PBD effect is indicated by the ratio $M_{(ND+P)}/M_{(ND)}$ (curves ii in Fig. 6-10c-f) and is observed to decrease as L/d , d/w and b/t increase but gain significance as

b/d increases. Also, the ratio $M_{(ND+P)}/M_{(ND)}$ is observed to generally be in good agreement with the pre-buckling deformation coefficient C_p (curve iii in Fig. 6-10c-f) except for short span cantilevers (i.e., small L/d ratios) where the $M_{(ND+P)}/M_{(ND)}$ ratios are higher than those of the C_p coefficient (Fig. 6-10c). The difference between $M_{(D+P)}/M_{(ND)}$ (curve vii) and $M_{(D)}/M_{(ND)}$ (curve viii) provides an indication of PBD effects, in the presence of distortion, and shows that the PBD effects increase with L/d (curve ii in Fig. 6-10c) but decreases when d/w, b/t and b/d increase (Fig. 6-10d-e). The PBD effect in the presence of distortion as provided by the ratio $M_{(D+P)}/M_{(ND)}$ (curve vii in Fig. 6-10c-e) is in excellent agreement with $C_p M_D/M_{ND}$ (curve v in Fig. 6-10c-e).

The difference between $M_{(ND+P+S)}/M_{(ND)}$ (curve i) and $M_{(ND+P)}/M_{(ND)}$ (curve ii) is an indicator of pre-buckling shear deformation effects on critical moments including PBD effects. The proximity of both curves suggest that shear deformation effects are negligible except for the short span cantilevers where curve (i) deviates from curve (ii) (Fig. 6-10c). In such cases, the inclusion of shear deformation effects leads to larger pre-buckling deformations and hence a larger pre-buckling deformation stiffening effect.

In the presence of distortional effects, the effect of shear deformation is observed by comparing the ratios $M_{(D+P+S)}/M_{(ND)}$ (curves vi in Fig. 6-10c-f) and $M_{(D+P)}/M_{(ND)}$ (curves vii). For the ratios of L/d, d/w and b/d, the difference between both curves is indistinguishable, suggesting that shear deformation effects are negligible. Pre-buckling shear deformation effect is observed to gain significance for sections with stocky flanges (i.e., small ratio of b/t) as evidenced by curves vi and vii (Fig. 6-10e).

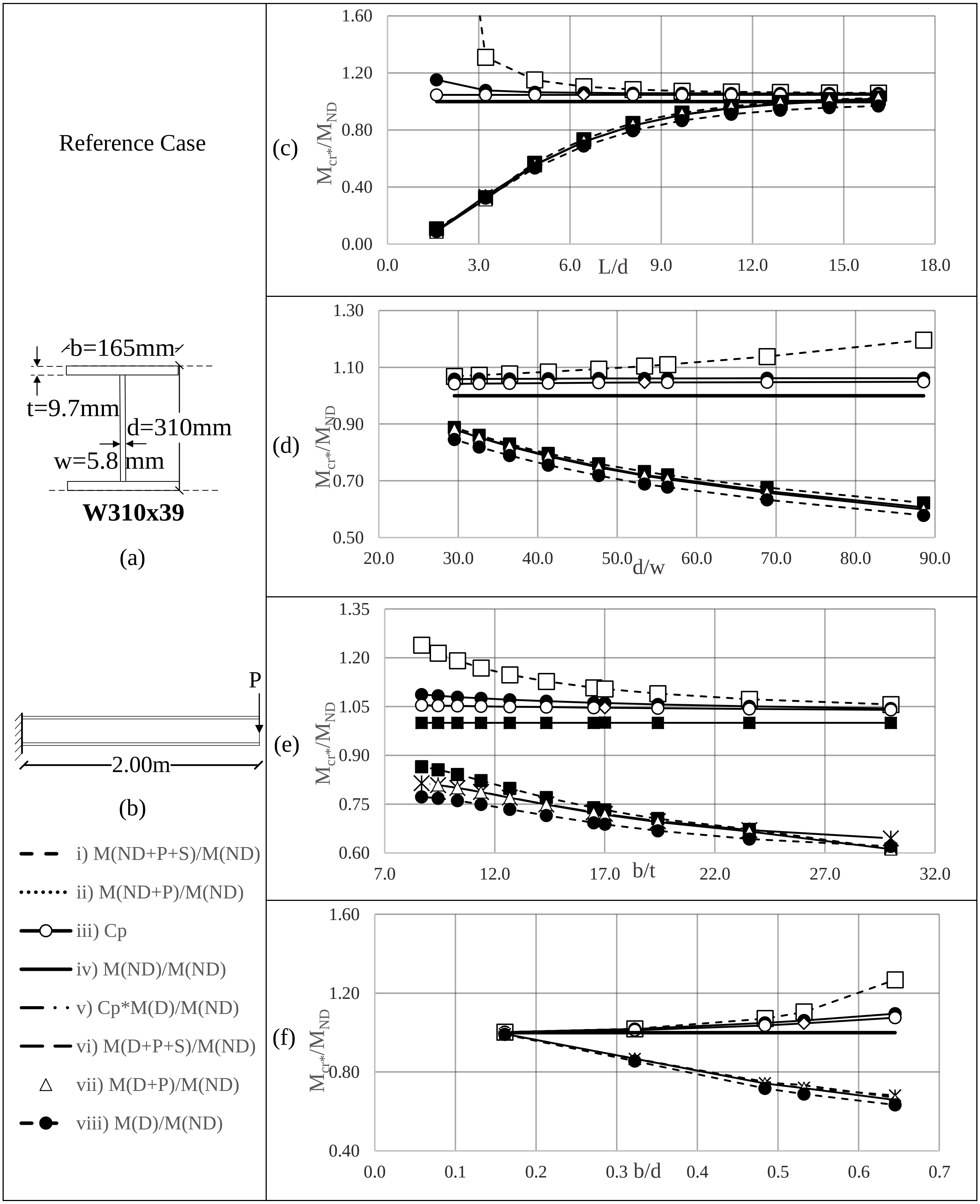

Fig. 6-10 a) Cross Section dimensions b) Loading scheme c-f) Ratio of various types of critical moments to the classical solution versus dimensionless parameters L/d , d/w , b/t and b/d

6.13.3. Example 3: Transverse load height effect

A 6m span simply supported beam (Fig. 6-11a) with a W250x33 cross-section with the geometric parameters in Fig. 6-11b, is subjected to a transverse point load which acting at mid-span. The load is offset from the shear center by a distance y such that $-h/2 \le y \le h/2$ and $y = -h/2$ denotes top flange loading and $y = h/2$ denotes bottom flange loading. It is required to investigate the effect of the load offset from the shear center on the critical moments. As expected, all types of analyses shows the critical moment is observed to decrease as the point of application of the load moves upward (Fig. 6-11d). All types of analyses considered are then normalized with respect to the critical moments M_{ND} predicted by the conventional analysis. The resulting critical moment ratio plots in Fig. 6-11c. When all effects combined are considered (pre-buckling, shear deformation, and distortional effects) the critical moment ratio $M_{(D+P+S)}/M_{(ND)}$ range from 100% for top flange loading to 106% for bottom flange loading, suggesting that it would be conservative to adopt load height effects based on the classical solution. When only distortional effects are considered, the $M_{(D)}/M_{(ND)}$ ratio ranged from 96% for bottom flange loading to 98% near bottom flange loading. When PBD and shear deformation effects are included, the $M_{(ND+P+S)}/M_{(ND)}$ ratio ranged from 104% for top flange loading to 108% bottom flange loading.

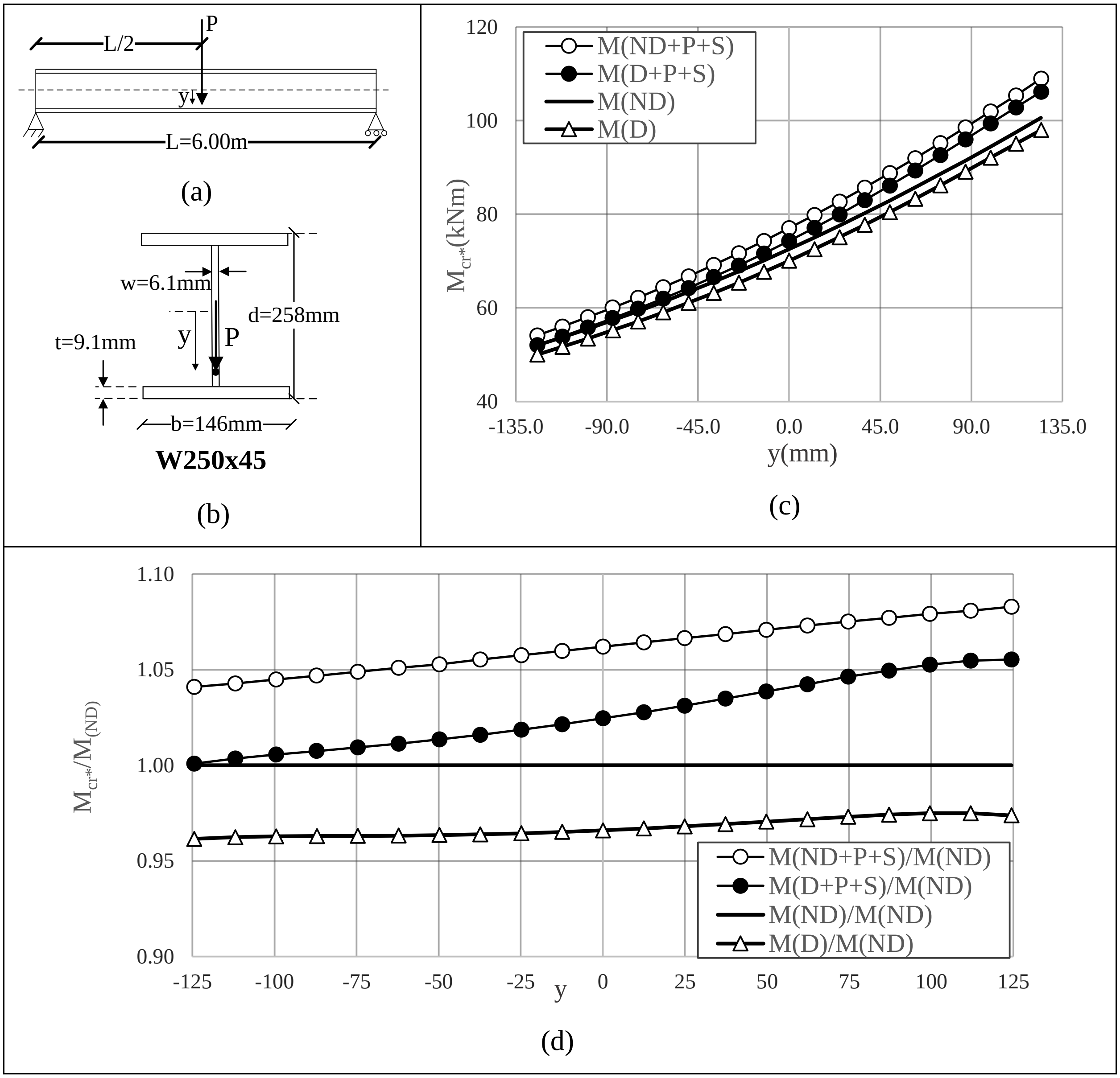

Fig. 6-11 a)Simply supported beam subjected to mid-span load offset from shear center b)geometric properties c) effect of load applied offset from the shear centre on critical moments d) effect of the load applied offset from the shear centre on the normalized critical moments

6.13.4. **Example 4: Longitudinal load height effect**

The beam column in Example 3 is re-considered while replacing the transverse load by a compressive axial load applied at one end. The load is offset from the shear center by a distance y such that $-h/2 \le y \le h/2$. In all analyses conducted, the pre-buckling nonlinear effects were supressed as evidenced by the presence of designator L (i.e., Linear pre-buckling analysis). As expected, the critical load has a peak value when the load is applied at the section centroid (Fig. 6-12a) and decreases as the offset of the point of load application is increased given the additional moments induced by the eccentricity. Fig. 6-12b depicts the critical loads normalized with respect to the case of non-distortional buckling analysis (ND)-L. The inclusion of distortional effects in Analysis (D)-L is observed to reduce the critical load. Distortional effects are observed to have a minimal effect when the load is applied concentrically with the section centroid and to increase as the point of load application moves farther from the section centroid. This is evidenced by the fact that $P_{cr}(D)/P_{cr}(ND)=1.00$ at $y=0$ and decreases to $P_{cr}(D)/P_{cr}(ND)=0.99$ when $y=\pm h/2$. The PBD effect is non-existent for the case of pure axial compression ($y=0$). It increases with the offset from the section centroid and peaks at $P_{cr}(ND+P+S)/P_{cr}(ND)=1.02$ when $y=\pm h/2$. A similar trend is shown when the combined effects of distortion and pre-buckling are considered. In this case, $P_{cr}(D+P+S)/P_{cr}(ND)=1.00$ at $y=0$ and peaks to $P_{cr}(D+P+S)/P_{cr}(ND)=1.01$ at $y=\pm h/2$.

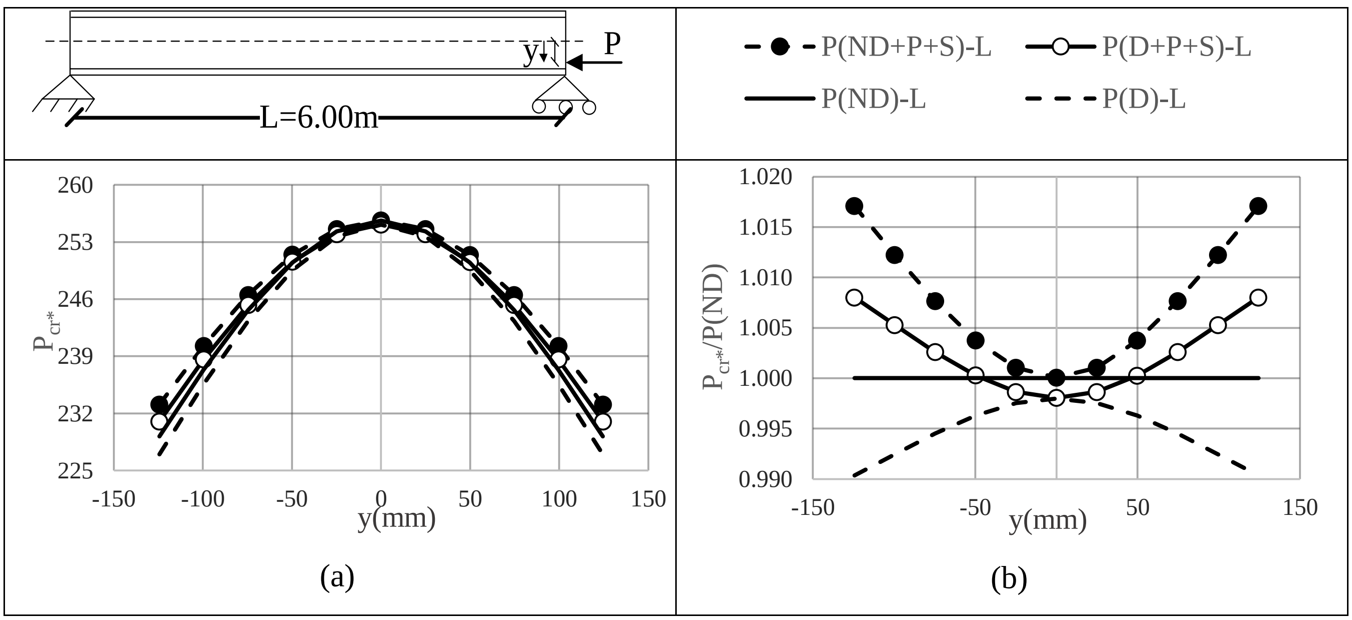

Fig. 6-12 Effect of the axial load offset from the shear centre on a) critical load b) normalized critical load

6.13.5. **Example 5: P-delta effect in beam columns**

A 8.0m span simply supported member (Fig. 6-13a) with a W250x45 cross-section (geometric parameters are provided on Fig. 6-13b), is subjected to a transverse point load $V=\lambda_{cr}180kN$ acting at mid-span and an axial point load $H=\lambda_{cr}(\alpha 1800kN)$ acting at the end $z=L$. The axial load multiplier α is varied in the range $0\le\alpha\le1$ to trace the $V-H$ transverse-axial force interaction diagram, and λ_{cr} is the critical load multiplier to be obtained from the eigen-value analysis. Both flanges of the member are laterally restrained at mid-span.

Four types of buckling analysis $(D),(ND),(D+P+S)$ and $(ND+P+S)$ are conducted. Since the member is axially loaded, for each type of buckling analysis, two possible types of pre-buckling analyses are possible; linear (denoted by the additional designation L) which omits the P-delta effect, and non-linear (denoted by NL). The interaction diagrams based on all eight type of solutions are depicted in Fig. 6-13c. As expected, a comparison of the NL types analysis to the corresponding L types of analysis are observed to reduce the critical transverse forces V for all types of buckling analyses. Also, in the absence of distortion, incorporating the pre-buckling deformation effect in the $(ND+P+S)$ analysis is found to be favourable compared to excluding it in the (ND) type of analysis. Similar observations are made for distortional analyses $(D),(D+P+S)$, where the inclusion of pre-buckling deformation effects is found to lead to an increase in the predicted critical force V.

The force-displacement curves are depicted for the cases $\alpha = 0.3$ (Fig. 6-13d) and $\alpha = 1$ (Fig. 6-13e). In both graphs, the load-deformation equilibrium paths are depicted and the points of onset of buckling as predicted by the $(D),(ND),(D+P+S)$ and $(ND+P+S)$ type eigen-value analyses in each case, after which the equilibrium path is deemed to be unstable.

As expected, the nonlinear pre-buckling analysis for the higher axial force $\alpha = 1$ exhibit a more nonlinear behaviour than that of the lower axial force $\alpha = 0.30$. The critical transverse force resulting from non-linear pre-buckling analysis (the dashed curves) are observed to be smaller than that based on a linear pre-buckling analysis (the continuous curves). In the case of the smaller axial force ratio $\alpha = 0.3$, the critical transverse load is greater than that based on the higher axial force $\alpha = 1$. The higher transverse load is observed to lead to larger pre-buckling transverse displacements.

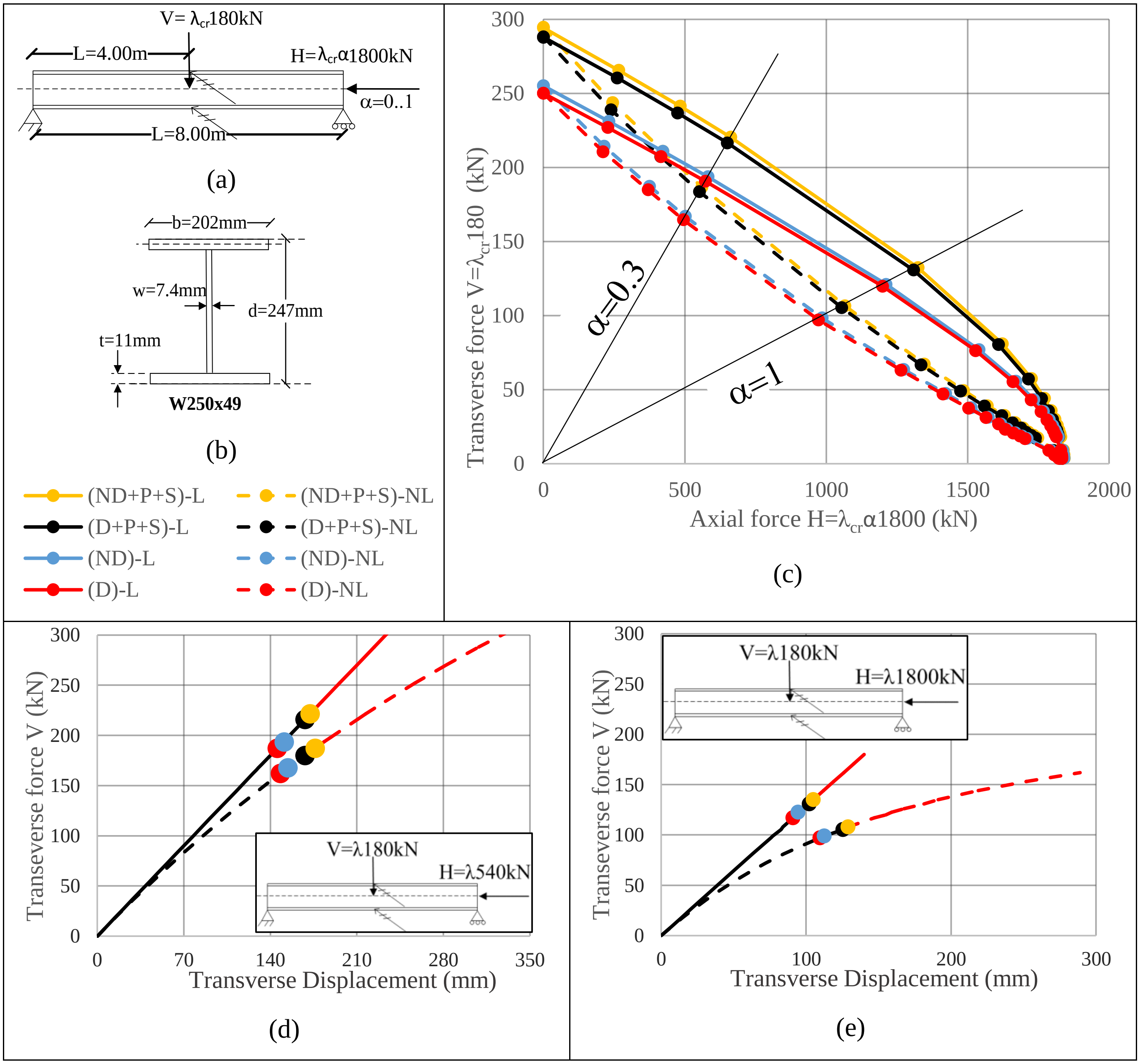

Fig. 6-13 a) Simply supported beam subjected to a mid-span transverse load and an axial end-node load b)geometric properties c) Buckling capacity resulting from interaction of transverse and axial forces d) force-displacement diagrams for $\alpha = 0.3$ and e) force-displacement diagrams for $\alpha = 1$

6.13.6. Example 6: Effect of the stiffeners on distortional critical moments

A 16.0m span simply supported plate girder (Fig. 6-14b) with 16.0m span is subjected to a point load acting at the mid-span(Fig. 6-14a). The normalized distortional critical moment M_D to the classical solution M_{ND} is obtained for a series of cases starting from the case where no stiffeners are provided and adding a pair of stiffeners sequentially starting from beam end and moving towards mid-span. (Fig. 6-14e) corresponding to 0, 2, 4, 6, 8, 10, 12, 14, 16, and 17 stiffeners, the last stiffener being located under the load. The first pair of stiffeners at both ends of the beam are observed to significantly increase the critical moment (i.e., 11%) in comparison to the strength gained by the addition of the stiffeners (i.e., 4.6%). Given that in practical situations, a bearing stiffener may be placed under the mid-span load, two additional cases have been investigated. In case 1 (Fig. 6-14c), the beam is stiffened by two pairs of stiffeners at each end and one stiffener at mid-span while in case 2 (Fig. 6-14d) another pair of stiffeners are added beside the middle stiffener. It is observed that a single stiffener at the point of the load (case 1) is nearly as effective as case 2 with a 0.73% difference in critical moments.

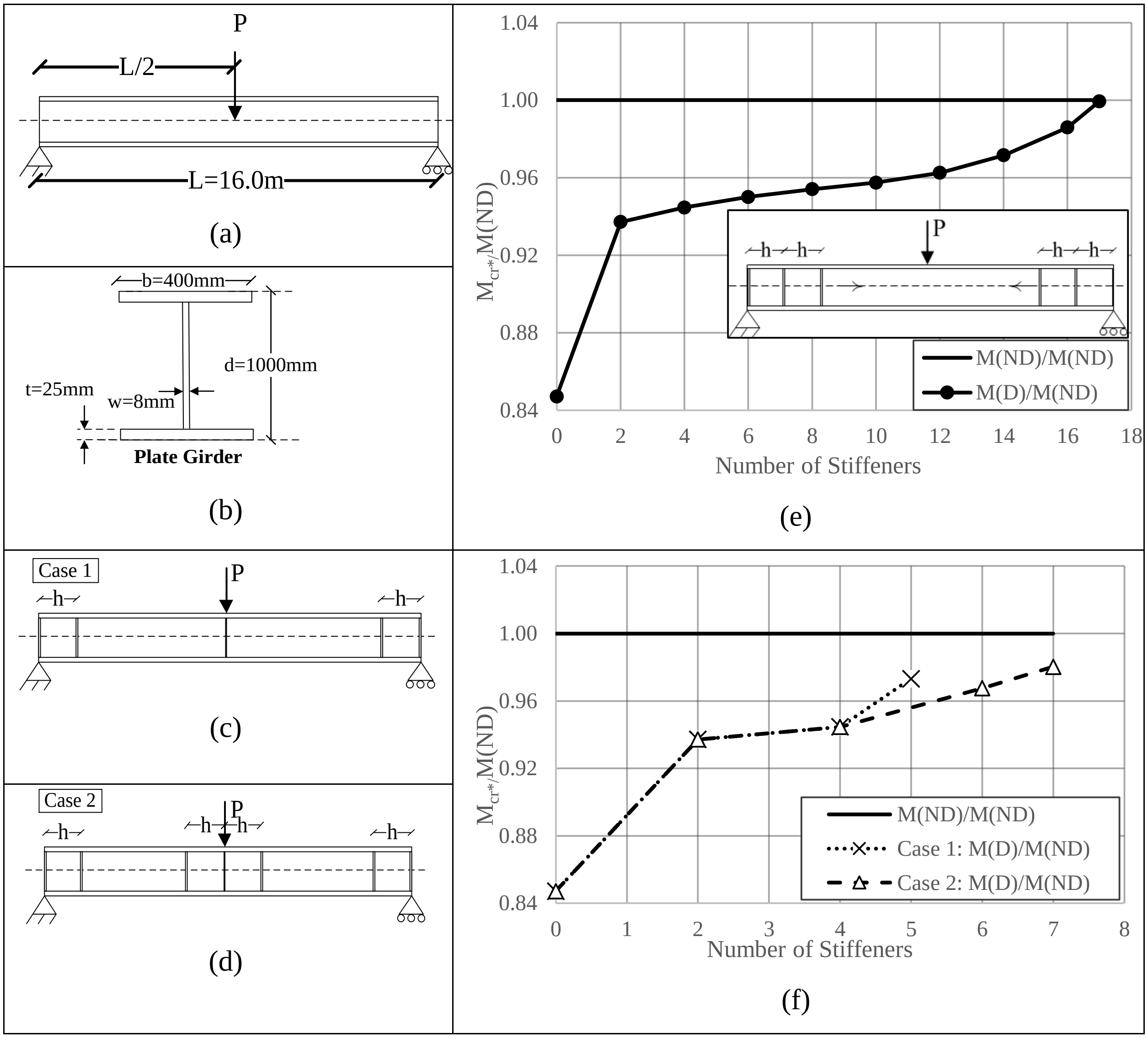

Fig. 6-14 a) simply supported plate girder subjected to mid-span load b) geometric properties c) case (1) includes five stiffeners d) case (2) includes seven stiffeners e) effect of stiffeners on distortional normalized critical moment f) effect of middle stiffeners on normalized critical moments

6.14. **Summary and conclusions**

A generalized distortional lateral torsional buckling finite element formulation is developed for members with doubly symmetric wide flanges. The lateral displacement of the web is interpolated using quintic Hermitian polynomials in the longitudinal direction and cubic Hermitian polynomials in the transverse direction. The formulation captures multiple non-conventional effects including (1) the softening effect due to web distortion, (2) the stiffening effect due to pre-buckling deformations, (3) the effects due to transverse load offset from the shear centre (4) pre-buckling shear deformation effects within the plane of the web, (5) the geometrically non-linear effects in the pre-buckling analysis, and (6) the stiffening effect due to the presence of transverse stiffeners. The validity of the solution is established through comparisons with 3D shell FEA results. The solution allows the investigation of the effects on the buckling load separately as well as assessing the interaction between various effects. The theory is applied to investigate a number of practical problems. The main findings are:

1- For the simply supported beams and cantilevers, web distortional effects are observed to gain significance as L/d decreases and become less significance as d/w or b/d decrease. In cantilevers, distortional effects are shown to be increased as b/t increases, whereas in simply supported beams, they are shown to be pronounced as b/t decreases.

2- In the absence of distortion, the PBD effects are shown to slightly decrease as L/d, d/w and b/t increase but to increase as b/d increases. In the presence of distortion, the PBD effect is shown to increase with L/d but to decrease as d/w. For cantilevers, when distortion is captured, the PBD effects are observed to decrease as b/t and b/d increase whereas in simply supported beams the PBD effects are shown to increase with b/t and b/d.

3- In most cases considered, the inclusion of shear deformation effects in pre-buckling analysis is shown to have a negligible effect on predicted buckling load. However, in short span beams, the incorporation of shear deformation effects in pre-buckling analysis was shown to increase the stiffening effect due to PBD.

4- In beam-columns, the inclusion of geometric non-linear effects in the pre-buckling analysis is associated with larger pre-buckling displacements due moment-axial compression interaction and is thus shown to reduce the predicted buckling strength of compared to solutions that omit geometric non-linear effects. In the examples investigated, this softening effect seems to overshadow the beneficial stiffening effect additional deformations may contribute to the PBD effects. Distortional and PBD effects are observed to increase as the ratio of transverse to axial forces increase.

5- For beams with transverse loads offset from the shear centre, distortional effects are observed to gain significance as the point of application of the load moves upwards, whereas the PBD effect is shown to gain significance as the point of application of load moves downwards. For the problem examined, the distortional and PBD effects seem to offset one another when the load is applied at the top flange, but have a net beneficial effect when the load is applied at the bottom flange.

6- For the investigated beam-column with a compressive force offset from the section centroid, the PBD and distortional effects are observed to increase as the load moves away from the centroid. The stiffening effect due to PBD is shown to be more significant compared to the softening effect induced by distortion.

7- For the simply supported plate girder with thin web considered, the placement of transverse stiffeners is observed to increase the lateral torsional buckling capacity of the member. Stiffeners located near both ends and at mid-span, are observed to be particularly effective in increasing the lateral torsional buckling capacity compared to other intermediate stiffeners. The provision of multiple stiffeners is shown to supress the distortional effects nearly entirely. This is evidenced by the fact that the member is able to attain the lateral torsional buckling strength as predicted by the classical Vlasov theory.

6.15. Appendix A – Matrices for the web

From Eq. (6.37), web elastic stiffness matrix $\mathbf{K_{EW}}$ and geometric stiffness matrices $\mathbf{K_{G1W}}$ and $\mathbf{K_{G2W}}$ are defined as

$$\mathbf{K_{EW}} = \sum_{i=1}^{4} \mathbf{k}_{(i)} \quad , \qquad \mathbf{K_{G1W}} = \sum_{i=1}^{5} \mathbf{k}_{\mathbf{g}(i)} + \sum_{i=1}^{7} \mathbf{k}_{\mathbf{pg}(i)} \quad , \qquad \mathbf{K_{G2W}} = \sum_{i=1}^{9} \mathbf{k}_{\mathbf{PG}(i)} \tag{6.47}$$

where $D = Et^3 \big/ 12\left(1-\nu^2\right)$ and stiffness matrices $\mathbf{k_1}$ - $\mathbf{k_4}$, $\mathbf{k_{g1}}$ - $\mathbf{k_{g5}}$, $\mathbf{k_{pg1}}$ - $\mathbf{k_{pg7}}$ and $\mathbf{k_{PG1}}$ - $\mathbf{k_{PG9}}$ are defined as

$$\mathbf{k}_i = \int_0^L \int_{-h/2}^{h/2} f\left(y,z\right) dydz$$

$\mathbf{k}_i$	$f\left(y,z\right)$	$\mathbf{k}_i$	$f\left(y,z\right)$
$\mathbf{k_1}$	$\mathbf{D}\mathbf{M}_{,zz}\mathbf{M}^{\mathbf{T}}_{,zz}$	$\mathbf{k_{pg5}}$	$2\nu D\mathbf{M}_{,yz}v_{p,z}\mathbf{M}^{\mathbf{T}}_{,yy}$
$\mathbf{k_2}$	$\mathbf{D}\mathbf{M}_{,yy}\mathbf{M}^{\mathbf{T}}_{,yy}$	$\mathbf{k_{pg6}}$	$2D\left(1-\nu\right)\mathbf{M}_{,yz}v_{p,z}\mathbf{M}^{\mathbf{T}}_{,yy}$
$\mathbf{k_3}$	$2\nu D\mathbf{M}_{,zz}\mathbf{M}^{\mathbf{T}}_{,yy}$	$\mathbf{k_{pg7}}$	$2D\left(1-\nu\right)\mathbf{M}_{,yz}\left[\left(\frac{1}{2}-\frac{y}{h}\right)w_{,zTp}+\left(\frac{1}{2}+\frac{y}{h}\right)w_{Bp,z}\right]\mathbf{M}^{\mathbf{T}}_{,yz}$
$\mathbf{k_4}$	$2D\left(1-\nu\right)\mathbf{M}_{,yz}\mathbf{M}^{\mathbf{T}}_{,yz}$	$\mathbf{k_{PG1}}$	$D\mathbf{M}_{,yz}v^2_{p,z}\mathbf{M}^{\mathbf{T}}_{,yz}$

$\mathbf{k}_{\mathbf{g1}}$	$N_{zp}\mathbf{M}_{,z}\mathbf{M}_{,z}^{\mathbf{T}}$	$\mathbf{k}_{\mathbf{PG2}}$	$D/h^2\,\mathbf{M}_{,yz}\left(-w_{Tp}+w_{Bp}\right)^2\mathbf{M}_{,yz}^{\mathbf{T}}$
$\mathbf{k}_{\mathbf{g2}}$	$N_{zp}\dfrac{w^2}{12}\mathbf{M}_{,\mathrm{yz}}\mathbf{M}_{,\mathrm{yz}}^{\mathbf{T}}$	$\mathbf{k}_{\mathbf{PG3}}$	$2D\nu/h\,\mathbf{M}_{,yz}\left(-w_{Tp}+w_{Bp}\right)v_{p,z}\mathbf{M}_{,yz}^{\mathbf{T}}$
$\mathbf{k}_{\mathbf{g3}}$	$N_{yzp}\mathbf{M}_{,\mathrm{y}}\mathbf{M}_{,z}^{\mathbf{T}}$	$\mathbf{k}_{\mathbf{PG4}}$	$D(1-\nu)/2\,\mathbf{M}_{,yy}v_{p,z}^2\mathbf{M}_{,yy}^{\mathbf{T}}$
$\mathbf{k}_{\mathbf{g4}}$	$N_{yzp}\dfrac{w^2}{12}\mathbf{M}_{,\mathrm{yz}}\mathbf{M}_{,\mathrm{yy}}^{\mathbf{T}}$	$\mathbf{k}_{\mathbf{PG5}}$	$D(1-\nu)/2\,\mathbf{M}_{,yz}\left[\left(\frac{1}{2}-\frac{y}{h}\right)w_{Tp,z}+\left(\frac{1}{2}+\frac{y}{h}\right)w_{Bp,z}\right]^2\mathbf{M}_{,yz}^{\mathbf{T}}$
$\mathbf{k}_{\mathbf{g5}}$	$N_{yzp}\dfrac{w^2}{12}\mathbf{M}_{,\mathrm{yz}}\mathbf{M}_{,zz}^{\mathbf{T}}$	$\mathbf{k}_{\mathbf{PG6}}$	$D(1-\nu)/2h^2\,\mathbf{M}_{,zz}\left(-w_{Tp}+w_{Bp}\right)^2\mathbf{M}_{,zz}^{\mathbf{T}}$
$\mathbf{k}_{\mathbf{pg1}}$	$2D\mathbf{M}_{,yz}v_{\mathrm{p},z}\mathbf{M}_{,zz}^{\mathbf{T}}$	$\mathbf{k}_{\mathbf{PG7}}$	$D(1-\nu)\mathbf{M}_{,yy}\left[\left(\frac{1}{2}-\frac{y}{h}\right)w_{Tp,z}+\left(\frac{1}{2}+\frac{y}{h}\right)w_{Bp,z}\right]v_{p,z}\mathbf{M}_{,yz}^{\mathbf{T}}$
$\mathbf{k}_{\mathbf{pg2}}$	$2D/h\,\mathbf{M}_{,yy}\left(-w_{Tp}+w_{Bp}\right)\mathbf{M}_{,yz}^{\mathbf{T}}$	$\mathbf{k}_{\mathbf{PG8}}$	$D(1-\nu)\mathbf{M}_{,yy}\left(-w_{Tp}+w_{Bp}\right)v_{p,z}\mathbf{M}_{,zz}^{\mathbf{T}}$
$\mathbf{k}_{\mathbf{pg3}}$	$\dfrac{2D\nu}{h}\mathbf{M}_{,\mathrm{zz}}\left(-w_{Tp}+w_{Bp}\right)\mathbf{M}_{,yz}^{\mathbf{T}}$	$\mathbf{k}_{\mathbf{pg4}}$	$\dfrac{2D(1-\nu)}{h}\mathbf{M}_{,\mathrm{zz}}\left(-w_{Tp}+w_{Bp}\right)\mathbf{M}_{,yz}^{\mathbf{T}}$
$\mathbf{k}_{\mathbf{PG9}}$	$D(1-\nu)\mathbf{M}_{,zz}\left[\left(\frac{1}{2}-\frac{y}{h}\right)w_{Tp,z}+\left(\frac{1}{2}+\frac{y}{h}\right)w_{Bp,z}\right]\left(-w_{Tp}+w_{Bp}\right)\mathbf{M}_{,yz}^{\mathbf{T}}$		

where $N_{zp}=\sigma_{zp}w$ and $N_{yzp}=2\tau_{yzp}w$

6.16. **Appendix B – Matrices for flanges**

The matrices relevant to the top flange are provided in the following. From Eq. (6.38), the elastic stiffness matrix $\mathbf{K}_{\mathbf{ET}}$ and geometric stiffness matrices $\mathbf{K}_{\mathbf{G1T}}$, $\mathbf{K}_{\mathbf{G2T}}$ and $\mathbf{K}_{\mathbf{3GT}}$ of top flange are defined as

$$\mathbf{K}_{\mathbf{ET}}=\sum_{i=5}^{7}\mathbf{k}_{(i)},\ \mathbf{K}_{\mathbf{G1T}}=\sum_{i=6}^{7}\mathbf{k}_{\mathbf{g}(i)}+\sum_{i=8}^{14}\mathbf{k}_{\mathbf{pg}(i)},\qquad \mathbf{K}_{\mathbf{G2T}}=\sum_{i=10}^{57}\mathbf{k}_{\mathbf{PG}(i)},\qquad \mathbf{K}_{\mathbf{G3T}}=\sum_{i=1}^{16}\mathbf{k}_{\mathbf{3PG(i)}} \qquad (6.48)$$

where stiffness matrices $\mathbf{k}_{\mathbf{5}}$ - $\mathbf{k}_{\mathbf{7}}$, $\mathbf{k}_{\mathbf{g6}}$ - $\mathbf{k}_{\mathbf{g8}}$, $\mathbf{k}_{\mathbf{pg8}}$ - $\mathbf{k}_{\mathbf{pg14}}$, and $\mathbf{k}_{\mathbf{PG10}}$ - $\mathbf{k}_{\mathbf{PG57}}$, $\mathbf{k}_{\mathbf{3PG1}}$ - $\mathbf{k}_{\mathbf{3PG16}}$ are defined as

$$\mathbf{k}_i=\int_0^L f\left(-h/2,z\right)dz$$

$\mathbf{k}_i$	$f\left(-h/2,z\right)$	$\mathbf{k}_i$	$f\left(-h/2,z\right)$

$\mathbf{k}_5$	$EI_{yT}\mathbf{M}_{,zz}\mathbf{M}_{,zz}^{\mathbf{T}}$	$\mathbf{k}_{\mathbf{PG34}}$	$G\frac{h^2}{4}A_T\mathbf{M}_{,zz}\theta_{xp}^2\mathbf{M}_{,zz}^{\mathbf{T}}$
$\mathbf{k}_6$	$EI_{\omega T}\mathbf{M}_{,yzz}\mathbf{M}_{,yzz}^{\mathbf{T}}$	$\mathbf{k}_{\mathbf{PG35}}$	$GhA_T\mathbf{M}_{,zz}\left(v_{p,z}+\theta_{xp}\right)\theta_{xp}\mathbf{M}_{,y}^{\mathbf{T}}$
$\mathbf{k}_7$	$4GI_{xT}\mathbf{M}_{,yz}\mathbf{M}_{,yz}^{\mathbf{T}}$	$\mathbf{k}_{\mathbf{PG36}}$	$GhA_T\mathbf{M}_{,zz}w_{Tp,z}\theta_{xp}\mathbf{M}_{,z}^{\mathbf{T}}$
$\mathbf{k}_{\mathbf{g6}}$	$\sigma_{zTp}A_T\mathbf{M}_{,z}\mathbf{M}_{,z}^{\mathbf{T}}$	$\mathbf{k}_{\mathbf{PG37}}$	$-GhI_{xT}\mathbf{M}_{,zz}\theta_{xp}\theta_{xp,z}\mathbf{M}_{,yz}^{\mathbf{T}}$
$\mathbf{k}_{\mathbf{g7}}$	$\sigma_{zTp}\left(I_{xT}+I_{yT}\right)\mathbf{M}_{,yz}\mathbf{M}_{,yz}^{\mathbf{T}}$	$\mathbf{k}_{\mathbf{PG38}}$	$-4GI_{xT}\mathbf{M}_{,yz}\theta_{xp,z}w_{Tp,z}\mathbf{M}_{,z}^{\mathbf{T}}$
$\mathbf{k}_{\mathbf{pg8}}$	$2EI_{yT}\mathbf{M}_{,zz}\left(\theta_{xp}+v_{p,z}\right)\mathbf{M}_{,yz}^{\mathbf{T}}$	$\mathbf{k}_{\mathbf{PG39}}$	$\sigma_{zTp}\frac{h}{2}A_T\mathbf{M}_{,y}\theta_{xp,z}\mathbf{M}_{,y}^{\mathbf{T}}$
$\mathbf{k}_{\mathbf{pg9}}$	$2EI_{yT}\mathbf{M}_{,zz}\theta_{xp,z}\mathbf{M}_{,y}^{\mathbf{T}}$	$\mathbf{k}_{\mathbf{PG40}}$	$\sigma_{zTp}hA_T\mathbf{M}_{,y}\left(\theta_{xp}+v_{p,z}\right)\mathbf{M}_{,yz}^{\mathbf{T}}$
$\mathbf{k}_{\mathbf{pg10}}$	$-EI_{yT}\frac{h}{2}\mathbf{M}_{,zz}\theta_{xp,zz}\mathbf{M}_{,z}^{\mathbf{T}}$	$\mathbf{k}_{\mathbf{PG41}}$	$-\sigma_{zTp}I_{yT}\mathbf{M}_{,yz}\theta_{xp}\mathbf{M}_{,zz}^{\mathbf{T}}$
$\mathbf{k}_{\mathbf{pg11}}$	$EI_{yT}\frac{h}{2}\mathbf{M}_{,zz}\theta_{xp}\mathbf{M}_{,zzz}^{\mathbf{T}}$	$\mathbf{k}_{\mathbf{PG42}}$	$-\sigma_{zTp}I_{yT}\mathbf{M}_{,yz}\theta_{xp,z}\mathbf{M}_{,z}^{\mathbf{T}}$
$\mathbf{k}_{\mathbf{pg12}}$	$-EI_{yT}\frac{h}{2}\mathbf{M}_{,yzz}\theta_{xp}^2\mathbf{M}_{,zz}^{\mathbf{T}}$	$\mathbf{k}_{\mathbf{PG43}}$	$2\sigma_{zTp}I_{yT}\mathbf{M}_{,yz}\theta_{xp,z}\theta_{xp}\mathbf{M}_{,y}^{\mathbf{T}}$
$\mathbf{k}_{\mathbf{pg13}}$	$-4GI_{xT}\mathbf{M}_{,yz}\theta_{xp,z}\mathbf{M}_{,z}^{\mathbf{T}}$	$\mathbf{k}_{\mathbf{PG44}}$	$\sigma_{zTp}I_{yT}\mathbf{M}_{,yz}\theta_{xp}^2\mathbf{M}_{,yz}^{\mathbf{T}}$
$\mathbf{k}_{\mathbf{pg14}}$	$4GI_{xT}\mathbf{M}_{,yz}w_{Tp,z}\mathbf{M}_{,yz}^{\mathbf{T}}$	$\mathbf{k}_{\mathbf{PG45}}$	$-\sigma_{zTp}\frac{h}{2}A_T\mathbf{M}_{,z}\theta_{xp}\mathbf{M}_{,zz}^{\mathbf{T}}$
$\mathbf{k}_{\mathbf{PG14}}$	$EI_{yT}\mathbf{M}_{,y}\theta_{xp,z}^2\mathbf{M}_{,y}^{\mathbf{T}}$	$\mathbf{k}_{\mathbf{PG46}}$	$-\sigma_{zTp}\frac{h}{2}A_T\mathbf{M}_{,z}\theta_{xp,z}\mathbf{M}_{,z}^{\mathbf{T}}$
$\mathbf{k}_{\mathbf{PG15}}$	$EI_{yT}\mathbf{M}_{,yz}\left(\theta_{xp}+v_{p,z}\right)^2\mathbf{M}_{,yz}^{\mathbf{T}}$	$\mathbf{k}_{\mathbf{PG47}}$	$-\sigma_{zTp}I_{yT}\mathbf{M}_{,yz}\theta_{xp}\mathbf{M}_{,zz}^{\mathbf{T}}$
$\mathbf{k}_{\mathbf{PG16}}$	$2EI_{yT}\mathbf{M}_{,y}\left(\theta_{xp}+v_{p,z}\right)\theta_{xp,z}\mathbf{M}_{,yz}^{\mathbf{T}}$	$\mathbf{k}_{\mathbf{PG48}}$	$-\sigma_{zTp}I_{yT}\mathbf{M}_{,yz}\theta_{xp,z}\mathbf{M}_{,z}^{\mathbf{T}}$
$\mathbf{k}_{\mathbf{pg13}}$	$-EI_{yT}\mathbf{M}_{,zz}\theta_{xp}v_{p,z}\mathbf{M}_{,zz}^{\mathbf{T}}$	$\mathbf{k}_{\mathbf{PG49}}$	$-2\sigma_{zTp}I_{yT}\mathbf{M}_{,yz}\theta_{xp,z}\theta_{xp}\mathbf{M}_{,y}^{\mathbf{T}}$
$\mathbf{k}_{\mathbf{pg14}}$	$-EI_{yT}\mathbf{M}_{,zz}\theta_{xp,z}v_{p,z}\mathbf{M}_{,z}^{\mathbf{T}}$	$\mathbf{k}_{\mathbf{PG50}}$	$-\sigma_{zTp}I_{yT}\mathbf{M}_{,yz}\theta_{xp}^2\mathbf{M}_{,yz}^{\mathbf{T}}$
$\mathbf{k}_{\mathbf{PG10}}$	$EI_{yT}\mathbf{M}_{,y}\theta_{xp,z}^2\mathbf{M}_{,y}^{\mathbf{T}}$	$\mathbf{k}_{\mathbf{PG51}}$	$-\sigma_{zTp}hI_{yT}\mathbf{M}_{,yz}\theta_{xp,z}\mathbf{M}_{,yz}^{\mathbf{T}}$
$\mathbf{k}_{\mathbf{PG11}}$	$EI_{yT}\mathbf{M}_{,yz}\left(\theta_{xp}+v_{p,z}\right)^2\mathbf{M}_{,yz}^{\mathbf{T}}$	$\mathbf{k}_{\mathbf{PG52}}$	$-\sigma_{zTp}\frac{h}{2}I_{yT}\mathbf{M}_{,yz}\theta_{xp}\theta_{xp,z}\mathbf{M}_{,zz}^{\mathbf{T}}$

$\mathbf{k}_{\mathbf{PG12}}$	$2EI_{yT}\mathbf{M}_{,\mathrm{y}}\left(\theta_{xp}+v_{p,z}\right)\theta_{xp,z}\mathbf{M}^{\mathbf{T}}_{,\mathrm{yz}}$	$\mathbf{k}_{\mathbf{PG53}}$	$\sigma_{zTp}\dfrac{h}{2}I_{yT}\mathbf{M}_{,\mathrm{yz}}\theta^2_{xp,z}\mathbf{M}^{\mathbf{T}}_{,z}$
$\mathbf{k}_{\mathbf{PG13}}$	$E\dfrac{h^2}{16}I_{yT}\mathbf{M}_{,\mathrm{z}}\theta^2_{xp,zz}\mathbf{M}^{\mathbf{T}}_{,\mathrm{z}}$	$\mathbf{k}_{\mathbf{PG54}}$	$-\sigma_{zTp}hI_{yT}\mathbf{M}_{,\mathrm{yz}}\theta_{xp}\mathbf{M}^{\mathbf{T}}_{,\mathrm{zz}}$
$\mathbf{k}_{\mathbf{PG14}}$	$E\dfrac{h^2}{16}I_{yT}\mathbf{M}_{,\mathrm{zzz}}\theta^2_{xp}\mathbf{M}^{\mathbf{T}}_{,\mathrm{zzz}}$	$\mathbf{k}_{\mathbf{PG55}}$	$\sigma_{zTp}\dfrac{h}{2}I_{yT}\mathbf{M}_{,\mathrm{yz}}\theta_{xp}\theta_{xp,zz}\mathbf{M}^{\mathbf{T}}_{,\mathrm{z}}$
$\mathbf{k}_{\mathbf{PG15}}$	$-E\dfrac{h^2}{8}I_{yT}\mathbf{M}_{,\mathrm{zzz}}\theta_{xp}\theta_{xp,zz}\mathbf{M}^{\mathbf{T}}_{,\mathrm{z}}$	$\mathbf{k}_{\mathbf{PG56}}$	$-\sigma_{zTp}\dfrac{h}{2}I_{yT}\mathbf{M}_{,\mathrm{yz}}\theta^2_{xp}\mathbf{M}^{\mathbf{T}}_{,\mathrm{zzz}}$
$\mathbf{k}_{\mathbf{PG16}}$	$-EI_{yT}\mathbf{M}_{,\mathrm{zz}}v_{p,z}\theta_{xp}\mathbf{M}^{\mathbf{T}}_{,\mathrm{zz}}$	$\mathbf{k}_{\mathbf{PG57}}$	$\sigma_{zTp}\dfrac{h^2}{2}A_T\mathbf{M}_{,\mathrm{yz}}\theta_{xp}\theta_{xp,z}\mathbf{M}^{\mathbf{T}}_{,\mathrm{y}}$
$\mathbf{k}_{\mathbf{PG17}}$	$-EI_{yT}\mathbf{M}_{,\mathrm{zz}}v_{p,z}\theta_{xp,z}\mathbf{M}^{\mathbf{T}}_{,\mathrm{z}}$	$\mathbf{k}_{\mathbf{3PG1}}$	$\sigma_{zTp}\dfrac{h^2}{16}A_T\mathbf{M}_{,\mathrm{zz}}\theta^2_{xp}\mathbf{M}^{\mathbf{T}}_{,\mathrm{zz}}$
$\mathbf{k}_{\mathbf{PG18}}$	$-E\dfrac{h}{2}I_{yT}\mathbf{M}_{,\mathrm{yz}}\left(\theta_{xp}+v_{p,z}\right)\theta_{xp,zz}\mathbf{M}^{\mathbf{T}}_{,\mathrm{z}}$	$\mathbf{k}_{\mathbf{3PG2}}$	$\sigma_{zTp}\dfrac{h^2}{16}A_T\mathbf{M}_{,\mathrm{z}}\theta^2_{xp,z}\mathbf{M}^{\mathbf{T}}_{,\mathrm{z}}$
$\mathbf{k}_{\mathbf{PG19}}$	$E\dfrac{h}{2}I_{yT}\mathbf{M}_{,\mathrm{yz}}\left(\theta_{xp}+v_{p,z}\right)\theta_{xp}\mathbf{M}^{\mathbf{T}}_{,\mathrm{zzz}}$	$\mathbf{k}_{\mathbf{3PG3}}$	$\sigma_{zTp}\dfrac{h^2}{8}A_T\mathbf{M}_{\mathrm{zz}}\theta_{xp}\theta_{xp,z}\mathbf{M}^{\mathbf{T}}_{,z}$
$\mathbf{k}_{\mathbf{PG20}}$	$-E\dfrac{h}{2}I_{yT}\mathbf{M}_{,\mathrm{y}}\theta_{xp,z}\theta_{xp,zz}\mathbf{M}^{\mathbf{T}}_{,\mathrm{z}}$	$\mathbf{k}_{\mathbf{3PG4}}$	$\dfrac{1}{4}\sigma_{zTp}A_T\mathbf{M}_{,zz}\theta^2_{xp}\mathbf{M}^{\mathbf{T}}_{,zz}$
$\mathbf{k}_{\mathbf{PG21}}$	$E\dfrac{h}{2}I_{yT}\mathbf{M}_{,\mathrm{y}}\theta_{xp}\theta_{xp,z}\mathbf{M}^{\mathbf{T}}_{,\mathrm{zzz}}$	$\mathbf{k}_{\mathbf{3PG5}}$	$\dfrac{1}{4}\sigma_{zTp}A_T\mathbf{M}_{,\mathrm{z}}\theta^2_{xp,z}\mathbf{M}^{\mathbf{T}}_{,z}$
$\mathbf{k}_{\mathbf{PG22}}$	$-EhI_{yT}\mathbf{M}_{,\mathrm{yz}}\theta_{xp,z}v_{p,z}\mathbf{M}^{\mathbf{T}}_{,\mathrm{zz}}$	$\mathbf{k}_{\mathbf{3PG6}}$	$\dfrac{1}{2}\sigma_{zTp}A_T\mathbf{M}_{,zz}\theta_{xp}\theta_{xp,z}\mathbf{M}^{\mathbf{T}}_{,z}$
$\mathbf{k}_{\mathbf{PG23}}$	$-EhI_{yT}\mathbf{M}_{,\mathrm{yzz}}\theta_{xp}v_{p,z}\mathbf{M}^{\mathbf{T}}_{,\mathrm{zz}}$	$\mathbf{k}_{\mathbf{3PG7}}$	$\dfrac{h^2}{4}\sigma_{zTp}I_{yT}\mathbf{M}_{,\mathrm{yzz}}\theta^2_{xp}\mathbf{M}^{\mathbf{T}}_{,\mathrm{yzz}}$
$\mathbf{k}_{\mathbf{PG24}}$	$GA_T\mathbf{M}_{,\mathrm{y}}\left(\theta_{xp}+v_{p,z}\right)^2\mathbf{M}^{\mathbf{T}}_{,\mathrm{y}}$	$\mathbf{k}_{\mathbf{3PG8}}$	$\dfrac{h^2}{4}\sigma_{zTp}I_{yT}\mathbf{M}_{,\mathrm{yz}}\theta^2_{xp,z}\mathbf{M}^{\mathbf{T}}_{,\mathrm{yz}}$
$\mathbf{k}_{\mathbf{PG25}}$	$GA_T\mathbf{M}_{,z}w^2_{Tp,z}\mathbf{M}^{\mathbf{T}}_{,z}$	$\mathbf{k}_{\mathbf{3PG9}}$	$\dfrac{h^2}{2}\sigma_{zTp}I_{yT}\mathbf{M}_{,\mathrm{yzz}}\theta_{xp}\theta_{xp,z}\mathbf{M}^{\mathbf{T}}_{,\mathrm{yz}}$
$\mathbf{k}_{\mathbf{PG26}}$	$GI_{xT}\mathbf{M}_{,\mathrm{yz}}w^2_{Tp,z}\mathbf{M}^{\mathbf{T}}_{,\mathrm{yz}}$	$\mathbf{k}_{\mathbf{3PG10}}$	$-\dfrac{h}{2}\sigma_{zTp}A_T\mathbf{M}_{,\mathrm{zz}}\theta_{xp}v_{p,z}\mathbf{M}^{\mathbf{T}}_{,\mathrm{y}}$
$\mathbf{k}_{\mathbf{PG27}}$	$GI_{xT}\mathbf{M}_{,\mathrm{z}}\theta^2_{xp,z}\mathbf{M}^{\mathbf{T}}_{,\mathrm{z}}$	$\mathbf{k}_{\mathbf{3PG11}}$	$-\dfrac{h}{2}\sigma_{zTp}A_T\mathbf{M}_{,\mathrm{z}}\theta_{xp,z}v_{p,z}\mathbf{M}^{\mathbf{T}}_{,\mathrm{y}}$

$\mathbf{k}_{\mathbf{PG28}}$	$3\frac{t^2}{20}GI_{xT}\mathbf{M}_{,\mathrm{yz}}\theta_{xp,z}^2\mathbf{M}_{,\mathrm{yz}}^{\mathbf{T}}$	$\mathbf{k}_{\mathbf{3PG12}}$	$-\frac{h}{2}\sigma_{zTp}A_T\mathbf{M}_{,\mathrm{z}}\theta_{xp}v_{p,z}\mathbf{M}_{,\mathrm{yz}}^{\mathbf{T}}$
$\mathbf{k}_{\mathbf{PG29}}$	$-4GI_{xT}\mathbf{M}_{,\mathrm{yz}}\theta_{xp}\theta_{xp,z}\mathbf{M}_{,\mathrm{y}}^{\mathbf{T}}$	$\mathbf{k}_{\mathbf{3PG13}}$	$\frac{h}{2}\sigma_{zTp}A_T\mathbf{M}_{,\mathrm{zz}}\theta_{xp}\theta_{xp,z}\mathbf{M}_{,\mathrm{yz}}^{\mathbf{T}}$
$\mathbf{k}_{\mathbf{PG30}}$	$GhI_{xT}\mathbf{M}_{,\mathrm{yz}}\theta_{xp,z}^2\mathbf{M}_{,\mathrm{z}}^{\mathbf{T}}$	$\mathbf{k}_{\mathbf{3PG14}}$	$\frac{h}{2}\sigma_{zTp}A_T\mathbf{M}_{,\mathrm{yz}}\theta_{xp,z}^2\mathbf{M}_{,\mathrm{z}}^{\mathbf{T}}$
$\mathbf{k}_{\mathbf{PG31}}$	$-GhI_{xT}\mathbf{M}_{,\mathrm{yz}}\theta_{xp}\theta_{xp,z}\mathbf{M}_{,\mathrm{zz}}^{\mathbf{T}}$	$\mathbf{k}_{\mathbf{3PG15}}$	$\frac{h}{2}\sigma_{zTp}A_T\mathbf{M}_{,\mathrm{yzz}}\theta_{xp}^2\mathbf{M}_{,\mathrm{zz}}^{\mathbf{T}}$
$\mathbf{k}_{\mathbf{PG32}}$	$2GA_T\mathbf{M}_{,\mathrm{y}}\left(\theta_{xp}+v_{p,z}\right)w_{Tp,z}\mathbf{M}_{,\mathrm{z}}^{\mathbf{T}}$	$\mathbf{k}_{\mathbf{3PG16}}$	$\frac{h}{2}\sigma_{zTp}A_T\mathbf{M}_{,yzz}\theta_{xp}\theta_{xp,z}\mathbf{M}_{,z}^{\mathbf{T}}$
$\mathbf{k}_{\mathbf{PG33}}$	$-2GI_{xT}\mathbf{M}_{,\mathrm{y}}\left(\theta_{xp}+v_{p,z}\right)\theta_{xp,z}\mathbf{M}_{,\mathrm{yz}}^{\mathbf{T}}$		

Similar expressions can be written for the bottom flange are obtained be setting $y = h/2$ instead of $y = -h/2$. As a result, the bottom flange matrices corresponding to1 $\mathbf{k}_{\mathbf{pg10}}$ - $\mathbf{k}_{\mathbf{pg12}}$, $\mathbf{k}_{\mathbf{PG18}}$ - $\mathbf{k}_{\mathbf{PG23}}$, $\mathbf{k}_{\mathbf{PG35}}$ - $\mathbf{k}_{\mathbf{PG37}}$, $\mathbf{k}_{\mathbf{PG39}}$ - $\mathbf{k}_{\mathbf{PG40}}$, $\mathbf{k}_{\mathbf{PG45}}$ - $\mathbf{k}_{\mathbf{PG46}}$, $\mathbf{k}_{\mathbf{PG55}}$ - $\mathbf{k}_{\mathbf{PG56}}$ and $\mathbf{k}_{\mathbf{3PG10}}$ - $\mathbf{k}_{\mathbf{3PG16}}$ are similar to those of the top flange matrices but multiplied by -1 and the remaining bottom flange matrices are identical to those of the top flange.

6.17. Appendix C

The second variation of the total potential energy (Eq. (6.42)), takes the matrix form

$$\bar{\bar{\Pi}} = \left\langle \hat{\mathbf{u}}_{\mathbf{b-1}}^{\mathbf{T}} \;\vdots\; \hat{\mathbf{u}}_{\mathbf{b-i}}^{\mathbf{T}} \;\vdots\; \hat{\mathbf{u}}_{\mathbf{b-2}}^{\mathbf{T}} \right\rangle^{\mathbf{T}} \begin{bmatrix} \mathbf{k}_{\mathbf{t-11}} & \mathbf{k}_{\mathbf{t-1i}} & \mathbf{k}_{\mathbf{t-13}} \\ \mathbf{k}_{\mathbf{t-1i}}^{\mathbf{T}} & \mathbf{k}_{\mathbf{t-ii}} & \mathbf{k}_{\mathbf{t-i3}} \\ \mathbf{k}_{\mathbf{t-13}}^{\mathbf{T}} & \mathbf{k}_{\mathbf{t-i3}}^{\mathbf{T}} & \mathbf{k}_{\mathbf{t-33}} \end{bmatrix} \begin{Bmatrix} \hat{\mathbf{u}}_{\mathbf{b-1}} \\ \hat{\mathbf{u}}_{\mathbf{b-i}} \\ \hat{\mathbf{u}}_{\mathbf{b-2}} \end{Bmatrix} \tag{6.49}$$

From Eq. (6.44), one enforces the kinematic constraint on nodal displacements($\hat{\mathbf{u}}_{\mathbf{b-i}}$) of node i, i.e.

$$\hat{\mathbf{u}}_{\mathbf{b-i}(10\times1)} = \mathbf{C}_{10\times6}\hat{\underset{\sim}{\mathbf{u}}}_{\mathbf{b-i}(6\times1)}$$

hence, the structure nodal displacement vector $\hat{\mathbf{u}}_{\mathbf{b}}$ is transformed to the modified structure nodal displacements vector $\hat{\underset{\sim}{\mathbf{u}}}_{\mathbf{b}}$, i.e.,

$$\left\{\begin{array}{c}\hat{\mathbf{u}}_{\mathbf{b-1}}\\ \hdashline \hat{\mathbf{u}}_{\mathbf{b-i}}\\ \hdashline \hat{\mathbf{u}}_{\mathbf{b-2}}\end{array}\right\}_{\mathbf{10n\times1}}=\begin{bmatrix}\mathbf{I} & & \\ & \mathbf{C}_{\mathbf{10\times6}} & \\ & & \mathbf{I}\end{bmatrix}_{(\mathbf{10n\times1})\times(\mathbf{10n}-4)}\left\{\begin{array}{c}\hat{\mathbf{u}}_{\mathbf{b-1}}\\ \hdashline \underset{\sim}{\hat{\mathbf{u}}}_{\mathbf{b-i}}\\ \hdashline \hat{\mathbf{u}}_{\mathbf{b-2}}\end{array}\right\}_{(\mathbf{10n}-4)\times\mathbf{1}} \tag{6.50}$$

From Eq. (6.50) by substituting into Eq. (6.49), the modified second variation of total potential energy is recovered as

$$\bar{\bar{\Pi}}=\underset{\sim}{\bar{\mathbf{u}}}_{\mathbf{b}}^{\mathbf{T}}\underset{\sim}{\mathbf{K}}_{\mathbf{T}}(\lambda)\underset{\sim}{\bar{\mathbf{u}}}_{\mathbf{b}}=\left\langle \hat{\mathbf{u}}_{\mathbf{b-1}}^{\mathbf{T}} \;\vdots\; \underset{\sim}{\hat{\mathbf{u}}}_{\mathbf{b-i}}^{\mathbf{T}} \;\vdots\; \hat{\mathbf{u}}_{\mathbf{b-2}}^{\mathbf{T}}\right\rangle^{\mathbf{T}}\begin{bmatrix}\mathbf{I} & & \\ & \mathbf{C}_{\mathbf{10\times6}}^{\mathbf{T}} & \\ & & \mathbf{I}\end{bmatrix}\left[\begin{array}{c:c:c}\mathbf{k}_{\mathbf{t-11}} & \mathbf{k}_{\mathbf{t-1i}} & \mathbf{k}_{\mathbf{t-13}}\\ \hdashline \mathbf{k}_{\mathbf{t-1i}}^{\mathbf{T}} & \mathbf{k}_{\mathbf{t-ii}} & \mathbf{k}_{\mathbf{t-i3}}\\ \hdashline \mathbf{k}_{\mathbf{t-13}}^{\mathbf{T}} & \mathbf{k}_{\mathbf{t-i3}}^{\mathbf{T}} & \mathbf{k}_{\mathbf{t-33}}\end{array}\right]\begin{bmatrix}\mathbf{I} & & \\ & \mathbf{C}_{\mathbf{10\times6}} & \\ & & \mathbf{I}\end{bmatrix}\left\{\begin{array}{c}\hat{\mathbf{u}}_{\mathbf{b-1}}^{\mathbf{T}}\\ \hdashline \underset{\sim}{\hat{\mathbf{u}}}_{\mathbf{b-i}}^{\mathbf{T}}\\ \hdashline \hat{\mathbf{u}}_{\mathbf{b-2}}^{\mathbf{T}}\end{array}\right\}$$

Thus, one obtains the entries of the modified structure stiffness matrix $\underset{\sim}{\mathbf{K}}_{\mathbf{T}}(\lambda)$ as

$$\underset{\sim}{\mathbf{K}}_{\mathbf{T}}(\lambda)_{(\mathbf{10n-4})\times(\mathbf{10n-4})}=\left[\begin{array}{c:c:c}\mathbf{k}_{\mathbf{t-11}} & \mathbf{k}_{\mathbf{t-1i}}\mathbf{C} & \mathbf{k}_{\mathbf{t-13}}\\ \hdashline \mathbf{C}^{\mathbf{T}}\mathbf{k}_{\mathbf{t-1i}}^{\mathbf{T}} & \mathbf{C}^{\mathbf{T}}\mathbf{k}_{\mathbf{t-ii}}\mathbf{C} & \mathbf{C}^{\mathbf{T}}\mathbf{k}_{\mathbf{t-i3}}\\ \hdashline \mathbf{k}_{\mathbf{t-13}}^{\mathbf{T}} & \mathbf{k}_{\mathbf{t-i3}}^{\mathbf{T}}\mathbf{C} & \mathbf{k}_{\mathbf{t-33}}\end{array}\right]=\left[\begin{array}{c:c:c}\mathbf{k}_{\mathbf{E-11}} & \mathbf{k}_{\mathbf{E-1i}}\mathbf{C} & \mathbf{k}_{\mathbf{E-12}}\\ \hdashline \mathbf{C}^{\mathbf{T}}\mathbf{k}_{\mathbf{E-1i}}^{\mathbf{T}} & \mathbf{C}^{\mathbf{T}}\mathbf{k}_{\mathbf{E-ii}}\mathbf{C} & \mathbf{C}^{\mathbf{T}}\mathbf{k}_{\mathbf{E-i2}}\\ \hdashline \mathbf{k}_{\mathbf{E-12}}^{\mathbf{T}} & \mathbf{k}_{\mathbf{E-i2}}^{\mathbf{T}}\mathbf{C} & \mathbf{k}_{\mathbf{E-22}}\end{array}\right]$$

$$+\lambda\left[\begin{array}{c:c:c}\mathbf{k}_{\mathbf{G1-11}} & \mathbf{k}_{\mathbf{G1-1i}} & \mathbf{k}_{\mathbf{G1-12}}\\ \hdashline \mathbf{C}^{\mathbf{T}}\mathbf{k}_{\mathbf{G1-1i}}^{\mathbf{T}} & \mathbf{C}^{\mathbf{T}}\mathbf{k}_{\mathbf{G1-ii}} & \mathbf{C}^{\mathbf{T}}\mathbf{k}_{\mathbf{G1-i2}}\\ \hdashline \mathbf{k}_{\mathbf{G1-12}}^{\mathbf{T}} & \mathbf{k}_{\mathbf{G1-i2}}^{\mathbf{T}} & \mathbf{k}_{\mathbf{G1-22}}\end{array}\right]+\lambda^{2}\left[\begin{array}{c:c:c}\mathbf{k}_{\mathbf{G2-11}} & \mathbf{k}_{\mathbf{G2-1i}} & \mathbf{k}_{\mathbf{G2-12}}\\ \hdashline \mathbf{C}^{\mathbf{T}}\mathbf{k}_{\mathbf{G2-1i}}^{\mathbf{T}} & \mathbf{C}^{\mathbf{T}}\mathbf{k}_{\mathbf{G2-ii}} & \mathbf{C}^{\mathbf{T}}\mathbf{k}_{\mathbf{G2-i2}}\\ \hdashline \mathbf{k}_{\mathbf{G2-12}}^{\mathbf{T}} & \mathbf{k}_{\mathbf{G2-i2}}^{\mathbf{T}} & \mathbf{k}_{\mathbf{G2-22}}\end{array}\right]$$

$$+\lambda^{3}\left[\begin{array}{c:c:c}\mathbf{k}_{\mathbf{G3-11}} & \mathbf{k}_{\mathbf{G3-1i}} & \mathbf{k}_{\mathbf{G3-12}}\\ \hdashline \mathbf{C}^{\mathbf{T}}\mathbf{k}_{\mathbf{G3-1i}}^{\mathbf{T}} & \mathbf{C}^{\mathbf{T}}\mathbf{k}_{\mathbf{G3-ii}} & \mathbf{C}^{\mathbf{T}}\mathbf{k}_{\mathbf{G3-i2}}\\ \hdashline \mathbf{k}_{\mathbf{G3-12}}^{\mathbf{T}} & \mathbf{k}_{\mathbf{G3-i2}}^{\mathbf{T}} & \mathbf{k}_{\mathbf{G3-22}}\end{array}\right]$$

6.18. List of symbols

Subscripts T, B and W denote the correspondence to Top and Bottom flanges and the Web respectively.

γ_{xzT}	Total shear strain within the xz plane for the top flange
$\gamma_{xzLT},\gamma_{xzNT}$	Linear and nonlinear contributions of the shear strain within the xz plane for the top flange
$\gamma_{xzTp},\gamma_{xzTb}$	Pre-buckling and buckling contributions of the shear strain within the xz plane for the top flange
γ_{yz}	Total shear strain within the yz plane for the web

$\gamma_{yzL}, \gamma_{yzN}$	Linear and nonlinear contributions of the shear strain within the yz plane for the web
$\gamma_{yzp}, \gamma_{yzb}$	Pre-buckling and buckling contributions of the shear strain within the yz plane for the web
$\sigma_{zp}(y,z), \sigma_{zTp}(z), \sigma_{zBp}(z)$	Pre-buckling normal stresses within the web, top and bottom flanges
$\sigma_{zb}(y,z), \sigma_{zTb}(z), \sigma_{zBb}(z)$	Buckling normal stresses within the web, top and bottom flanges
$\sigma_{yp}(y,z)$	Pre-buckling transverse stresses within the web
λ	Buckling load multiplier
$\varepsilon_{zB}, \varepsilon_{zT}, \varepsilon_{z}$	Total normal strain along the *z* direction
$\varepsilon_{zLT}, \varepsilon_{zNT}, \varepsilon_{zL}, \varepsilon_{zN}$	Linear and nonlinear contributions of normal strain along the *z* direction
$\varepsilon_{zTp}, \varepsilon_{zp}, \varepsilon_{zTb}, \varepsilon_{zb}$	Pre-buckling and buckling contributions of normal strain
ε_{y}	Total transverse strain along the *y* direction
$\varepsilon_{yL}, \varepsilon_{yN}$	Linear and nonlinear contributions of transverse strain along the *y* direction
ε_{yb}	Buckling contributions of transverse strain
θ_{Bb}, θ_{Tb}	Angle of twist at the flange to web junction onset of buckling
θ_{x0}, θ_{xL}	Strong-axis angle of rotation at both ends of the element
$\theta_{xp}(z)$	Pre-buckling strong-axis angle of rotation expression
$\Delta_{b}(z)$	The vertical distance travelled by the transverse load
ν	Poisson’s ratio
Π	Total energy of the system
$\tau_{yzp}(y,z), \tau_{yzb}(y,z)$	Pre-buckling and buckling shear stresses within the plane of the web
τ_{xzT}	Total shear stresses within the plane of the top flange

τ_{xzTp}	Pre-buckling shear stresses within the plane of the flange
A_B, A_T, A_W, A	Cross sectional areas for bottom and top flanges, web and the entire section
b	Flange width
C	Matrix of kinematic constraints
D	Flexural rigidity of the web
E	Modulus of elasticity
F	Structure nodal force vector
G	Shear modulus
$H_1(y) \sim H_4(y)$	Cubic shape functions
h	Height of the cross section, measured along the flanges centerline
I_{xF}, I_{xxW}, I_{yF}	Moment of inertia about x and y axes
I_x	Cross sectional moment of inertia about x axis
K_D	Structure geometric displacement-base stiffness matrix
K_E	Structure elastic stiffness matrix
K_G	Structure geometric force-base stiffness matrix
K_{EB}, K_{ET}, K_{EW}	Buckling elastic stiffness matrix
$K_{G1B}, K_{G1T}, K_{G1W}$	Buckling first order geometric stiffness matrix
$K_{G2B}, K_{G2T}, K_{G2W}$	Buckling second order geometric stiffness matrix
K_{G3B}, K_{G3T}	Buckling third order geometric stiffness matrix
K_T	Total buckling stiffness matrix
K_{Tp}	Structure pre-buckling tangent stiffness matrix
K_V	Contribution of the load potential energy
$k_1 - k_7$	Buckling elastic stiffness sub-matrices

k_{g1} - k_{g7}	Buckling geometric stiffness sub-matrices
k_{pg1} - k_{pg14}	Buckling first order geometric stiffness sub-matrices due to PBD effect
k_{PG1} - k_{PG60}	Buckling second order geometric stiffness sub-matrices due to PBD effect
k_{3PG1} - k_{3PG16}	Buckling third order geometric stiffness sub-matrices due to PBD effect
L	Beam span
$M_{20\times1}(y,z)$	Vector of element shape functions
M_1, M_2	Bending moments at both ends of the element
$M_P(z)$	Pre-buckling strong-axis bending moment expression for the element
$M_{(ND)}$	Critical moments based on classical solution
$M_{(ND+P)}$	Critical moments based on classical solution including PBD effect
$M_{(ND+P+S)}$	Critical moments based on classical solution including PBD and shear deformations effect
$M_{(D)}$	Critical moments based on distortional solution
$M_{(D+P)}$	Critical moments based on distortional solution including PBD effect
$M_{(D+P+S)}$	Critical moments based on distortional solution including PBD and shear deformations effect
$N_P(z)$	Pre-buckling normal force expression for the element
N_{zp}	Pre-buckling normal traction across the edge of the web
N_{yzp}	Pre-buckling shear traction across the edge of the web
n_B, n_T, n	Normal component of local coordinate system
P_1, P_2	Axial forces at both ends of the element

$Q_{1\times 6}(z)$	Vector of quintic shape functions
$Q_x(y)$	Cross sectional first moment of inertia about x axis
$q_y(z)$	Transverse distributed load, along *z* axis
$q_z(z)$	Longitudinal distributed load, along *z* axis
t	Thickness of the flange
U_B, U_T, U_W	Internal strain energy
u_{Bb}, u_{Tb}	Lateral displacements at the flanges centroid onset of buckling
$\widehat{u}_B(x, n_B, z), \widehat{u}_T(x, n_T, z), \widehat{u}_b(y, z)$	Total lateral displacement (from Configurations 1 to 4)
u_b	Lateral displacements of the web onset of buckling
$\hat{u}_b$	Vector of buckling nodal displacements
u_p	pre-buckling nodal displacement vector
$\hat{\mathbf{u}}_{\mathbf{b}(20\times 1)}$	Buckling nodal displacements vector
V	Total potential energy gained by the loads
V_1, V_2	Transverse shear forces at both ends of the element
$V_P(z)$	Pre-buckling shear force expression for the element
$\widehat{v}_B(x, n_B, z), \widehat{v}_T(x, n_T, z), \widehat{v}(n, y, z)$	Total transverse displacement (from Configurations 1 to 4)
v_0, v_L	Transverse displacement at both ends of the element
$v_p(z)$	Pre-buckling transverse displacement
w	Web thickness
$\widehat{w}_B(x, n_B, z), \widehat{w}_T(x, n_T, z), \widehat{w}(n, y, z)$	Total longitudinal displacement (from Configurations 1 to 4)
$w_{Bp}(z), w_{Tp}(z)$	Pre-buckling longitudinal displacement for top and bottom flanges
w_0, w_L	Longitudinal displacement at both ends of the element

$y_{qy}(z)$, $y_{qz}(z)$ curves define the load distance from the shear centre for loads $q_y(z)$ and $q_z(z)$

6.19. References

Ádány, S., and Schafer, B. W. (2008). "A full modal decomposition of thin-walled, single-branched open cross-section members via the constrained finite strip method." *Journal of Constructional Steel Research*, 64(1), 12-29.

Anderson, J. M., and Trahair, N. S. (1972). "Stability of Monosymmetric Beams and Cantilevers." *Journal of the Structural Division, ASCE*, 98(1), 269-286.

Andrade, A., and Camotim, D. (2004). "Lateral-torsional buckling of prismatic and tapered thin-walled open Pre-buckling deflection effects on stability of thin-walled beams with open sections beams: assessing the influence of pre-buckling deflections." *Journal of steel and composite structures*, 4(4), 281-301.

Andreassen, M. J., and Jönsson, J. (2012). "Distortional solutions for loaded semi-discretized thin-walled beams." *Thin-Walled Structures*, 50(1), 116-127.

ANSI/AISC 360-16 (2016). "ANSI/AISC 360-16." *Specification for structural steel buildings*, American Institute of Steel Construction (AISC), Chicago, IL.

AS/NZS 4600-05 (2005). "AS/NZS 4600 Cold Formed Steel Structures." Standards Australia (SA), Sydney, Australia. .

Barsoum, R. S., and Gallagher, R. H. (1970). "Finite element analysis of torsional and torsional–flexural stability problems." *International Journal for Numerical Methods in Engineering*, 2(3), 335-352.

Bradford, and Ronagh (1997). "Generalized Elastic Buckling of Restrained I-Beams by FEM." *Journal of Structural Engineering*, 123(12), 1631-1637.

Bradford, M. A. (1985). "Distortional buckling of monosymmetric I-beams." *Journal of Constructional Steel Research*, 5(2), 123-136.

Bradford, M. A. (1986). "Inelastic distortional buckling of I-beams." *Computers & Structures*, 24(6), 923-933.

Bradford, M. A. (1988a). "Buckling of elastically restrained beams with web distortions." *Thin-Walled Structures*, 6(4), 287-304.

Bradford, M. A. (1988b). "Elastic buckling modes in steel tee-beams." Civil Engineering Transactions, I.E. Aust, 36-38.

Bradford, M. A. (1990a). "Lateral-distortional buckling of tee-section beams." *Thin-Walled Structures*, 10(1), 13-30.

Bradford, M. A. (1990b). "Stability of mono-symmetric beam-columns with thin webs." *Journal of Constructional Steel Research*, 15(4), 323-339.

Bradford, M. A. (1992a). "Buckling of doubly-symmetric cantilevers with slender webs." *Engineering Structures*, 14(5), 327-334.

Bradford, M. A. (1992b). "Lateral-Distortional buckling of steel I—Section members." *Journal of Constructional Steel Research*, 23(1–3), 97-116.

Bradford, M. A. (1999). "Elastic distortional buckling of tee-section cantilevers." *Thin-Walled Structures*, 33(1), 3-17.

Bradford, M. A., and Trahair, N. S. (1981). "Distortional Buckling of I-Beams." *Journal of the Structural Division, ASCE*, 107(2), 355-370.

Bradford, M. A., and Trahair, N. S. (1982). "Distortional buckling of thin-web beam-columns." *Engineering Structures*, 4(1), 2-10.

CAN-CSA S16-14 (2014). "Handbook of Steel Construction." *CSA-S16-14 Specification*, Canadian Institute of Steel Construction, CA.

Chajes, A., and Churchill, J. (1987). "Nonlinear Frame Analysis by Finite Element Methods." *Journal of Structural Engineering*, 113(6), 1221-1235.

Chen, W. E. I., and Ye, J. (2010). "ELASTIC LATERAL AND RESTRAINED DISTORTIONAL BUCKLING OF DOUBLY SYMMETRIC I-BEAMS." *International Journal of Structural Stability and Dynamics*, 10(05), 983-1016.

Chin, C. K., Al-Bermani, F. G. A., and Kitipornchai, S. (1992). "Stability of thin-walled members having arbitrary flange shape and flexible web." *Engineering Structures*, 14(2), 121-132.

Clark, J. W., and Knoll, A. H. (1958). "Effect of deflection on lateral buckling strenght." *J. Engrg. Mech. Div. ASCE*, 84(2), 1596:1591-1596:1518.

Dekker, N. W., and Kemp, A. R. (1998). "A simplified distortional buckling model for doubly symmetrical I-sections." *Canadian Journal of Civil Engineering*, 25(4), 718-727.

EN-1993-1-1-05 (2005). "Eurocode 3: Design of Steel Structures-General Rules and Rules for Buildings." European Committee of Standardization (CEN), Brussels, Belgium.

Erkmen, R. E., and Attard, M. M. (2011). "Lateral–torsional buckling analysis of thin-walled beams including shear and pre-buckling deformation effects." *International Journal of Mechanical Sciences*, 53(10), 918-925.

Friedman, Z., and Kosmatka, J. B. (1993). "An improved two-node timoshenko beam finite element." *Computers & Structures*, 47(3), 473-481.

Gjelsvik, A. (1981). *The theory of thin walled bars / Atle Gjelsvik*, Wiley, New York, NY, USA.

Hancock, G. J. (1978). "Local, Distortional, and Lateral Buckling of I-Beams." *Journal of the Structural Division*, 104(11), 1787-1798.

Hancock, G. J., Bradford, M. A., and Trahair, N. S. (1980). "Web distortion and flexural-torsional buckling." *Journal of the Structural Division, ASCE*, 106(7), 1557-1571.

Hassan, R., and Mohareb, M. (2015). "Distortional lateral torsional buckling for simply supported beams with web cleats." *Canadian Journal of Civil Engineering*, 42(12), 1091-1103.

Hong, G., Wang, C., and Kanok-Nukulchai, W. (1993b). "Elastic Buckling of Circular Plates Allowing for Prebuckling Deformation." *Journal of Engineering Mechanics*, 119(5), 905-916.

Hong, G. M., Wang, C. M., and Tan, T. J. (1993a). "Analytical buckling solutions for circular Mindlin plates: inclusion of inplane prebuckling deformation." *Arch. Appl. Mech.*, 63(8), 534-542.

Hughes, O., and Ma, M. (1996a). "Lateral Distortional Buckling of Monosymmetric Beams under Point Load." *Journal of Engineering Mechanics*, 122(10), 1022-1029.

Kalkan, I., and Buyukkaragoz, A. (2012). "A numerical and analytical study on distortional buckling of doubly-symmetric steel I-beams." *Journal of Constructional Steel Research*, 70(0), 289-297.

Kumar, A., and Samanta, A. (2006c). "Distortional buckling in monosymmetric I-beams: Reverse-curvature bending." *Thin-Walled Structures*, 44(7), 721-725.

Liew, K. M., Xiang, Y., and Kitipornchai, S. (1996). "Navier's solution for laminated plate buckling with prebuckling in-plane deformation." *International Journal of Solids and Structures*, 33(13), 1921-1937.

Ma, M., and Hughes, O. (1996b). "Lateral distortional buckling of monosymmetric I-beams under distributed vertical load." *Thin-Walled Structures*, 26(2), 123-145.

Machado, S. P., and Cortínez, V. H. (2005). "Lateral buckling of thin-walled composite bisymmetric beams with prebuckling and shear deformation." *Engineering Structures*, 27(8), 1185-1196.

Mohri, F., Damil, N., and Potier-Ferry, M. (2012). "Pre-buckling deflection effects on stability of thin-walled beams with open sections." *Steel and Composite Structures*, 13(1), 71-89.

Mohri, F., and Potier-Ferry, M. (2006). "EFFECTS OF LOAD HEIGHT APPLICATION AND PRE-BUCKLING DEFLECTIONS ON LATERAL BUCKLING OF THIN-WALLED BEAMS." *Journal of steel and composite structures*, 6(5), 401-415.

Ng, M. L.-H., and Ronagh, H. R. (2004). "An Analytical Solution for the Elastic Lateral-Distortional Buckling of I-section Beams." *Advances in Structural Engineering*, 7(2), 189-200

Ng, M. L., and Ronagh, H. R. (2009). "An Analytical Solution for the Elastic Lateral-Distortional Buckling of I-section Beams." *Advances in Structural Engineering*, 7(2).

Pezeshky, P., and Mohareb, M. (2014). "Distortional theory for the analysis of wide flange steel beams." *Engineering Structures*, 75, 181-196.

Pezeshky, P., and Mohareb, M. (2015). "Finite-Element Formulations for the Distortional Analysis of Wide Flange Steel Beams." *Journal of Engineering Mechanics*, 04015071.

Pi, Y., and Trahair, N. (1992b). "Prebuckling Deflections and Lateral Buckling. I: Theory." *Journal of Structural Engineering*, 118(11), 2949-2966.

Pi, Y., and Trahair, N. (1992c). "Prebuckling Deflections and Lateral Buckling. II: Applications." *Journal of Structural Engineering*, 118(11), 2967-2985.

Pi, Y., and Trahair, N. (2000). "Distortion and Warping at Beam Supports." *Journal of Structural Engineering*, 126(11), 1279-1287.

Pi, Y., Trahair, N., and Rajasekaran, S. (1992a). "Energy Equation for Beam Lateral Buckling." *Journal of Structural Engineering*, 118(6), 1462-1479.

Roberts, T., and Azizian, Z. (1983a). "Instability of Thin Walled Bars." *Journal of Engineering Mechanics*, 109(3), 781-794.

Roberts, T. M., and Azizian, Z. G. (1983d). "Influence of pre-buckling displacements on the elastic critical loads of thin walled bars of open cross section." *International Journal of Mechanical Sciences*, 25(2), 93-104.

Roberts, T. M., and Jhita, P. S. (1983b). "Lateral, local and distortional buckling of I-beams." *Thin-Walled Structures*, 1(4), 289-308.

Ronagh, H. R., and Bradford, M. A. (1994). "Some notes on finite element buckling formulations for beams." *Computers & Structures*, 52(6), 1119-1126.

Samanta, A., and Kumar, A. (2006b). "Distortional buckling in monosymmetric I-beams." *Thin-Walled Structures*, 44(1), 51-56.

Samanta, A., and Kumar, A. (2008). "Distortional buckling in braced-cantilever I-beams." *Thin-Walled Structures*, 46(6), 637-645.

SIMULIA. 2011a. Abaqus/CAE Analysis, version 6.11-1Dassault Systemes.

SIMULIA. 2011b. Abaqus/CAE User's Manual, version 6.11-1Dassault Systemes.

Trahair, N. S. (2009). "Lateral–distortional buckling of monorails." *Engineering Structures*, 31(12), 2873-2879.

Trahair, N. S., and Woolcock, S. T. (1973). "Effect of major axis curvature on I-beam stability." *J. Engrg. Mech. Div. , ASCE*, 99(1), 85-98.

Vacharajittiphan, P., Woolcock, S. T., and Trahair, N. S. (1974). "Effect of In-Plane Deformation on Lateral Buckling." *Journal of Structural Mechanics*, 3(1), 29-60.

Vlasov, V. Z. (1961). *Thin walled elastic beams*, Israel Program for Scientific Translations, Jerusalem, Israel. Available from Office of Technical Services, US Department of Commerce,Washington, D.C.

Vrcelj, Z., and Bradford, M. A. (2006a). "Elastic distortional buckling of continuously restrained I-section beam–columns." *Journal of Constructional Steel Research*, 62(3), 223-230.

Wang, C. M., Chin, C. K., and Kitipornchai, S. (1991). "Parametric study on distortional buckling of monosymmetric beam-columns." *Journal of Constructional Steel Research*, 18(2), 89-110.

Wang, C. M., Liew, K. M., Xiang, Y., and Kitipornchai, S. (1992d). "Application of Trefftz theory in thin-plate buckling with in-plane pre-buckling deformations." *International Journal of Mechanical Sciences*, 34(9), 681-688.

Xiang, Y., Wang, C., Liew, K., and Kitipornchai, S. (1993). "Mindlin Plate Buckling with Prebuckling In-Plane Deformation." *Journal of Engineering Mechanics*, 119(1), 1-18.

Ziegler, H. (1983c). "The influence of inplane deformation on the buckling loads of isotropic elastic plates." *Ing. arch*, 53(1), 61-72.

Zirakian, T., and Showkati, H. (2006d). "Distortional buckling of castellated beams." *Journal of Constructional Steel Research*, 62(9), 863-871.

Zirakian, T., and Showkati, H. (2007). "Experiments on Distortional Buckling of I-Beams." *Journal of Structural Engineering*, 133(7), 1009-1017.

Chapter 7

Summary-Conclusion-Recommendation-Future work

7.1. Summary of contributions

The present dissertation has developed a distortional theory and a family of finite elemens for the static analysis of members with wide flange cross-sections. The theory is intended for the static analysis of members with mono-symmetric wide flange cross-sections under general loadings (Chapters 3) and the finite element formulations in chapter 4 extended the distortional solutions for more complex span configurations. A distortional buckling finite element formulation was then developed for doubly-symmetric wide flange steel beams subjected to general axial and transverse loading (Chapter 6). All finite elements developed were 1D beam elements involving discretization only along the longitudinal coordinate. Yet, the elements captured 3D aspects of the response (such as distortion) at a fraction of the computational and modelling effort involved in 3D shell analysis. The contributions and aspects of the distortional static theory are summarized under Section 7.1.1 , those of the distortional buckling theory are summarized under Section 7.1.2 while additional contributions are provided under Section7.1.3.

7.1.1. Contributions related to the distortional static theory

1- The governing differential equations and associated boundary conditions were formulated based on the principle of minimum total potential energy. Two sets of coupled differential equations were obtained along with the possible boundary conditions. The first set characterizes the longitudinal-transverse response and involves three displacement fields and the second set characterizes the lateral-torsional response and involves four displacement fields.

2- Closed form solutions were developed for the resulting coupled differential equations under general loading.

3- The longitudinal-transverse solution captures shear deformation effects within the plane of the web in a manner comparable to the Timoshenko beam theory while the lateral-torsional response captures web distortion as well as local and global warping.

4- Two sets of distortional finite elements were formulated. In the first set of elements, cubic and linear Hermitian shape functions are adopted to interpolate nodal displacements while in the second set of elements, the closed form solution obtained is employed to formulate special shape functions. Each set of elements consists of two finite elements, one characterizing the longitudinal-transverse response and the other one characterizing the lateral-torsional response. All four elements have two nodes. The longitudinal-transverse elements had two end nodes with four degrees of freedom per node while the lateral-torsional had two end nodes with eight degrees of freedom per node.

5- A mesh study is performed to establish the convergence characteristics of the finite elements developed. Also, comparisons of results with those based on 3D shell FEA models show the validity of the closed form and the finite element solutions developed.

6- The applicability of the new theory is demonstrated in a number of practical problems including beams subjected to torsion and laterally loaded beams with only one of the flanges restrained.

7.1.2. Contributions related to the distortional buckling theory:

1. A LTB finite element was developed for the lateral torsional buckling analysis of beam-columns of doubly-symmetric cross sections subjected to general loading. The formulation captures the effects of web distortion, pre-buckling deformation, pre-buckling shear deformation, pre-buckling geometric nonlinearity, local and global warping, load height, and presence/absence of transverse stiffeners.
2. The theory is able to characterize the effect of any combination of features and evaluate the individual contribution of each feature as well as the combined effect of multiple features on the predicted buckling loads
3. The lateral displacement of the web is interpolated using quintic Hermitian polynomials along the longitudinal direction and cubic Hermitian polynomials in the transverse direction. The resulting element consists of two end nodes with 10 buckling degrees of freedom per each node.
4. Where web distortion is to be suppressed due to the presence of transverse stiffeners (or for comparison with classical non-distortional buckling solutions) a technique for enforcing the associated kinematic constraints has been developed and implemented.
5. The inclusion of pre-buckling terms into the formulation was observed to lead to a cubic eigenvalue problem in the unknown buckling load multiplier. This contrasts with classical buckling solutions and those based on commercial programs where pre-buckling effects are omitted leading to the linearized eigen-value problem.
6. The validity of the solutions based on the present buckling theory has been established through comparisons with various solutions including shell FEA analyses based on the S4R element in Abaqus, and beam buckling analyses based on the element of Barsoum and Gallagher (1970).

7.1.3. Additional contributions

1. The closed form solutions in Chapter 3, geometric nonlinear solution in Chapter 5, and finite element formulations for the static and buckling theories developed in Chapters 4 and 6 been implemented under the Matlab platform.
2. As a pre-requisite to the distortional buckling theory developed in Chapter 6, a shear deformable geometric non-linear formulation is developed to characterize the pre-buckling equilibrium path. A formulation was developed to conduct such an analysis in Chapter 5. The formulation is based on special shape functions based on the exact static solution for linear Timoshenko beam to avoid shear locking. The element captures second order effects due to interaction of between strong axis moment and axial forces in beam columns.
3. Given that present buckling eigen-value buckling solutions in commercial programs, such as Abaqus, do not capture pre-buckling deformation effects, an innovative iterative procedure was developed to capture the PBD effect from present shell 3D FEA linearized buckling solutions. The iterative procedure involves conducting multiple successive shell FEA and involves significantly more effort than that based on the present solution which directly captures PBD effects. Nevertheless, it provides a basis to assess and establish the validity of the predictions of the present theory in capturing PBD effects.

7.2. Conclusions

The following conclusions can be made based on the results of the distortional static theory;

1. For beams under torsion, the static distortional theory indicates that the deformational response largely depends on the type of twisting moments applied to the section. For instance, the response was shown to vary significantly depending on whether the twisting moment is applied in the form of equal and opposite horizontal forces applied to the web ends, or as equal and opposite vertical forces applied to the bottom flange tips, or to the top flange tips. The difference in response was corroborated
2. Due to web distortion, the angles of twist of top and bottom flanges were shown to differ. At the tip of a cantilevers under twisting moments, the average angle of twist for the whole section is shown to be smaller compared to that predicted by the Vlasov theory. Near the cantilever root however, the angle of twist is typically larger compared to that predicted by the Vlasov theory.
3. For cantilevers and beams with overhangs subjected to twisting moments, the presence of stiffeners is shown to have a significant effect on reducing the lateral displacement.

The following additional conclusions can be made based on the results of distortional buckling theory:

1- For a given beam with span L and a wide flange cross section of height d , flange width b , flange thickness t and web thicknesses w, numerical results based on the present distortional theory indicate that in simply supported beams and cantilevers, web distortional effects become significant as the span-to-depth ratio L/d decreases and become less important as either d/w or b/d decrease. Also, in simply supported beams, distortional effects are shown to increase as b/t decreases whereas in cantilevers, they are observed to become pronounced as b/t increases.

2- In the presence of distortion, the PBD effect is shown to increase as L/d or b/d increase but to reduce as d/w or b/t increase. In the absence of distortion, the PBD effects are shown to slightly decrease as L/d , d/w or b/t increase but to increase as b/d increases.

3- In general, the pre-buckling shear deformation effect is shown to slightly increase the predicted buckling resistance where PBD effect is included compared to analyses that account for PBD effect while neglecting shear deformation effects. In contrast, for short span cantilevers, accounting for shear deformation effects is observed to increase the stiffening effect due to PBD.

4- In beam-columns, the inclusion of geometric nonlinear effect (P-delta effect) during the pre-buckling stage, is associated with a large pre-buckling transverse displacements and larger strong axis bending moments and thus the buckling resistance of the member is observed to reduce compared to that based on a linear pre-buckling analysis. Also, the numerical examples indicate that the deteriorating effect induced by the magnification of strong-axis bending moments due to the presence of axial compression is significantly higher than the beneficial PBD effect resulting from the additional pre-buckling displacements caused by the P-delta effect. Hence the critical moments predicted are lower than those based on a linear pre-buckling analysis.

5- For simply supported beams with transverse loads offset from the shear centre, distortional effects are shown to gain significance as the point of load application moves upwards whereas the PBD effect is observed to gain significance as the point of load application moves downwards. Also, the distortional and PBD effects seem to compensate for one another when the load is applied at the top flange, but have a net beneficial effect when the load is applied at the bottom flange.

6- In beam-columns with a compressive force offset from the section centroid, the PBD and distortional effects are observed to increase as the load moves away from centroid. The stiffening effect due to PBD is observed to be more significant as opposed to the softening effect induced by distortion.

7- In simply supported plate girders with a slender web under mid-span point load, the presence of transverse stiffeners is observed to increase the buckling resistance of the member. Stiffeners located near both ends and at the point of application of the load at mid-span, are observed to be particularly effective in increasing the distortional lateral torsional buckling capacity of the girder compared to other intermediate stiffeners. The provision of multiple stiffeners along the beam is shown to supress the distortional effects nearly entirely. The predicted LTB resistance approached such case is observed to agree with that based on the classical non-distortional Vlasov theory.

7.3. Recommendations for future work

Recommendations for future work include:

1- The distortional theory developed accounts for several non-conventional effects not accounted for in present steel design standards (i.e., distortional effects, pre-buckling deformation effect, etc.). It is of interest to re-assess present design methodologies in light of the new theory, conduct a large database of runs, and possibly develop design factors that account for distortional effects and pre-buckling deformations. Such refinements are expected to lead to improved design rules with more consistent probabilities of failure than present rules.

2- The present distortional theory is suited to determine the distortional LTB resistance of members that are laterally supported at one of the flanges. Relevant applications include continuous beams with continuous lateral and torsional support at the top through a concrete slab or with discrete lateral braces provided by secondary steel members.

3- Both distortional theories developed account for shear deformation effects in the web but have neglected shear deformations in the flanges. It is of interest to add shear deformation effects in the flanges by considering each of the two flanges as Timoshenko beams.

4- It is of interest to extend the formulation for members with mono-symmetric wide flange cross sections and tapered beams.

5- While the present research has adopted distortional kinematics to develop a static and buckling theories, it is of interest to extend the work to develop a distortional dynamic analysis theory based on the same kinematics for the analysis of beams under dynamic loads.

Barsoum, R. S., and Gallagher, R. H. (1970). "Finite element analysis of torsional and torsional–flexural stability problems." *International Journal for Numerical Methods in Engineering*, 2(3), 335-352.